Cranfield University

School of Mechanical Engineering

Ph.D. Thesis

Academic Year 1997 - 98

M. J. Swainson

Evaluation of the potential of solar chimneys to drive natural ventilation in non domestic buildings

Supervisor W. J. Batty

December 1997

ABSTRACT

The solar chimney allows natural ventilation to be achieved during periods when the wind velocities are low and the difference between internal and external air temperatures is minimal. The correct design of such building components requires that designers have appropriate design tools available to them that are both effective and easy to use. The aim of this project was to evaluate design tools currently available and if appropriate to provide a tool that would allow the effects of variations in key physical parameters to be evaluated.

Two design tools are currently available to designers; zonal models and CFD programmes. Both of these were however found to be unsuitable for the evaluation of the performance of a solar chimney. Zonal models assume that the air within a zone is fully mixed which results in the effects of variations in physical parameters on the mass flow rate being incorrectly predicted. CFD programmes require validation of any models developed before confidence in the predictions can be established, it was found however that data for such validation was not available for realistic flow configurations.

An experimental rig was designed and tested to ensure that the uncertainty in the data produced was both minimised and accurately quantified.

A detailed review of the sensitivity of a CFD programme to model and input variables was undertaken allowing development of an appropriate model. Comparison of the results of the experimental investigation and CFD predictions showed that the CFD programme, utilising the $k\varepsilon$ turbulence model accurately predicted air flow rates through a solar chimney across a range of key physical parameter variations.

Within the limits of the validity determined for the CFD model, a detailed parametric investigation was then undertaken.

The result of the parametric investigation was the development of a design tool appropriate for the determination of the effects of variations of the key physical variables on the mass flow rate through a solar chimney.

ACKNOWLEDGEMENTS

I would like to thank Dr. Bill Batty for his guidance throughout the duration of this project. My thanks also go to Mr C. Knight and all of the support staff at Cranfield University who have helped me at every stage of my work. For the loan of equipment, the shell of my rig and hours of discussion, my thanks to Chris Martin of EMC Ltd.

To family and friends, my thanks for maintaining my state of relative sanity and of course to Niki Curtis for putting up with the last three years.

Finally, to the memory of my father, Mr T. G. Swainson for his unswerving support and encouragement throughout the years.

TABLE OF CONTENTS

APPENDICES

LIST OF FIGURES

CHAPTER ONE

CHAPTER TWO

CHAPTER THREE

3.7. Basic rig design for solar chimney investigation
3.8. Final design of experimental rig
3.9. Positioning of instrumentation within experimental rig
3.10. Model of experimental solar chimney inlet used to establish the inlet profile of the air across a range of mass flow rates

CHAPTER FOUR

4.1. Measured mass flow rate into and out of the solar chimney at two heights with high aspect ratios (i.e. $\geq$15:1)
4.2. Measured mass flow rate into and out of the solar chimney at two heights with low aspect ratios (i.e. $\leq$ 10:1)
4.3. Comparison of the methods of calculating energy transfer within the chimney.
4.4. Energy transferred from the plate throughout a clear day
4.5. Energy transferred from the plate and mass flow rate for a range of plate to inlet air temperature differences
4.6. Rig stratification creating temperature difference $T_{rig} > T_{inlet}$
4.7. Vertical air temperature profile within rig
4.8. Influence of external stack temperature on mass flow rate of a fully mixed space with a heat source.
4.9. Effect on mass flow rate of elevation of rig air temperature above inlet air temperature.
4.10. Influence of plate height and inlet height on mass flow rate
4.11. Mass flow rate for different aspect ratios with a plate height of 1.5m
4.12. Mass flow rate for different aspect ratios with a plate height of 2.25m
4.13. Mass flow rate for different aspect ratios with a plate height of 3.0m
4.14. Mass flow rate for different aspect ratios with a plate height of 3.75m
4.15. Variations in mass flow rate from maximum for all rig heights at an energy transfer rate of 100 W/m^2.
4.16. Channel depth giving the maximum flow compared to the depth of a turbulent natural convection boundary layer, calculated using equation 2.15.
4.17. Effect of channel depth in relation to depth corresponding to maximum flow rate on mass flow rate for all rig heights at 100 W/m^2.
4.18. Temperature elevation of the plate above inlet air temperature at an energy transfer rate of 100 W/m^2 for each of the experimental plate heights
4.19. Local convective heat transfer coefficient for each of the plate heights at an energy transfer rate of 100 W/m^2
4.20. Convective heat transfer coefficients for different plate heights across a range of rates of energy transferred from the plate to the air
4.21. Mass flow rate predictions using equations 4.1. to 4.4.
4.22. Predicted mass flow rates using equations 4.7. to replace equation 4.4.
4.23. Mass flow rates predicted by the model proposed by Borgers et al compared to experimental results.

CHAPTER FIVE

5.18. CFD predictions of flow at the outlet of the chimney for a low aspect ratio configuration showing the occurrence of reversed flow and the cross flow at the channel outlet.
5.19. Outlet air temperature profiles for all aspect ratios for a rate of energy transferred from the plate of 100W/m^2.

CHAPTER SIX

6.1. Model developed for the parametric testing of the solar chimney flow configuration
6.2. Channel depth corresponding to maximum mass flow rate for the parametric investigations at a rate of energy transferred from the plate of 100 W/m^2.
6.3. The influence of stack height and rate of energy transferred from the plate on the maximum mass flow rate
6.4. Comparison of the effect of the rate of energy transferred from the plate on the normalised maximum mass flow rate for two different stack heights.
6.5. Effect of normalised channel depth and inlet height on the mass flow rate for a stack height of 4m and a rate of energy transferred from the plate of 100 W/m^2.
6.6. Effect of normalised channel depth and inlet height on the mass flow rate for a stack height of 4m and a rate of energy transferred from the plate of 100 W/m^2.
6.7. The effect of different stack heights on the normalised mass flow rate when the inlet height and channel depth were altered at a constant rate of energy transferred from the plate of 100 W/m^2.
6.8. The effect of different rates of energy transferred from the plate on the normalised mass flow rate when the inlet height and channel depth were altered at a constant stack height of 4m
6.9. Determination of the value of the normalised inlet height and channel depth from the actual dimensions (mm)
6.10. Determination of the normalised mass flow rate M_A from normalised values of the inlet height and channel depth
6.11. Determination of the normalised mass flow M_B from the normalised mass flow rate M_A and the rate of energy transferred from the plate (W/m^2)
6.12. Determination of the mass flow rate (g/s) from the normalised mass flow rate M_B and stack height (m)
6.13. Percentage difference between predicted mass flow rate of model using equations 6.14. to 6.20. and those predicted by the CFD model
6.14. Comparison of the actual velocity profile within a solar chimney as predicted in the parametric investigation with that of a turbulent fully developed flow of the same mass flow rate

LIST OF TABLES

CHAPTER SIX

6.1. Identified range of input variables for the parametric investigation
6.2. Values of input variables used in the example calculation of mass flow rate in figures 6.9. to 6.12.

NOTATION

Symbol	Meaning		Unit
A	Area		m^2
Ab	Cross sectional area of boundary layer		m^2
b	Boundary layer depth	Equation 2.15.	m
B	Matrix in dynamic model	Equation C.18.	
Bi	Biot number	Equation C.4.	
Cd	Discharge coefficient		
C_f	Skin friction coefficient	Equation 5.8.	
Cp	Specific heat at constant pressure		J/kg °C
d	Depth of channel		m
d_h	Hydraulic diameter $4 \frac{\text{Area}}{\text{Perimeter}}$		m
D	Normalised channel depth	Equation 6.2.	
f	Friction factor	Equation 2.28.	
Fo	Fourier number	Equation C.2.	
g	Gravitational force		m/s^2
Gr_h	Grashof number based on temperature difference		
Gr_h^*	Grashof number based on heat flux		
h	Height		m
h_c	Convective heat transfer coefficient		W/m^2 °C
H	Normalised inlet height	Equation 6.3.	
k	Turbulent kinetic energy	Equation 5.5.	
k	Thermal conductivity		W/°C m
K	Pressure loss coefficient	Equation 2.27.	
$\dot{m}$	Mass flow rate		kg/s
M	Normlised mass flow rate		
Nu_h	Nusselt number	Equation 2.19.	
P	Absolute pressure		Pa
P_s	Stack pressure		Pa
Pr	Prantl number	Equation 2.17.	
q	Heat transfer rate		W
q''	Heat flux		W/m^2
Q	Volumetric flow rate		m^3/s
Q''	Matrix in dynamic model	Equation C.18.	
Re	Reynolds number	Equation 2.4.	
t	Time		s
T	Temperature		K
u	Velocity		m/s
u_∞	Free stream velocity		m/s
U	Uncertainty		
U	Fractional uncertainty		%
w	Width of boundary layer		m
W	Weights matrix	Equation 6.11.	

x	Length		m
y	Distance normal to plate		m
y^+	Nondimensional wall distance	Equation 5.6.	

Greek letters

α	Thermal diffusivity		m^2/s
β	Coefficient of thermal expansion		
ΔP	Pressure difference		Pa
ΔT	Temperature difference		K
ε	Emissivity		
θ_g	Non dimensional temperature	Equation 2.25.	
μ	Viscosity		kg/ms
ν	Kinematic viscosity		m^2/s
ξ	Efficiency	Equation 2.35.	
ρ	Density		kg/m^3
ρ_0	Density at 273 K		kg/m^3
σ	Stefan Boltzman constant		
τ_w	Wall shear stress		N/m^2
ω	Temperature gradient	Equation 2.5.	K/m

Subscripts

1 & 2	Identifiers	
A	Normalised mass flow rate identifier	
abs	Absorbed by the plate	
atrium	Atrium environment	
B	Normalised mass flow rate identifier	
channel	Channel formed by heated plate and back wall	
chimney	Air heated within chimney	Figure 1.8
conv	Convective heat flux	
d	Channel depth	
exhaust	Exhausting from rig to external	
external	External environment	
g	Glazing to solar chimney	
gap	Space between heated plate and glazing	
glass	Glazed wall within Trombe wall channel or solar chimney	
h	Height	
i	Opening identifier	Equation 2.1.
inlet	Channel inlet	
input	weights matrix identifier	

internal	Internal environment	
j	Opening identifier	Equation 2.1.
losses	Overall losses	Equation 2.26.
m	Measured value	
max	Maximum	
mean	Mean	
n	Total number of uncertainty variables	
outlet	Channel outlet	
output	weights matrix identifier	
p	Heated plate of channel	
plate	Heated plate of channel	
rad	Radiated heat flux	
reference	Reference	
rig	Rig air	
rig wall	Rig structure	
sol	Solar heat flux	
solar heated	Air heated within atrium	Figure 1.5
Total	Total	
Trans	Transmitted	
wall	High thermal mass wall within Trombe wall channel	

CHAPTER ONE

THE BACKGROUND TO NATURAL VENTILATION AND THE SOLAR CHIMNEY AS A VENTILATION DRIVER

1.1 Introduction

Interest in naturally driven ventilation for the provision of a comfortable internal environment has been growing in northern Europe for a number of years. The reasons for this interest are examined and the implications for non-domestic buildings are discussed. The use of natural driving forces requires that the physical principles are fully understood. These are therefore explained and a range of examples showing how they have been utilised in different design solutions discussed.

1.2 Ventilation of non domestic buildings

The primary purpose of ventilation is to provide an acceptable quality of internal climate for the occupants of a building. This requires a continuous supply of oxygen and the removal of CO_2 and odours from the occupied space. Additionally ventilation removes any pollutants that may be contained within a building due to the processes undertaken or the materials contained. Ventilation may also be used to remove heat from spaces and contribute to the provision of thermally comfortable conditions. To protect the fabric of the building from potential deterioration ventilation is also required to remove moisture.

In the UK, with its mild maritime climate, most buildings in the past required only heating in the cooler seasons. Ventilation in summer was provided largely through the use of windows and doors to allow cooling by maintaining a large air change rate. In the heating season ventilation was minimised and usually achieved through infiltration. Up to the 19th. century buildings size was limited largely by structural considerations however during the 19th. century advances in structural design and construction methods allowed the development of larger buildings. The resulting internal environment in many of the larger public buildings of the period was reported to be unhealthy due to inadequate ventilation[1]. Some designers, such as Sir J Jebb[2], did address

this and designed buildings containing systems that promoted ventilation by natural means. By 1900 mechanical systems of ventilation had been developed and became widely adopted within larger buildings in Europe. Therefore the development of natural ventilation techniques to remove heat gains from large buildings in northern Europe was never fully addressed by building designers.

This is in sharp contrast to buildings developed in hotter climates where natural ventilation was always utilised to remove heat gains. In these climates the style of the architecture especially regarding spatial relationships vividly reflects this function. Towers and courtyards were developed to promote the natural driving forces required to achieve comfortable internal conditions or provide cool sheltered conditions outside.

In the UK the development of the Building Regulations, especially after the oil crisis of the 1970's, has focused on heat losses and thus the winter operation of buildings. In this way the energy implications of the summer operation of buildings was broadly ignored. The result of this was that the fabric of a building was seen as the prime source of energy loss in winter, walls became highly insulated and windows reduced in size and/or double glazed. Infiltration was reduced with tighter construction methods being adopted. The move to deep plan buildings and the rise in the use of office machinery resulted in large internal heat gains and associated problems of overheating. This was further exacerbated in the 1980's as global standardisation of office type buildings and the desire for an international corporate image drove office designs toward fully glazed facades which resulted in high solar gains in summer. The overall result of these changes has been that during much of the year the adoption of full air conditioning was the only way to prevent overheating.

In 1992 Roaf[3] noted that in the south east of the UK nearly all new and 50% of refurbished offices were being fitted with air conditioning. A review of several newly designed buildings in 1996[4] showed that at the top end of the market this trend had been slowed with examples of fully naturally ventilated buildings or buildings adopting a mix of natural and mechanical ventilation. All of these buildings had been designed to limit solar gains in summer with frequent use of solar shading to minimise the potential for overheating and thus reduce the need for comfort cooling.

1.2.1 The perceived need for air conditioning

At the design stage the heating and cooling loads of a building must be quantified to enable the mechanical plant to be sized. In the past the calculation of loads was undertaken using steady state calculations. Such methods omit the dynamic effects of a buildings structure which can attenuate its response to diurnal swings in ambient temperatures. Use of the Admittance method with idealised CIBSE weather data has been shown to be wholly unrealistic[5]. This method assumes a repeating cycle of extreme daily temperatures which in reality do not occur for extended periods of time. The result of such a calculation is a repeating cycle of building loads required to offset an ambient condition that does not occur in reality and consequently may lead to oversized systems.

In addition to the space environmental conditioning load arising from ambient conditions of temperature and insolation, an assessment of the internal heat gains must be undertaken. The standard method of achieving this is to use the data published by CIBSE[6], however there is evidence that the allowance made for office equipment is significantly over estimated[7] [8]. This is especially so with electrical equipment as manufacturers are constantly striving to reduce power consumption and thus heat generation. Such equipment is also not always functioning at full capacity and so appropriate utilisation factors must be applied. The figures that became the normal in the 1980's, i.e. 40 W/m^2, are therefore now considered[9][10] as significantly in excess of those currently appropriate i.e. 15 W/m^2.

The result of both of these methodologies for load calculations is the perception that the risk of overheating is greater than it actually is. Thus in many cases full conditioning is then the only method of controlling the predicted internal temperatures in summer. In reality however, the actual requirement for comfort cooling may be significantly below that perceived, making the option of natural ventilation as the primary means of heat removal more appropriate for a high percentage of non domestic buildings in the UK.

1.2.2 Ventilation and thermal comfort

Attempts to define an air temperature at which people would be comfortable, considering all other pertinent variables were first introduced in the 1920's[11]. Designers used an index to determine the effect of each variable on the air

temperature. This produced an effective air temperature representing that perceived by a buildings occupants.

In 1972 Fanger[12] produced an environmental index that could be used to calculate an appropriate mix of parameters that would provide thermal comfort. This resulted in a set of comfort charts used for a combination of any two variables. From such charts, given detailed information on the air characteristics within the space, designers were able to predict the air temperature that should be provided in a space for given levels of activity and clothing. The result of this was that through the inclusion of large conditioning plants within buildings, a constant internal temperature was provided regardless of the style of office building design, ambient conditions and running cost.

This idea that a single temperature can be defined as being the optimum for thermal comfort has remained largely unchallenged until recently[13]. Evans[14] questioned whether the occupants of a building would tolerate or even prefer fluctuating internal temperatures on a diurnal and seasonal basis.

Humphreys[15] undertook investigations into free running buildings that suggested that the occupants were comfortable with a wide range of temperatures, that related to the season. The possibility of a thermal comfort model based on such aspects as season and building type as well as activity and clothing levels has been suggested and is now being actively investigated[16]. This type of model has been referred to as 'adaptive', as it is thought to correspond more closely to human behaviour and its ability to adapt than the single temperature solution widely used at present.

In addition to the broad question of thermal comfort the subject of sick building syndrome has been much investigated[17] in the last few years with findings indicating that non air conditioned buildings are generally less likely to produce symptoms than fully sealed and conditioned ones.

In free running buildings Leaman[18] found that people are more likely to tolerate greater discomfort if they have personal control over the conditions or are allowed to alter their style of dress freely. This is counter to the move in the 1970's and 80's where control was increasingly centralised and buildings totally sealed to allow precise plant control. This point was again highlighted in

a survey by Ellis[19] where 89% of people surveyed said they preferred non conditioned buildings i.e. not centrally controlled.

1.2.3 Environmental aspects

Many scientists believe that the climate will become warmer as a consequence of the emissions into the atmosphere of greenhouse gasses.

Currently energy used in all types of buildings in the UK accounts for around 50% of CO_2 emissions[7] and the bulk of energy use (60%) in buildings in the commercial and public sectors is for space heating and air conditioning. Added to this, air conditioning requires three to four times as much energy as heating[20] and air conditioning and mechanical ventilation is the fastest growing consumer of energy in buildings and estimated to account for nearly 10% of the CO_2 emissions from building operation[21].

In light of these facts there is a need to address the continuing expansion of air conditioning if the government's pledged target of reducing CO_2 emissions to 1990 levels by the year 2000, as agreed in 1993 with the ratification of the Framework Convention on Climate Change, is to be met. This commitment was further reinforced by the Labour Party in its manifesto[22] which promised a 20% cut in CO_2 emissions between 1990 and 2010. The pressure to find alternatives to full air conditioning for buildings will therefore continue to grow as the government seeks to achieve its goals.

Conclusion on the move to adopt air conditioning and why this should be abated

The development of mechanical ventilation and refrigeration systems and changes in architectural fashion have led to largely non passive means being adopted for the conditioning of larger buildings in northern Europe especially to meet anticipated occupant comfort needs in the summer season. The continued increase in adoption of such systems has significant implications for the natural environment and raises questions about what internal environment building occupants find most comfortable. The vernacular architecture of the region however offers no real solutions to the problem of natural ventilation in larger buildings. Possible passive solutions must therefore be investigated and evaluated to ensure that inappropriate solutions are not adopted. If this is not undertaken faith in naturally driven ventilation systems will not be gained and the largely unnecessary move to full conditioning with cooling will continue.

The implications of adopting natural ventilation are now considered along with methods available to achieve practical solutions.

1.3 The potential of natural ventilation in non domestic buildings

CIBSE in their Application Manual on natural ventilation[7] state that a naturally ventilated building could be up to 15% cheaper to build, due to the savings in plant and fittings. This is however questioned by Wyatt[23] who states that naturally ventilated buildings are not a cheap option and may well cost more than a simple conditioned one. The reason for this being that the cost of exposed structural-mass finishes and openable windows may be considerably greater than the savings made from the omission of plant. Additionally the design costs for such buildings may be greater as more detailed modelling will be required to evaluate the building's dynamic response over a wide range of weather and seasonal ambient conditions.

Running costs for conditioning systems are suggested by CIBSE[7] to be up to 40% and Clements-Croome[24] to vary between 40 - 70% less for a naturally ventilated building when compared to a similar fully conditioned building.

The greatest potential motivation for building occupiers to move to natural ventilated buildings is the potential effect on occupant productivity through the psychological perception of control they gain over their internal environment. This potential link was suggested by Raw[25] who linked productivity and perception of control over the internal environment. Wyatt[23] noted that if the result of reduced energy consumption was a bad indoor climate, the costs arising from reduced productivity would be many times more than that of the energy saved. Sherman[26] placed the relative costs of running an office building into context;

Expenditure	$/ft^2/Yr
Energy	2
Maintenance	3
Tax	4
Rent	40
Productivity	300

Table 1.1. Relative costs of running an office building in US[26]

Table 1.1. indicates that a small increase in the productivity of the workforce would mask any savings made on energy. However, the converse is also true. Natural ventilation designs must therefore be fully evaluated at the design stage as the implications for building owners of uncertainty in the performance of a design are very large and may well result in adoption of air conditioning as a safe option.

1.4 Air conditioning and regulations

The Building Regulations in the UK[27] are generally seen as a standard to aim for and not the minimum standard to which a building should comply. It is against this backdrop that the lack of guidance for building designers on the summer operation of buildings has led to the free adoption of air conditioning with only the cost implications in most cases influencing the final design. Maldonado[28] interestingly notes that in many southern European countries where the move to air conditioning has been very widespread, estimated at 900% increase in installations per year in Portugal, the building regulations have also failed to address means of reducing the cooling loads in buildings in summer.

The BREEAM labelling scheme[29], recently introduced in the UK by the BRE, offers building designers a way of voluntarily rating their buildings with respect to environmental impact. One of the key approaches to raising the rating of a building is through the adoption of natural ventilation. In this way the reduced impact of a building on the environment can be quantified relative to other buildings. Better ratings with the BREEAM scheme are now becoming seen as tools for enhancing corporate image and better marketability of buildings[30]. This scheme could therefore help to increase the move towards more naturally ventilated buildings by increasing demand for buildings with lower environmental impact.

In contrast to this voluntary scheme the most recent edition to the UK Building Regulations applied to ventilation, Part F[31] , introduced standards for the provision of ventilation in non domestic buildings for the first time but makes no provision that the need for air conditioning has to be evaluated to meet the regulations. In contrast the need to prove to the authorities that a building requires conditioning has existed in Denmark since 1977[32]. With the broad

similarity between the climates of Denmark and the UK it is logical that this requirement will be introduced in the UK eventually.

The result of such a move and continuing awareness of environmental impact of buildings adopting full conditioning will be that alternative, in some cases naturally driven, ventilation systems will be sought. Proven solutions must therefore be available for adoption by building designers to prevent wholly inappropriate systems being constructed, resulting in uncomfortable internal environments.

1.5 Methods of achieving natural ventilation

Natural ventilation of buildings is achieved by utilising the naturally induced pressure differences between the inside and outside of a building. In the UK these pressure differences have been traditionally used to ventilate buildings through the use of windows;

Wind induced pressure differences;

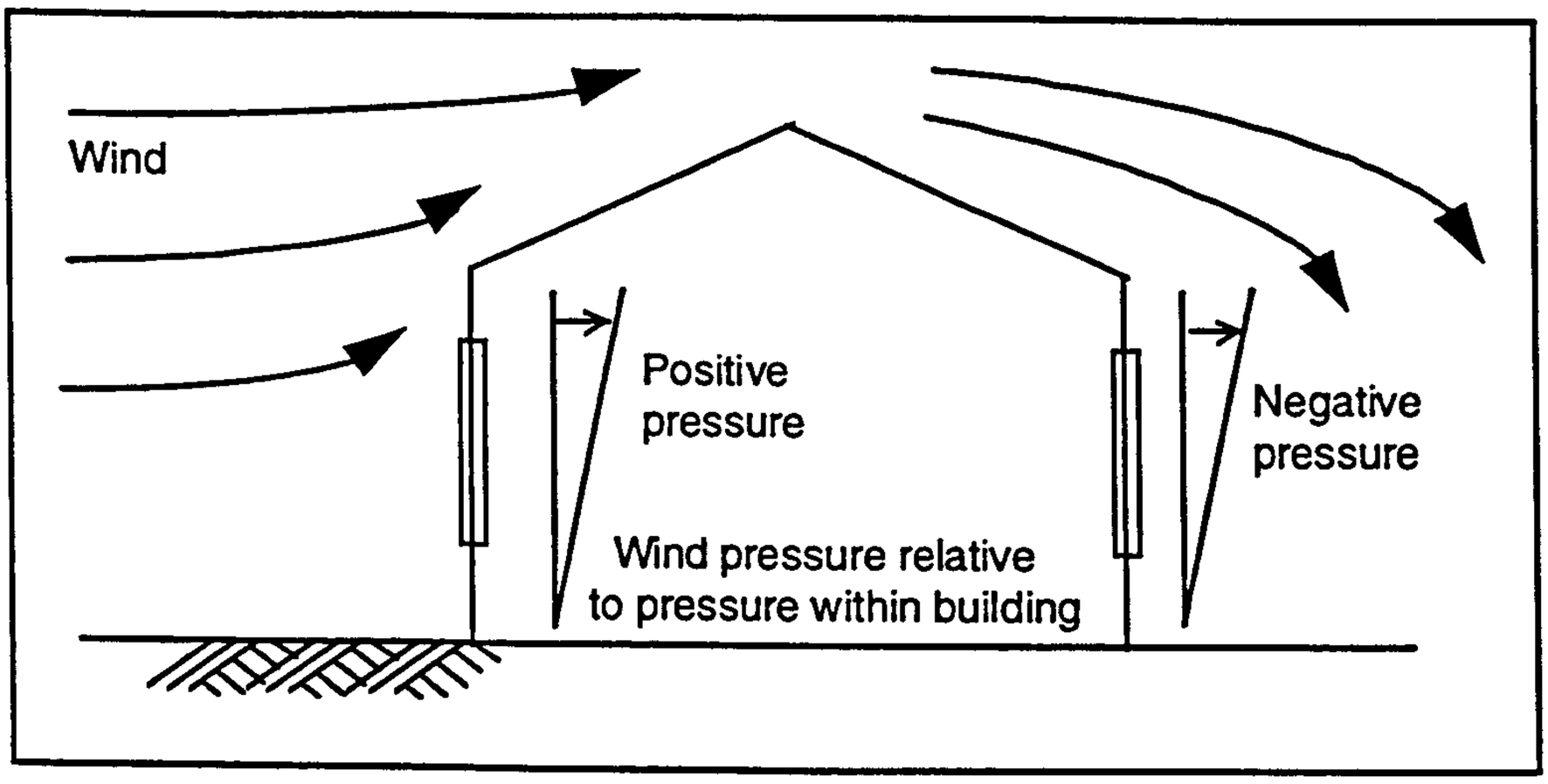

Figure 1.1. Wind induced ventilation

Temperature induced pressure differences (stack effect);

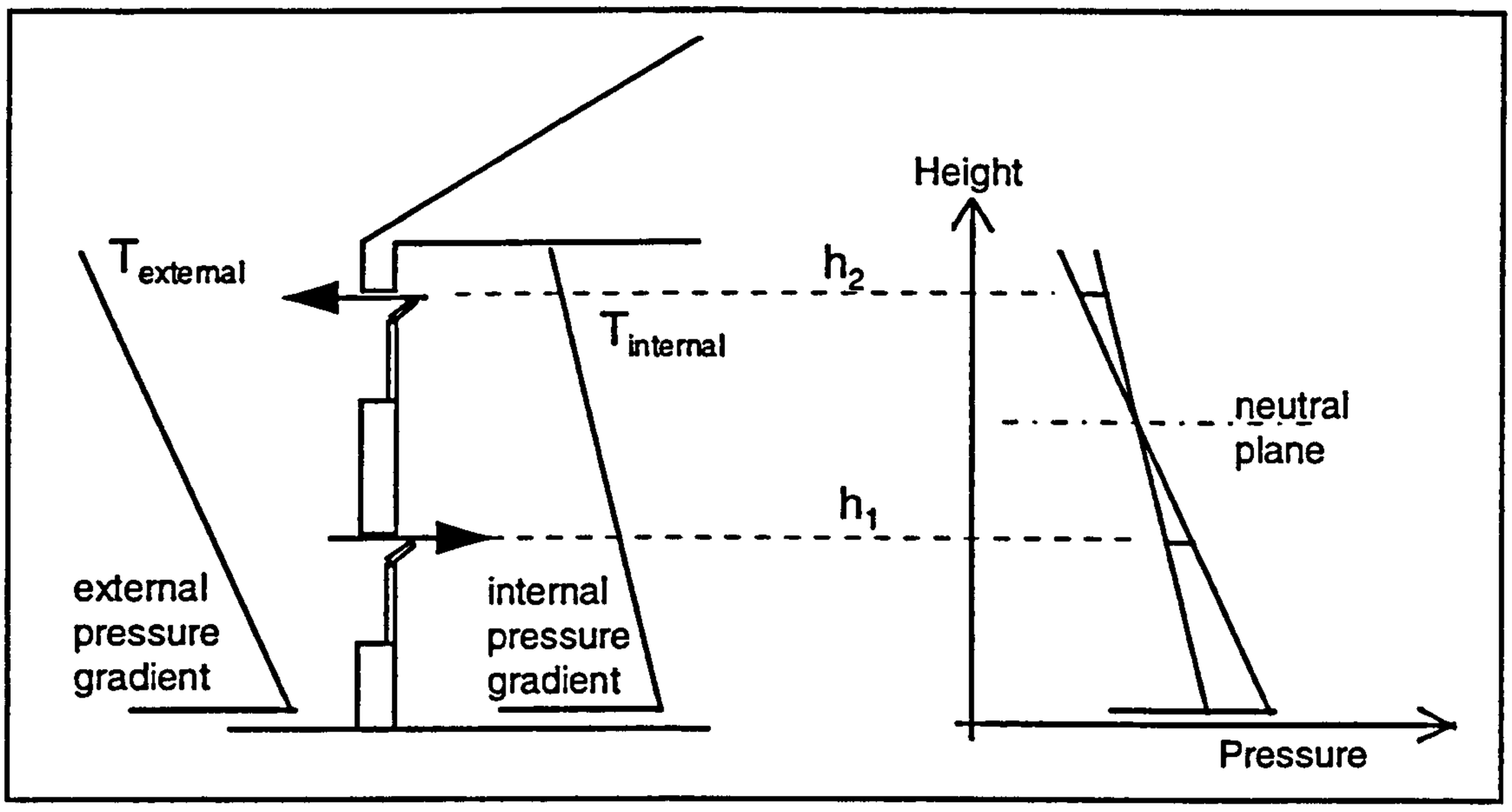

Figure 1.2. Stack induced ventilation

Although the exact values are open to significant variation due to the micro climate, Liddament[33] and Etheridge[34] both compared the relative magnitude of wind induced pressure differences and those created by stack effect. They concluded that similar pressure differences result for typical low rise buildings in urban environments. Therefore both wind and stack induced driving forces should be considered for a natural ventilation strategy.

The potential of a building to be effectively ventilated by wind induced pressure differences is influenced by a large number of variables, including; wind direction and speed, nature and position of openings, and the nature of surrounding countryside or adjacent buildings. The wind is also highly variable and this therefore raises the question of how ventilation is achieved during periods when the wind induced pressure differences are small due to low wind speeds. One of the most critical times for this is in the summer season when strong anticyclonic weather systems may predominate for extended periods of time. At such times the solar gains to a building may be high, combined with minimal wind speeds. Although disputed by Jones[35] as an unrealistic meteorological phenomena for most locations, the assumption that the wind is minimal and therefore the natural driving force for the ventilation is stack induced alone, places the strictest test upon a building design to achieve effective naturally driven ventilation.

Baker[36] noted that except in climates where the wind is very reliable the limiting case has to be that of no wind i.e. stack driven ventilation alone. Thus this investigation is limited to the case of minimal wind where ventilation relies upon stack induced flows only. In this way the potential of a ventilation design to provide an adequate ventilation rate in critical circumstances can be assessed.

1.6 Stack induced pressure differences

Stack induced pressure differences between the internal and external air masses of a building are created by differences in temperature of the air bodies and thus density. The pressure at any given height is given by;

$$P_h = P - \rho g h \qquad \text{Equation 1.1.}$$

Thus both the internal and external pressure gradients, can be described by;

$$\frac{dP}{dh} = - \rho g \qquad \text{Equation 1.2.}$$

If it is assumed that air is a perfect gas then the pressure gradient can be expressed in terms of temperature as;

$$\frac{dP}{dh} = - \rho_0 \; g\left(\frac{273}{T}\right) \qquad \text{Equation 1.3.}$$

Therefore for two uniform stacks of air the pressure difference can be expressed as;

$$\Delta P = P_{external} \sim P_{internal} \qquad \text{Equation 1.4.}$$

$$\Delta P = P_{external} - P_{internal} - g h \left(\rho_{external} - \rho_{internal}\right) \qquad \text{Equation 1.5.}$$

Expressed in terms of air mass temperatures:

$$\Delta P = P_{external} - P_{internal} - \rho_0 \, g \, h \, 273 \left(\frac{1}{T_{external}} - \frac{1}{T_{internal}}\right)$$

Equation 1.6.

In a naturally ventilated building the values of $P_{internal}$ and $P_{external}$, the values of atmospheric pressure, will be equal and therefore can be omitted from equation 1.6. If however mechanical ventilation systems are in use then the internal / external pressure difference may be significant. In such situations this must be considered when calculating the overall pressure difference between the internal and external air masses.

1.7 Methods of achieving stack induced ventilation

At the single storey level the use of windows or vents at different heights will induce stack flows as shown below:

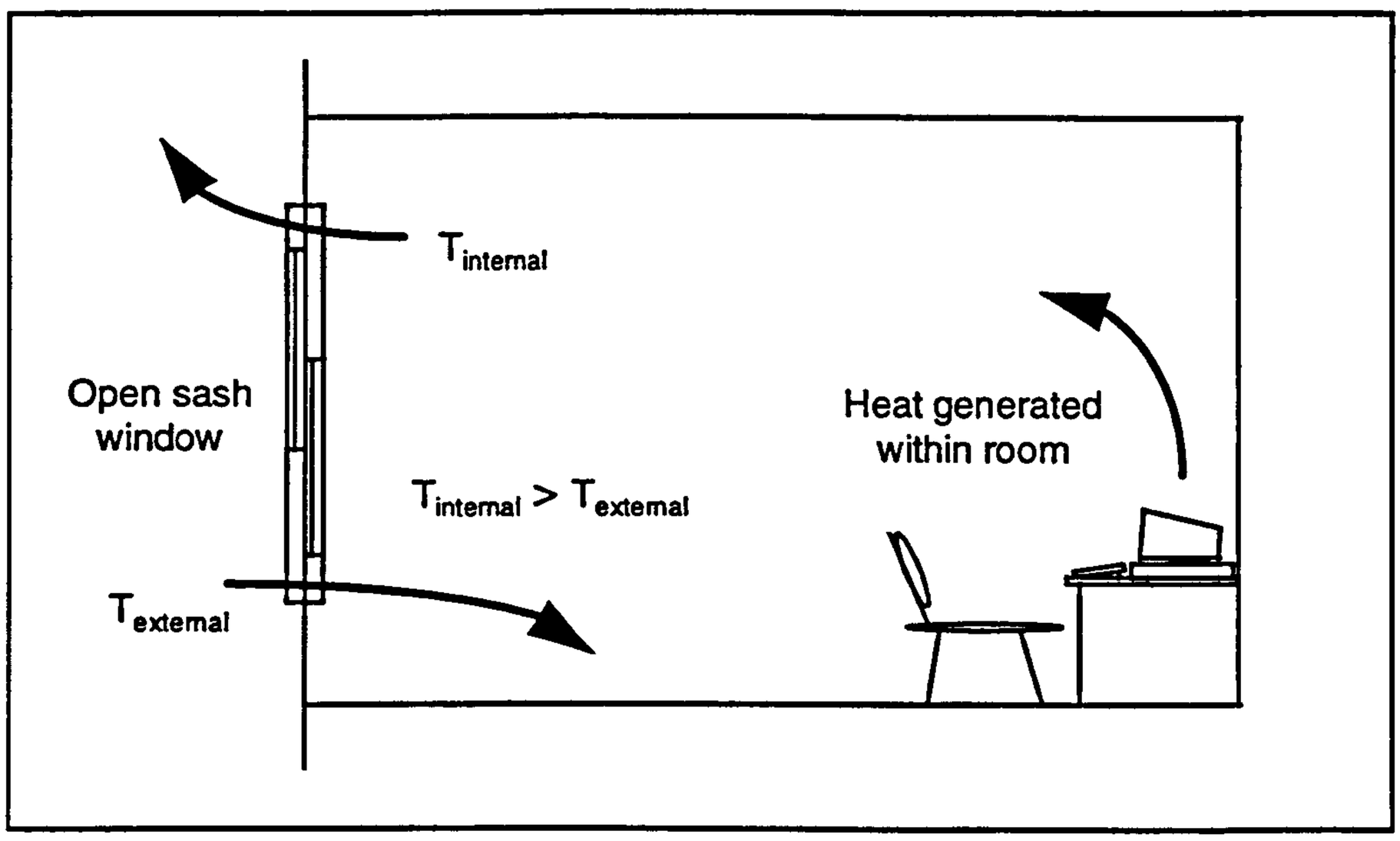

Figure 1.3. Ventilation via sash windows

As can be seen from equation 1.6. the stack pressure induced is directly proportional to the height over which the temperature difference between the air masses occurs. Thus to create significant flow rates over a single storey in summer would require that the internal air temperature were raised significantly above that externally. This may result in the internal air temperature exceeding that which is comfortable for the occupants of the space. Therefore to achieve naturally driven ventilation on a storey by storey basis many alternative methods of enhancing the effective height of the stack have been adopted. These fall into two broad categories;

1.7.1 Extending the stack height within the internally occupied space.

If there is no restriction on the vertical height of the occupied spaces within a building then this can be increased, allowing a greater level of stratification within that space. In this way occupant comfort is not impaired and the stack pressure available to drive the ventilation enhanced.

An alternative method of achieving the height is through the use of atria. These are now widely used in deep plan buildings to minimise the depth of the occupied zone to a level that can be effectively cross ventilated. In this way exhaust air from the occupied space is allowed to spill out into the atrium, drawing in cooler air through the occupied space.

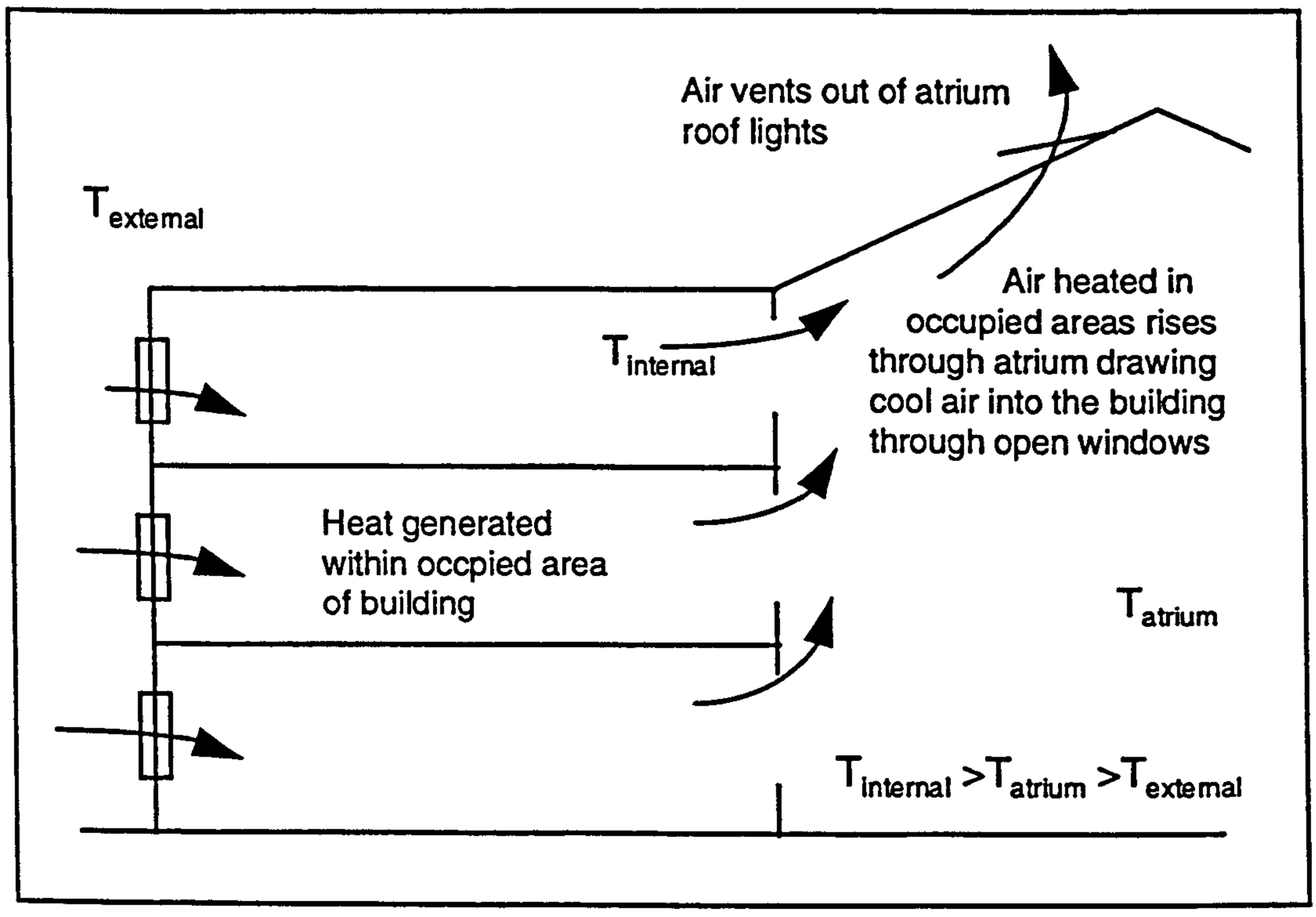

Figure 1.4. Use of atria to induce ventilation in occupied spaces

The drawback with this approach in hot summer conditions is that to prevent internal spaces overheating, high ventilation rates are required to remove heat gains. However to achieve such high ventilation rates through naturally induced stack pressures, requires that the temperature of the air within the building is significantly greater than that externally. Thus to maintain such flow rates requires that the temperature elevation of the air within the building is considerable, creating uncomfortable internal conditions for the buildings

occupants. This has led some designers to fit solar shading blinds at the roof section of atria in the hope that the heating of the air at the top of the atrium, via solar gains to the blinds, will induce greater stack pressures. The effectiveness of this approach however is limited as the height over which the temperature elevation occurs is relatively small and thus the effect on the induced stack pressure is minimal.

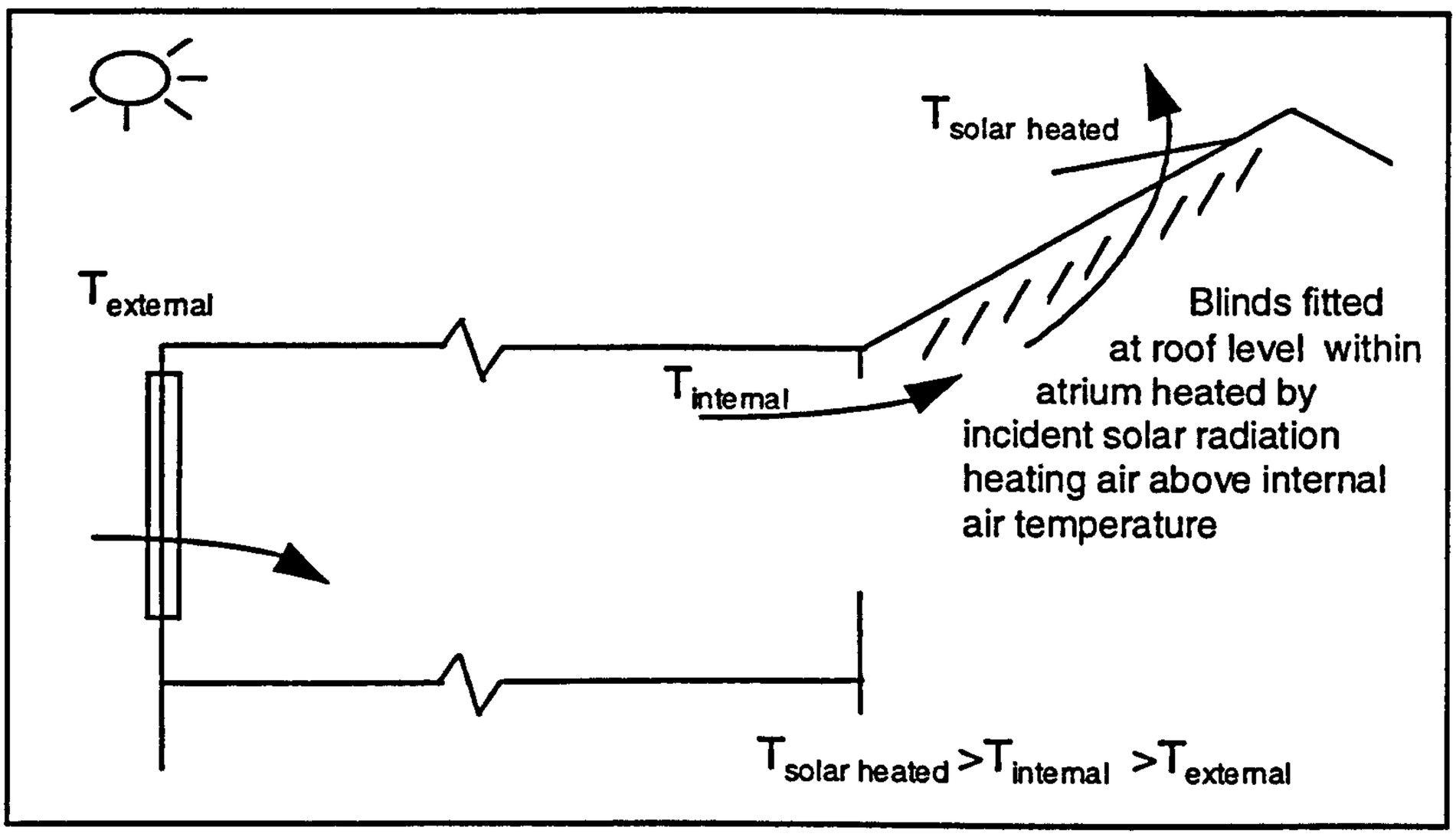

Figure 1.5. The use of solar shading intended to help induce air flows by heating the exhaust air at roof level .

1.7.2 Extending the stack height outside the occupied space.

The use of chimneys to increase the height over which internally created stack pressure differences occur has been adopted in several buildings recently in the UK. The most notable of these is the Queens Building at DeMontfort University[37]. In this building the chimneys are designed to enhance the stack pressures created in large internal spaces. Chimney heights of 13.3m, serve large internal spaces which allow significant stratification to build up without impairing the comfort of the occupants.

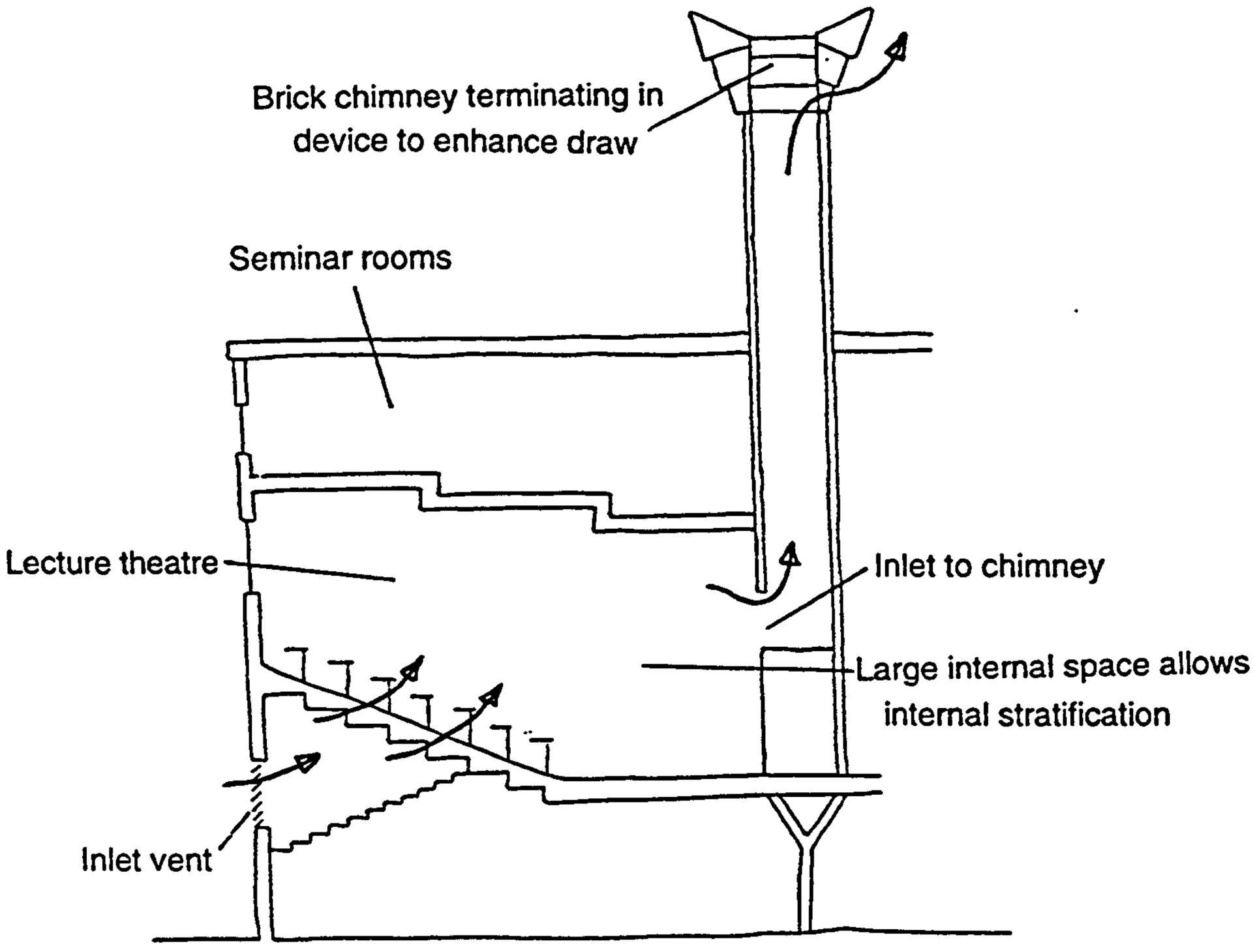

Figure 1.6. Ventilation of Queens Building, Demontfort University

In buildings with smaller floor to floor heights the potential of achieving such levels of stratification internally is rarely possible without impairing occupant comfort thus alternative methods have been sought.

A very effective method of overcoming this problem is the heating of the exhaust air after it has left the occupied zone of a building, then allowing this air to rise up a chimney drawing in fresh air through the occupied zone. This technique was adopted in the 1800's as detailed by Billington[1]. One of the largest examples of such a ventilation system in the UK. was the prison at Pentonville designed by Sir. J. Jebb[38]. Small fires were lit at the base of the chimneys in summer to raise the temperature of the exhaust air well above that of the outside air. In this way air was drawn in at basement level and through the cells of the three storey building throughout the summer, regardless of the ambient temperature. Jebb[2] noted that the fire was needed because wind forces alone could not be relied upon to produce the necessary circulation.

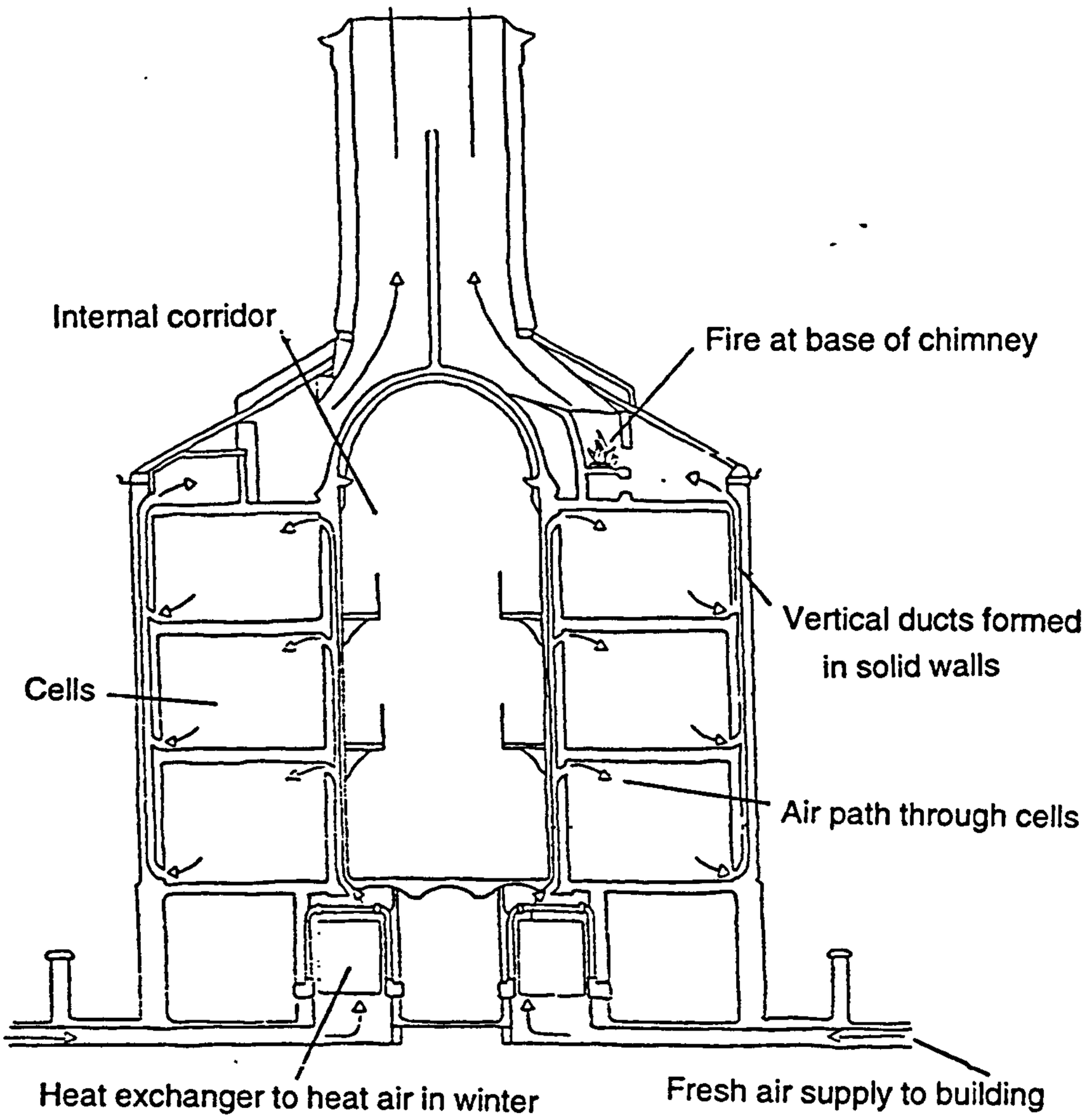

Figure 1.7. Ventilation of Pentonville Prison[38]

The use of fires or independent heating systems to enhance the stack temperature is not justified today, however the coincidence of the highest solar gains with periods of greatest potential overheating does raise the possibility of using solar energy to increase the temperature of the stack after it has left the occupied zone. A term used to describe such building components by Baker[36] is 'solar chimney'.

This approach has been adopted in warm climates where it was noted by Bansal[39] that internal / external temperature differences in summer were too small to have any practical natural ventilation application. Thus some form of heating had to be adopted to enhance the stack induced pressure differences. Bouchair[40] proposed a similar application in very hot dry climates where ventilation during the day is undesirable, due to extreme ambient temperatures. A thermally heavy chimney constructed on the south west facade of domestic buildings is heated during the day while the vents at the top

and bottom of the chimney are kept closed. At night the vents are opened and the heat stored in the chimney structure heats the exhaust air to a temperature greater than ambient. Thus air is drawn through the building throughout the night.

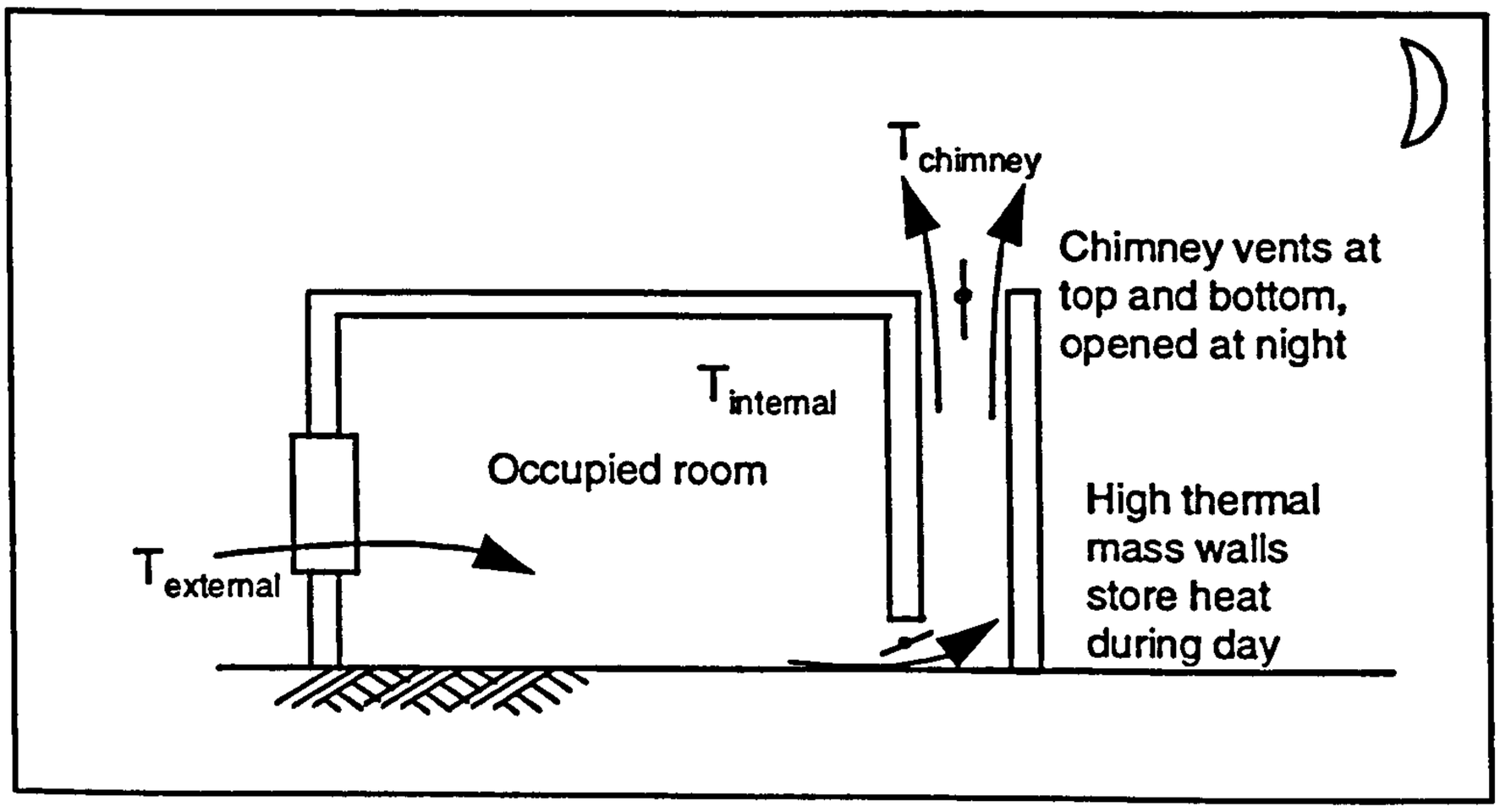

Figure 1.8. High thermal mass solar chimney proposed by Bouchair.

In N Europe where external temperatures are generally below those within occupied spaces, the need is for daytime removal of heat gains. The use of solar energy to enhance the stack pressure in chimneys has to date been limited, with one of the few examples being in Germany. Raatschen[41] describes a double facade consisting of vertical air shafts where temperatures are enhanced in summer by solar gains. In the UK, in some situations, impractical solutions have been adopted where solar panels have been introduced onto a chimney. For example at Wood Green Community Mental Health Centre Bellow[42] it was reported that the ventilation was induced by a set of chimneys which terminate in 1.0m high solar panels referred to as 'solar accelerators'. As with the use of blinds at the top of atrium, the fitting of a heater at the top of a chimney has a minimal effect to the overall stack pressure due to the small height over which the temperature elevation occurs. This inappropriate use of the potential of a solar chimney was noted by Baker[43] who commented that such designs would probably be ineffective due to the inadequate height of the column of heated air.

One recently designed building that did offer a great potential to evaluate the effectiveness of solar chimneys was the new energy efficient office at BRE at Garston[44]. Early design drawings, Figure 1.9. illustrate clearly how the fully glazed chimneys were intended to operate. The expamet, heated by the sun,

would induce a flow of air up the chimney. In conversation with the design engineers[45] however it was commented that actual quantification of the effectiveness of the solar aspect of the chimney had not been undertaken and that it was considered to be marginal. The final design of the chimneys reflects this feeling with only one side of the chimneys being of glass blocks and the others of opaque materials and inclusion of paddle fans to induce air movement if wind and stack induced rates are insufficient. An article[46] promoting the passive features of this building stated that with respect to summer ventilation 'because the stacks are faced with glass blocks, solar heating should stimulate this ventilation'. Thus confirming largely that the solar aspect of the chimneys was not an over-riding feature of the ventilation strategy and any ventilation gains were largely considered as fortuitous.

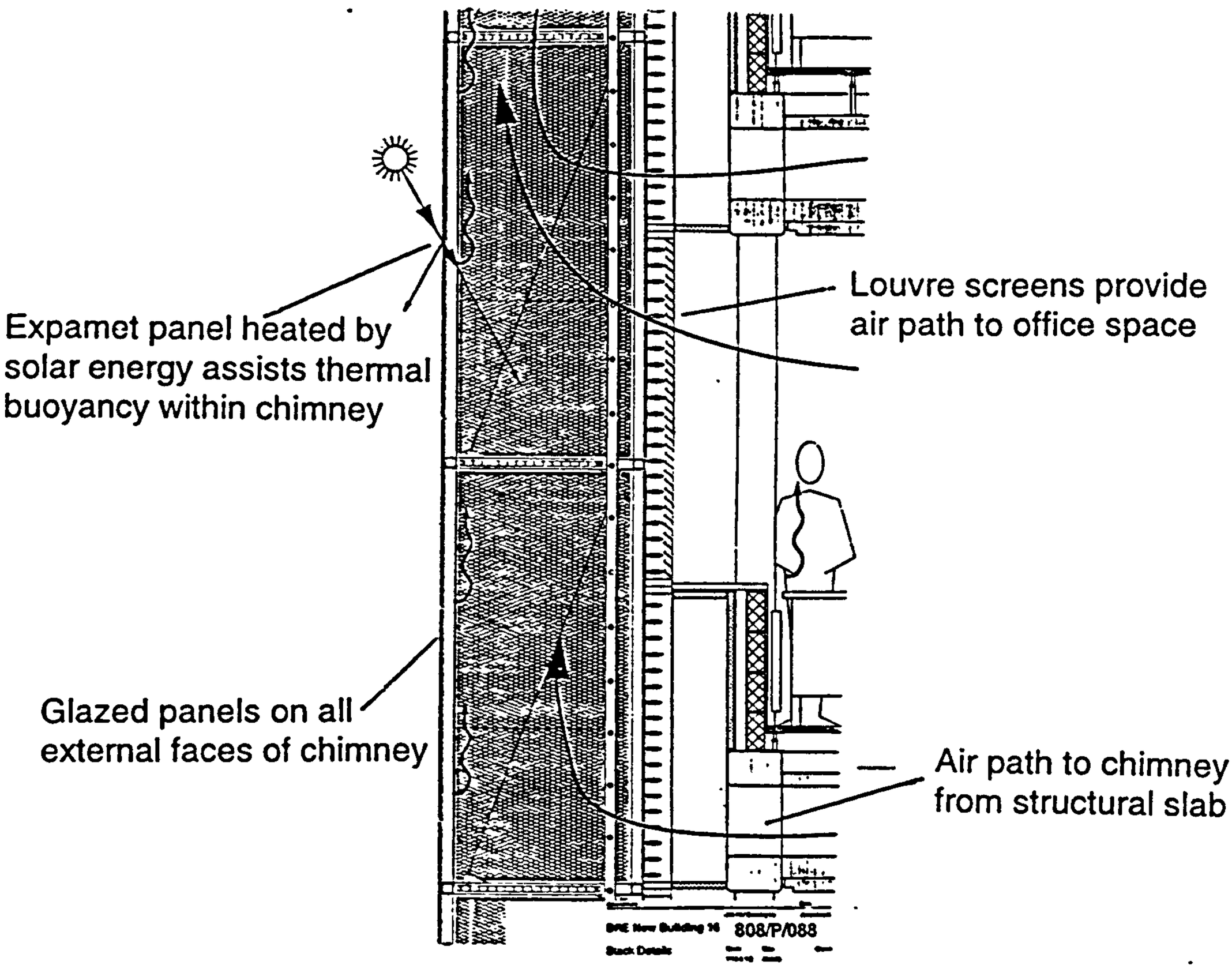

Figure 1.9. Early design ideas for the ventilation strategy of the BRE energy efficient office using solar assisted chimneys[47]

A preliminary study by Swainson[48] noted that simple air flow models often used to evaluate natural ventilation within buildings were not suitable for predicting the flows within a solar chimney or the effects of changes to physical parameters. This therefore raises the question of the ability of building designers to evaluate the potential ventilation drive of such chimneys which must be undertaken if they are to be designed to operate effectively.

1.8 Conclusion and proposal

The move to adopt air conditioning within larger buildings has implications for both the ambient environment and the comfort, and thus productivity, of the building occupants. With north European vernacular architecture not providing proven solutions to effectively ventilate large buildings for removal of heat gains, attempts have been made by building designers to provide this through a range of passive means. However some solutions are only applicable to specific types of building, for example high levels of internal stratification require large floor to ceiling heights which may not be appropriate for office type buildings. In other cases components appear to have been used inappropriately or designs modified to largely remove passive solar features. In these later cases questions are therefore raised about the potential of available evaluation methods to allow investigation of the effectiveness of designs and the effects of changes to key physical parameters.

The aim of this project is therefore to investigate if the potential of a solar chimney to operate as a natural ventilation driver can be evaluated by existing methods and if not to provide such a solution.

The proposed objectives that will allow this aim to be realised are:

Review all existing methods appropriate to the prediction of the driving potential of a solar chimney.

Review all work in areas associated with naturally induced channel flows to assess if any existing models or data sets could be used to describe the operation of a solar chimney.

If suitable data sets do not exist that can be used to test models of a chimney, then an experimental investigation must be undertaken to obtain such data.

Test the existing methods and models against an appropriate data set of chimney operation.

If the review indicates that non of the available calculation methods are suitable for the needs of building designers then undertake to provide such a solution.

1.9 References Chapter One

1. Billington, N. and Roberts, B., Building Services Engineering: A Review of its Development, Pergamon Press Ltd., Oxford, UK, 1Ed., 1982.

2. Dale, K., Within these walls, Building Services, 32 - 33, December, 1992.

3. Roaf, S., Ozone Loopholes. A Case Study of Air Conditioning in Britain, Proceedings 2nd. World Congress on Renewable Energy, Reading, September, 1992.

4. Spring, M., Working order, Building, Issue 24, 50 - 55, 14th. June, 1996.

5. EDSL, Comparison of Dynamic Simulation and the Admittance Procedure using CIBSE Section A8 Example Office, Environmental Design Solutions Ltd., Stony Stratford.

6. CIBSE, Internal Heat Gains, CIBSE Guide, A7, CIBSE, 1986.

7. CIBSE, CIBSE Application Manual, Natural Ventilation in Buildings, Draft version, CIBSE, December, 1994.

8. Hastings, S., Myths in Passive Solar Design, Solar Energy, Vol. 55, No. 6, 445 - 451, 1995.

9. Parsloe, C., Overengineering in Building Services. An International Comparison of Design and Installation Methods, BSRIA TR21/95, BSRIA, 1995.

10. Pekka, M., Hannu, P. and Wilkins, D., Measurement of office buildings equipment loads, Proceedings 6th. International Conference on Indoor Air Quality and Climate, Helsinki, July, 1993.

11. Houghton, F. and Yagloglou, C., Determining lines of equal comfort, Trans. ASHVE, Vol. 21, 1923.

12. Fanger, P., Thermal Comfort, McGraw-Hill, 1970.

13. Griffiths, I., Field Studies of Thermal Comfort in Passive Solar Buildings, Proceedings 2nd. European Conference on Architecture, Paris, December, 1989.

14. Evans, B., Product Review, AJ Focus: HVAC, AJ, 43 - 55, September, 1995.

15. Humphreys, M., Thermal comfort requirements, climate and energy, Proceedings 2nd. World Congress on Renewable Energy, Reading, UK, September, 1992.

16. Willis, S., Keeping control of comfort, Building Services, 43, February, 1995.

17. Wilson, S. and Hedge, A., The office environment survey: a study of building sickness, Building Use Studies, May, 1987.

18. Leaman, A., A demand side perspective, BRE Seminar, Window design for natural ventilation - just hot air?, Garston, May, 1993.

19. Ellis, R., The British Office Market - The Workplace of Tomorrow; the consumers view, 1994.

20. EC., Natural and Low Energy Cooling in Buildings, European Commission Directorate - General XVII for Energy, May, 1994.

21. Berry, R., Department of Environment support for low - energy ventilation research in the UK, Natural Ventilation Group Forum, Proceedings CIBSE/ASHRAE Joint National Conference, Harrogate, UK, September, 1996.

22. Anon, Cutting energy use heads Blair agenda, Energy in Buildings & Industry, 2, September, 1997.

23. Wyatt, T., Better balanced buildings, HAC, 14 - 18, April, 1996.

24. Clements-Croome, T., Future horizons in building environmental engineering, Proceedings CIBSE/ASHRAE Joint National Conference, Harrogate, UK, September, 1996.

25. Raw, G., Roys, M. and Leaman, A., Further findings from the office environmental survey, Proceedings 5th. International Conference on Indoor Air Quality and Climate, Toronto, Canada, 1990.

26. Shearman, M., Revising ASHRAE 62 Ventilation Standard, A breath of fresh air: a new look at ventilation standards, CIBSE ASHRAE and natural ventilation groups seminar, BRE, Garston, 14th. March, 1996.

27. HMSO, The Building Regulations 1991, Various editions.

28. Maldonado, E. and de Oliveira Fernandes, E., Building thermal regulations: why has summer been forgotten?, Proceedings 3rd. European Conference on Architecture. Florence, Italy, May, 1993.

29. BRE, Building Research Establishment Assessment Method (BREEAM) for new offices, BRE, 1993.

30. Daniels, K., The Technology of Ecological Building, Birkäuser Verlag, Basel, 1995.

31. HMSO, Approved Document F, Means of ventilation, 1995 edition, HMSO, 1995.

32. Anon, BRF headquarters Copenhagen, Case Studies of Energy Efficient Non Domestic Buildings, Cambridge Architectural Research Limited, Cambridge, 1994.

33. Liddament, M., Aspects of natural ventilation in passively heated buildings, Proceedings 2nd. UK-ISES Conference, The Efficient Use of Energy in Buildings, Cranfield University, September, 1986.

34. Etheridge, D. and Sandberg, M., Building Ventilation, Theory and Measurement, J. Wiley & Sons., UK, 1996.

35. Jones, A., Private communication, Environmental Design Solutions Ltd., June, 1996.

36. Baker, N., Notes on the natural ventilation of atria, Proceedings I. Mech. E. Seminar, Atrium Engineering, 26 June, 1990.

37. Eppel, H. and Lomas, K., Simulating the thermal performance of naturally ventilated spaces: A case study, Proceedings PLEA Conference, Spain, 1991.

38. Surveyor-General of Prisons, Construction, Ventilation and Details of Pentonville Prison, 1844, Contained in; British Parliament Papers, Crime and Punishment in Prisons II, Conditions and Discipline in Prisons, 1823 - 1845.

39. Bansal, N., Mathur, R. and Bhandari, M., Solar chimney for enhanced stack ventilation, Building and Environment, Vol. 28, No. 3, 373 - 377, 1993.

40. Bouchair, A., Solar induced ventilation in the Algerian and similar climates, PhD. Thesis, University of Leeds, 1989.

41. Raatschen, W., Energy and ventilation performance of double facade office buildings, Proceedings BEP '94 Conference, York, April, 1994.

42. Anon, Care in the community, AJ, 25 - 34, 8th. December, 1994.

43. Baker, N., Energy and Environment in Non-Domestic Buildings, Cambridge Architectural Research Ltd., Cambridge.

44. Gethings, B., Private communications, June, 1995.

45. Thomas, R., Private communications, May, 1995.

46. Anon, Actively promoting passive architecture, Building Services & Environmental Engineer, 18, June, 1997.

47. Fielden Clegg Design, BRE New building 16, Drawing No. 808/P/088, Fielden Clegg Design, Bath, 1995.

48. Swainson, M., Investigation into the Potential of Thermosyphoning Air Panels to Drive Natural Ventilation in Buildings, MSc. Thesis, Cranfield University, 1994.

CHAPTER TWO

METHODS OF PREDICTING NATURAL VENTILATION FLOWS FOR BUILDING DESIGNERS, A REVIEW OF CURRENT METHODS AND WORK IN THE AREA

2.1 Introduction

Chapter one raised the question of the effectiveness of current design tools to fully describe the flow through a building component such as a solar chimney. The existing models have been reviewed and their appropriateness for application to such building components discussed.

Extensive work has been undertaken in the area of natural convective flows over flat plates and within channels, this is reviewed to assess if any simple models have been developed that can be applied to a solar chimney.

In light of the findings of the review, the methods of achieving the objectives of this project are set out.

2.2 Presently available methods of predicting naturally induced ventilation within buildings

There are broadly three different types of mathematical models used to evaluate the ventilation of buildings by natural driving forces. These are:

- Fully empirical. This method relies upon simple mathematical correlation equations developed from regression analysis of experimental data. Such models are often referred to as infiltration models.

- Semi empirical. These models are based on solving the steady state continuity equation of mass balance, equation 2.1. However they also rely upon experimentally derived empirical data to describe the flow characteristics of the openings in the building envelope and internal partitions. These models are known as zonal models.

$$\rho_{external} \sum_{i} Q_i + \rho_{internal} \sum_{j} Q_j = 0 \qquad \text{Equation 2.1.}$$

- Solution of the fundamental equations describing fluid flow. This method of modelling numerically solves the fundamental mathematical equations that describe the fluid flow and is know as computational fluid dynamics (CFD).

One general assumption that is common to all of the mathematical models described is that the naturally occurring driving pressures are considered to be steady, i.e. that the induced flow is in a steady state. This assumption can lead to significant errors in the prediction of wind induced flows, as the turbulence of the wind is such that a steady driving force is never experienced. Etheridge et al[1] assessed the errors induced by such an assumption to be up to 20%. For temperature induced flows however, the change in driving forces, due to changes in temperature difference between internal and external air masses, is relatively slow and therefore the assumption of a steady state is not unrealistic.

2.2.1 Fully empirical models

Etheridge et al[2] reported that the earliest models of this type were developed in 1940. These models were based on experimentally measured data of ventilation rates induced for a given combination of meteorological variables or for a pre-described pressurisation level of the building. The aim was therefore to assess the background ventilation or leakage of the whole building envelope. Such models are very limited in application as the generality of the leakage between even buildings of the same type in different locations is low due to variations in construction quality and local microclimate. These models are therefore not designed to allow the effects of variations in the physical parameters of a single component on the ventilation rate to be assessed. Fully empirical models therefore offer no assistance to building designers for the design of specific building components such as solar chimneys.

2.2.2 Semi empirical models

These are split into two categories based on how the internal spaces of a building are treated.

- Single zonal models:

Which assume that the internal mass of air is fully mixed and not divided i.e. there is no flow resistance to air passage between any side of the building envelope. Such an assumption is appropriate for small single room buildings, however this type of model is often used for domestic type buildings[2]. In such cases the presence of several internal rooms restricts the full internal homogeneity of the air mass and thus makes the assumption of a single fully mixed zone incorrect. The mass balance equation 2.1. is resolved across the building envelope between the ambient and the internal zone.

- Multi zonal models:

Consider that the internal space of the building is divided into a series of zones and the air movement between these zones is via defined flow resistances. Within each zone the air is assumed to be fully mixed. The models achieve an airflow solution by resolving the mass balance defined by equation 2.1. between all linked zones and across the building envelope.

Zonal models can be used to predict air flows within a building before it has been constructed and also to assess the influence of different physical variables on the induced ventilation rate. Therefore the potential exists for a building designer to use a zonal model for the investigation of the effects of a solar chimney on whole building ventilation.

The potential application of such models to a solar chimney type building component is now investigated.

Data requirements

As with any mathematical model of a physical process the data used in the calculations will determine the accuracy of the final answer and thus the ability of the model to predict performance over a range of situations reliably.

The data required by a zonal model is;

- distribution of openings
- flow characteristics of openings
- temperature distribution of the air within the zones

Distribution of openings

To calculate the induced flow rates between zones and through the building envelope, the relative height of the openings through which the air can flow must be defined. Consideration of equation 2.2. indicates that the induced stack pressure is directly related to the height over which the temperature difference of the two air masses occurs.

$$\Delta P = P_{external} - P_{internal} - \rho_0 \, g \, h \, 273 \left(\frac{1}{T_{external}} - \frac{1}{T_{internal}} \right)$$

Equation 2.2.

For purpose built ventilation components defining such heights is relatively simple and evaluation of the influence of variations in the height can be undertaken to assess ventilation sensitivity to this variable.

Flow characteristics of openings and ventilation routes

The air flow through a purpose provided opening is dependant upon the open area and the geometry of the orifice. For most purpose provided openings the area is relatively easy to define, but the geometry, and thus the influence the opening will have on the air flow, is much more complex. To obtain accurate data on the flow rate induced by a given pressure differential across an orifice, experimental investigation is required.

In the absence of detailed experimental data, assumptions about the orifice geometry must be made.

Some models, both single and multi zonal, assume that all openings designed for ventilation, can be defined by the common orifice equation, equation 2.3.

$$Q = Cd \, A \sqrt{\left(\frac{2 \, \Delta P_{inlet}}{\rho} \right)}$$

Equation 2.3.

Where Cd is the discharge coefficient

Liddament[3] notes that the flow through large openings is usually turbulent and thus the common orifice equation is appropriate. Etheridge et al[2] confirms this by stating that for sharp edged orifices, where the height of the opening is significantly greater than the length, and the Reynolds number (Re), defined by equation 2.4., is sufficiently high (>>100), then the value of Cd is constant at a value of 0.61.

$$Re = \frac{u\, d_h}{v} \qquad \text{Equation 2.4.}$$

This value is used in the simple single zonal model proposed by CIBSE[4] and a value of 0.62 is proposed for use in the dynamic thermal modelling software TAS[5]. Both of these models use the common orifice equation to describe all of the purpose provided openings. Thus the level of user input is reduced to inputting the area of the opening.

With models such as ESP[6] and COMIS[7] each opening can be defined through a range of different flow component equations. Clarke et al[6] reports that ESP has 21 flow component equations available that require from 1 to 17 parameters to be input by the user. Such high levels of complexity may be appropriate for the research environment but designers require simple and reliable tools where sensitivity to input parameters can be easily assessed.

Some models allow flow through purpose provided ducts or chimneys to be modelled. This requires details of the physical variables and factors such as the friction factor. Such factors are related to surface roughness and have an effect on the flow of air related to the air velocity. Thus if such components are to be included in a flow model then a high level of detail is required in order to obtain realistic results.

Overall therefore the potential of a zonal model to predict flows through openings is influenced by the level of detail known about them. If this is low, but they can be considered as sharp edged orifices, then the use of equation 2.3. is in many cases appropriate and in some models limited to this form only.

Temperature distribution of the air within the building

As stated previously a zonal model assumes that the air within any zone is fully mixed, i.e. the temperature is uniform in all directions.

Within small rooms of a building this may be the case, but in situations where internal stratification occurs this assumption may lead to significant errors in the predicted stack pressure due to incorrect definition of the height over which a temperate difference exists.

To overcome this in large spaces Liddament[3] proposes the use of equation 2.5. where the linear temperature gradient can be input as required.

$$P_h = P_{h=0} - g\,\rho_0\,273\left[\frac{1}{\omega}\ln(\omega\,h + T_{h=0})\right]_{h=0}^{h=h} \qquad \text{Equation 2.5.}$$

Where ω is the temperature gradient (K/m)

Other models such as COMIS[7] allow a room to be split into any number of horizontal zones. In this way a level of stratification that is not pre-defined can be input by the model user and its effect assessed.

One of the major drawbacks with zonal models until recently has been that the temperature of the air within each of the spaces was required as an input before the model could be run. Investigations into the interaction of a buildings structure with the ventilation were therefore limited and required manual iterations between zonal and thermal models. To overcome this problem many examples of linked zonal and dynamic thermal models now exist[5][6] where the stack induced flow is calculated based on the result of the overall thermal model energy balance. Iterations between the models are then undertaken until convergence is achieved at each time step in terms of both fabric temperature and mass flow in each zone.

Zonal models can be used to effectively model ventilation rates within spaces when the air is fully mixed or when stratification occurs. Thus for whole building applications such models offer a valuable tool to test the sensitivity of ventilation to variations in physical variables at the design stage. Validation data for models has been made available[8] and their application is the area of investigation of a significant recent international research project[9].

Application of a zonal model to a building component such as a solar chimney however requires that the type of flow occurring within such components is adequately modelled by the assumptions made in the zonal model. The solar

heating of a solar chimney creates a natural convective boundary layer along the internal surface of the plate. The temperature variation of the air within the chimney is therefore constant in neither the vertical or the horizontal direction. The assumption therefore of a horizontally homogeneous mass of air is a significant simplification, the influence of which cannot be assessed through the use of a zonal model.

The method of calculation of flow rate for a zonal model must be considered to assess its applicability to a boundary layer type flow.

Figure 2.1. shows the basic layout of a single zone. For simplicity the inlet is considered to be significantly smaller that the outlet. In this way the effect of varying one orifice can be investigated.

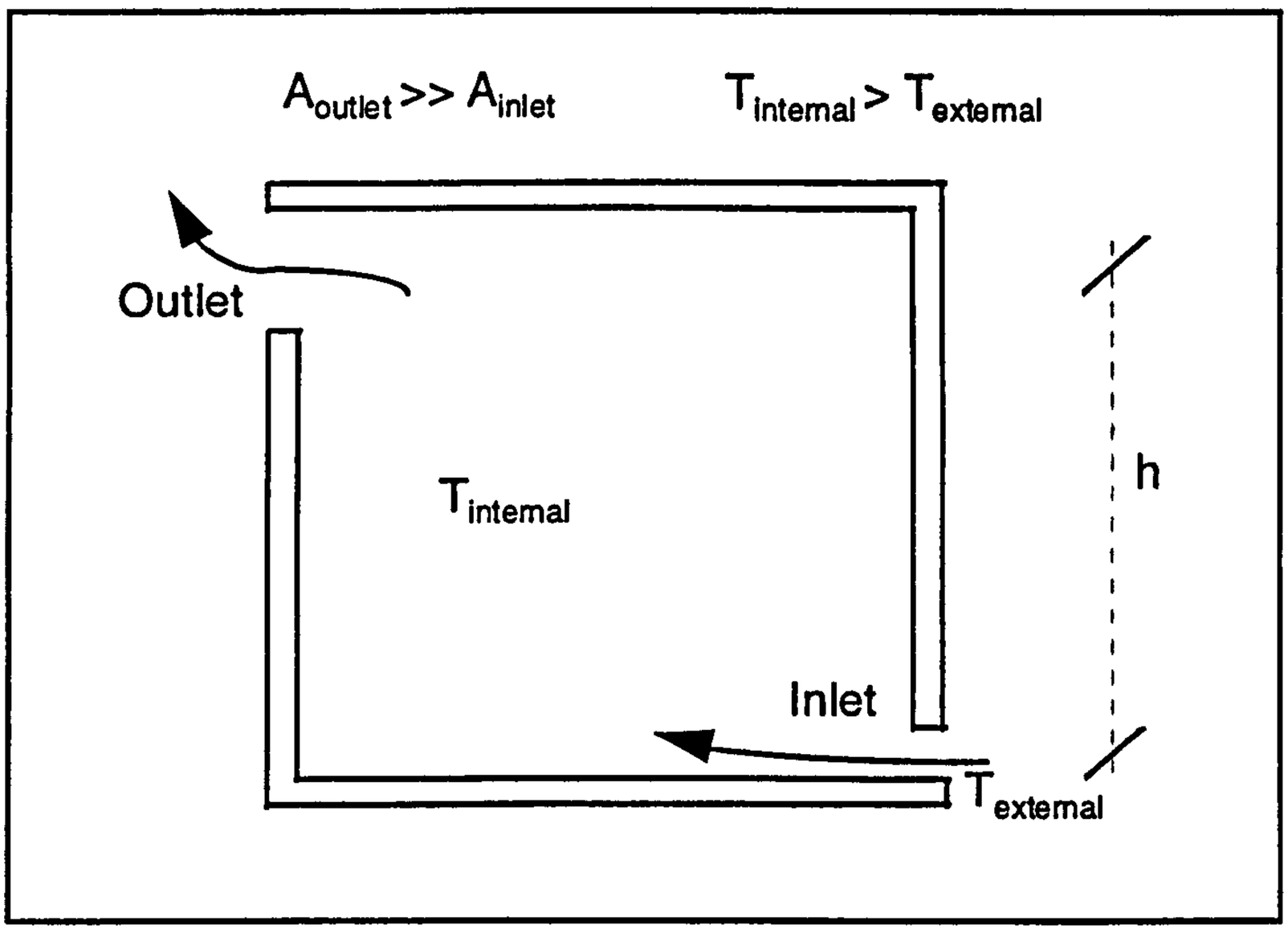

Figure 2.1. Layout of a single zonal model to assess the effect of inlet opening on the mass flow rate.

In the simplest zonal model a constant internal temperature is set and the influence of the inlet size on the mass flow rate can be determined.

CIBSE Guide A4[4] gives equation 2.6. for the calculation of the mass flow rate created by constant internal and external temperature differences.

$$\dot{m} = \rho \ Cd \ A \left(\frac{2 \ \Delta T \ h \ g}{T_{mean} - 273} \right)^{0.5}$$ Equation 2.6.

Where $\Delta T = (T_{internal} - T_{external})$ Equation 2.7.

$$T_{mean} = \left(\frac{T_{external} + T_{internal}}{2} \right)$$ Equation 2.8.

From equation 2.6. it is apparent that the area of the inlet and the mass flow rate are related linearly. Thus any changes in inlet area will have a corresponding effect on the mass flow rate predicted.

A more appropriate model is to assume that a space has a constant internal heat gain. In such cases the zonal model approach assumes that the heat from the source is fully mixed within the space. The temperature of the air is then calculated through the following energy balance:

Energy gain within room = energy removed from room by air

i.e. $q'' = \dot{m} \ Cp \ \Delta T$ Equation 2.9.

$$\dot{m} = \rho \ Cd \ A \left(\frac{2 \ \Delta P_{inlet}}{\rho} \right)^{0.5}$$ Equation 2.10.

$$P_s = \rho_0 \ g \ h \ 273 \left(\frac{1}{T_{external}} - \frac{1}{T_{internal}} \right)$$ Equation 2.11.

In steady state it can be assumed that for the configuration presented in figure 2.1. the stack pressure created is equal to the pressure difference acting across the inlet.

i.e. $\Delta P_{inlet} = P_s$ Equation 2.12.

Equations 2.9. to 2.12. can be solved iteratively for any level of q'' and inlet area. From these equations it is evident that increasing the inlet area will always increase the mass flow rate.

If however a boundary layer flow is considered, created by a temperature difference between a heated wall and a mass of air, the resulting velocity profile for such a flow can be defined by equation 2.13. proposed by Eckert at al[10].

$$u = C\left(\frac{h}{b}\right)^{\frac{1}{7}}\left(1 - \frac{h}{b}\right)^{4} \qquad \text{Equation 2.13.}$$

$$\text{Where } C = 1.185\left(\frac{\nu}{h}\right) Gr_h^{\frac{1}{2}}\left(1 + 0.494\,(Pr)^{\frac{2}{3}}\right)^{-\frac{1}{2}} \qquad \text{Equation 2.14.}$$

$$\text{and} \quad b = 0.565\,(Gr_h)^{-\frac{1}{10}}\,Pr^{-\frac{8}{15}}\left(1 + 0.494\,(Pr)^{\frac{2}{3}}\right)^{-\frac{1}{10}} h \qquad \text{Equation 2.15.}$$

$$\text{Where } Gr_h = \frac{g\,\beta\,\Delta T\,h^3}{\nu^2} \qquad \text{Equation 2.16.}$$

$$Pr = \frac{\nu}{\alpha} \qquad \text{Equation 2.17.}$$

For an air mass of 20°C Bouchair et al[11] integrated across the boundary layer and proposed equation 2.18. for the calculation of the mass flow rate within a turbulent naturally convective boundary layer.

$$\dot{m} = 0.15\,\rho\ b\ w\,C \qquad \text{Equation 2.18.}$$

Equation 2.18. predicts the mass flow rate that occurs in a natural boundary layer. Considering this with respect to a zonal model highlights the fundamental difference in the two types of air flow. Air flow rates predicted by a zonal model always continue to increase with increasing size of the inlet orifice. In contrast the flow induced by a boundary layer has a natural maximum flow rate, above which it will not increase regardless of increases in inlet orifice area.

From this discussion it is evident that the assumption of fully mixed air masses for zonal models when predicting air flows is highly appropriate. However for a boundary layer flow induced by natural convection, the assumption of a fully mixed air mass is incorrect and the result of this on the induced mass flow rate and the influence of variations of key physical variables is largely unquantified.

Swainson[12] noted considerable differences when a zonal model was used to predict mass flow rate through a solar chimney. Awbi[13] compared the results of a zonal model and CFD model predictions and obtained differences of between 4 and 21%. These, it was claimed, were due to the inability of the zonal model to take account of the true flow configurations and because turbulence was predicted more accurately by the CFD model.

Thus if zonal models are to be used for the prediction of natural convection flows within boundary layers then it is important that the different characteristics of such flows are incorporated into the model.

2.2.3 Computational Fluid Dynamics

The numerical simulation of the thermofluid processes involves the solution of a set of coupled, non linear, second order partial differential equations. These differential equations express the 'conservation laws' for mass, momentum and thermal energy. In addition to these equations, if the flow is turbulent, a model describing the effects of turbulence upon the flow must also be solved.

The numerical solution of these equations requires some discretisation of the flow domain into a set of non-overlapping cells, forming a computational grid. The differential equations may then be integrated over each cell of the domain which leads to a set of algebraic equations. These algebraic equations are then solved in a finite volume model iteratively. The iterative solution continues until the imbalance in the equations is sufficiently small to be considered negligible. This is known as convergence.

This process was developed largely by the aerospace industry[14] to assist in the design of aircraft. Until recently CFD models were limited in other applications to academic and R&D organisations, mainly because of their level of complexity and lack of a user friendly interface. However improvements in computer hardware and the development of graphical user interfaces has opened up CFD to building applications. In this area it is now used for investigating air movement within buildings, for the evaluation of thermal comfort and the assessment of pressure distributions on building facades due to wind.

CFD is capable of modelling the air flows induced by natural convection and predicting the effects of changes in the physical variables. Thus for application

to a building component such as a solar chimney, CFD offers advantages over zonal models for such flow situations. However although CFD is a very powerful tool, it does suffer from limitations which are now considered:

- As previously mentioned a sophisticated level of user knowledge is required to obtain meaningful predictions from CFD programmes. The sensitivity of the final predictions to variations in input variables, particularly the air properties at the inlet and boundary conditions, is very high and requires a high level of engineering judgement if realistic predictions are to be obtained.

- The time involved in setting up a model of a flow domain and then running the software to a converged solution is significant. Small flow domains may require several hours but full three dimensional domains of large spaces often require several days to achieve a converged solution. Additionally the level of convergence for natural convective flows is not high[2] and so considerable user judgement is required to determine when convergence has been achieved.

- The grid developed for the flow domain and the mathematical methods utilised for the solving of the defining equations all influence the resulting predictions[15] . Such influences require evaluation for each flow configuration modelled. Therefore a significant level of model testing and validation is required prior to the full modelling being undertaken.

- The question of turbulence modelling with CFD codes is an area of intense research[2] with Schetz[16] noting that this was still an unresolved problem of classical physics. To allow CFD models to predict the flow when turbulence exists, mathematical turbulence models have been developed. Holmes et al[17] noted that the most widely used turbulence model, the k-epsilon ($k\,\varepsilon$) model, is semi empirically based on data for fully turbulent forced convective flows. Thus its application requires the use of a number of experimentally determined constants, which may not be appropriate for all flow conditions and in particular naturally driven convection air flows.

Considering the range of limitations described, Holmes et al[17] and Awbi[18] both suggest that CFD predictions of flow should always be checked against those of experimental investigations of similar flow configuration. In this way

the validity of the predictions can be checked before further parametric testing is undertaken using CFD programmes.

It is of interest to note how the aerospace industry views CFD modelling; Bussoletti[14] reported that when engineers were questioned as to their requirements of CFD, the most important area was that of accuracy of agreement with test data with respect to trends. To evaluate this up to five or more examples of validation were sighted as being required to provide confidence in the validated results and to justify the use of CFD as a design tool that could be relied upon. The identification of the need for agreement with the trend of test data highlights how CFD is used in this industry, with absolute agreement between results seen as of lower importance.

Work has been undertaken on the production of standard natural convection flow configurations that can be used to validate CFD predictions[19][20]. However many are highly simplified, usually being limited to flows on flat plates or within boxes. Data for the validation of model predictions of flows in a solar chimney type configuration do not exist. Thus the ability of a CFD programme to accurately predict the trends in operation due to variations in physical variables requires investigation before it is used for parametric studies.

Borth et al[21] noted that although CFD is becoming more widely available, there were few published examples where CFD had been used on a commercial basis by design engineers. This is put down to the level of user understanding required to obtain results and the lack of good data for validation of simulation results.

Overall therefore CFD offers the opportunity to investigate the flows occurring in a solar chimney, however significant work must be undertaken to validate model predictions before it can be used with a high level of confidence.

2.2.4 Conclusion of the presently available models

The use of full empirical models of building ventilation requires experimental results on which to base the equations and thus for new building components this approach is not appropriate.

Zonal models make significant assumptions about the homogeneity of the air mass within zones. This is appropriate for rooms within a building where full

mixing may largely be achieved, however for building components such as a solar chimney where air movement is due to natural convection and limited by the development of a boundary layer, the effects of this simplification are as yet unquantified. Thus the applicability of zonal models to such flow configurations requires investigation.

CFD offers the opportunity to address all of the simplifications of the Zonal model approach to modelling, however significant model validation is required prior to its use for parametric testing. In a design situation such a requirement in both computer time and operator hours may reduce the opportunities available to undertake such investigations.

Overall, none of the available modelling methods offered an appropriate means by which a designer could evaluate confidently the potential of a solar chimney to drive natural ventilation. The flow induced by a heated plate was therefore investigated to assess if any work in associated areas could be used to describe the operation of a solar chimney.

2.3 Review of work appropriate to a solar chimney

The basic solar chimney configuration is shown in figure 2.2.

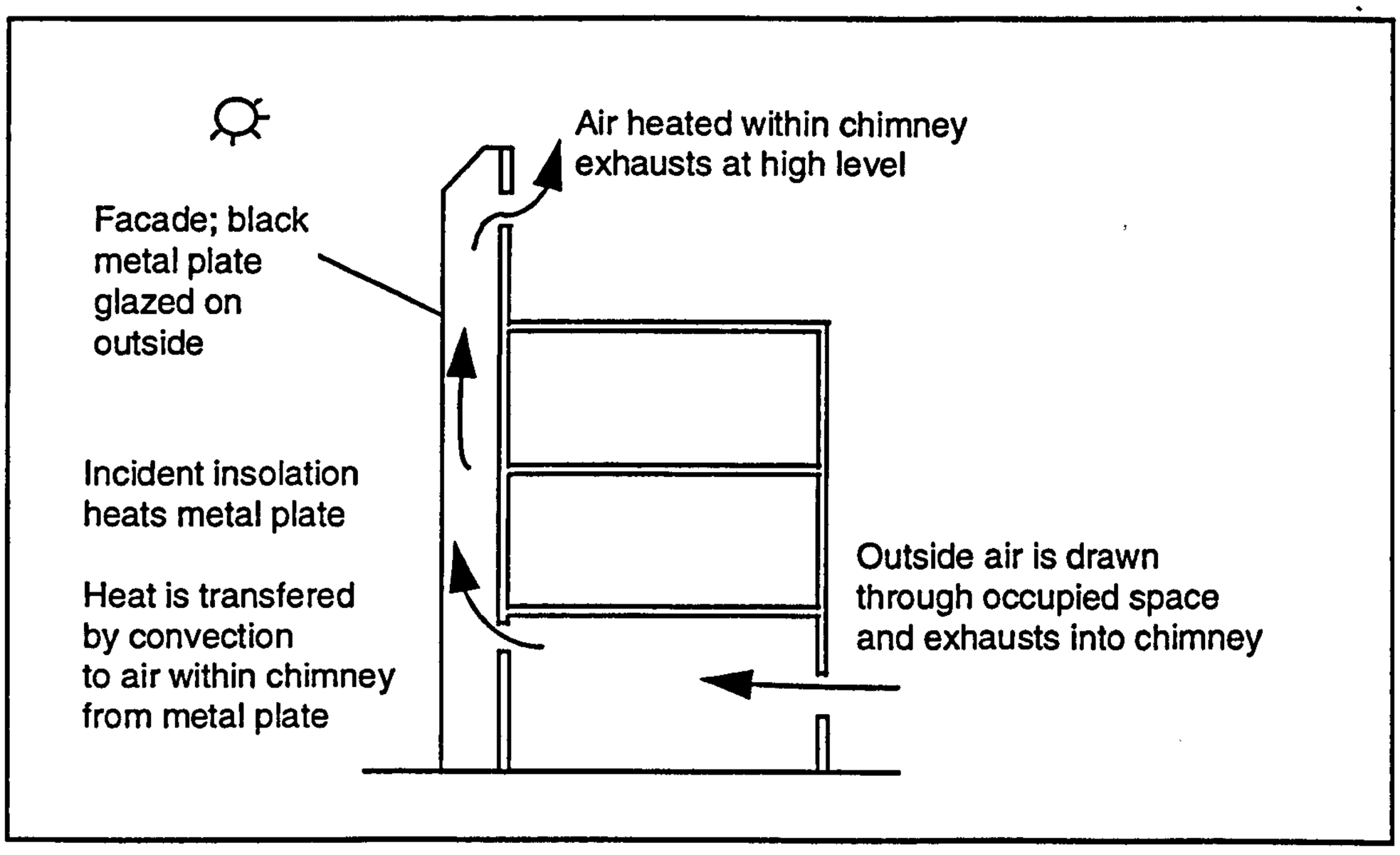

Figure 2.2. Basic layout of a solar chimney[22]

From figure 2.2. it can be seen that the driving force within a solar chimney is the natural convective heat transfer from the plate of the chimney. It is from this point that the evaluation of appropriate methods of describing the operation of such a building component is undertaken.

2.3.1 Air flows induced by a heated flat plate

The main area of interest for natural convection from a vertical flat plate has been the quantification of the heat transfer coefficient[23] and determination of the transition to, and nature of, turbulent flows.

The most usual form of the heat transfer coefficient related to the height, h, up a vertical flat plate, is expressed through the Nusselt number (Nu_h).

$$Nu_h = \frac{h_c\, h}{k} \qquad \text{Equation 2.19.}$$

And this is expressed in terms of the Grashof number (Gr_h)

$$Nu_h = c\, Gr_h^{\,a}\, Pr^b \qquad \text{Equation 2.20.}$$

Where a, b and c are constants governed by the flow regime

The transition to turbulent flow has significant influence upon the heat transfer coefficient and is dependant upon both height of the point of interest up the plate and upon the temperature difference between the plate and the air.

The Grashof number is used to define the onset of turbulence with a number of $Gr_h > 1.5*10^9$ being recommended by Etheridge et al[2] as signifying this transition.

Churchill et al[24] produced correlations describing the heat transfer coefficient across the whole flow regime from laminar to turbulent and thus could be used for any value of Gr_h. These equations are now widely quoted[25][26] for convective heat transfer from flat plates.

The determination of the mass flow rate created due to the temperature difference between a vertical flat plate and the adjacent air has received

significantly less attention. Bouchair[11] used the equations describing the boundary layer developed by Eckert[10] to produce equation 2.18. Etheridge et al[2] state that the equations produced by Eckert are adequate for calculation to within 20% however the solution was not general. Etheridge et al[2] proposed a solution for air with a temperature of approximately 20°C, as:

$$\dot{m} = 0.00275\,\Delta T^{0.4}\ h^{1.2}\,\rho \qquad \text{Equation 2.21.}$$

Comparison of the predictions derived from equations 2.18. and 2.21. for a vertical flat plate with temperature differences of up to 20°C and heights up to 10m, showed the predictions to be within 12%. Both of these equations are however adequate for flat plates in unrestricted air masses that allow the boundary layer to grow up the full height of the plate. For a boundary layer flow within a channel, all of the air that is drawn into the boundary layer must be drawn up through the channel. Thus there is a fundamental difference in the nature of a flow induced by a flat plate and that occurring in a channel.

2.3.2 Natural convective flows within channels

The interest in natural convection within channels has been led by the vast array of applications that rely upon such flows, such as; cooling of electronic components, cooling fins on machinery and the heating of buildings by passive solar means.

Webb et al[27] report that the pioneering experimental work in this area was undertaken in 1942, however follow up work was not undertaken until the 1960's and 70's. Although much of the work is concerned with small flows in the laminar regime it is of interest to consider the flow phenomena that have been encountered with such flow configurations.

Miyatake et al[28] investigated both numerically and experimentally a range of flows in an asymmetrically heated channel. The results presented show clearly that for long channels the velocity profile became parabolic while for short channel lengths the flow remained close to that of a flat plate.

Miyatake et al[28] proposed an equation for the determination of the flow rate in which the flow assumed a parabolic velocity profile. No equations were given for flows within channels that had not reached a parabolic velocity profile and therefore the generality of the equations was significantly limited.

It was also noted that the effect of the unheated plate decreased as the depth of the channel increased. This led Miyatake to conclude that at some point the heated plate would act in the same manner as a single heated plate in a stationary mass of fluid. This, it was proposed, would happen when flow reversal occurred on the non heated side of the channel, however no such flow phenomena were reported in the experimental investigation

Webb et al[27] confirmed the thinking of Miyatake et al by noting that as the plate spacing of an asymmetrically heated channel was increased, the heat transfer rate approached that of a flat plate.

Anand et al[29] undertook a detailed numerical investigation of the effect of channel aspect ratio, the ratio of channel height to depth, on the convective heat transfer coefficient for laminar flow regimes.

The results presented show clearly that a marked peak in the heat transfer rate was achieved as the aspect ratio was altered. The results are shown in figure 2.3.

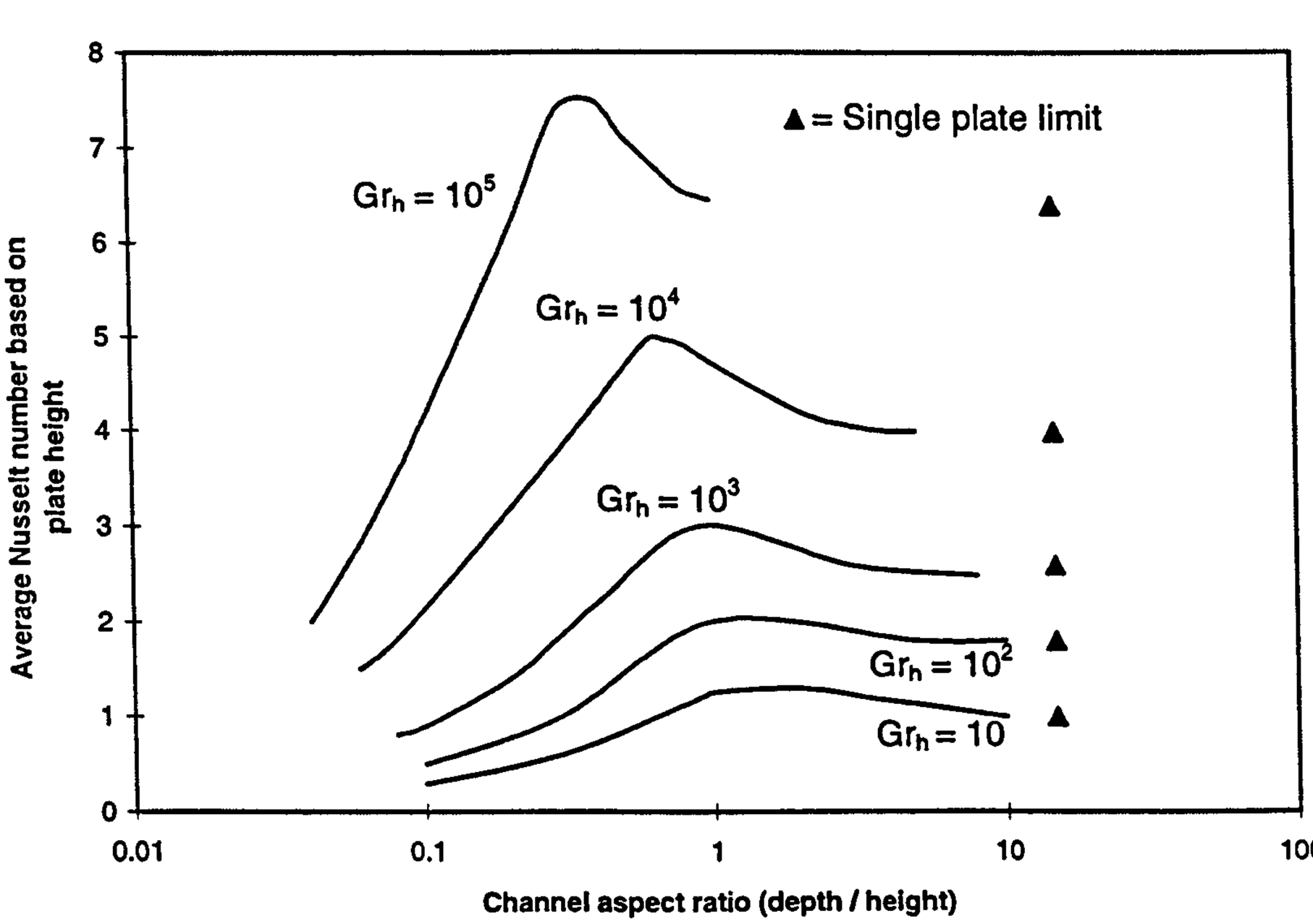

Figure 2.3. Results of Anand et al[29] showing the effect of channel aspect ratio on average Nusselt number

Anand et al[29] put the increase in the heat transfer coefficient above that of a flat plate down to the 'chimney effect'. However reasons for this effect were not put forward. Anand et al[29] also noted that as the Grashof number increased the effect of the unheated plate became more marked. Although the maximum Grashof number investigated was $1*10^5$, it was suggested that for higher values, the aspect ratio at which the maximum heat transfer coefficient occurs would be above that established for Grashof number of $1*10^5$.

At aspect ratios below the maximum where the channel depth decreases the heat transfer coefficient falls rapidly.

Sparrow et al[30] undertook a numerical and experimental investigation into the effect of plate spacing on natural convection within an asymmetrically heated channel with a uniform wall temperature. It was noted that many investigators presented their results of heat transfer coefficient in terms of the Nusselt and Grashof number based on the plate spacing. Sparrow et al[30] commented that presentation of the results in a variable that remains constant, such as the channel height was preferable as it allows the influence of channel aspect ratio on the resultant variables to be identified immediately.

In agreement with the findings of Anand et al[29], Sparrow et al[30] found that there were plate spacings that produced higher convective heat transfer coefficients than that of a flat plate. Thus confirming the presence of a 'chimney effect' which raised the coefficient up to 5% above that of a flat plate with the same Grashof number. At small plate spacings the coefficient fell off quickly and was highly sensitive to the aspect ratio.

Sparrow et al[30] investigated the boundary layer width for the corresponding Grashof numbers and found close agreement between this width and the inter plate spacing corresponding to the maximum Nusselt number. They comment that the heat transfer coefficient is largely insensitive to the plate spacing when the boundary layer does not span the interplate space, but as soon as the plate spacing is reduced to below the boundary layer width the sensitivity becomes high.

Sparrow et al[30] proposed an explanation of the 'chimney effect' referred to by Anand et al[29]: For a channel where the boundary layer is equal to the plate spacing, then the flow is created by the hydrostatic pressure differences within the channel. Thus, all of the air within the boundary layer at the exit must be

drawn into the channel through the channel inlet, resulting in an effectively forced convective flow within the lower region of the channel. As the plate spacing is increased, the effect of the air moving through the lower sections of the channel is reduced until, at the flat plate limit, all of the air entering the boundary layer is drawn from the stationary mass adjacent to the boundary layer. This is shown in figure 2.4.

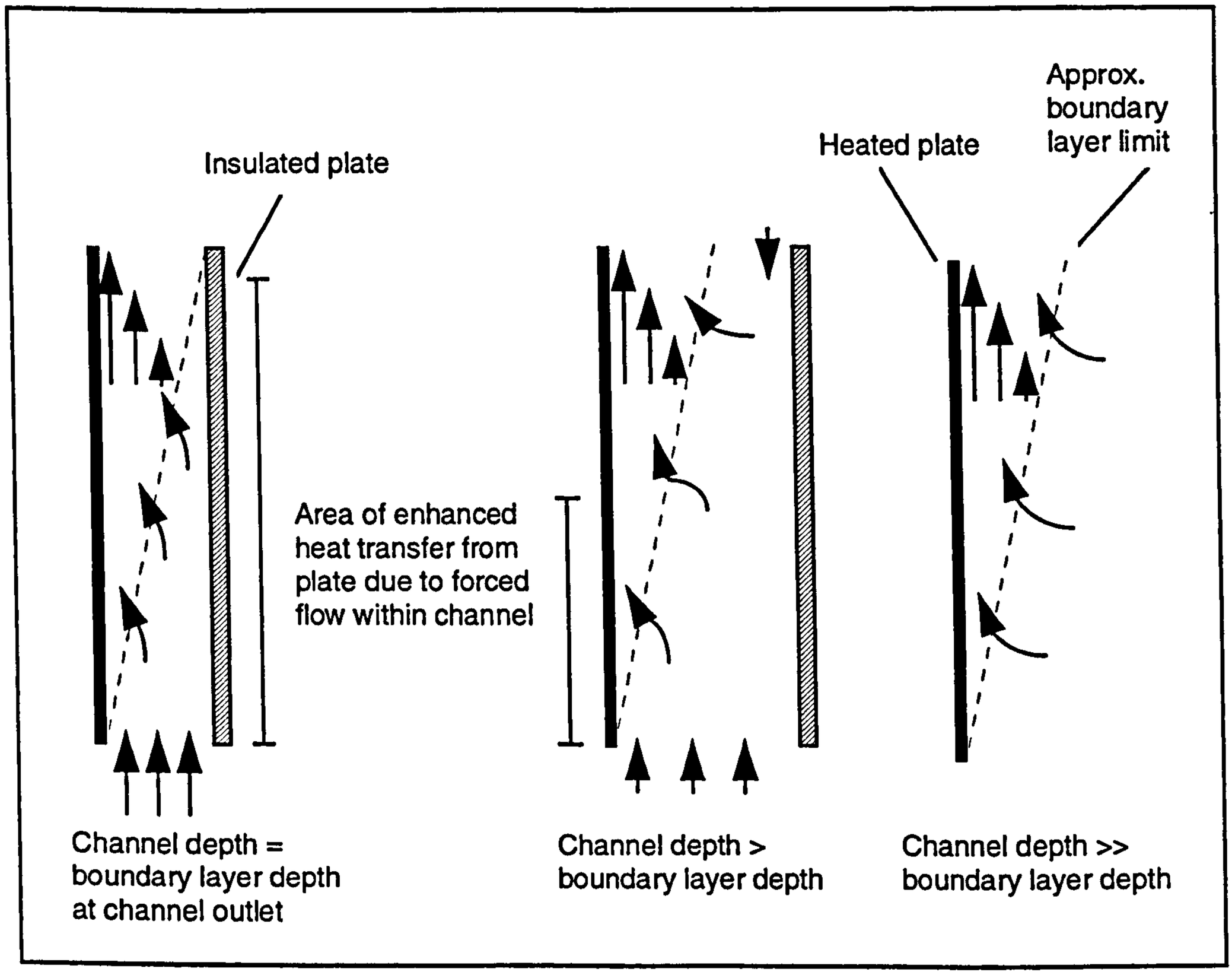

Figure 2.4. Chimney effect as described by Sparrow et al[28]

As the plate spacing reduces below that of the boundary layer depth, thermal stratification occurs within the channel and the heat transfer rate is reduced. The results of Anand et al[29] however show that for a constant heat flux into the plate the effect of this was less marked than for the assumption of a constant plate temperature. This is because for a constant heat flux the plate temperature will continue to rise above that of the adjacent air within the channel to maintain the energy balance.

Neither of these investigations however were extended to consider the effects of these flow phenomena on the induced mass flow rate.

Katoh et al[31] noting the lack of results presented for turbulent flows presented a series of results for an experimental investigation into a 5.0m high constant heat flux plate.

The channel aspect ratios of plate height to channel depth were 100, 50 and 25:1. These were all significantly below the maximum heat transfer coefficient aspect ratios predicted by Anand et al[29] for a laminar regime. Katoh et al[31] presented results showing that as the aspect ratio increased the heat transfer coefficient decreased. Thus implying that for turbulent flows the heat transfer ratio is also affected by channel plate spacing and that for high aspect ratios the rate falls off markedly.

Again no attempt was made to show the effect on the mass flow rate induced, however velocity profiles for each of the three aspect ratios at a single Grashof number were given and so an approximate mass flow rate was calculated by the author. The velocity of the air in the narrow channel was significantly above that of the other two however the overall mass flow rate fell from 80 l/s at an aspect ratio of 25:1 to 40 l/s at 100:1. Thus indicating that the fall in the heat transfer coefficient is accompanied by a corresponding fall in mass flow rate as the aspect ratio is reduced.

So far all of the studies considered that the flows within the channel enter at the lower opening and exit at the upper opening. Sparrow et al[32] challenged this by presenting results from an experimental investigation where flow visualisation was employed to determine the actual flow movement. The results of this investigation show clearly that for certain flow configurations a re-entrant flow occurs at the upper channel opening. The degree of penetration of the reverse flow was directly influenced by the aspect ratio of the channel and the Rayleigh number. The penetration increased with a decrease in aspect ratio and an increase in Grashof number.

However, Sparrow et al[32] showed that the presence of the reverse flow had no noticeable effect on the value of the heat transfer coefficient. It was suggested that the reverse flow existed because the boundary layer does not meet the unheated wall, and thus behaves as for a flat plate configuration. In such a configuration the air required to replace that drawn into the boundary

layer is drawn from the upper opening rather than up the whole length of the channel as indicated in figure 2.4.

The implication of reverse flow on the mass flow rate within such a channel flow was not considered. However such findings do imply that the flow rate may be highly sensitive to changes in plate spacing beyond that where the boundary layer just spans the channel.

Kihm et al[33] obtained close agreement between experimental results and numerical predictions of the depth of flow reversal within a heated channel. However, again the influence of this on the mass flow rate was not reported.

Moshfegh et al[23] used numerical methods to investigate a channel flow to model the heat removal from PV cells mounted on a building facade. The investigation covered both the laminar and turbulent flow regimes and for a facade height of 6.5m; the aspect ratio was varied from 26.0 to 30.95. The resulting velocity profiles show that at the lower aspect ratios the flow rate was the greatest. Thus confirming the results of Katoh et al[31]. No attempt to correlate the mass flow rate was presented.

From the preceding review of literature of flows created within channels it is evident that specific models for the calculation of the mass flow rate induced have not been developed. Added to this the flow phenomena that occur within channels are complex and will influence the flow rate, thus any model developed must take account of these factors.

Chang et al[34] developed a numerical model to investigate natural convective flows within an asymmetrically heated channel. Correlations to describe the mass flow rate induced were produced. A separate equation was developed for each aspect ratio investigated. Thus the subsequent investigation of aspect ratios other than those reported is not possible, reducing the applicability of the results for general use.

The investigations referred to so far have generally considered laminar flow regimes and offer little guidance on the mass flow rate induced within channels. A review of work in the area of passive solar heating components was therefore undertaken to assess if any applied studies had been undertaken that would offer a better insight into the flow induced in such flow configurations.

2.3.3 Building components for passive solar heating of buildings

One of the key differences between a passive solar building element and a solar chimney is the overall objective of the component. A passive solar heater aims to maximise the heat transfer into the building whereas a solar chimney looks to maximise the mass flow rate induced. In this latter application the degree of heating of the air is not the key variable. However, as was shown in the investigations into channels, most of the work undertaken considers the key variable to be the heat transfer coefficient.

Work within the area of passive solar heating elements has concentrated upon the Trombe wall configuration as shown in figure 2.5. Investigations into this component have been undertaken through three approaches;

- numerically solving the partial differential equations that describe the fluid motion,
- solving the energy balance of the components and the induced flow,
- through experimental observations.

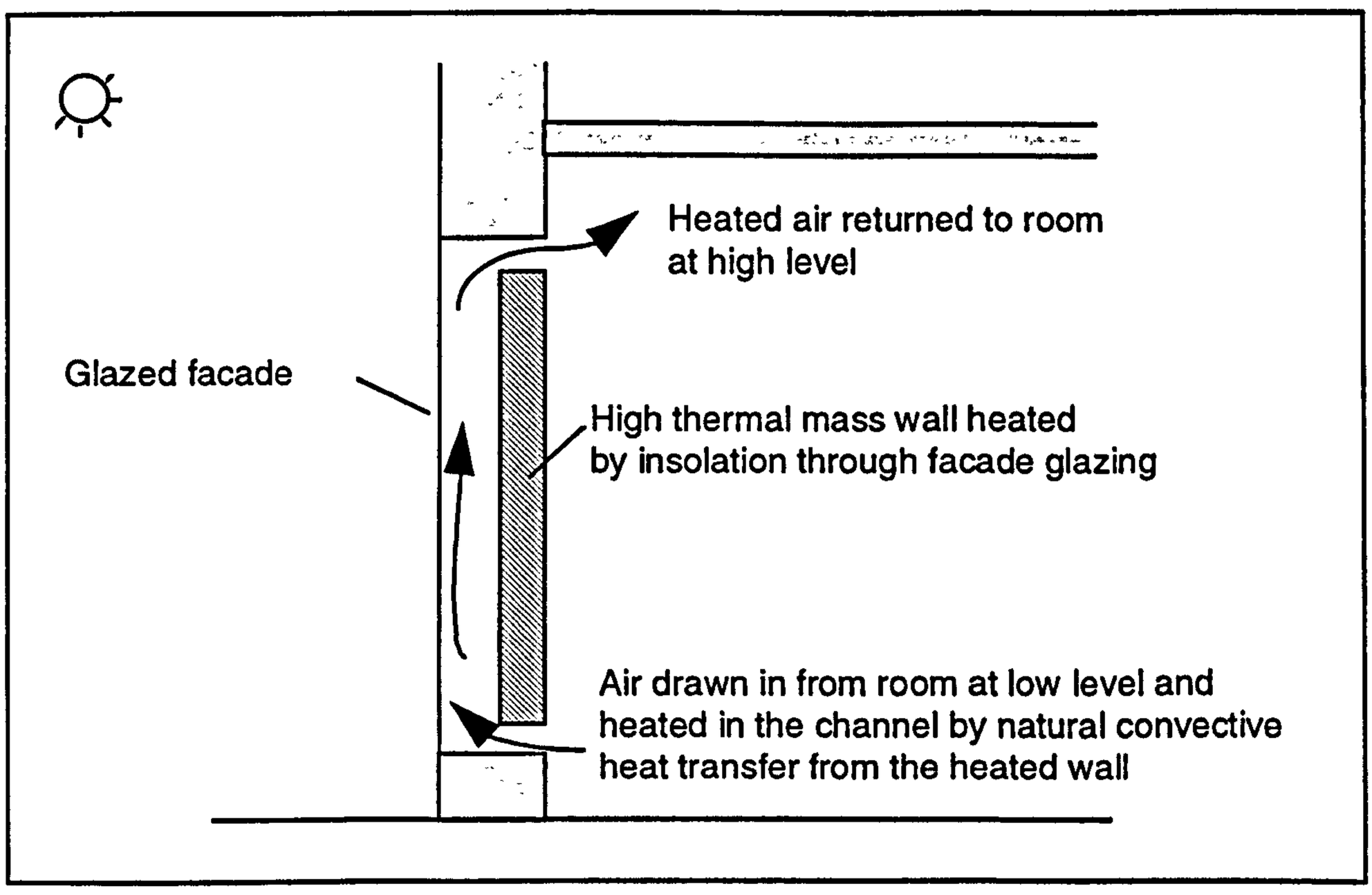

Figure 2.5. A typical Trombe wall configuration

Hobday[35] provides a full review of the development of building components designed for the passive solar heating of buildings. This review however concentrates upon the practical aspects of the components rather than addressing the influences of key physical variables on the mass flow rate induced.

CFD based investigations

Two investigators Pratt[36] and Akbari et al[37] studied Trombe wall systems numerically and made the assumption that the inlet profile of the air was uniform. Both investigators allowed for pressure losses in the inlet by assuming head losses from empirical equations of an orifice. This was then imposed on the numerical model to act against the stack pressure set up by the boundary layer.

Akbari et al[37] investigated the effect of differing levels of asymmetric heating of the channel walls and presented the results in a form that allowed the volumetric flow rate to be calculated from a range of channel heights and degrees of asymmetric heating. The results however took no account of the effect of the channel depth on the flow rate.

Borgers et al[38] undertook an investigation where the transition to a turbulent flow was calculated and the effects included in the subsequent calculations. As with the previous investigations however the inlet profile of the channel was assumed to be uniform. Borgers et al[38] extended his work to consider the effects of channel depth and produced a correlation equation for the flow rate based on a non-dimensional glazing temperature (θ_g) and a Grashof number based on channel depth. Predictions based on Borgers et al[38] correlation equation 2.22. are shown in figure 2.6.

$$\dot{m} = \rho 10^{-(c + f\,|\log H|^{\alpha})} \qquad \text{Equation 2.22.}$$

Where $c = e\,\theta_g^{\beta}$ Equation 2.23.

$$H = \frac{h}{Gr_d\, d} \qquad \text{Equation 2.24.}$$

$$\theta_g = \frac{T_g - T_{inlet}}{T_{wall} - T_{inlet}}$$ Equation 2.25.

and α, β , e and f are variables based on the Grashof number

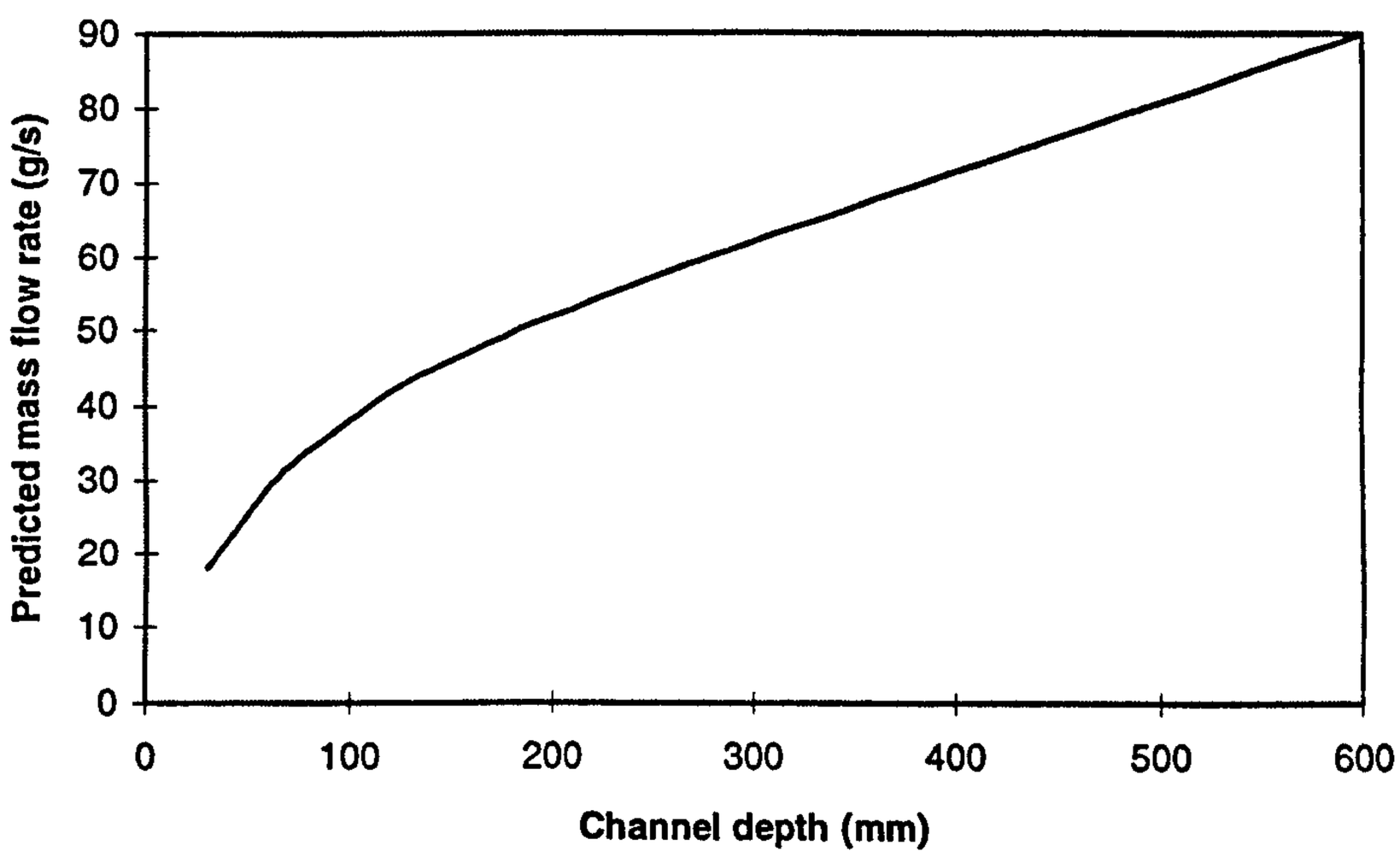

Figure 2.6. Influence of plate spacing on the predicted mass flow rate for a non dimensional glass temperature (θ_g) of 0.1 using equation 2.22.

The correlation proposed by Borgers et al[38] shows a continuous increase in flow rate as the aspect ratio is decreased. There is therefore no sign of a flow rate maximum or subsequent fall off due to flow reversal as predicted by Sparrow et al[32].

Tichy[39] extended the work of Akbari et al[37] and Borgers et al[38] to include a range of inlet frictional losses appropriate for ductwork. The aim was to assess the effect of inlet pressure losses on the performance of the Trombe wall.

The conclusion that Tichy[39] drew was that the value of the frictional losses at the inlet had a direct effect upon the mass flow rate within the Trombe wall but that the overall energy balance remained constant. Thus the energy delivered by the component was largely not influenced by the losses at the inlet. Tichy[39] comments finally that there are so many factors that affect the performance of a passive solar building component that the influence of the inlet losses are marginal. Such a statement is however only appropriate if the energy delivered is the only variable that the component performance is to be measured by.

With a solar chimney the mass flow rate is of prime importance and thus the influence of the inlet losses are of paramount interest.

It is interesting to note that in 1997 Kheireddine et al[40] furthered the work of Tichy[39] by extending the numerical grid outside the inlet of the channel. This allowed the determination of the value of inlet friction coefficient numerically. The flow regime was laminar and the inlet flow in the same axis as that of the channel. Overall therefore it is apparent that work in this area has largely considered simple flow configurations with few investigators studying practical configurations or turbulent flows. Ben Yedder et al[41] confirmed this commenting that within a Trombe wall type enclosure no work had been undertaken on turbulent flows with one wall of the enclosure acting as thermally massive, which is the true configuration of such a building component.

Robert et al[42] considered the Trombe wall type component in detail and discussed the problems of defining the pressure losses within the flow channel. The inlet and outlet he claimed could be approximated by 'usual engineering methods' but the flow within the channel could not be treated in the same way. Due to the thermally induced velocity profile Robert et al[42] questions the use of the Moody Diagram or other equivalent formulas for determination of the pressure loss coefficients. However no further details of pressure loss coefficients were given and no subsequent work in this area appears to have addressed the differences of such a flow to that of a fully developed pipe or duct flow.

One of the few published studies of a flow configuration similar to that of a solar chimney was undertaken by Fleming et al[43]. This study considered a thermosyphon loop with multiple inlets. The results presented illustrate the effects of inlet size and level of plate heating on the flow distribution and the occurrence of reverse flows. No correlations were however produced for mass flow rate in terms of these variables.

Overall therefore even though many of the investigations reviewed were claimed to be based on building components such as the Trombe wall, few practical flow configurations were actually studied. Added to this most numerical investigations have made little attempt to address the question of the induced mass flow rate concentrating largely on heat transfer issues.

The energy balance approach

Many investigators into solar air heaters[44][45] have chosen to solve the energy balance within such components as a means of evaluating their performance. Such modelling of the air flow however relies largely upon the zonal modal approach of defining the bulk air temperature to allow the stack pressures to be calculated.

Most of these studies have been aimed at evaluating the long term operation of the system and thus simplified the system to allow long term simulations to be run. In simplifying the model Utzinger[46] proposed that the flow rate was set i.e. effectively fan driven. This allowed the effect of different flow rates to be established, however the appropriateness of this approach must be questioned as both the heat output and mass flow rate are dependant variables. Using a constant value for one of them will therefore significantly affect the other, the influence of which was not reported.

Zikerm et al[47] undertook a detailed analysis of a Trombe wall configuration. In this investigation the air temperature within the channel was assumed to rise linearly and thus the stack pressure was calculated based on the mean of the inlet and outlet temperatures. However, only the pressure losses at the inlet and outlet of the solar heater were considered. Thus the influence of the chimney channel on the mass flow rate was not addressed.

The significant simplifications required by this approach, to the solving of the mass flow induced by a solar building component, reduce its appropriateness for the evaluation of the influence of the physical parameters on the flow rate.

Experimental investigations

Akbarzadeh et al[48] undertook an experimental investigation into a Trombe wall noting that from flow visualisation the inlet caused the flow to be turbulent throughout the height of the channel. This therefore raises questions as to the validity of the assumption of a laminar flow regime made by many investigators undertaking numerical investigations[36][37].

Akbarzadeh et al[48] investigated the effect of changing the height of the inlet and also the aspect ratio of the channel. With a fixed channel height of approximately 2.5m it was found that reductions of height of the inlet from

0.095 to 0.045m had a significant influence upon the mass flow rate, reducing it noticeably. Variations in the height of the inlet above 0.095m however showed little influence. The reduction of the flow rate at an inlet height of 0.045m was accompanied by an increase in exit air temperature. However the overall efficiency of the component was reduced as the losses to the external air were increased by the higher glazing temperatures.

Variations in the channel aspect ratio showed little influence on the overall performance. However as the performance was measured in terms of the energy delivered from the Trombe wall, assumptions as to the effect of the changes on the flow rate cannot be made.

Hocevar[49] investigated the velocity profiles within a Trombe wall channel and concluded that they were complex and a function of the channel depth, ambient temperature, insolation, wall surface temperature and the overall height of the channel above the inlet. No attempt to correlate the flow rate to any of these variables was, however, made.

La Pica et al[50] also investigated the Trombe wall configuration and presented a range of results for three different channel aspect ratios; 40:1, 24:1 and 18:1. Results for each of these aspect ratios was given for a constant heat flux wall with energy inputs ranging from 48 to 317 W/m^2.

The experimental rig was constructed inside a chamber, thus removing the uncertainty associated with experiments open to variations of ambient conditions. The volumetric flow rate was accurately measured at the inlet by traversing a velocity probe through 96 points within the opening. The temperature of the air was also measured at the inlet. The temperature rise of the air was used to calculate the energy gained by the air. La Pica et al[50] claimed that three temperature probes fitted within the exit would allow an average temperature rise to be calculated. This however ignores the fact that neither the velocity or temperature profile of the air would be flat. Thus the energy rise of the air was not well described by the temperature measured at the centre of the outlet and mass flow rate at the inlet.

The inlet and outlet openings were altered in size to match that of the channel, thus at low aspect ratios the outlet was relatively large and although the temperature variation across the outlet may have been small, the velocity variation would have been significant. The effect of this is shown in figure 2.7.

where, as the aspect ratio is reduced it is apparent that the difference in the energy measurements increased. This could not be explained by increased losses to ambient as the wall temperature fell as the aspect ratio decreased.

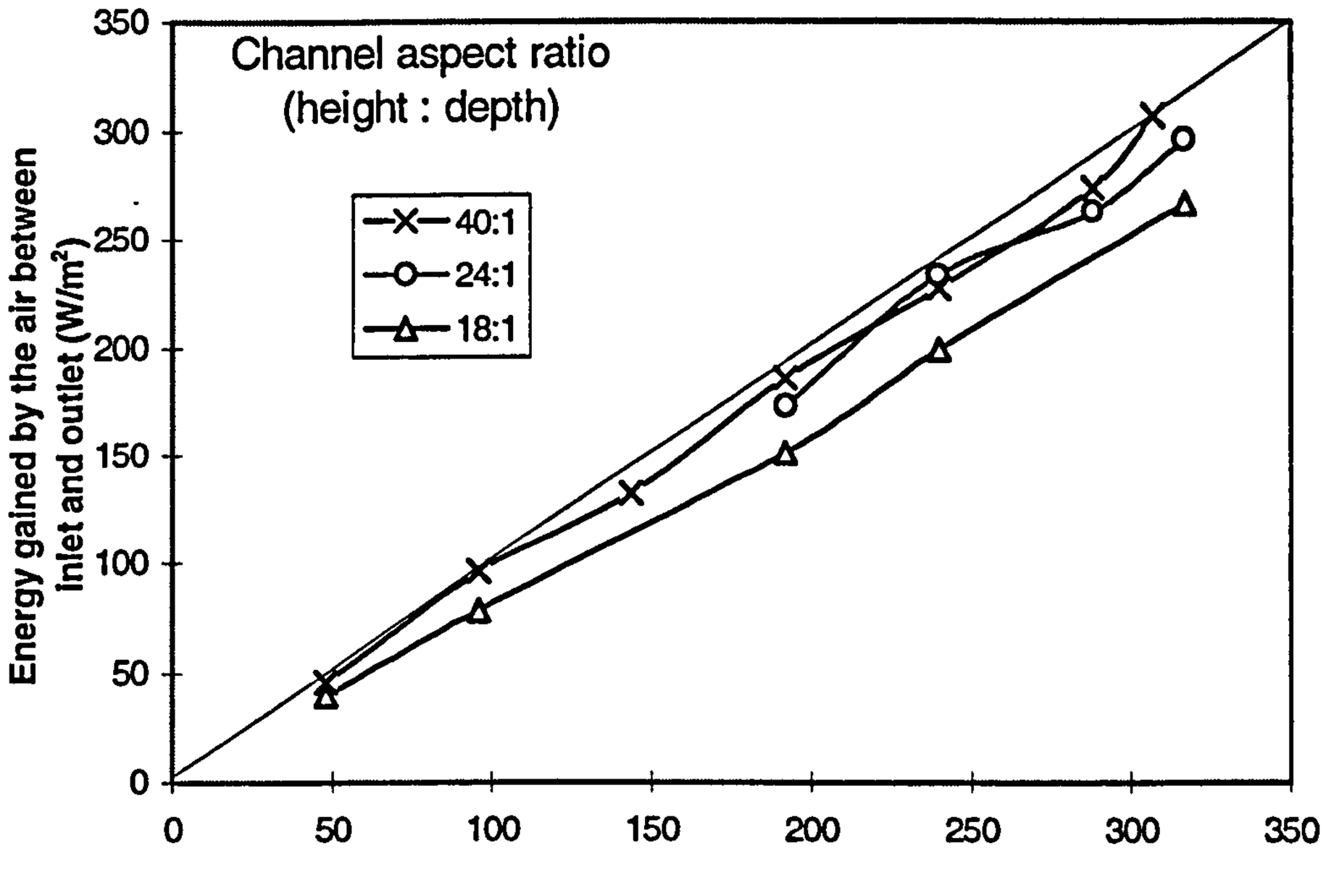

Figure 2.7. Comparison of energy given off the wall to that calculated as gained by the air (La Pica et al[50]).

La Pica et al[50] presents results for the Nusselt number showing that it increases markedly as the aspect ratio decreases. However as Sparrow[28] noted, the influence of the heat transfer coefficient can not be truly isolated when the Nusselt and Grashof numbers are both expressed in terms of the aspect ratio. In addition to this the results were calculated based upon the energy gained by the air and not that transferred from the wall.

When the heat transfer coefficient was recalculated, by the author, based upon the inlet air to plate temperature difference and the energy transferred from the wall, the coefficient was found to vary significantly less than reported by La Pica et al[50].

Channel	Temperature		Temperature difference	La Pica results		Recalculated results
Aspect ratio	Wall (°C)	Inlet air (°C)	(°C)	Nusselt number (Nu_d)	Heat transfer coefficient ($W/m^2°C$)	Average heat transfer coefficient ($W/m^2°C$)
1:40	62.6	24.9	37.7	21.7	7.5	6.4
1:24	57.3	22.8	34.5	39.3	8.2	7.0
1:18	55.9	21.5	34.4	44.4	6.8	7.0

Table 2.1. Results for experimental investigation of convective heat transfer coefficient, recalculated based on plate and inlet air temperature at 240 W/m^2

The results for the influence of aspect ratio on the mass flow rate are however of interest and were not affected by uncertainties in the temperature rise of the air within the channel. They show that as the aspect ratio is increased from 18:1 to 24:1 the mass flow rate fell slightly, however the fall was significant when the aspect ratio was increased to 40:1. No attempt to correlate the findings was made.

Overall it is evident therefore that the experimental investigations into passive solar components offer little insight into the operation of low thermal mass thermosyphon devices designed to provide air flow in natural ventilation systems.

2.3.4 Conclusion of work in areas associated with the solar chimney

From this review of work in areas associated with the types of flow induced in a solar chimney it is apparent that very little work of practical use has been undertaken.

The work undertaken into channel type flows, although mainly concerned with laminar flows, highlighted the significant influence the presence of a second plate has on the flow induced from a heated flat plate. However, as all of the work was aimed at the evaluation of heat transfer coefficients, little guidance is offered as to the influence of channel configurations on the mass flow rates induced in such channels.

Numerical investigations into the modelling of building components have often simplified the flow configuration to such an extent that significant assumptions about inlet pressure drops had to be made. The appropriateness and influence of such assumptions was not fully tested against experimental data and thus the usefulness of the results for application to actual building components is questionable.

The popular method of solving the system energy balance to evaluate the performance of solar systems relies upon zonal model based assumption of a fully mixed air mass within the channel. Therefore work in this area throws no light upon the influence of channel configuration on mass flow rates.

The reported experimental work is largely aimed at evaluating the heat transfer rates and the mass flow rate is not widely reported. The development of sufficient data to assess the ability of numerical model predictions of flow rates appears not to have been undertaken. The experimental investigations reported also highlight some of the practical problems associated with such work.

2.4 Review of work on the solar chimney

The solar chimney as a broad principle has received considerable recent coverage. Both the BRE[22] and EC[51] in separate guides to natural ventilation and cooling within buildings respectively refer to solar chimneys. Diagrams are used to show the basic principle but guidance as to how such a building component should be sized is not given.

CIBSE[52] elude to a solar chimney through a double facade arrangement in their Application Manual on Natural Ventilation in Buildings, however again no specific design advice is given and the only approach presented to calculate flow rates is through that of a zonal model.

Haisley[53] laid down the basic concepts, producing details of a complete cooling and ventilation system that included an evaporative cooling device for the supply air and a solar chimney to raise the temperature of the exhaust air. Haisley considers the pressure drops in all components of the system, but

offers no insight into appropriate values or the sensitivity of the flow rate to changes in any of the physical parameters.

Bansal et al[54] produced a mathematical model of a solar chimney and considered the effect of differences in the discharge coefficient on the mass flow rate. However the air within the chimney was considered to be fully mixed and no guidance as to an appropriate range of values of discharge coefficient were given. Thus the predictions of mass flow rate are based on the zonal model assumption and no account of the channel aspect ratio was taken, reducing the usefulness of the model.

One of the most detailed investigations published into a solar chimney was undertaken by Bouchair[11]. As previously described in Chapter One, the prime aim of this investigation was to evaluate the potential of providing overnight ventilation in hot arid climates. For this Bouchair[11] proposed a thermally massive structure. In mild climates, such as the UK, the requirement is for day time ventilation and therefore thermally lightweight structures are more appropriate. Apart from this detail however the principle of the solar chimney is the same.

Bouchair studied many aspects of the solar chimney for application in hot arid climates including orientation[55] and the ability of the chimney to drive ventilation throughout the night[56]. Of most interest to the present investigation was the work undertaken to predict the mass flow rate of the chimney.

Bouchair[11] investigated the chimney both theoretically and through a detailed experimental study. The experimental rig allowed both the aspect ratio of the chimney and the size of the inlet to be altered for a range of plate temperatures.

The experimental results show clear trends of mass flow rate as other physical variables were altered.

Figure 2.8. shows the influence of channel depth and inlet size for a range of plate to inlet air temperature differences. As the channel depth was increased the mass flow increased and then declined gradually. This was more defined with the smaller inlet. As the inlet area was increased both the maximum flow rate and the channel depth at which it occurs increased.

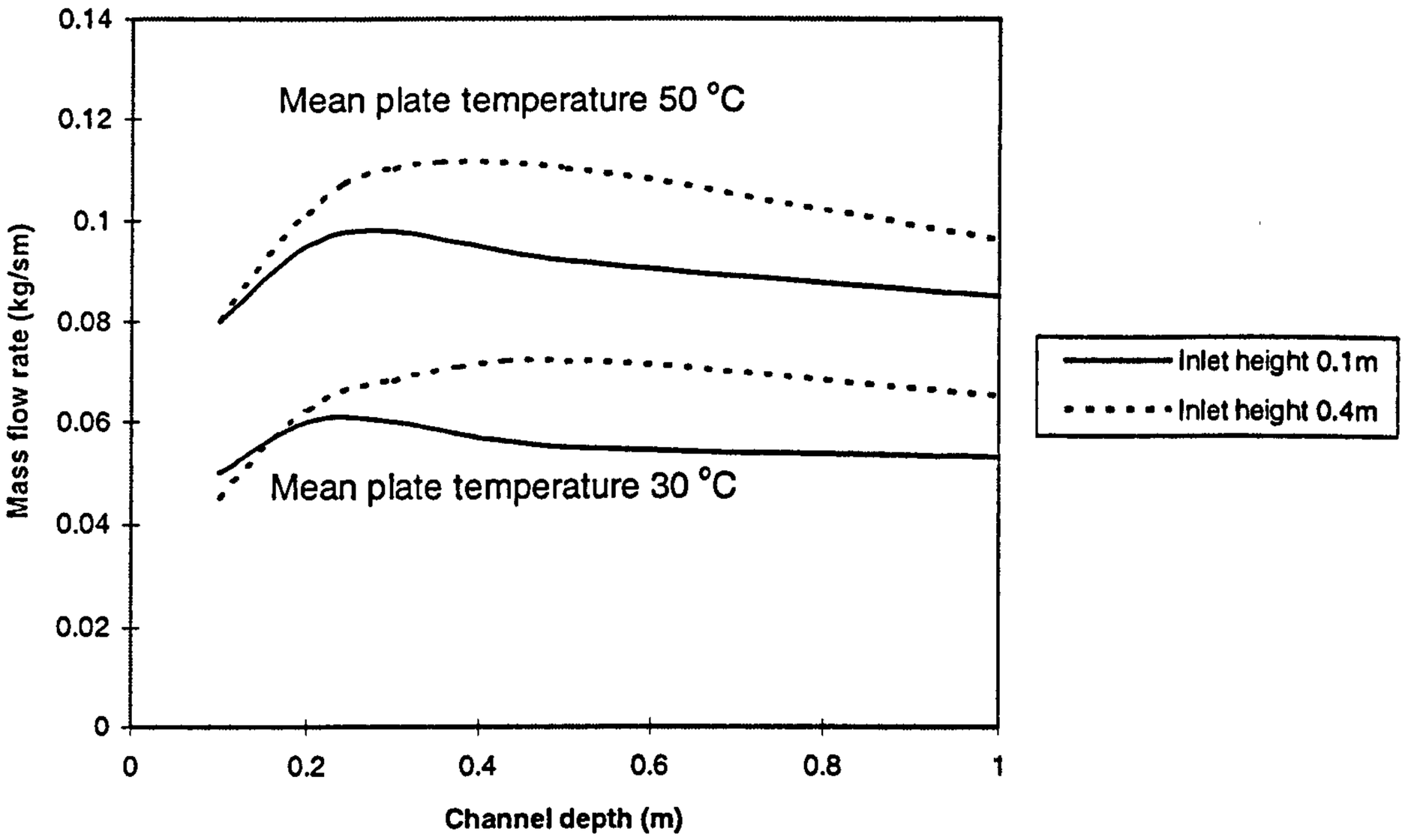

Figure 2.8. Experimental results of the influence of channel depth and inlet opening size on mass flow rate induced[56]

Bouchair[11] investigated the channel depth at which the maximum flow occurred. Flow visualisation showed that as the channel depth was increased, past this maximum flow point, reverse flow at the outlet was observed. This therefore confirms the findings of Sparrow et al[32] and indicates that flow reversal does influence the mass flow rate through the inlet of such a channel. Bouchair used the equations proposed by Eckert et al[10], equation 2.15., to determine if the channel depth corresponding to the maximum flow was linked to the boundary layer width. For a channel of height 1.95m the calculated boundary width was 0.13m. Bouchair[11] therefore proposed that the maximum flow occurred when the boundary layers just met in a symmetrically heated channel i.e. at a channel depth of approximately 0.26m.

This proposal is however only appropriate for flows with inlets of 0.1m high. With the inlet height at 0.4m, the channel depth corresponding to maximum flow rate is significantly greater than that of the boundary layer widths. This point was not raised by Bouchair[11] and implies that the channel depth at which maximum flow rate occurs was influenced by the resistance to the flow imposed by the inlet opening as well as boundary layer width.

Bouchair[11] then investigated the operation of the solar chimney theoretically.

Bouchair[11] firstly considered the mass flow rate created by a free boundary layer through the use of the boundary layer width and velocity profile suggested by Eckert et al[10]. This flow rate was however not then used for any part of the calculation[57], other than to provide a first estimate for subsequent iterative calculations.

Bouchair[11] proposed that the stack pressure created by the heating of the air within the channel was matched by the pressure losses in the components that made up the flow path of the air. i.e.

$$P_s = P_{losses} = P_{inlet} + P_{channel} + P_{outlet} \qquad \text{Equation 2.26.}$$

$$\text{Where } P_{outlet} = \frac{K \rho u_{outlet}^2}{2} \qquad \text{Equation 2.27.}$$

and K is the pressure loss coefficient

Bouchair[11] proposed that the pressure loss at the outlet was equal to one pressure head i.e. K = 1. However Fried et al[58] states that if the velocity profile of the air is not uniform then the pressure loss at the outlet may be significantly greater. Thus the value of K was directly influenced by channel depth of the chimney and not constant as assumed by Bouchair[11].

$$P_{channel} = 4 f h \frac{\rho u_{channel}^2}{4 d} \qquad \text{Equation 2.28.}$$

Where *f* is the friction factor of the channel obtained from the Moody diagram

$$\text{and} \quad P_{inlet} = \frac{K \rho u_{inlet}^2}{2} \qquad \text{Equation 2.29.}$$

Unlike Tichy[39], Bouchair[11] did not use the pressure loss coefficient for ductwork which meant that the value of K had to be determined. Bouchair[11] proposed the following relationship:

$$T_{outlet} = T_{plate} - (T_{plate} - T_{inlet}) \exp^{\left(\frac{-h}{a}\right)} \qquad \text{Equation 2.30.}$$

$$\text{Where } a = \frac{\dot{m}\, Cp}{5.81 + 4.1\left(\frac{\dot{m}}{\rho A}\right) 2w} \qquad \text{Equation 2.31.}$$

$$P_s = 3463\ h\left(\frac{T_{mean} - T_{inlet}}{T_{mean}\ T_{inlet}}\right) \qquad \text{Equation 2.32.}$$

$$\text{Where } T_{mean} = \frac{T_{outlet} + T_{inlet}}{2} \qquad \text{Equation 2.33.}$$

$$P_{losses} = \frac{K \rho\ u^2_{inlet}}{2} + 4f\ h \frac{\rho\ u^2_{channel}}{4d} + \frac{\rho\ u^2_{outlet}}{2} \qquad \text{Equation 2.34.}$$

Therefore, as the pressure losses are equal to the stack pressure created, by taking the experimentally obtained values for mass flow rate the value of K at the inlet was calculated. The problem with this approach is that the value of K is then used to fit the mathematical model to the experimental data rather than the theoretical model predicting the flow through the chimney.

Bouchair[11] compared the values of K determined from the experimental data with those of pressure losses in an appropriate duct configuration. For an inlet height of 0.1m Bouchair[11] found K equal to 0.4 to 0.7 with the published data giving 1.3, for an inlet height of 0.4m the experiments gave K equal to 1.8 to 7.7 and the published data about 3.2. Part of this variation will be due to the effects of the pressure losses at the exit varying as the channel depth influenced the profile of the air exiting the chimney. This was however not taken into account by Bouchair[11].

Therefore the approach adopted by Bouchair[11] is only appropriate for the configurations that he tested experimentally and is not a general model, requiring the variable K to be fitted to get correct predictions. Thus its appropriateness for designers of different types of building components is very limited.

Awbi et al[13] also carried out an investigation into solar chimneys and used the experimental results of Bouchair to test his 'simplified analytical approach'.

The model developed was based on the same assumptions as that of Bouchair[11], i.e. the stack pressure created equals the pressure losses due to the air flow and the pressure loss at the exit was constant and equal to one pressure head loss regardless of velocity profile of the air. There was therefore again a need to determine the value of K for the inlet, however in this paper Awbi et al[13] gave no results of theoretical predictions.

In a later paper Awbi[59] approached the problem slightly differently. In this case the pressure losses within the channel and at the exit were subtracted from the stack pressure leaving a net pressure loss across the inlet. The inlet was treated as an orifice through the use of equation 2.3.

Awbi[59] gave no values of Cd however one must have been assumed appropriate to the type of inlet of Bouchair's[11] rig. In this way therefore the equations describing the chimney could then be solved iteratively for a given plate temperature. Awbi[59] presents results for his analytical approach against those of Bouchair et al[11] showing close agreement, however it is not apparent what value of discharge coefficient was used or if one value allowed the affects of different inlet heights to be predicted.

Both the models proposed by Bouchair[11] and Awbi[59] consider the effects of friction within the chimney channel. In this way the reductions in the flow rate at high aspect ratios can be predicted, however the effects of low aspect ratios are not addressed. Therefore again the models proposed are somewhat simplified and lack generality.

Awbi[59] finally considered the efficiency of a solar chimney. This was defined as:

$$\xi = \frac{T_{outlet} - T_{inlet}}{T_{wall} - T_{inlet}} \qquad \text{Equation 2.35.}$$

From this equation it was implied that the efficiency of the solar chimney falls as the temperature of the air at the exit falls. If the actual requirement of a solar chimney is considered, this is the inverse of what is required. For a given wall temperature the lower the air temperature at the exit the greater the mass flow rate that must occur to maintain the energy balance i.e. for the purposes of ventilation this represents high efficiency.

Overall therefore the investigations into the operation of a solar chimney have been based upon the zonal model principle of heat gain to the whole air mass within the chimney. Attempts at predicting the changes in mass flow rate with aspect ratio have only addressed the issue of frictional losses within the channel and not considered the effects of reverse flows, even though such flow phenomena were reported in experimental investigations.

2.5 Conclusions drawn from the assessment of models currently available and literature in the area

This review of the models and literature appropriate to the determination of the mass flow rate induced in a building component such as a solar chimney has highlighted the significant lack of guidance available to designers of such components.

The simplifications inherent to the mathematical models require investigation as they do not allow the effect of channel flow to be fully assessed. CFD on the other hand offers an ideal solution. However, the time and operator skill required along with the need for validation of any models developed, limits its use in practical design situations.

From the review of the literature concerning buoyancy induced flows within channels it is apparent that the question of the mass flow rate has not been widely addressed and when it has the models produced have been based on zonal model assumptions and only consider the effects of channel friction and not possible flow reversal.

There is therefore a need for a model or set of correlation equations that can describe the mass flow rate through such a building component in terms of the physical variables of the channel.

2.6 Methods of achieving project aim

From the review undertaken it was apparent that sufficient data does not exist to validate a CFD model and undertake a parametric testing regime of the typical flow configuration found in a solar chimney. A data set was therefore established to undertake such a study.

The production of a suitable data set for the validation of a CFD model required that the level of accuracy of the data was high. Due to the potential physical problems of full scale rig investigations, the area of scale models was addressed by Swainson et al[60]. A report on the findings of the investigation into this is given in Appendix A. The result of the study however highlighted the fact that to obtain full similarity of flow and heat transfer, a full scale investigation was the only truly reliable approach.

The aim of this project was therefore achieved as follows:

Development of a suitable rig to obtain a data set for the validation of a CFD model and the testing of any appropriate existing models.

Testing of existing models and prediction methods against the experimental data.

Development of a CFD model and validation against the experimental data.

Undertaking of parametric testing of the chimney physical variables to assess their influence on the mass flow through a solar chimney.

Development of a means of presenting the results of the investigation that can be used by building designers to evaluate the influence of physical parameters on the potential flow rate.

2.7 References Chapter Two

1. Etheridge, D., Modelling of air infiltration in single and multi cell buildings, Energy and Buildings, Vol. 10, 185 - 192, 1988.

2. Etheridge, D. and Sandberg, M., Building Ventilation. Theory and Measurement, J. Wiley & Sons., UK, 1996.

3. Liddament, M., Air Infiltration Calculation Techniques - An Application Guide, AIVC, 1986.

4. CIBSE, Air Infiltration and Natural Ventilation, CIBSE Guide A4, 1986.

5. EDSL, TAS User Manual, Revision 8.0, EDSL Ltd., 1996.

6. Clarke, J. and Hensen, J., An approach to the simulation of coupled heat and mass flows in buildings. Proceedings 11th. AIVC Conference, Belgirate, Italy, 1990.

7. Feustel, H. and Raynor - Hoosen, A., COMIS Fundamentals, Berkeley, USA, 1990.

8. Furbringer, J., Compagnon, R. and Roulet, C., The LESO building, Weather & aeraulic data set for validation, Proceedings of AIVC Workshop on Data Base, Warwick, March, 1990.

9. Liddament, M., Two airflow studies completed, Air Infiltration Review, Vol. 17, No. 4, 10 - 12, 1996.

10. Eckert, E. and Jackson, T., Analysis of turbulent free-convection boundary layer, NACA Technical Note No. 2207, 1950.

11. Bouchair, A., Solar induced ventilation in the Algerian and similar climates, PhD. Thesis, University of Leeds, UK, 1989.

12. Swainson, M., Investigation into the potential of thermosyphoning air panels to drive natural ventilation in buildings, MSc. Thesis, Cranfield University, UK, 1994.

13. Awbi, H, and Gan, G., Simulation of solar-induced ventilation, Proceedings 2nd. World Congress on Renewable Energy, Reading, September, 1992.

14. Bussoletti J. E. CFD calibration and validation. The challenges of correlating computational model results with test data, Proceedings 18th. AIAA Aerospace ground testing conference. Colorado Springs, USA, June, 1984.

15. Baker, A. and Kelso, R., On validation of CFD procedure for room air motion prediction, ASHRAE Transactions, Vol. 96, No. 1, 760 - 774, 1990.

16. Schetz, J. and Fuhs, A., Handbook of Fluid Dynamics and Fluid Machinery, Volume 1, J. Wiley & Sons, UK., 1996.

17. Holmes, M. and Whittle, G., How accurate are the predictions of complex air movement models, Building Serv. Eng. Res. Technol., Vol. 8, 29 - 31, 1987.

18. Awbi, H., The role of numerical solutions in room air distribution design, Proceedings Roomvent 90, Oslo, Norway, 1990.

19. Chen, Q., Moser, A. and Suter, P., A database for assessing indoor airflow, air quality, and draught risk, IEA Annex 20, Subtask 1, Research Item 1.23, 1992.

20. Henkes, R. and Hoogendoorn, C., Comparison exercise for computations of turbulent natural convection in enclosures, Numerical Heat Transfer, Part B, Vol. 28, 59 - 78, 1995.

21. Borth, J. and Suter, P., Influence of mesh refinement on the numerical prediction of turbulent air flow in rooms, Proceedings Roomvent 94, 15 - 17 June, Krakow, Poland, 1994.

22. BRE., Natural ventilation in non domestic buildings, Digest 399, 1994.

23. Moshfegh, B. and Sandberg, M., Investigation of fluid flow and heat transfer in a vertical channel heated from one side by PV elements, Part 1, Proceedings World Renewable Energy Congress, 15 - 21 June, Denver Colorado, USA, 1996.

24. Churchill, S. and Chu, H., Correlating equations for laminar and turbulent free convection from a vertical plate, Int. J. heat Mass Transfer, Vol. 18, 1323 - 1329, 1975.

25. Incropera, F. and DeWitt, D., Fundamentals of Heat and Mass Transfer, 3rd. Ed., J. Wiley & Sons, New York, 1990.

26. Burmeister, L., Convective Heat Transfer, 2nd. Ed., J. Wiley & Sons, New York, 1993.

27. Webb, B. and Hill, D., High Rayleigh number laminar natural convection in an asymmetrically heated vertical channel, J. of Heat Transfer, Vol. 111, 649 - 656, 1989.

28. Miyatake, O., Fuji, T., Fuji, M. and Tanaka, H., Natural convection heat transfer between vertical parallel plates, Heat transfer Japanese Research, Vol. 3, 25 - 33, 1973.

29. Anand, N., Kim, S. and Fletcher, L., The effect of plate spacing on free convection between heated parallel plates, Journal of Heat Transfer, Vol. 114, 515 - 518, 1992.

30. Sparrow, E. and Azevedo, L., Vertical channel natural convection spanning between the fully - developed and the single - plate boundary layer limit, Int. J. Heat Mass Transfer, Vol. 28, No. 10, 1847 - 1857, 1985.

31. Katoh, Y., Miyamoto, M., Kurima, J. and Kaneyasu, S., Turbulent free convection heat transfer from vertical parallel plates, JSME International Journal, Series 2, Vol. 34, No. 4, 496 - 501, 1991.

32. Sparrow, E., Chrysler, G. and Azevedo, L., Observed flow reversals and measured - predicted Nusselt numbers for natural convection in a one - sided heated vertical channel, Journal of Heat Transfer, Vol. 106, 325 - 332, 1984.

33. Kihm, K., Kim, J. and Fletcher, L., Onset of flow reversal and penetration length of natural convective flow between isothermal vertical walls, Journal of Heat Transfer, Vol. 117, 776 - 779, 1995.

34. Chang, T. and Lin, T., On the reversed flow and oscillating wake in an asymmetrically heated channel, Int. J. for Numerical Methods in Fluids, Vol. 10, 443 - 459, 1990.

35. Hobday, R., Passive solar - energy air - heating wall panels, PhD. Thesis, Cranfield University, UK, 1987.

36. Pratt, R. and Karaki, s., Natural convection between vertical plates with external frictional losses - application to Trombe walls, Proceedings 3rd. National Passive Solar Conference, 1979.

37. Akbari, H. and Borgers, T., Free convective laminar flow within the Trombe wall channel, Solar Energy, Vol. 22, 165 - 174, 1979.

38. Borgers, T. and Akbari, H., Free convective turbulent flow within the Trombe wall channel, Solar Energy, Vol. 33, No. 3/4, 1984.

39. Tichy, J., The effect of inlet and exit losses on free convective laminar flow in the Trombe wall channel, Journal of Solar Engineering, Vol. 105, 187 - 193, 1983.

40. Kheireddine, A., Houla Sanda, M., Chaturvedi, S. and Mohieldin, T., Numerical prediction of pressure loss coefficient and induced mass flux for laminar natural convective flow in a vertical channel, Energy, Vol. 22, No. 4, 413 - 423, 1997.

41. Ben Yedder, R. and Bilgen, E., Turbulent natural convection and conduction in enclosures bounded by a massive wall, Int. J. Heat Mass Transfer, Vol. 38, No. 10, 1879 - 1891, 1995.

42. Robert, J., Peube, J. and Trombe, F., Experimental study of passive air - cooled flat - plate solar collectors, Energy Conservation in Heating, Cooling, and Ventilating Buildings, Hemisphere Publishing Corp., Washington, USA, 1978.

43. Fleming, J. and Ruhul Amin, M., Conjugate natural convection in a planar thermosyphon with multiple inlets, Int. J. Heat mass Transfer, Vol. 39, No. 1, 49 - 59, 1996.

44. Parker, B., Colliver, D. and Walton, L., Sensitivity of air - type solar collector efficiency to design changes, Transactions of the ASAE, Vol. 3, 915 - 920, 1984.

45. Mullick, S. and Samdarashi, S., An improved technique for computing the top heat loss factor of a single flat - plate collector with single glazing, Journal of Solar Energy Engineering, Vol. 110, 262 - 267, 1988.

46. Utzinger, D., Klein, S. and Mitchell, J., The effect of air flow rate in collector - storage walls, Solar Energy, Vol. 25, 511 - 519, 1980.

47. Zrikem, Z. and Bilgen, E., Theoretical study of a composite Trombe - Mitchel wall solar collector system, Solar Energy, Vol. 39, 409 - 419, 1987.

48. Akbarzadeh, A., Charters, W. and Lesslie, D., Thermocirculation characteristics of a Trombe wall passive test cell, Solar Energy, Vol. 28, 461 - 468, 1982.

49. Hocevar, C., Thermocirculation data for instantaneous efficiencies for Trombe walls, Proceedings 4th. National Passive Solar Conference, ISES-AS, 1979.

50. La Pica, A., Rodono, G. and Volpes, R., An experimental investigation on natural convection of air in a vertical channel, Int. J. Heat Mass Transfer, Vol. 36, No. 3, 611 - 616, 1993.

51. EC DG XVII, Natural and Low Energy Cooling in Buildings, Thermie Programme maxibrochure. 1994.

52. CIBSE, CIBSE Application Manual, Natural Ventilation in Buildings, Draft version, CIBSE, December, 1994.

53. Haisley, R., Solar chimney theory: Basic Precepts, Proceedings Passive and Hybrid Cooling International Conference, Miami Beach, USA, November , 1981.

54. Bansal, N., Mathur, R. and Bhandari, M., Solar chimney for enhanced stack ventilation, Building and Environment, Vol. 28, No. 3, 373 - 377, 1993.

55. Bouchair, A. and Fitzgerald, d., The optimum azimuth for a solar chimney in hot climates, Energy and Buildings, Vol. 12, No. 2, 135 - 140, 1988.

56. Bouchair, A., Solar chimney for promoting cooling ventilation in southern Algeria, Building Serv. Eng. Res. Technol. Vol. 15, No. 2, 1994.

57. Bouchair, A., Private communications, December, 1996.

58. Fried, E. and Idelchik, I., Flow Resistance, A Design Guide For Engineers, Hemisphere Publishing Corp., New York, 1989.

59. Awbi, H., Design considerations for naturally ventilated buildings, Renewable Energy, Vol. 5, Part 2, 1081 - 1090, 1994.

60. Swainson, M. and Batty, W., A review of physical modelling techniques to aid in the design of naturally ventilation building components, Proceedings CIBSE National Conference, Eastbourne, October, 1995.

CHAPTER THREE

DESIGN AND DEVELOPMENT OF A RIG FOR THE INVESTIGATION OF A SOLAR CHIMNEY

3.1 Introduction

The need for a reliable data set against which existing models describing stack induced air flow can be assessed was highlighted in Chapter Two. With CFD programmes capable of modelling complex geometries, it was important that if CFD modelling was to be used to develop design aids for actual building components, then the experimental rig should be based on a practical building component configuration.

As highlighted in Chapter 2, work on realistic configurations of channel flow such as that in a solar chimney, has been limited. The problems identified in the experimental work undertaken by La Pica [1] demonstrated the ease with which basic assumptions about the flow of air can significantly affect the practical use of experimental results. Therefore the sensitivity of the key dependant variables to uncertainty in the input data was tested. In this way the level of uncertainty in the results could be evaluated and minimised through the design of the experimental rig.

3.2 Approach to the design of the rig

The need for high quality data from the experimental investigation required that the level of uncertainty in each of the results obtained was minimised, i.e. the level of confidence that the results were within a given band was high. To achieve such a level of confidence required that the sources of uncertainty were identified, quantified and as far as possible minimised.

The data required for the validation of mathematical air flow models could be obtained in one of two ways:

- Directly by measurement, in which case the level of uncertainty was associated with the instruments and techniques used.

- Indirectly through calculations using a range of measurements and associated variables. In this case the level of uncertainty would be related

both to the measured data and any other variables required for the calculation.

The air flow within a solar chimney resulted from the convective heat transfer from a plate heated by solar energy. There were therefore two variables against which the flow rate of the chimney could be expressed: the plate to air temperature difference or the value of the energy transferred from the plate to the air.

Temperature difference

The plate and air temperatures could both be measured directly and thus only incur uncertainties associated with the instruments used.

Energy transferred from the plate

The energy transferred from the plate to the air could not be directly measured accurately and thus required calculating from a range of measurements and associated variables. There were two methods by which this could be undertaken:

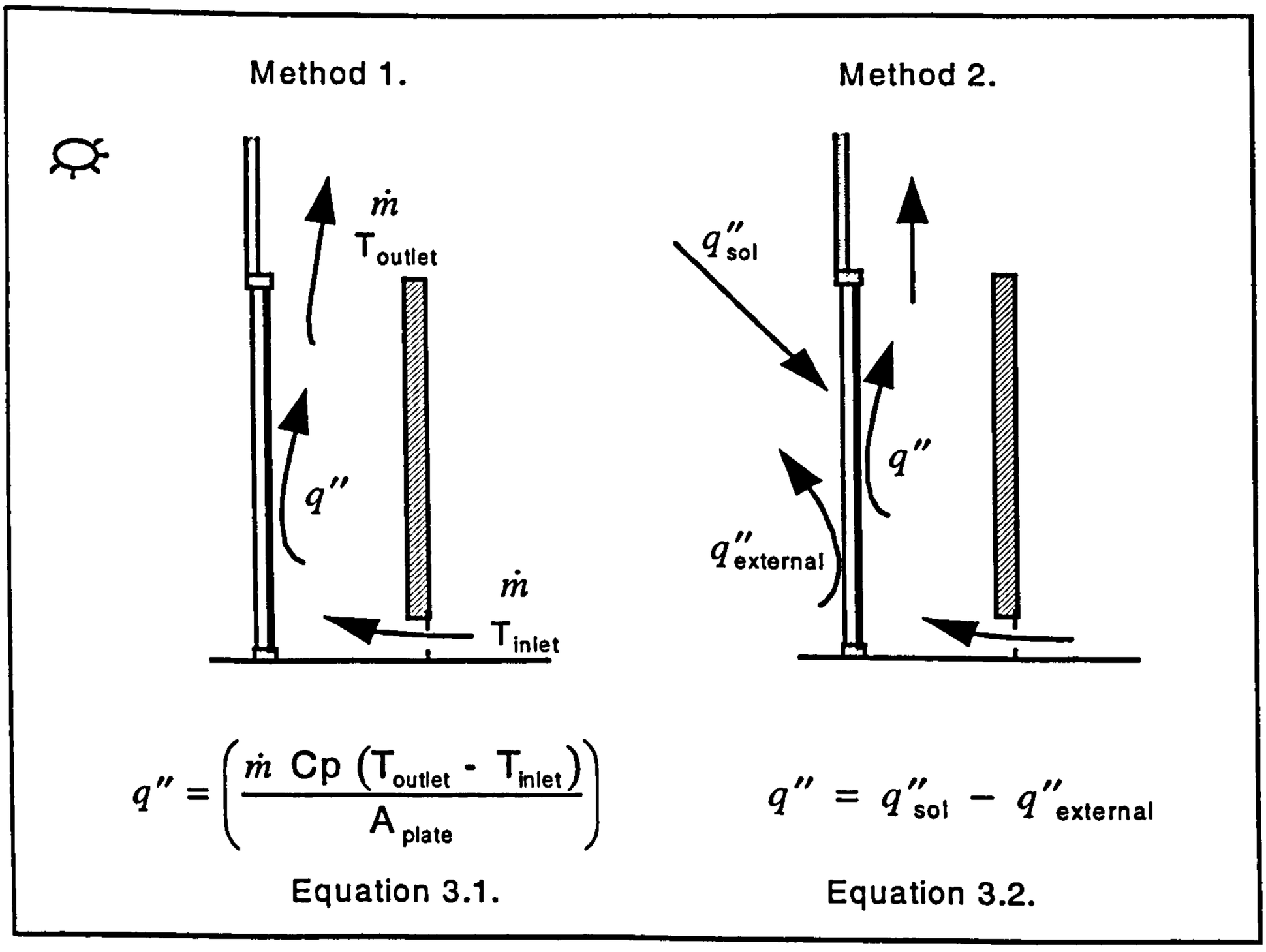

$$q'' = \left(\frac{\dot{m}\ Cp\ (T_{outlet} - T_{inlet})}{A_{plate}} \right)$$

Equation 3.1.

$$q'' = q''_{sol} - q''_{external}$$

Equation 3.2.

Figure 3.1. The two methods of calculating the energy transferred from the plate to the air within the chimney.

Method 1.

This method relied upon the accurate measurement of both the air temperature and velocity profiles at the inlet and outlet of the chimney. Accurate measurement of low air velocities was inherently difficult and thus the level of uncertainty associated with such measurements was relatively high[2] [3]. Additionally, as both mass flow rate and energy gained by the air required the use of air velocity measurements, uncertainties in this variable would tend to be magnified when the dependant variables were compared.

Method 2.

With this method the energy balance at the plate between the solar energy absorbed by the plate and the energies transferred from the plate to the outside environment and to the air within the chimney required calculating. There were therefore several sources of uncertainty, both with the measurements and through the calculations undertaken. These uncertainties were; the accuracy with which the solar energy absorbed by the plate could be obtained from the measured solar data and the ability with which the balance between the energy transferred from the plate to the outside environment and that within the chimney could be resolved.

Conclusion as to the best approach to the rig design

Consideration of the prime purpose of the experimental results, i.e. that of comparison with mathematical models and in particular CFD predictions of the flow created by an isoflux plate, provided the key to which variable was to be used as the independent variable. If plate temperature was used as the independent variable, then as plate temperature distribution was related to the flow within the chimney, this would require that the plate temperature was input accurately to a CFD model to obtain a correct prediction of the mass flow rate. This approach would therefore only allow comparisons where actual plate temperatures for a given heat flux were known a priori from the experimental investigation. This would therefore restrict the potential of further parametric testing of chimney configurations to that modelled experimentally.

Thus for the purpose of comparison between measured data and CFD predictions it was deemed most appropriate to express the mass flow rate in terms of the energy transferred from the plate to the air. Of the two methods

available for calculating this, the calculation of the energy balance at the plate eliminated the need for accurate velocity profile measurements at the chimney outlet. Such measurements were inherently difficult as highlighted previously and further complicated by the likelihood of reverse air flows, as demonstrated by Sparrow et al [4].

The level of uncertainty in the energy balance approach is now considered.

3.3 Quantification of uncertainty in the resultant data by sensitivity analysis.

This required that:

- The level of uncertainty in all the variables that influence the operation of the chimney were identified and quantified.
- The sensitivity of the key independent variable to the uncertainty in the dependant variables was established. In this way the total level of uncertainty in the resultant data could be quantified and methods of reducing the uncertainty through the rig design and experimental procedure undertaken.

To undertake a sensitivity analysis of a physical process required that a mathematical model was developed that allowed the effects of the levels of uncertainty identified in the physical variables to be tested.

Once the level of uncertainty within the model had been established and as far as possible reduced to a minimum, it was important that the mathematical model was empirically validated to ensure that it accurately predicted the physical process within the level of confidence calculated.

3.3.1 Uncertainty in model input variables.

The only practical method of obtaining realistic values of the level of uncertainty associated with the variables that could not be directly measured, was to undertake a literature search of all quoted values for each variable. In this way the range of values obtained gave a good idea of the extent of the most likely values for each variable and thus its associated uncertainty.

The sources of information were: CIBSE[5] and ASHREA[6] manuals and Heat transfer texts[7][8].

Table 3.1. shows the range of values between which the variables are most likely to fall and also the most frequently quoted value or the mean, if no value was predominant.

Variable	Range of values	
	Max / Min	Most common
Conductivity of glass (W/m °C)	1.4 / 0.78	1.1
Density of glass (kg/m^3)	2700 / 2500	2500
Cp of glass (kJ/kg °C)	0.84 / 0.75	0.8
Conductivity of plate (W/m °C)	240 / 236	237
Density of plate (kg/m^3)	2707 / 2700	2700
Cp of plate (kJ/kg °C)	0.903 / 0.896	0.900
Emissivity of glass	0.95 / 0.88	0.9
Absorptivity of glass (/m)	12 / 4	8
Width of glass (mm)	+/- 0.2	4
Width of plate (mm)	+/- 0.1	2
Internal convective heat transfer coefficient (+/- 50%) (W/m^2 °C)	11.25 / 3.75	7.5
Inter plate / glazing convective heat transfer coefficient (+/- 25%) (W/m^2 °C)	4.38 / 2.63	3.5
External convective heat transfer coefficient Laminar (+/- 50%)	6.45 / 2.15	4.3
Turbulent (+/- 50%) (W/m^2 °C)	24.9 / 8.30	16.6
Temperature of ambient environment (°C)	$T_{external}$ 0~ -6	$T_{external}$ -6

Table 3.1. Identified ranges of uncertainty for all variables effecting the flow within a solar chimney

3.3.2 Approach to undertaking the sensitivity analysis

Two basic approaches may be used for a sensitivity analysis;

- the simultaneous approach
- the one at a time approach

With the simultaneous approach all of the variables are varied across the range of identified uncertainty simultaneously and through the analysis of a large number of simulations, the overall level of uncertainty in the results is established. The Monte Carlo Technique is often used for this type of analysis[9]. The disadvantage of this method is that although interaction of each of the uncertainties in the various variables is fully accounted for, the effect of individual variables is masked. Thus for the purpose of refining the rig or the experimental procedure to minimise the effects of the uncertainty

through knowledge of the effects of individual variables, this approach is of little assistance.

The one at a time approach is so called because a model is developed and the result noted when all of the variables are at their most likely values. Then the value of each variable in turn is varied across the range of uncertainty identified. In this way the effect of the uncertainty in each of the variables is identified explicitly and quantified.

The major drawback of this method is that by testing each variable independently it assumes that the effect of each variable is independent of all others and that it is linear across the range tested. The validity of this assumption could however be tested.

Conclusion of the approach to undertaking the sensitivity analysis

To enable the model to be assessed for the influence of uncertainties in individual variables, the one at a time approach was adopted. The result of a one by one testing regime allowed the variables that cause the greatest level of uncertainty in the measured data to be readily identified and ranked in order of influence. The result of such ranking identified the major sources of uncertainty and thus allowed effort to be concentrated, through the design of the rig to minimise the effects of such variables.

3.3.3 Sensitivity of solar radiation transmitted through the glazing to uncertainty in associated variables

The value of the solar radiation transmitted through the glazing depended upon the level of both direct and diffuse (sky and ground reflected) solar radiation components incident upon the glazing and the amount of radiation transmitted through the glazing. The values of both of the components of incident solar radiation could be measured and were subject to the accuracy of the instruments used. The value of transmitted radiation was however dependant upon the physical properties of the glass and the angle of incidence of both components of solar radiation.

The variables that affect the value of transmitted solar radiation were identified and the ranges of their uncertainty established.

Variable	Value	Range of uncertainty
Extinction coefficient (/m)	8	+/- 50%
Glass thickness (mm)	4	+/- 0.2
Angle of incidence of incident diffuse solar radiation (°)	59.5	+/- 5
Glass refractive index	1.52	+/- 0.02
Day number		+/-1
Time (minutes)		+/- 5
Latitude and Longitude (″)		+/- 1
Orientation (°)	180	+/- 1

Table 3.2. Identified ranges of uncertainty for all variables effecting the value of solar radiation transmitted through the glazing.

The model of solar transmission by the glazing is given in Appendix B.

The sensitivity of solar radiation transmitted through the glazing to the uncertainties in the identified variables was assessed. The results of this are given in table 3.3. The angle of incidence of the solar radiation directly affects its transmission through glass, therefore variables whose uncertainty caused changes in the angle of incidence were quantified in terms of the change in this angle.

Variables	Effects of the identified level of uncertainty
Extinction coefficient and thickness	2.2 - 5.4 % difference in radiation transmitted
Angle of incidence of incident diffuse solar radiation	3.2 - 5 % difference in radiation transmitted
Glass refractive index	0.5 % difference in radiation transmitted
Day number	< 0.5° change in angle of incidence
Time	0 - 1° change in angle of incidence
Latitude and Longitude	< 0.02° change in angle of incidence
Orientation	0 - 1° change in angle of incidence

Table 3.3. Uncertainty in solar radiation transmitted through the glazing to identified uncertainty in the independent variables

The effect of an error in the angle of incidence on the solar radiation transmitted through the glazing was dependant upon the actual angle of incidence. The effect on solar radiation transmitted was therefore calculated for errors in a range angles of incidence.

Angle of incidence (°)	% Changes in solar radiation transmitted for given errors in angle of incidence			
	+2°	+1°	-1°	-2°
40	-0.3	-0.2	0.1	0.2
60	-1.8	-0.9	0.8	1.5
70	-5.1	-2.4	2.2	4.3
80	-16.9	-8.2	7.7	14.9
85	-40.3	-19.7	19.0	37.1

Table 3.4. Percentage change in solar radiation transmitted for a range of angles of incidence.

From table 3.4. it can be clearly seen that an error in the angle of incidence of as little as 1° , potentially created a significant error in the calculated solar radiation transmitted through the glazing. This was further compounded by the fact that the experiments were conducted across the summer solstice period when the minimum angle of incidence for a vertical south facing facade rose from over 39° at equinox to over 62° at solstice.

3.3.4 Testing the level of uncertainty in solar variables.

With potentially such large errors being incurred in the calculation of the solar radiation dependant variable, a method of assessing the validity of the assumed levels of uncertainty was sought. The CM5 solarimeter manufactured by Kipp and Zonen[10] used in this investigation uses a matt black pyranometer to measure the incident flux. This is covered by two glass domes.

Consideration of the operation of such an instrument raised the question as to its effectiveness when used inside a space i.e. behind a sheet of glazing. The pyranometer is non sensitive to incident radiation wavelength however the two glass domes absorb any incident long wave radiation reducing transmission to the wavelength range 305 - 2800 nm i.e. the whole solar spectral distribution. Thus the addition of a third sheet of glass it was proposed, would not inhibit the operation of the pyranometer and, give a true reading of the solar radiation passing through such glazing. Although such operation was agreed by the

manufacturers[11], the calibrated accuracy was then not deemed to hold true. Alternative figures were not available however the manufacturers considered the effects to be small.

In light of this a series of tests were undertaken with both externally and internally mounted solarimeters. The direct and diffuse solar radiation components were measured externally and the equations given in Appendix B used to calculate the solar radiation transmitted through the glazing. This was then compared directly to the data obtained from the solarimeter mounted internally behind a sheet of glass.

The externally mounted global and diffuse solarimeters were mounted on a rig that had an orientation established to significantly better than 0.5° of azimuth[12]. All the solarimeters used in the test were calibrated against each other and a standard instrument with a manufacturers specified level of uncertainty of +/- 4.5%[10]. The maximum difference found was less than +/- 0.3% of the reading of the standard instrument at all times. Thus the maximum error of the instruments was taken to be +/- 4.8%.

The tests were undertaken over a period of 5 days with a variety of weather conditions, to enable the assumed effective angle of incidence of diffuse radiation to be assessed along with all other variables that affect the direct beam radiation.

Figure 3.2. shows the result of the comparison between the measured and calculated rate of solar radiation energy transmission through the glazing of the rig. The error bars associated with the calculated values of transmitted solar radiation are +/- 3%. Thus the certainty that the error due to the calculation procedure was within this value was very high for values of incident solar radiation greater than 100 W/m^2. The values less than this were at the extremes of the day when the angle of incidence was approaching 90° and the errors in transmission magnified.

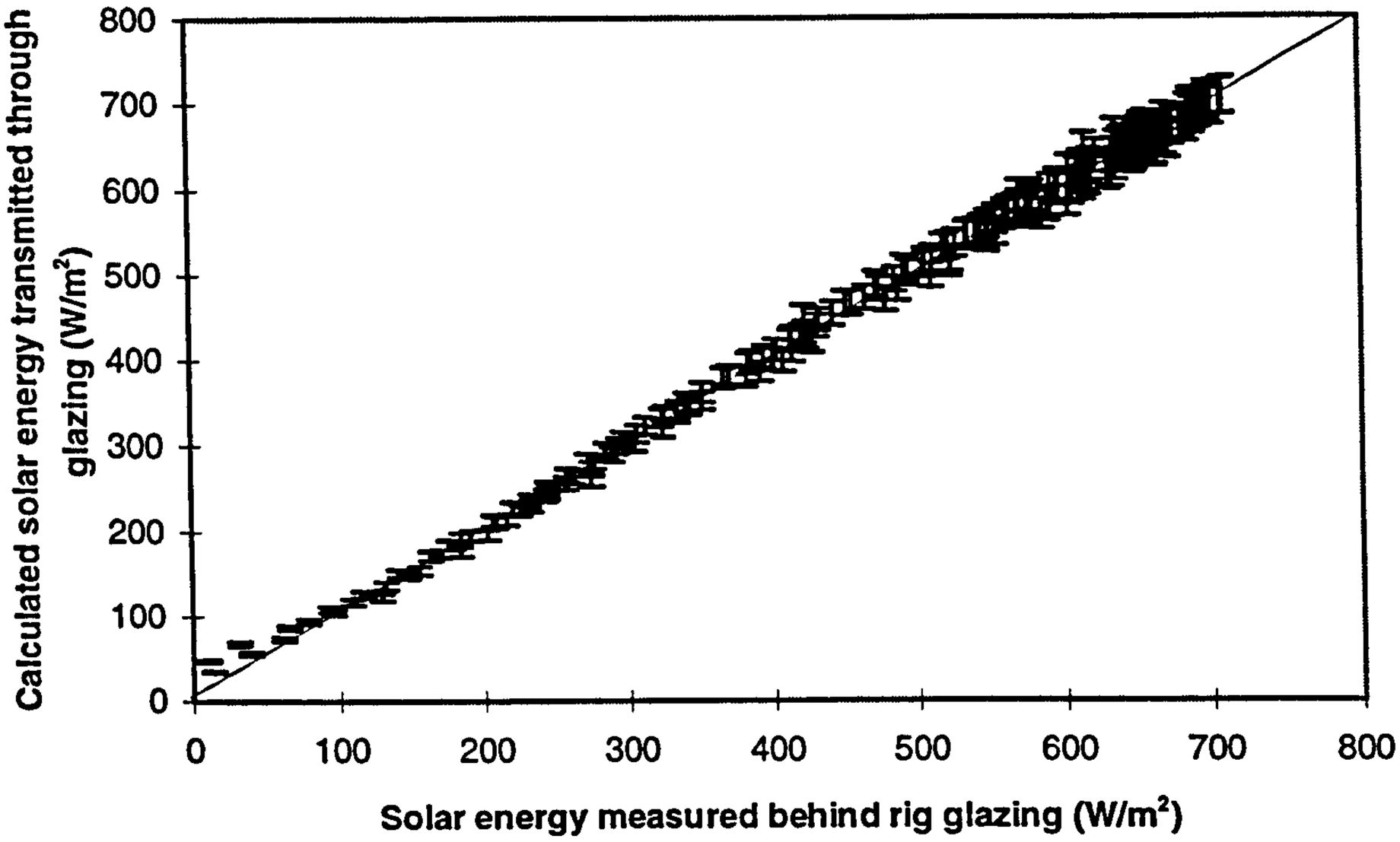

Figure 3.2. Comparison of calculated and measured solar radiation transmitted through glazing

For all experiments a lower value of 100 W/m^2 solar energy transmitted through the glazing and a maximum angle of incidence of 85° were set as the limits of data recording. In this way the overall uncertainty of the solar radiation transmitted through the glazing was considered to be reduced to an acceptable value with a high level of confidence. The highlighting of the potential uncertainty associated with time measurements was resolved by limiting the logging periods to one day. In this way the clock within the logger was checked daily and the level of uncertainty all but eliminated from this variable.

To calculate the overall uncertainty in the value of the solar radiation transmitted through the glazing, Taylor[13] suggested that for uncertainties that were random and independent, the product and quotient could be calculated through quadrature addition of the fractional uncertainties.

Such that; $U_{Total} = \sqrt{U_1^2 + U_2^2 + ... + U_n^2}$ Equation 3.3.

Where U_T is the total fractional uncertainty
U_1 is the fractional uncertainty in variable 1
n is the total number of variables

The uncertainties in the variables required for calculation of the solar radiation transmitted through the glazing were due to the instrument uncertainties and the calculations undertaken and thus were independent of each other. Thus the overall level of uncertainty in the solar radiation transmitted through the glazing was calculated as:

$$U_{Sol\ trans} = \sqrt{4.8\%^2 + 3\%^2} \qquad = +/- 5.7\%$$

3.3.5 Sensitivity analysis of solar chimney variables

To validate the mathematical model developed to test the sensitivity of the solar chimney required that the resultant data from the model could be directly compared to measured data whose level of uncertainty was both minimal and quantified. For this reason the energy transferred from the plate could not be used as quantification of the uncertainty in this variable had not been established. The plate temperature however, was measured with a high degree of confidence and was directly related to the energy transferred from the plate. This was therefore used as the variable against which the uncertainty in all of the other variables was tested.

Determination of the influence of the channel depth on the mass flow rate through a solar chimney was one of the key aims of this project. Previous work detailed in Chapter Two highlighted the potential influence of channel depth, therefore for the calculation of the uncertainty of the energy balance a single flat plate was considered. This removed any uncertainty associated with the depth of the channel used on the convective heat transfer coefficient and allowed it to be defined with more certainty.

To test the validity of the mathematical model of a flat plate subject to solar radiation, a rig was constructed adjacent to the proposed position of the solar chimney. Details of the construction are given in figure 3.3.

For the purpose of the analysis, the heat transfer was assumed to be one dimensional. This assumption was considered appropriate as the plate dimensions were 1.2 * 1.5 m and set back into the wall of the rig by 0.020 m, thus the overshadowing was minimal at all but extreme solar angles of incidence. Temperature measurements of the plate showed that across the central 1.0 m of the plate width the temperature variation with position was less

less than 0.3°C. This indicated that the assumption of one dimensional heat transfer was appropriate.

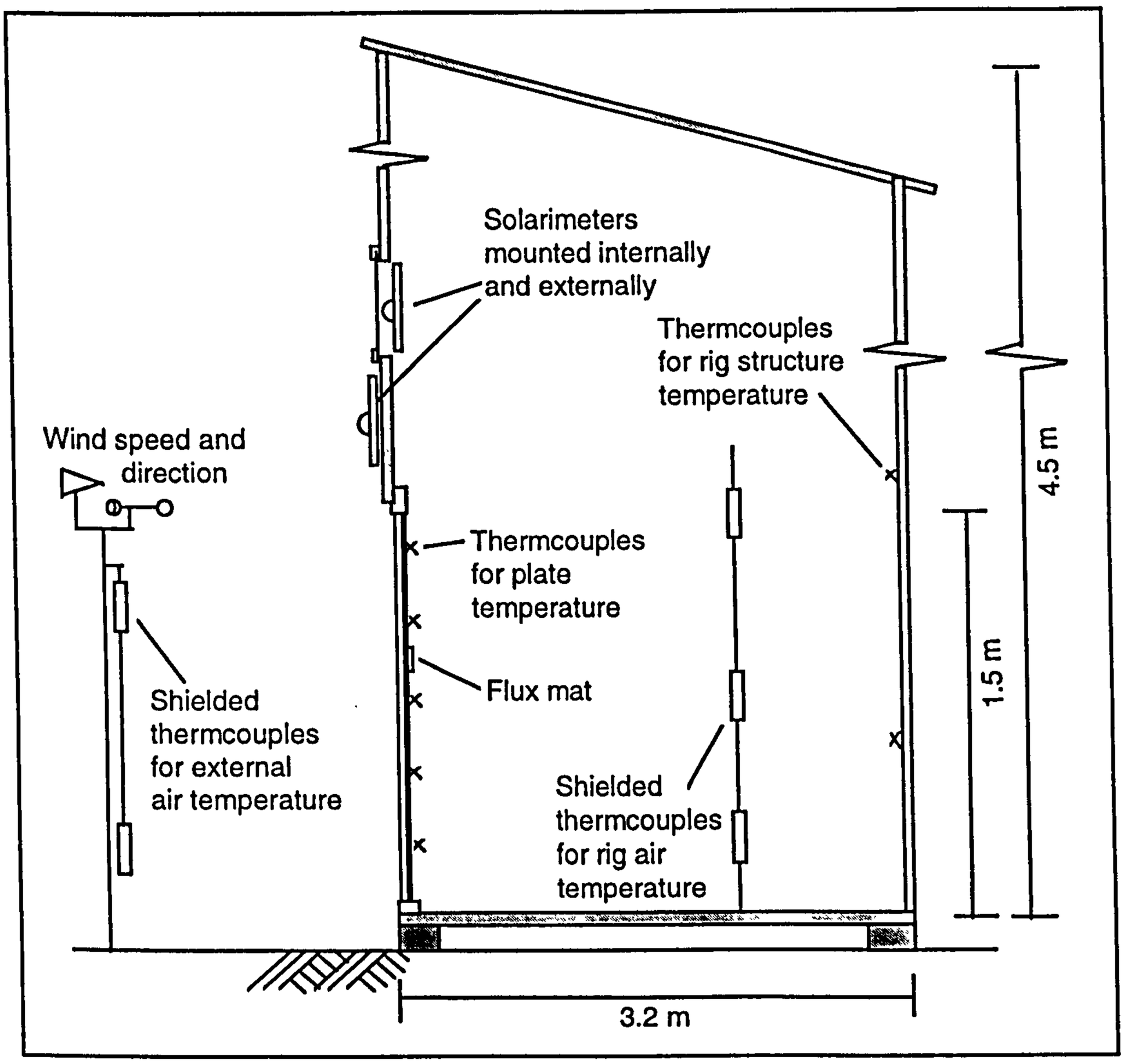

Figure 3.3. Instrumentation for logging of flat plate

The mathematical model developed of the flat plate is given in Appendix C.

The level of sensitivity of the plate temperature to the identified uncertainties in the variables was measured by establishing a base case response to a set of real weather data. This represented the model run with all the variables at their most likely values as identified in Table 3.1. The model was then run for each variable in turn at the minimum and then maximum values defined in Table 3.1. The change in temperature of the plate was recorded and represented the sensitivity of the plate to variations of the variables across the range of

uncertainty identified. The results of those variables that caused 0.1°C or greater change in temperature are shown in table 3.5.

Variable	Base case Value	Minimum case (Value) Temperature difference (°C)	Maximum case (Value) Temperature difference (°C)
Glass conductivity (W/m°C)	1.1	(0.8) +0.2	(1.4) -0.12
Glass emissivity	0.9	(0.88) +0.17	(0.92) -0.17
Plate emissivity	0.93	(0.91) +0.22	(0.95) -0.22
Emissivity of shed	1.0	(0.95) +0.42	(1.0) 0
Absorptivity of glass (/m)	8	(4) +0.23	(12) -0.29
Solar absorptivity of plate	0.93	(0.91) -0.52	(0.95) +0.52
Shed air temperature (°C)	12	(11.5) -0.24	(12.5) +0.24
External air temperature (°C)	10	(9) -0.12	(11) +0.12
Ambient temperature for radiation (°C)	10	(4) -0.17	(10) 0
Internal plate convective heat transfer coef. (W/m^2 °C)	7.5	(3.75) +6.9	(11.25) -4.75
Inter plate-glazing convective heat transfer coef. (W/m^2 °C)	3.5	(2.63) +0.41	(4.38) -0.37
External convective heat transfer coef. Laminar / turbulent (W/m^2 °C)	Laminar 4.3	(laminar 4.3) 0	(Turbulent 16.6) -2.43
External convective heat transfer coef. Laminar +/- 50% (W/m^2 °C)	4.3	(2.15) +0.89	(6.45) -0.67
External convective heat transfer coef. Turbulent +/- 50% (W/m^2 °C)	16.6	(8.3) +1.3	(24.9) -0.69
Solar radiation transmitted + / - 5.7 % (W/m^2)		(-5.7%) -1.48	(+5.7%) +1.48
Measured temperatures (°C)		-0.2	+0.2

Table 3.5. Results of sensitivity analysis for variables that produced a change in plate temperatures ≥ 0.1°C.

Table 3.6. shows the input variables in ranked order of their effect upon the plate temperature:

Variable	Absolute change in plate temperature (°C)
Internal plate convective heat transfer coefficient. +/- 50%	6.9
External convective heat transfer coefficient. Laminar / turbulent	2.43
Errors in solar radiation transmitted through glazing (+/- 5.7%)	1.48
External convective heat transfer coefficient equation. +/- 50%	1.3
Solar absorptivity of plate	0.52

Table 3.6. Ranked sensitivity of plate temperature to uncertainty in variables.

From table 3.6. it is apparent that the identified uncertainty of the convective heat transfer coefficients created the greatest levels of uncertainty in the plate temperature. There was therefore a need to investigate these identified levels of uncertainty and assess if they were appropriate and if they could be reduced.

3.3.6 Reduction of variable uncertainty

- Solar absorptivity of the plate.

  The long wave absorptivity of the plate was measured to an accuracy of +/- 2% using an emissometer [14]. The solar absorptivity of a surface may differ from that of the long wave. Incropera et al [7] however notes that black paint has a constant emissivity in both the long and solar spectrum. Thus the uncertainty level of +/- 2% could not be practically reduced and was considered as appropriate.

- Errors in calculation of solar energy transmitted through the glazing.

  The investigation into these errors have been detailed previously and the level of +/- 5.7% was appropriate considering the instruments used and levels of uncertainty associated with the variables that directly influence this calculation.

- Internal convective heat transfer coefficient.

  To reduce the uncertainty of the internal convective heat transfer coefficient, a heat flux mat was placed on the internal face of the plate and logged for a period of time. The uncertainty associated with the flux

mat was +/-5%. The heat flux mat was given the same internal coating as the plate to ensure that the radiative component of the flux leaving the mat was the same as that leaving the plate internal surface. The convective heat flux was then calculated as;

$$q''_{conv\ internal} = q''_{Total\ internal} - q''_{rad\ internal} \qquad \text{Equation 3.4.}$$

Where $q''_{rad\ internal}$ was calculated using plate and rig structure temperatures using equation 3.5.

$$q''_{rad\ internal} = \sigma\ \varepsilon_{plate}\ (T^4_{plate} - T^4_{rig\ wall}) \qquad \text{Equation 3.5.}$$

The absorptivity of the rig was assumed to be 1.0.

To calculate the overall level of uncertainty in the internal convective heat transfer coefficient required that the uncertainties resulting from both equations 3.4. and 3.5. were calculated. Taylor[13] suggested that if the uncertainties were random and independent then the sum or difference of the uncertainties could be calculated by adding the uncertainties in quadrature addition.

Such that; $U_{Total} = \sqrt{U_1^2 + U_2^2 + \ldots + U_n^2}$ Equation 3.6.

Where U_{Total} is the total uncertainty
U_1 is the uncertainty in variable 1
n is the total number of variables

The uncertainties in all of the variables required for calculation of the convective heat transfer coefficient were due to independent instrument uncertainties and thus were independent of each other.

From equation 3.5.

$$U_{q''_{rad\ internal}} = \sqrt{2\%^2 + \left(\frac{\sqrt{(4 * 0.2^2) + (4 * 0.2^2)}}{T_{mean}}\right)\%^2} = +/- 2.8\%$$

$$U_{q''_{internal}} = +/- 5\%$$

From equation 3.4. $U_{q''_{conv\ internal}} = \sqrt{5\%^2 + 2.8\%^2} = +/- 5.8\%$

Equation 3.7. was then used to calculate the convective heat transfer coefficient.

$$h_c = \frac{q''_{conv\ internal}}{T_{plate} - T_{rig}} \qquad \text{Equation 3.7.}$$

The overall uncertainty in the internal convective heat transfer coefficient was:

$$U_{h_c} = \sqrt{5.8\%^2 + \left(\frac{\sqrt{0.2^2 + 0.2^2}}{T_{mean}}\right)\%^2} = +/- \ 5.9\%$$

The flat plate was logged for a 6 day period to assess if the calculated value of uncertainty was appropriate. Figure 3.4. shows the results with error bars of +/- 5.9% applied. It can be seen that this level of uncertainty encompasses the best fit line established for the full 6 day period. This level of uncertainty was therefore taken as appropriate for the internal heat transfer coefficient.

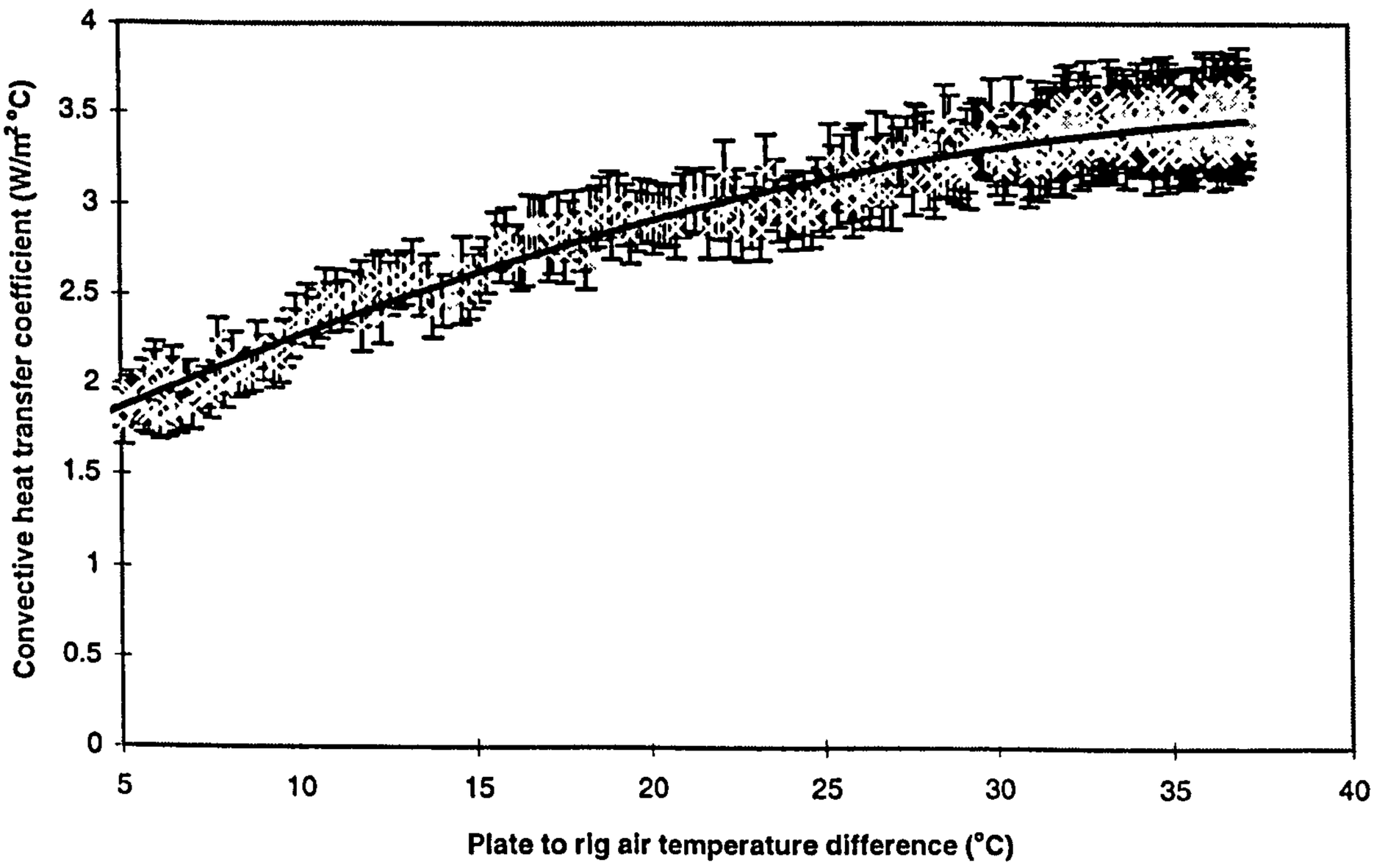

Figure 3.4. Internal heat transfer coefficient plotted against plate to air temperature difference for one day and best fit line for the 6 day period.

- External convective heat transfer coefficient.

  Lastly the question of reducing the uncertainty associated with the external convective heat transfer coefficient was addressed.

  The value of the flux absorbed by the plate and that transmitted internally had been calculated, thus considering the heat balance given in Equation 3.2. a correlation was sought for the external heat transfer coefficient between the glazing temperature and the external environmental variables.

An attempt was made to correlate the coefficient to the three variables; wind speed, direction and difference in glass and air temperature, however no correlation was achieved. A second attempt to correlate the heat flux to temperature difference and local wind speed across the glass, as measured at a distance of 0.075m normal to the glass was made. Again however no correlation could be achieved that would reduce the identified uncertainty.

As no adequate correlation could be established to solve the energy balance an alternative approach was sought. Having resolved the uncertainty in the internal convective heat transfer coefficient and obtained a value for the solar radiation absorbed by the plate, the energy balance for the flat plate could be solved. This therefore offered the following alternative; to monitor the flat plate alongside the chimney, solving the energy balance and thus obtaining a figure for the heat loss to the external environment at every logging interval. This required that the flat plate rig was fully instrumented and data logged throughout the duration of the investigation into the solar chimney. In the absence of any alternative means of calculating the heat lost to the ambient, this approach offered a practical solution and the potential to quantify the uncertainty in the energy transferred from the plate to the air within the solar chimney.

Quantification of the uncertainty in the external heat transfer coefficient required the addition of the uncertainties associated with the solar radiation absorbed by the plate and that transferred to the rig.

$$q''_{external} = q''_{sol} - \left(q''_{conv\ internal} + q''_{rad\ internal}\right) \qquad \text{Equation 3.8.}$$

$$q''_{sol} = q''_{soltrans} \times \text{Plate absorptivity} \qquad \text{Equation 3.9.}$$

$$U_{q''_{sol}} = \sqrt{5.7\%^2 + 2\%^2} = +/- \ 6.1\%$$

From equation 3.7.

$$U_{q''_{conv\ internal}} = \sqrt{5.9\%^2 + \left(\frac{\sqrt{0.2^2 + 0.2^2}}{T_{mean}}\right)\%^2} = +/- \ 6.0\%$$

$$U_{q''_{rad\ internal}} = +/- \ 2.8\%$$

$$U_{q''_{external}} = \sqrt{6.1\%^2 + 6.0\%^2 + 2.8\%^2} = +/- \ 9.0\%$$

3.3.7 Results of uncertainty reduction

The mathematical model was run with the new levels of uncertainty. The results of this are given in table 3.7.

Variable	Base case Value	Minimum case (Value) Temperature difference (°C)	Maximum case (Value) Temperature difference (°C)
Internal plate convective heat transfer coefficient. +/- 5.9%	7.5	(7.06) +0.81	(7.94) -0.54
External convective heat transfer coefficient. +/- 9.0%	16.6	(15.11) +0.21	(18.09) -0.11

Table 3.7. Resultant levels of uncertainty caused by key variables after measures taken to minimise their effects.

3.3.8 Testing independence of model input variables

As previously stated, one disadvantage of the one at a time approach to sensitivity testing is that it assumes that the effects of the input variables are linear and independent. To assess whether this was actually the case the model was run with all of the input variables applied simultaneously to give first a positive change in temperature and then a negative change. This gave the

upper and lower boundary values that were then plotted against the base case predicted temperatures with the individual errors arising from the identified uncertainty applied appropriately.

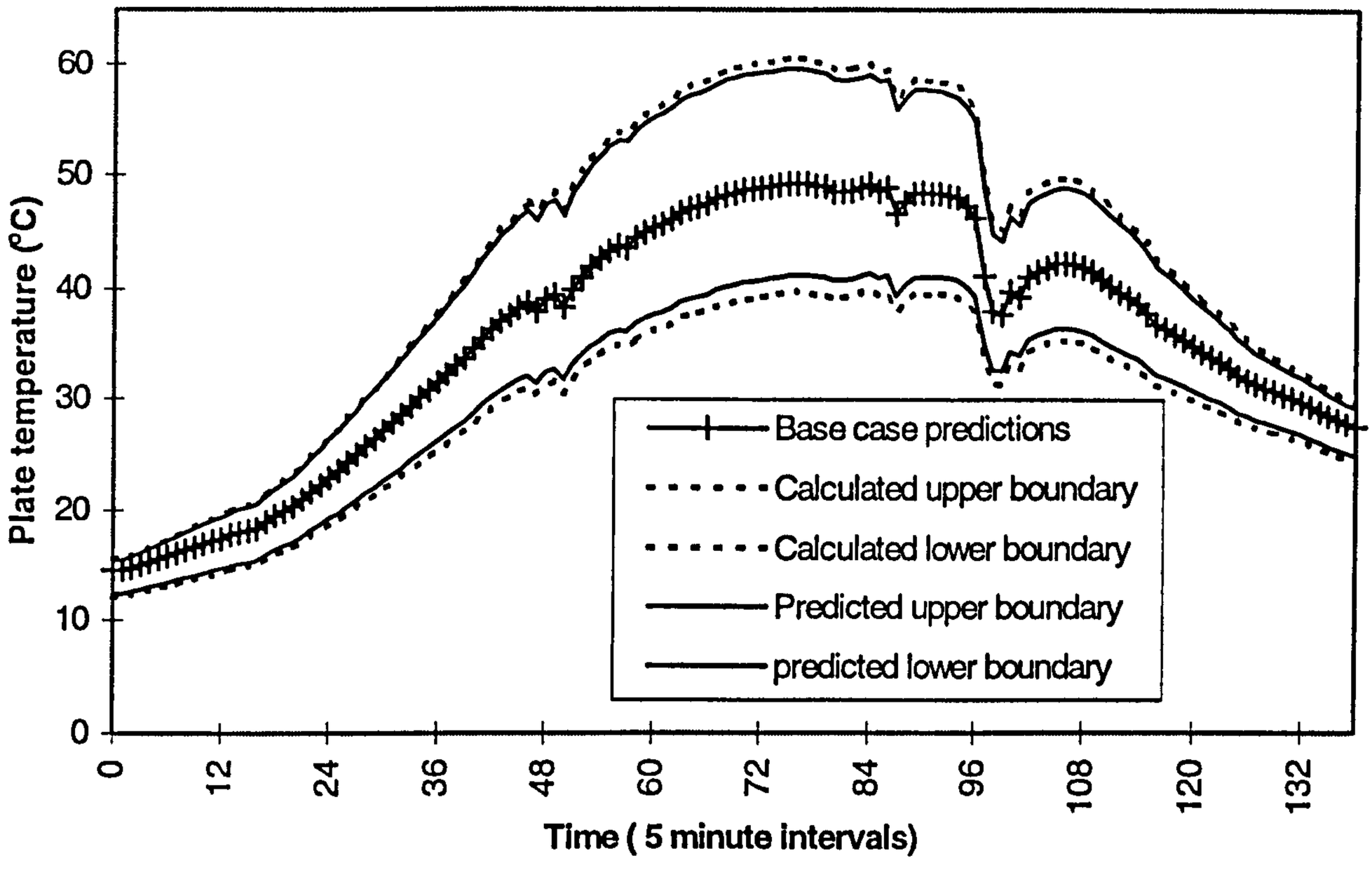

Figure 3.5. Comparison of calculated and predicted plate temperatures at the upper and lower boundaries

Figure 3.5. shows that the results are very similar for application of the uncertainties individually or simultaneously. This indicates that the assumption that the effects of variable uncertainty on the plate temperature were largely independent of each other was correct and the one at a time approach to sensitivity analysis was valid for this application.

3.3.9 Testing the validity of the mathematical model

For the analysis undertaken the bands of uncertainty adopted were such that there is a minimal i.e. less than 5% chance that each variable was outside the range identified. Thus the upper and lower bands of certainty had a 95% confidence level of not being exceeded.

The effect of the uncertainty in each variable was quantified and then the total level of uncertainty, positive and negative from the base case, was calculated through quadrature addition. These were then applied to the base case

predictions of the model giving the upper and lower limits of the 95% confidence band.

The uncertainty in the model variables and measured data can be applied separately to their respective data sets, however any results must then be compared statistically to assess if any error is significant. Alternatively Lomas et al [9] suggested that all of the uncertainties could be applied to one data set. Then if the other data set falls outside the band of predicted uncertainty, the error would be considered as significant and the presence of additional, possibly internal model errors established.

The later of these two approaches was adopted as it allows quick evaluation of the results, without recourse to statistical analysis of significance levels.

The uncertainty associated with the measurement of the plate temperatures is +/- 0.2°C with a 95% level of confidence. This was added in quadrature to the model variable uncertainties as defined in Equation 3.10.

Upper limit of uncertainty

$$U_{+5\%} = \sqrt{(U_1^2 + U_2^2 + \ldots + U_n^2 + U_m^2)} \qquad \text{Equation 3.10.}$$

Where U_m is the uncertainty due to measurements with a 95% confidence limit

$U_{1..n} \geq 0$

$U_m \geq 0$

Lower limit of uncertainty

$$U_{-5\%} = \sqrt{(U_1^2 + U_2^2 + \ldots + U_n^2 + U_m^2)} \qquad \text{Equation 3.11.}$$

Where $U_{1..n} \leq 0$

$U_m \leq 0$

The results of this analysis are shown in Figure 3.7.

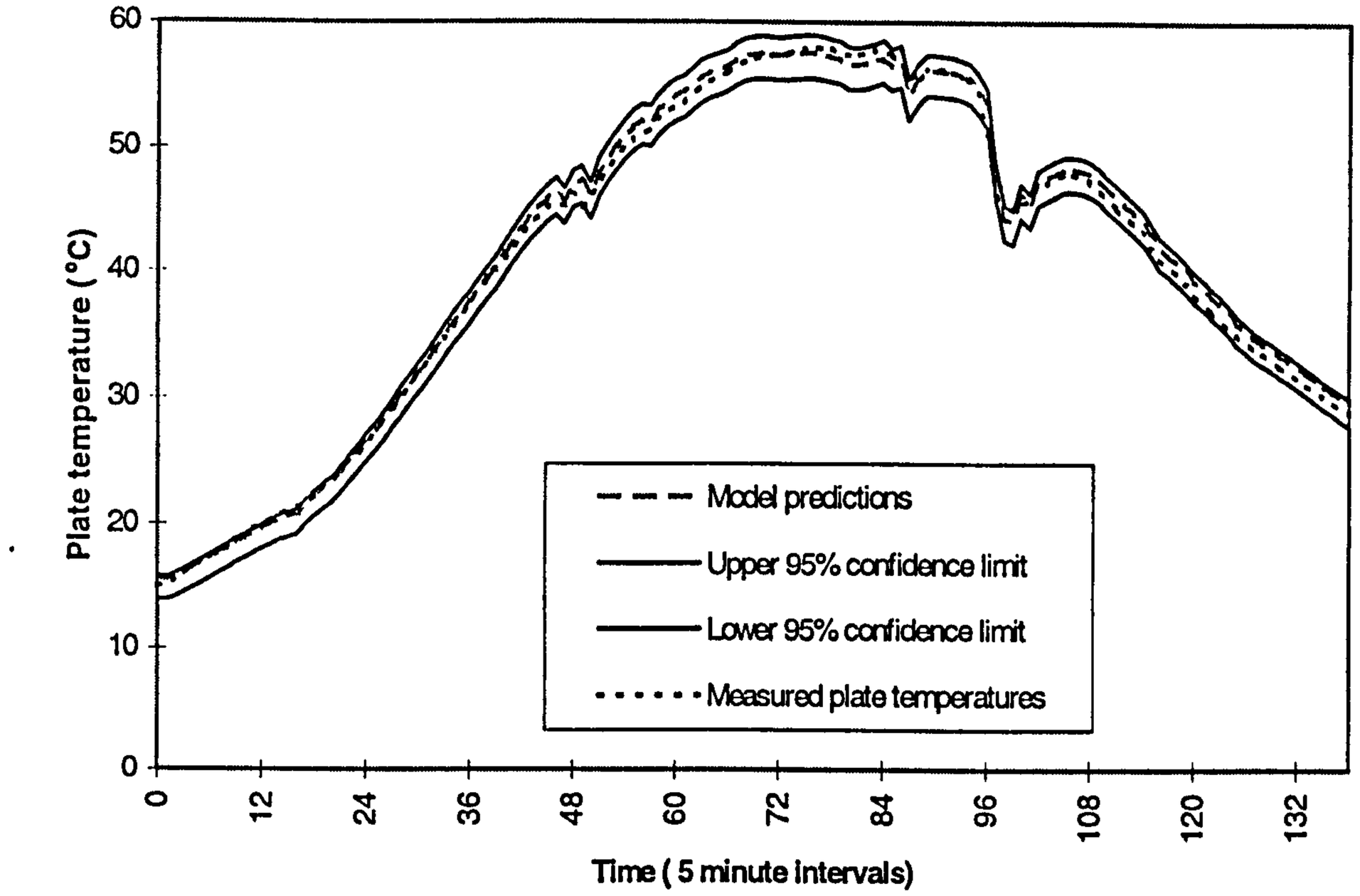

Figure 3.6. Comparison of measured data with the base case and upper and lower limits of the 95% confidence band.

Figure 3.6. shows that the actual measured value of the plate was within the 95% upper and lower confidence bands, indicating that the model predicted the response of the plate with a high level of confidence. Therefore the method of calculating the internal and external heat transfer coefficients was assumed to be effective within the levels of uncertainty adopted.

3.3.10 Total level of uncertainty in the energy transferred from the plate

Having established that the levels of uncertainty adopted were appropriate for the operation of the flat plate, the total uncertainty in the calculated energy transferred to the air within the chimney was calculated as follows:

From equation 3.2. $U_{q^*} = \sqrt{6.1\%^2 + 9.0\%^2} = +/- 10.9\%$

3.3.11 Conclusions and influences of sensitivity analysis approach to the rig design

The validation of the mathematical model showed that its ability to predict the plate temperature was high, when the external convective heat transfer coefficient was calculated through an energy balance calculation at the flat

plate. For the solar chimney therefore, the solving of the energy balance through the calculation of an external convective heat transfer coefficient in this way offered a robust method of calculating the energy transferred to the air within the chimney.

The result of this investigation was that the rig was designed to include the flat plate arrangement alongside the chimney rig as shown in plate 3.1. If this investigation had not been undertaken it would not have been possible to identify the major sources of uncertainty, reduce their effects and then quantify the level of uncertainty in the resultant data with such a high level of confidence. This would have resulted in the data being of substantially less use for comparison to and validation of, mathematical and CFD models of a solar chimney.

Plate 3.1. Front view of the experimental rig showing the flat plate to the right and the glazed panels of the solar chimney to the left

3.4 Establishing the data logging procedure

With the level of uncertainty in the data obtained from the experimental rig fully quantified, it was important that an appropriate data logging procedure was adopted. The continually varying nature of the environmental conditions required that the data logging procedure was capable of capturing the transient response of the plate to such inputs. The mathematical model developed for the sensitivity analysis was used to investigate the response of the plate to transient input variables.

The solar radiation absorbed by the plate was the input variable that was potentially subject the greatest and quickest levels of variation. Therefore the response of the plate temperature to variations in this variable was investigated.

To ensure that the true response of the plate was captured and that the volume of data was kept to a manageable level, two logging parameters were investigated:

1. The shortest time interval between data sampling required to ensure that the true response of the plate was captured.

To ensure that the sampling period was short enough to capture the response of the plate subject to a varying solar input, the mathematical model was run subject to a step variation in the level of solar energy absorbed by the plate. The values of all other variables of the model were maintained at the base case values detailed in Table 3.1. It was found that the plate responded by less than 25% of its full steady state response in 40 seconds. The data logger allowed a sampling interval of 30 seconds which was adopted as it ensured that the data sampled was a true reflection of the plate response to the variable input.

2. The longest period over which the sampled data could be averaged without masking the response of the plate to solar input variable.

To assess the effect of averaging the sampled data required that the level of attenuation of the plate temperature variations to the input was evaluated. One of the most effective methods of investigating this was to vary the frequency of the changes to the solar energy input variable. In this way the attenuation of

the response of the plate temperature could be established compared with the full response, had the plate been assumed to be at steady state i.e. assumed to have no thermal capacity. The mathematical model was set up with a sinusoidal variation in the solar radiation absorbed by the plate, based on time intervals of 1, 2, 5, 10, and 30 minutes varied about a mean of 100W/m^2 +/- 100W/m^2 . The input variations were continued until the oscillations in the plate temperature were stable. The results showed that cycles of the solar energy absorbed by the plate of less than 300 seconds were more than 80% attenuated. Thus the storage of data at 300 second intervals resulted in little loss of the plate response, longer periods would tend to mask variations in the plate response to the variable input.

From this investigation therefore the sampling period of 30 seconds and a storage period of 300 seconds was adopted. This had been shown to capture the transient response of the plate and not to mask such variations by averaging data over too long a period.

3.5 Design of the experimental rig

The rig used for the experimental investigation was situated in the Solar Annex of the Test Area at Cranfield University. The southerly elevation was open with low cut grass. The rig was constructed of timber with removable panels on the southerly facade. The inclusion of a solar chimney into the rig was therefore feasible and only required the height to be increased to allow a chimney height of up to 4.0 meters to be accommodated and the front panels replaced with glazed units.

The basic idea behind the rig is shown in figure 3.7.

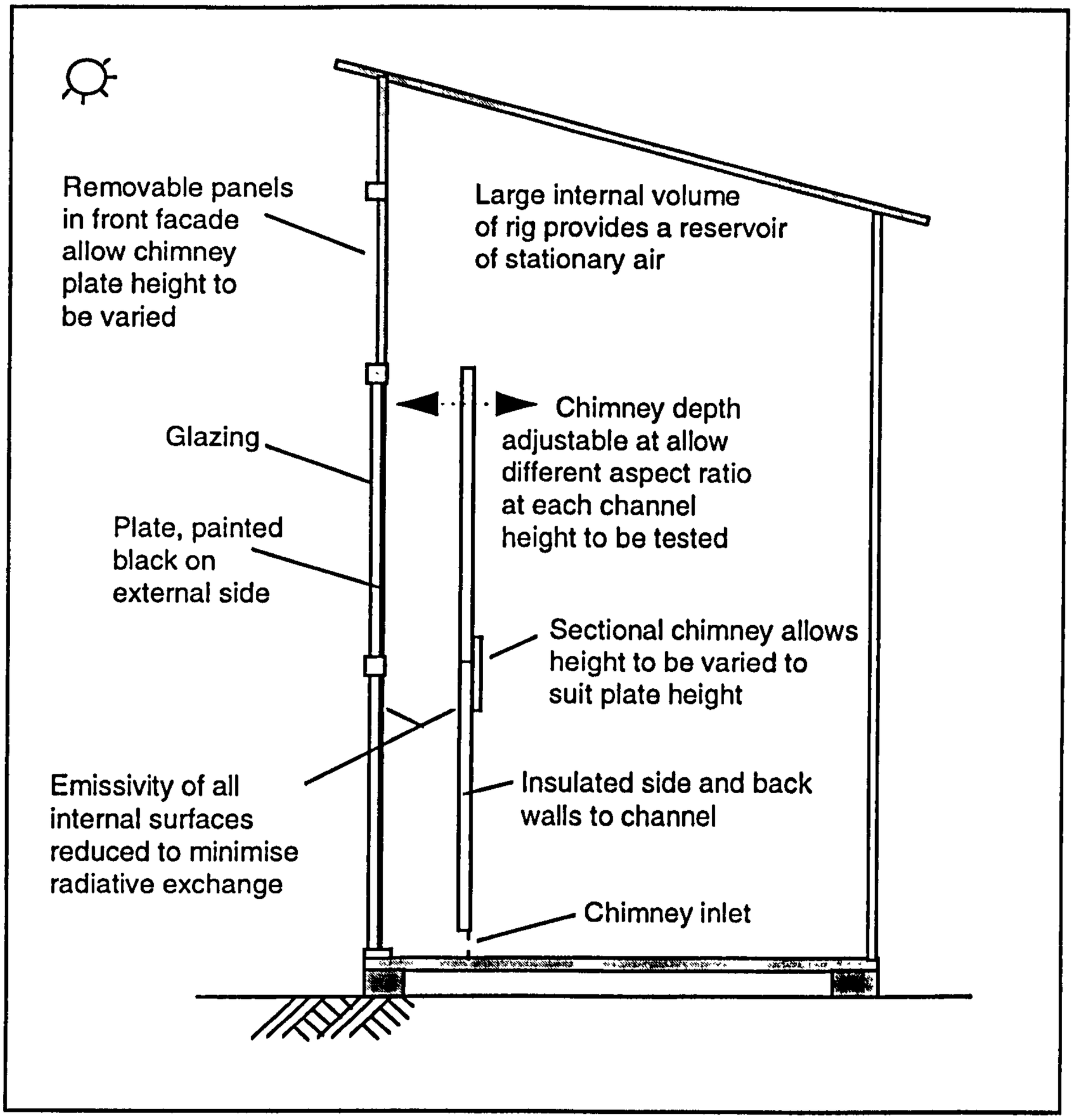

Figure 3.7. Basic rig design for solar chimney investigation

This arrangement allowed the stack pressure created within the chimney to act against a still reservoir of air. Initial trials with the flat plate arrangement however highlighted the fact that the level of stratification occurring within the rig was transient and reached a maximum of 10°C. Such a temperature gradient would have a significant influence on the mass flow rate through the solar chimney. Measures were therefore taken to minimise the occurrence of the stratification. This was most effectively achieved by allowing the hot air, exhausting from the chimney, to vent out of the rig at roof level. Fresh air was then allowed to enter the rig at approximately 1m below roof level. This resulted in mixing of the remaining volume of air within the rig.

Having determined the level of uncertainty in the energy transferred from the plate in the solar chimney it was important that all of this energy was transferred by convection to the air. To minimise radiative heat transfer from the plate its internal face was polished and the back and sides of the chimney channel were lined with aluminium foil. The emissivity of all internal surfaces was tested and found to be stable throughout the testing period at 0.04 with a level of uncertainty of +/- 2%.

To minimise heat transfer through the back and sides of the chimney, these elements were highly insulated. Various materials were considered for these elements, however 50mm Styrofoam Floormate[15] was chosen as it offered the advantage of having low thermal conductivity (0.024 W/mK) combined with a high structural strength. This allowed a sectional rig to be designed with a minimum of additional support and bracing.

The external surface temperature of the back of the channel was monitored and found not to rise above the temperature of the air within the rig. This indicated that the chimney was effectively acting as an asymmetrically heated channel with zero heat flux back and side walls.

The resulting design is shown in figure 3.8.

The inlet opening of a building component such as a solar chimney is subject to many different requirements ranging from its ability to be sealed in the event of a fire to its aesthetics. For the purpose of this investigation however an opening that could be accurately described mathematically was the prime requirement. The best opening for this was a sharp edged orifice, as the flow through such an opening was well described by Equation 2.3. To ensure that the velocity of the air passing through the inlet remained within the required velocity ranges of the measuring instruments, two different opening sizes were used. One 75mm and the other 150mm in height.

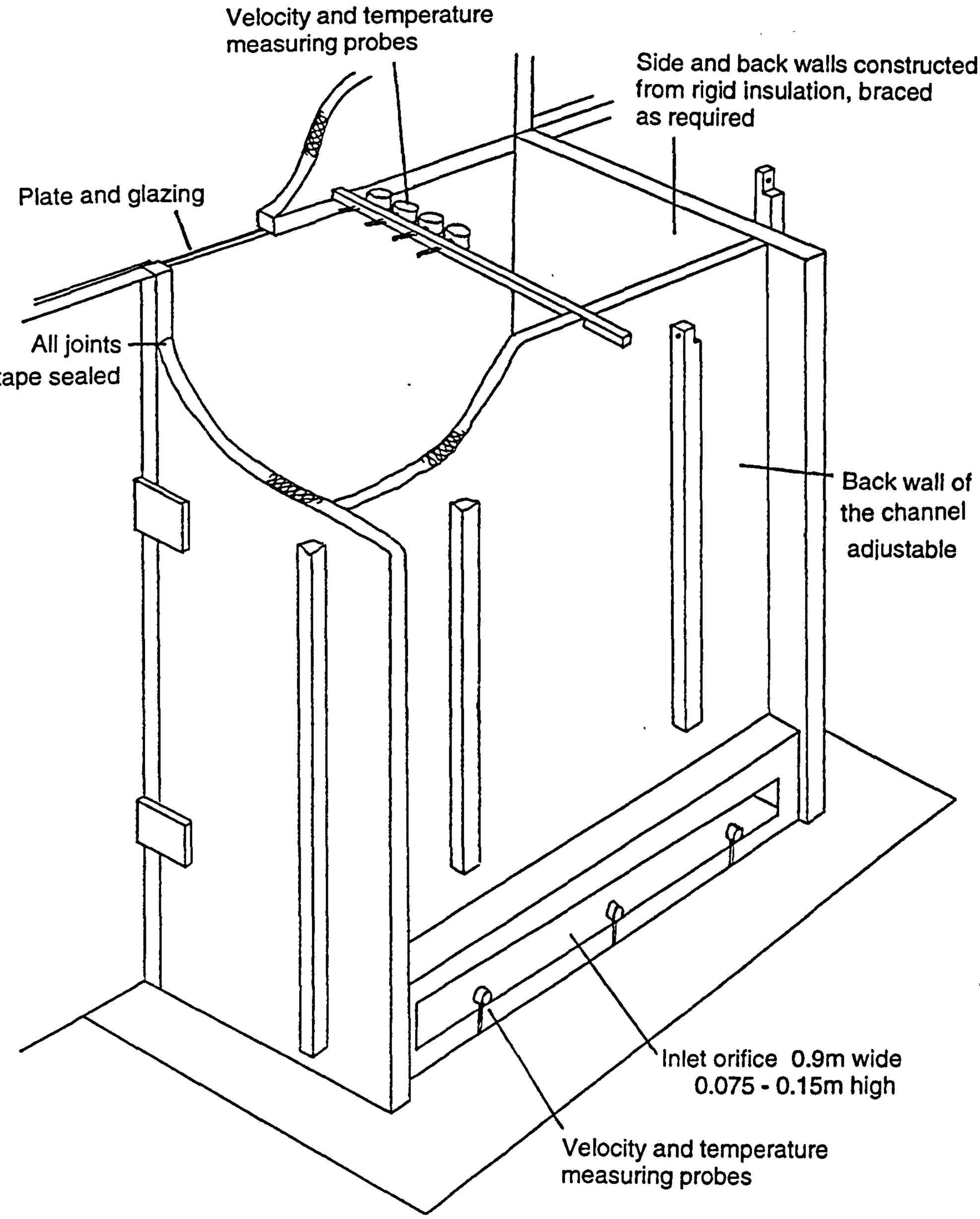

Figure 3.8. Final design of experimental rig

3.6 Instrumentation

All temperatures, except those obtained by the air velocity meters, were measured by copper / constantan (type T) thermocouples. All thermocouples were calibrated to +/- 0.2°C.

The following figure shows the distribution of temperature measurement positions throughout the experimental rig.

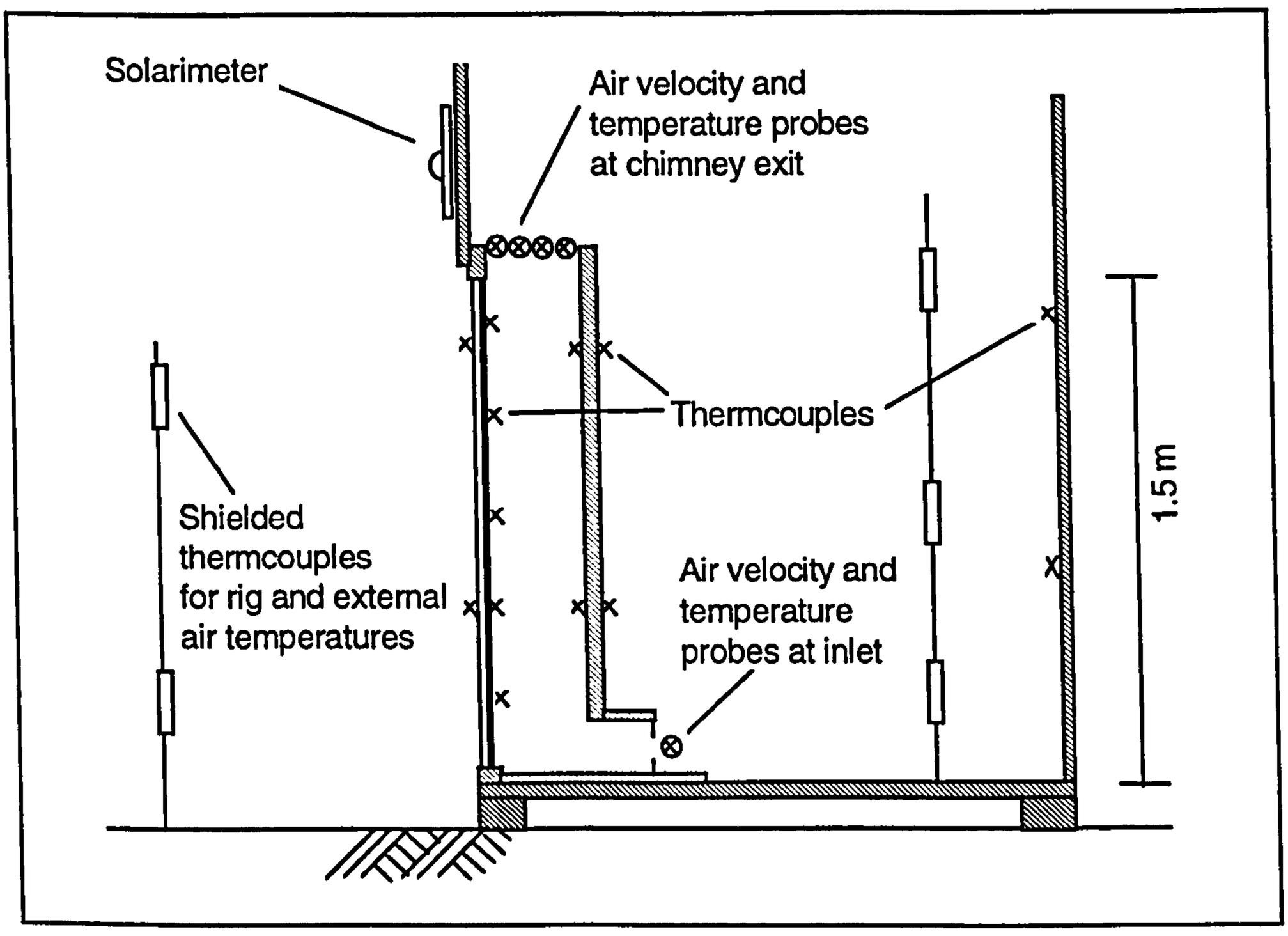

Figure 3.9. Positioning of instrumentation within experimental rig

All data was logged on a Delta T data logger [16] . This type of logger is capable of logging remotely for extended periods, however the sensitivity of the solar calculations to errors in time required that the logger was only run for one day at a time. This allowed the logger clock to be checked every day against a known time signal and thus this potential source of error was eliminated.

The error introduced by the recording of the data on the data logger was less that 0.1% of the logged value and was therefore not a significant additional source of error [16].

The solar insolation was measured by Kipp & Zonen CM5 solarimeters[10] as previously described in this Chapter.

3.6.1 Measurement of mass flow rate through the solar chimney

Spitler[2] noted the difficulties in attempting to measure low air velocities, concluding that for room air flow measurements the total error in any individual measurement was anticipated to be +12/-23%. Hobday[3] reported previous investigations into Trombe Walls where inaccuracies of up to 28% were incurred. These used single velocity measurements within the inlet duct and took no account of the inlet velocity profile. Hobday noted that the timing of smoke passing through a panel offered a reduction of such errors to between 10 and 20% for a given flow rate. Such high levels of uncertainty however reduce the usefulness of the results of an experimental investigation for comparison with mathematical models. Therefore the availability and suitability of accurate air velocity measuring instruments was examined. The requirements for this investigation were for an instrument that could measure both air velocity and temperature at a series of points, across a range of 0.05 to 1.0 m/s and 0 to 60°C. Multiple probes were required to obtain the profiles at the inlet and outlet of the chimney. The experimental rig was on a remote site with no mains power, the instruments were therefore required to operate by battery and provide an output signal appropriate for data logging.

Commercially there were found to be no instruments available therefore the potential of developing a suitable instrument was investigated. McNair[17] proposed an instrument based on high precision thermistors which proved to be appropriate for adaptation. Details of the instrument, adaptation, construction and calibration are given in Appendix D.

From the testing of the air velocity / temperature measurement instruments the following levels of uncertainty were established within 95% confidence:

Temperature	+/- 0.2%	between 5 and 60°C
Velocity	+/- 6%	between 0.05 and 0.8 m/s

The measurement of both the air velocity and temperature for the calculation of the mass flow rate at the inlet of the chimney required that the profile of both of these variables was determined accurately. The temperature was assumed to be constant as the chimney was to draw air from the rig and over the height of the inlet the temperature variation was negligible. The velocity profile however was dependant upon the mass flow rate, therefore to determine the flow rate, a full velocity profile was required.

The accurate monitoring of the velocity profile at the chimney inlet would have required a large number of probes. Therefore a rig was constructed to assess the actual profile and determine if a range of single point measurements could be used to accurately determine the flow rate.

A rig replicating the inlet configuration of the solar chimney was constructed, detailed in figure 3.10. The mass flow rate was accurately measured by a precision orifice plate[18] and manometer[19]. This allowed the flow rate to be determined to within +/-2%.

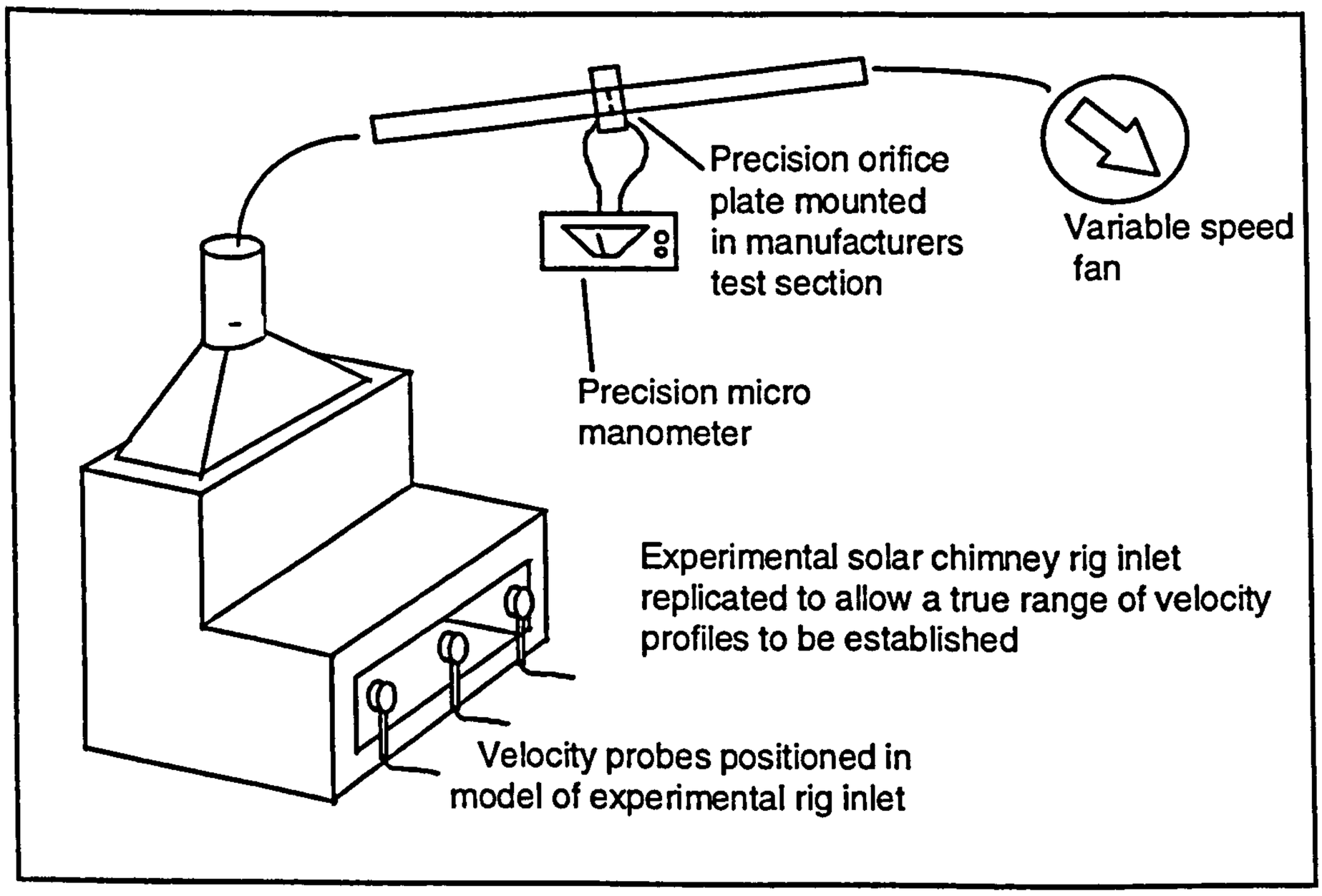

Figure 3.10. Model of experimental solar chimney inlet used to establish the inlet profile of the air across a range of mass flow rates

The mass flow rate was calculated by the velocity / temperature probes developed and compared with that measured via the orifice plate. It was found

that the mass flow rate calculated with the velocity / temperature probes with +/- 6% uncertainty applied fully encompassed the mass flow calculated with the orifice plate across both inlet sizes for velocities between 0.05 and 0.8 m/s. The uncertainty in the mass flow rate through the inlet was therefore taken as +/-6%.

3.7 Experimental procedure

To ensure that the range of experiments undertaken covered a wide range of variations in the independent variables the following testing matrix was undertaken.

	Plate height (m)			
	1.5	2.25	3.0	3.75
Inlet height (m)	0.075	0.075	0.15	0.15
Aspect ratios of channel investigated 5:1	Yes	Yes	6.67:1	No
7.5:1	Yes	Yes	Yes	8.3:1
10:1	Yes	Yes	Yes	Yes
15:1	Yes	Yes	Yes	Yes
20:1	Yes	Yes	Yes	Yes

Table 3.8. Range of physical variables investigated experimentally

The maximum physical channel depth that could be investigated was 0.45m. Therefore at the plate height of 3.75m the lowest aspect ratio of 5:1 could not be accommodated.

Each aspect ratio was logged for a minimum of 3 sunny days. This ensured that sufficient data across a wide range of values of energy transferred from the plate to the air within the chimney had been obtained. Thus any variations in flow rate, due to changes in other physical variables could then be easily identified and quantified.

Logging of the flat plate and the chimney, produced a considerable volume of data stored at 300 second intervals. It was therefore essential that the data was evaluated at the end of each experimental run to ensure that no random errors or instrument failures had occurred. To undertake the handling of the

data a visual basic program within the spread sheet Exel was written. This allowed the data to be sorted and presented graphically for evaluation without the need for manual handling.

The process of determining the overall level of uncertainty within the experimental results had highlighted two checking routes for calculations that offered the opportunity to evaluate the results for significant errors. These were; the calculation of the solar energy absorbed by the plate via the two methods highlighted previously and the checking of the mass flow rate by measurement of the velocity profile at the channel outlet. The uncertainty in the latter of these two could not be investigated until the rig was operating. The results of this are given in Chapter Four.

The flat plate was fully instrumented and temperatures logged at the same time as those in the chimney. This allowed the energy balance for the flat plate to be solved at each time interval. The determination of the energy transferred to the external environment then allowed the energy balance of the solar chimney plate to be calculated.

Although this was rather a circuitous route for the calculation of the energy transferred from the plate within the chimney, the level of uncertainty had been thoroughly investigated and was considered to be within the range established with a high degree of confidence.

The investigations into the sensitivity of the solar radiation calculations highlighted the effects of high angles of incidence. Therefore the maximum angle of incidence for which data was used was set at 85° and a lower limit on the solar energy absorbed by the plate of 100W/m^2.

3.8 Conclusion of the rig design

The need for a high level of confidence in the data obtained from the experimental investigation placed significant emphasis on the need to reduce and quantify the level of uncertainty in the results.

The sensitivity analysis undertaken allowed the identification of a method of calculating the key variable, energy transferred from the plate, to be calculated that at the outset of the investigation had not been envisaged. This resulted in

the uncertainty in the variable being reduced to an acceptable level with a high degree of confidence.

The sectional construction of the rig allowed a range of heights and channel depths to be investigated. The careful design of the joints and reduction of the internal emissivity ensured minimal infiltration and that the chimney would act as an asymmetrically heated channel.

To ensure that significant random errors were not included in the resultant data, calculation of the solar energy absorbed by the plate and mass flow rate was undertaken by two wholly separate methods. The results were then compared through a programmed data handling procedure that allowed inconsistencies to be readily highlighted.

3.9 References Chapter Three

1. La Pica, A., Rodono, G. and Volpes, R., An experimental investigation on natural convection of air in a vertical channel, Int. J. Heat Mass Transfer, Vol. 36, No. 3, 611 - 616, 1993.

2. Spitler, J., Pedersen, C., Fisher, D., Menne, P. and Cantillo, J., An experimental facility for investigation of interior convective heat transfer, ASHRAE Trans., NY-91-5-1, Vol. 97, 1991.

3. Hobday, R., Passive solar - energy air - heating wall panels, PhD. Thesis, Cranfield University, UK, 1987.

4. Sparrow, E., Chrysler, G. and Azevedo, L., Observed flow reversals and measured - predicted Nusselt numbers for natural convection in a one - sided heated vertical channel, Journal of Heat Transfer, Vol. 106, 325 - 332, 1984.

5. CIBSE, Thermal Properties of Building Structures, CIBSE Guide A3, 1986.

6. ASHRAE, ASHRAE Handbook, Fundamentals, ASHRAE, USA, 1981.

7. Incropera, F. and DeWitt, D., Fundamentals of Heat and Mass Transfer, 3rd. Ed., J. Wiley & Sons, New York, 1990.

8. Burmeister, L., Convective Heat Transfer, 2nd. Ed., J. Wiley & Sons, New York, 1993.

9. Lomas, K. and Bowman, N., Developing and testing tools for empirical validation, Final Report; An Investigation into Analytical and Empirical Validation Techniques for Dynamic Thermal Models of Buildings, BRE/SERC, Watford, 1988.

10. Kipp & Zonen, Instruction manual for Pyranometer CM5, Kipp & Zonen Ltd.

11. Manning, D., Kipp & Zonen Ltd., Private communications, August, 1995.

12. Lomas, K., Eppel, H., Martin, C. and Bloomfield, D., Empirical Validation of Thermal Building Simulation Programs Using Test Room Data, Final Report, Vol. 1, IEA, 1994.

13. Taylor, J., An Introduction to Error Analysis, Oxford University Press, USA, 1982.

14. Devices & Services, Instruction manual for Emissometer model AE, Devices & Services Co.

15. Dow, Floormate 500, Product information, Dow Construction Products, 1991.

16. Delta-T Devices, User Manual Version 2.01, Delta-T Logger, Delta-T Devices Ltd., 1993.

17. McNair, H. and Russell, M., Design of a thermistor thermometer and anemometer for room air measurement, The Gas Council, Report No. R&D/69/127, 1969.

18. Perflow Instruments, Precision orifice plate, Perflow Instruments Ltd., 1996.

19. Furness Controls, Micromanometer MDC, Furness Controls Ltd.

CHAPTER FOUR

RESULTS OF THE EXPERIMENTAL INVESTIGATIONS AND A COMPARISON OF THESE RESULTS WITH MATHEMATICAL MODELS

4.1 Introduction

The prime purpose for undertaking an experimental investigation of a solar chimney was to obtain a data set that could be used to test the ability of basic mathematical and CFD models to predict the air flow rate through such a building component.

The level of uncertainty in the key variables was investigated in Chapter Three. The results of initial tests to check that the presence of significant random errors could be identified are now presented.

The results of the experimental investigation are then presented with the influence of the physical variables upon the mass flow rate, the dependent variable of key interest, being detailed.

The data is then used to evaluate the potential of basic mathematical models to predict the operation of a solar chimney and to fully describe the influence of the physical variables investigated experimentally.

4.2 Initial testing of the rig and data handling procedure

4.2.1 Testing for inclusion of random errors

The key dependent variable of interest from the experimental investigation was the mass flow rate, expressed in terms of the energy transferred from the plate to the air. The level of uncertainty in each of these variables was evaluated in Chapter Three, however the possibility of random errors occurring could not be eliminated. Therefore initial testing was undertaken to assess if the occurrence of random errors could be detected.

The velocity and temperature profiles of the air exhausting from the chimney were of interest as they offered the opportunity to compare the CFD predictions of such profiles with those measured. The positioning of velocity / temperature probes at the chimney outlet had been designed to obtain such

data. The velocity and temperature profiles were however dependent upon many variables including; aspect ratio, energy transferred from the plate and the turbulence of the air. Therefore the level of uncertainty in these variables could not be practically defined.

For the purpose of assessing if random errors had been included in the mass flow data therefore, it was assumed that at best the uncertainty of the mass flow measured at the outlet would equal that of the inlet i.e. +/- 6%. The overall uncertainty was calculated by adding the uncertainties at the inlet and outlet in quadrature as recommended by Taylor[1]. This resulted in an overall level of uncertainty of +/- 8.5%.

Figure 4.1. shows the mass flow into and out of the chimney plotted against each other when the aspect ratio of the chimney was high i.e. $\geq$1:15, for two different chimney heights. At such aspect ratios the agreement was close and within the overall level of uncertainty anticipated.

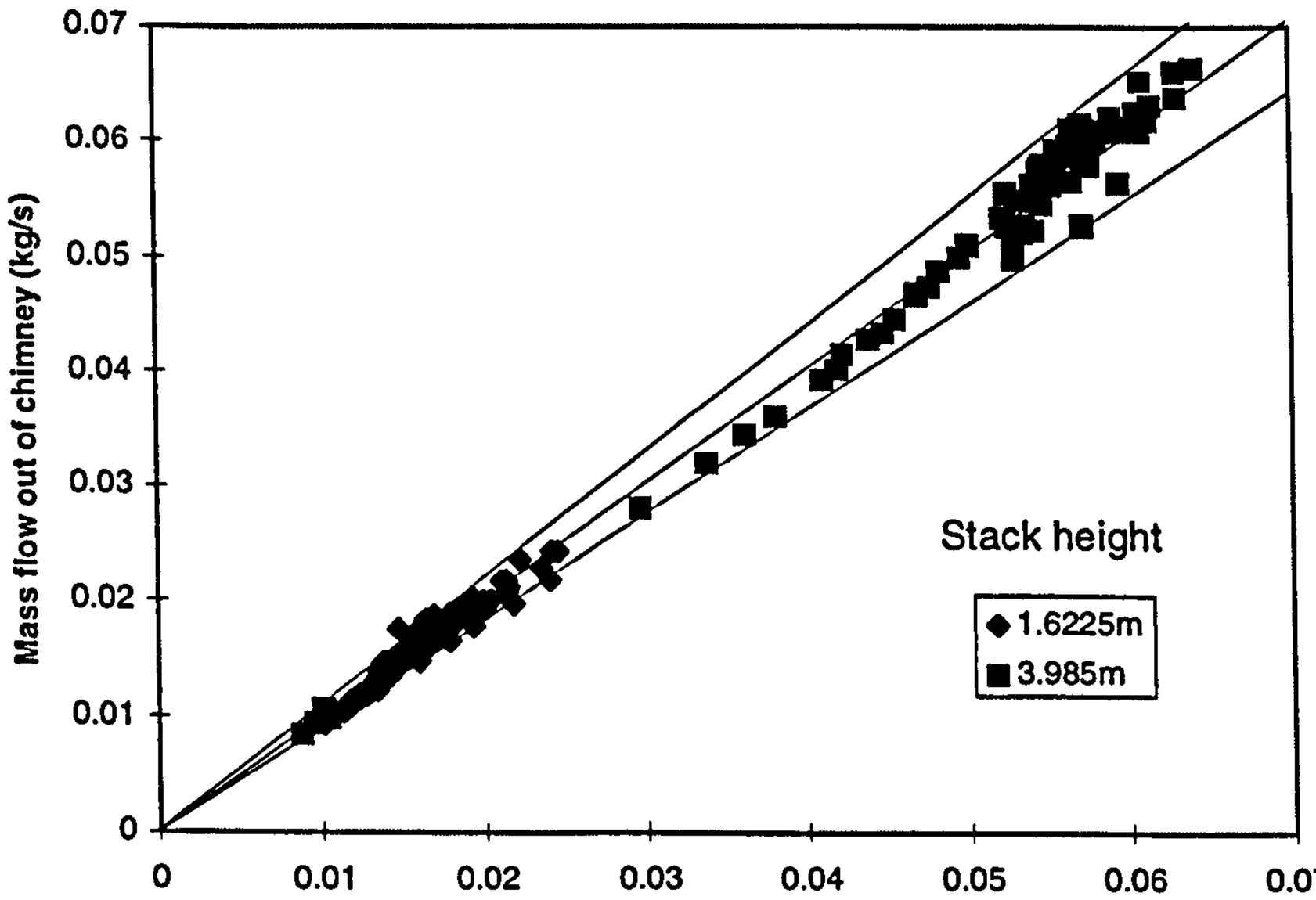

Figure 4.1. Measured mass flow rate into and out of the solar chimney at two heights with high aspect ratios (i.e. $\geq$ 15:1).

As the aspect ratio decreased, $\leq$ 10:1, recirculation was observed at the chimney outlet. As the direction of the flow could not be determined by the

velocity probes, the extent of the recirculation could only be determined through observation. This was undertaken by introducing smoke into the air flow at the chimney outlet to determine the flow direction. Consideration of equation 2.15., proposed by Eckert et al[(2)] defining the depth of a boundary layer, shows that it is only a weak function of plate to air temperature difference, the major influencing factor being the height of the plate. It was noted that the area of the outlet subject to recirculation was relatively constant throughout the logging period, indicating that the boundary layer depth did in fact remained largely constant.

In the absence of any other reliable method of determining the flow direction therefore, the mass flow calculated by the probes within the visualised area of flow reversal was taken to be into the chimney. This flow rate was then subtracted from that calculated by the other velocity probes. This allowed the mass balance to be tested for the low aspect ratio configurations i.e. $\leq$ 10:1.

Figure 4.2. shows the mass flow rates for the lower aspect ratios. It is evident that the balance is not as good as that obtained with high aspect ratio chimneys, however as a means of determining if significant random errors had been incurred, it offered an adequate check.

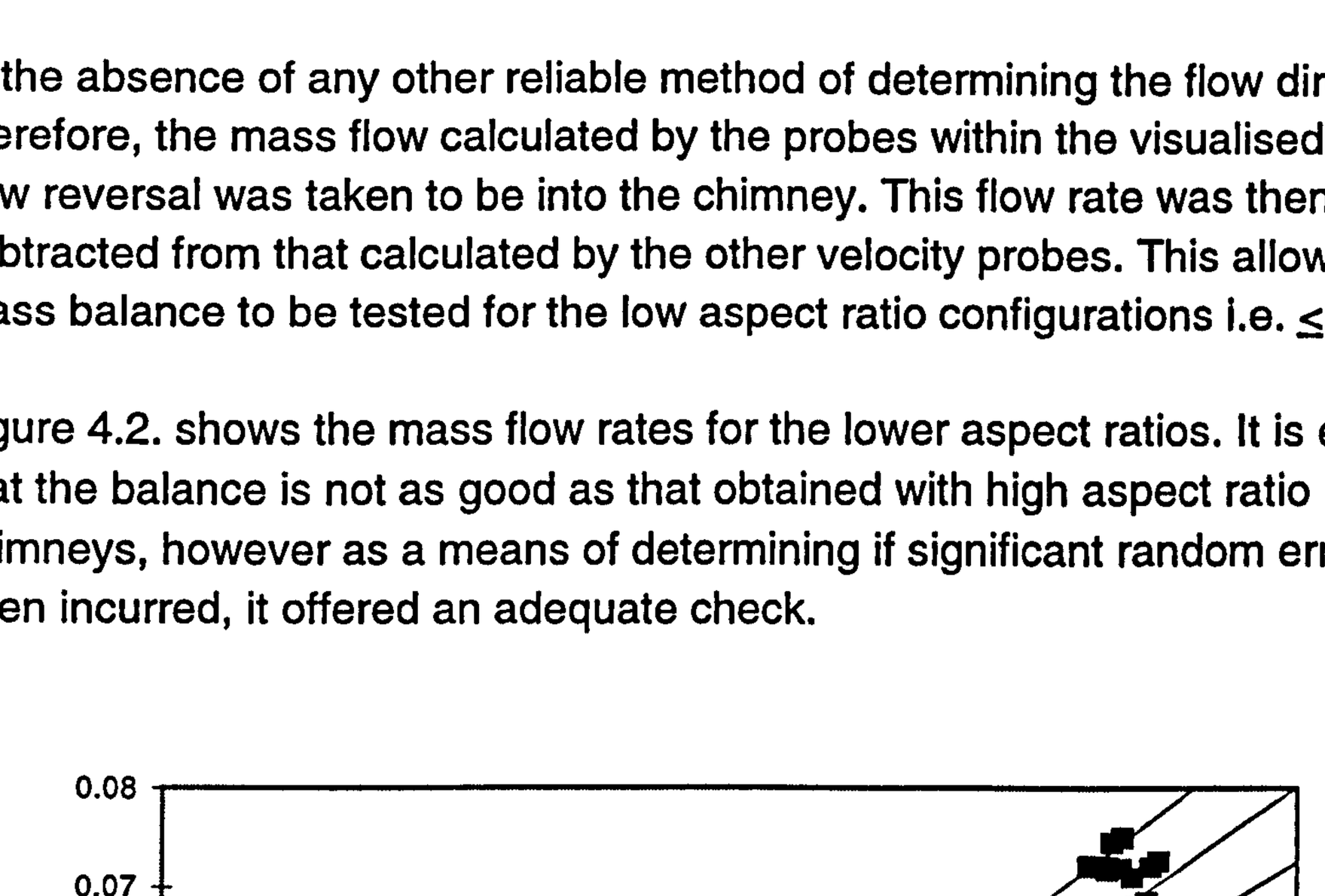

Figure 4.2. Measured mass flow rate into and out of the solar chimney at two heights with low aspect ratios (i.e. $\leq$ 10:1).

To test the calculation of the energy transferred to the air from the plate, to ensure that no random errors were included in this data, the energy gained by the air passing through the chimney was calculated. This required that the mass flow rate at the outlet and the temperature rise of the air within the chimney were solved. As demonstrated in figures 4.1. and 4.2. the accuracy of such calculations was variable and dictated by the aspect ratio of the chimney, however it was sufficient to provide a check for the occurrence of significant random errors.

Figure 4.3 shows both the calculated energy transferred from the plate to the air and the energy gained by the air for two different rig heights. The uncertainty band calculated for the energy transferred from the plate was applied to that data to allow the degree of difference to be evaluated.

Above the lowest values of energy transfer, the agreement between the two methods of calculation was generally good. This indicated that significant random errors were not included in this set of data.

Having established that the mass and energy flow rates, could be checked at the outlet of the chimney, this routine was incorporated into the data handling to allow the data to be checked after each logging period. In this way the potential of inclusion of large random errors into the data set was minimised.

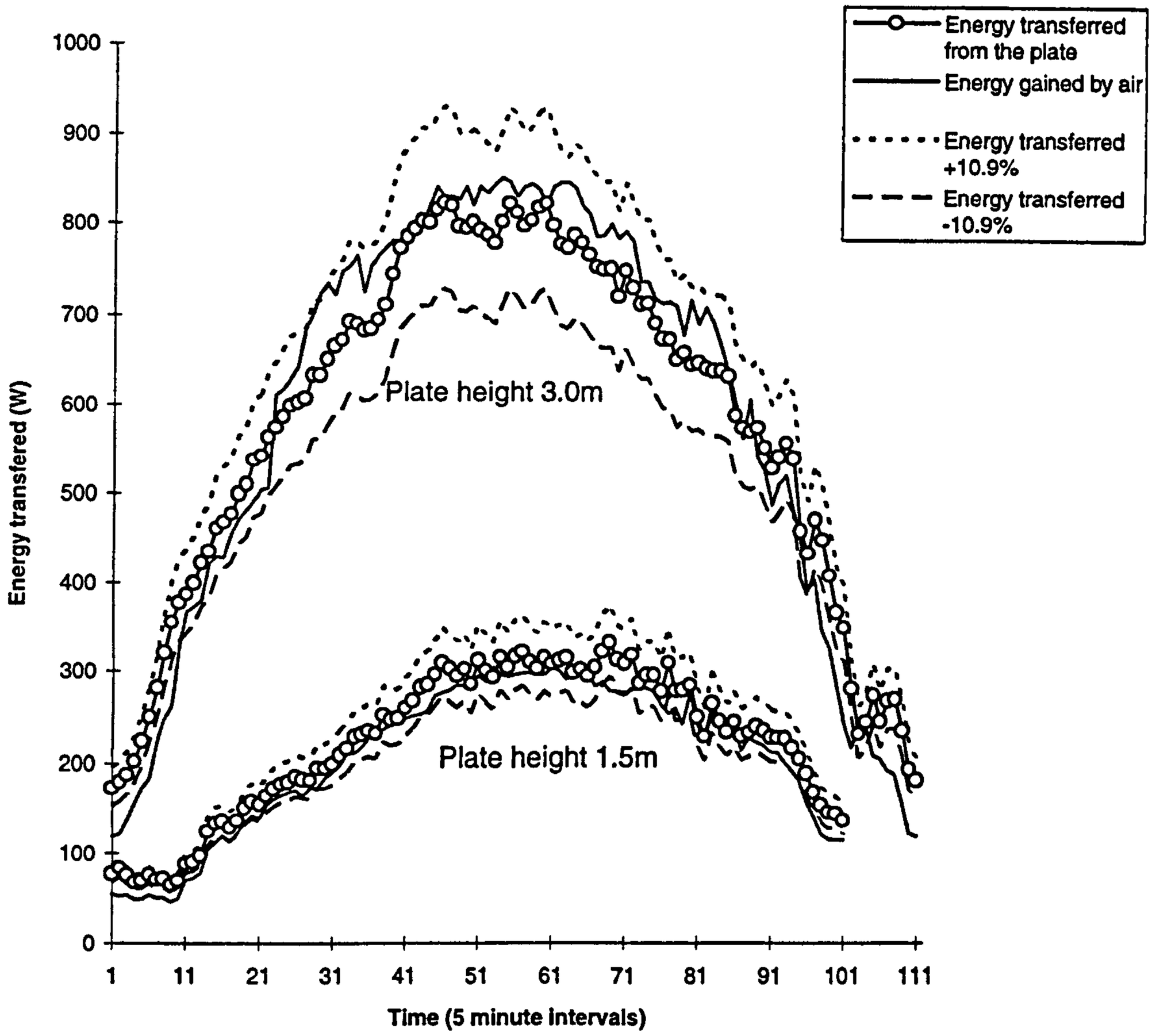

Figure 4.3. Comparison of the methods of calculating energy transfer within the chimney.

Conclusion of the testing of the check methods for the experimental rig.

The level of uncertainty in the calculated values of mass flow rate and energy transferred from the plate were established in Chapter Three. Although the confidence in these figures was high, the occurrence of random errors could not be eliminated or accounted for. It was therefore important that a method was found to check the data recorded. The use of the measurements at the chimney outlet, although subject to largely unquantifiable levels of uncertainty, provided a very effective method of checking the calculations. Therefore by comparing the results graphically while the data was being processed, the occurrence of any significant random errors was immediately identifiable. Consequently a high level of confidence in the data was established.

4.2.2 Stratification of air within the rig

During the initial testing of the rig it became clear that, particularly on days with clear skies, the mass flow rate was influenced by more than just the energy transferred from the plate to the air. An example of the data obtained for a day with clear skies is given in figures 4.4 and 4.5.

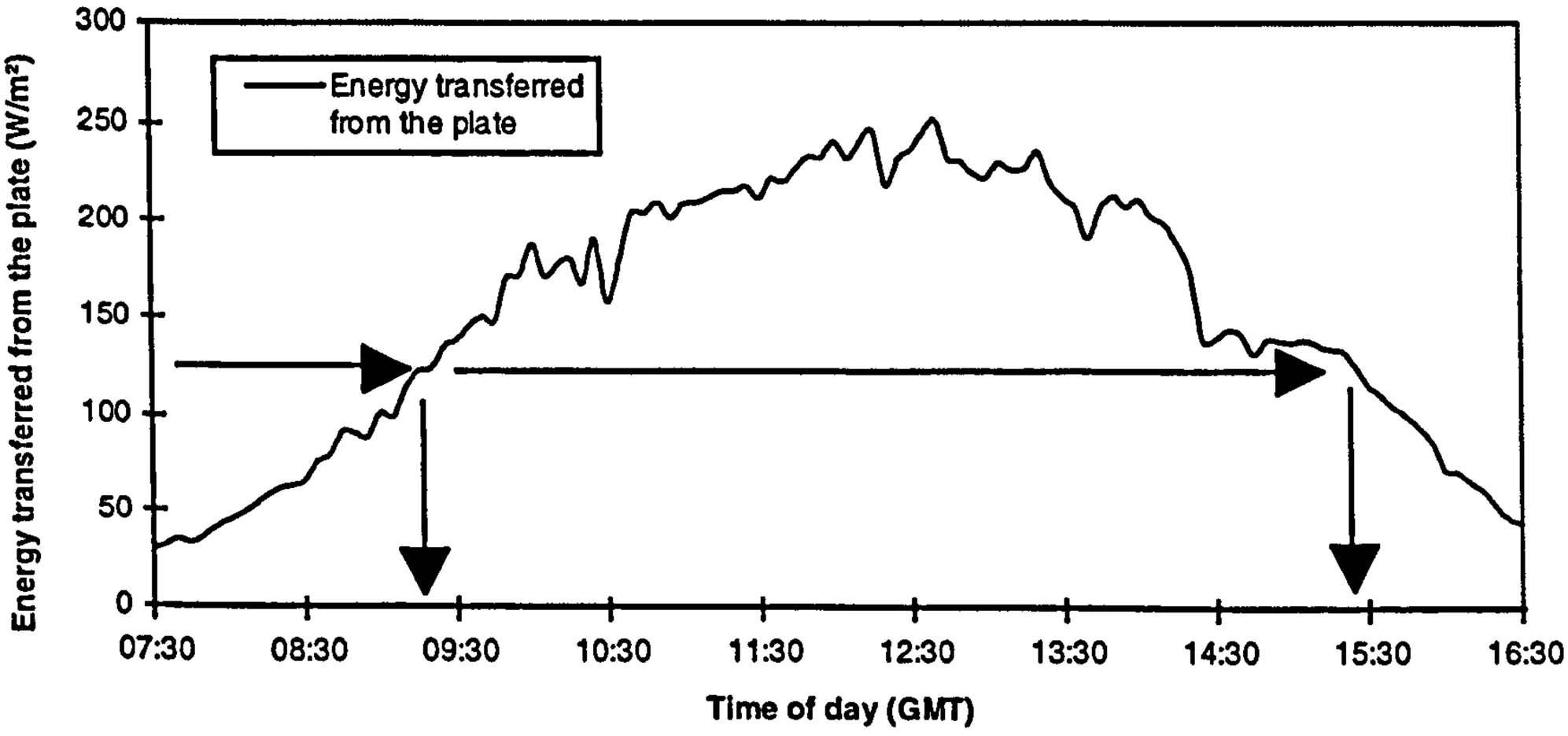

Figure 4.4. Energy transferred from the plate throughout a clear day

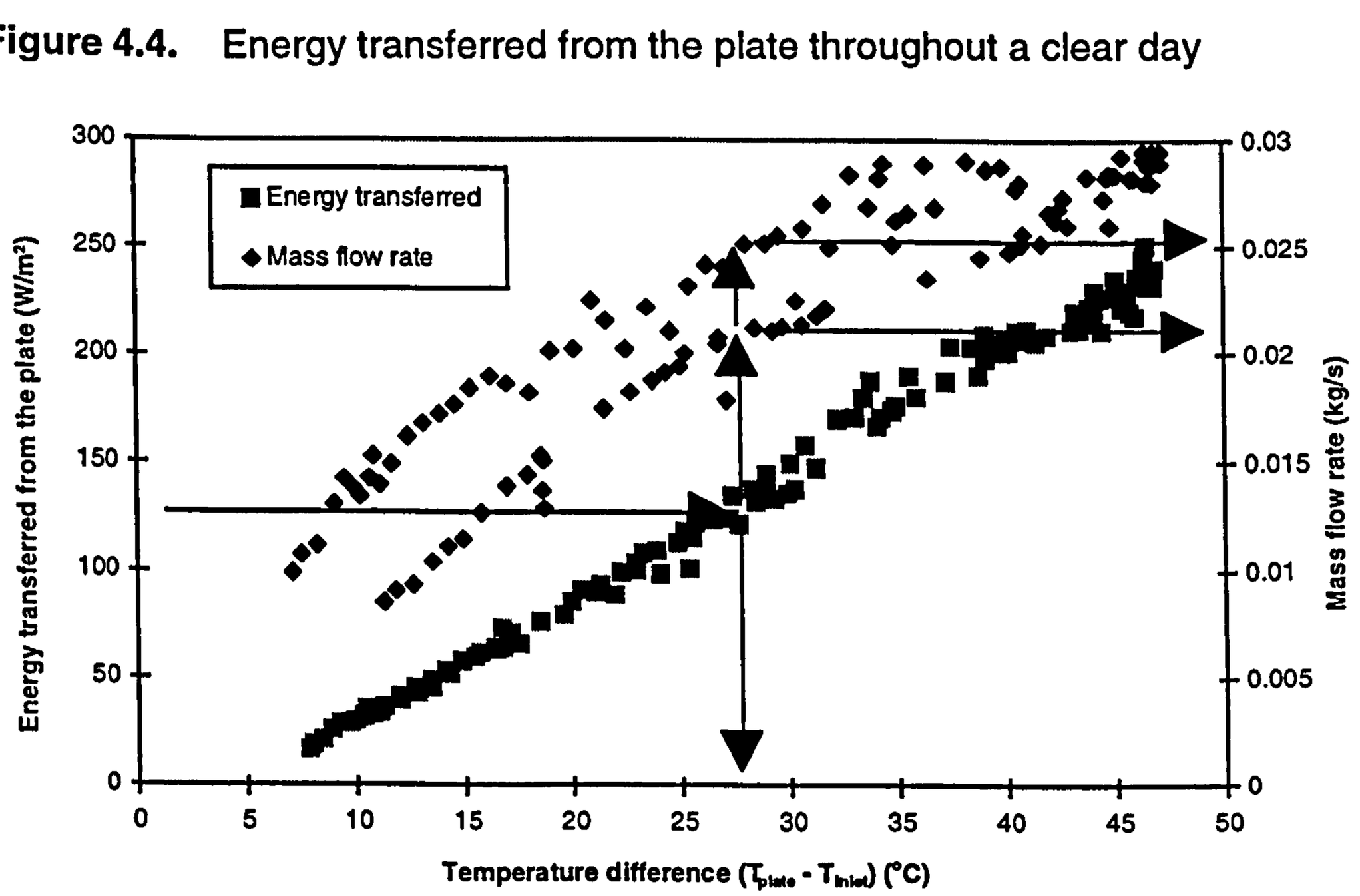

Figure 4.5. Energy transferred from the plate and mass flow rate for a range of plate to inlet air temperature differences

From the profile of the energy transferred from the plate in figure 4.4. it was evident that the level of solar insolation had been high throughout the day. However figure 4.5. shows that for a given value of energy transferred from the plate there was a relatively large level of scatter of the measured mass flow rate and at times evidence of two distinct flow rates.

Initial investigations showed that there were in fact two distinct flow rates, dependent upon the time of the day. Investigations into the instrumentation produced no apparent answers for this systematic, rather than random difference. The temperature compensation of the velocity measuring instruments was investigated and eliminated. Finally the level of stratification within the rig was investigated.

The floor of the rig was thermally isolated from the ground by an air gap of at least 200mm. However it was found that on days where the ambient temperature rose sharply and significantly in the morning, the temperature of the rig floor was relatively slow to respond. The effect of this was that, although the mass of the air within the rig was largely fully mixed at the prevailing outside air temperature, the air in direct contact with the rig floor was noticeably cooler throughout the morning. As the chimney inlet was at floor level this meant that the inlet air was at a lower temperature than the rig air mass. Figure 4.6.

Figure 4.7 shows the profile of the rig air temperature in the morning of a day when the air temperature outside rose sharply due to high insolation. It is evident that only the temperature probe at the inlet to the chimney registered a lower temperature, the remaining mass of air within the rig was well mixed.

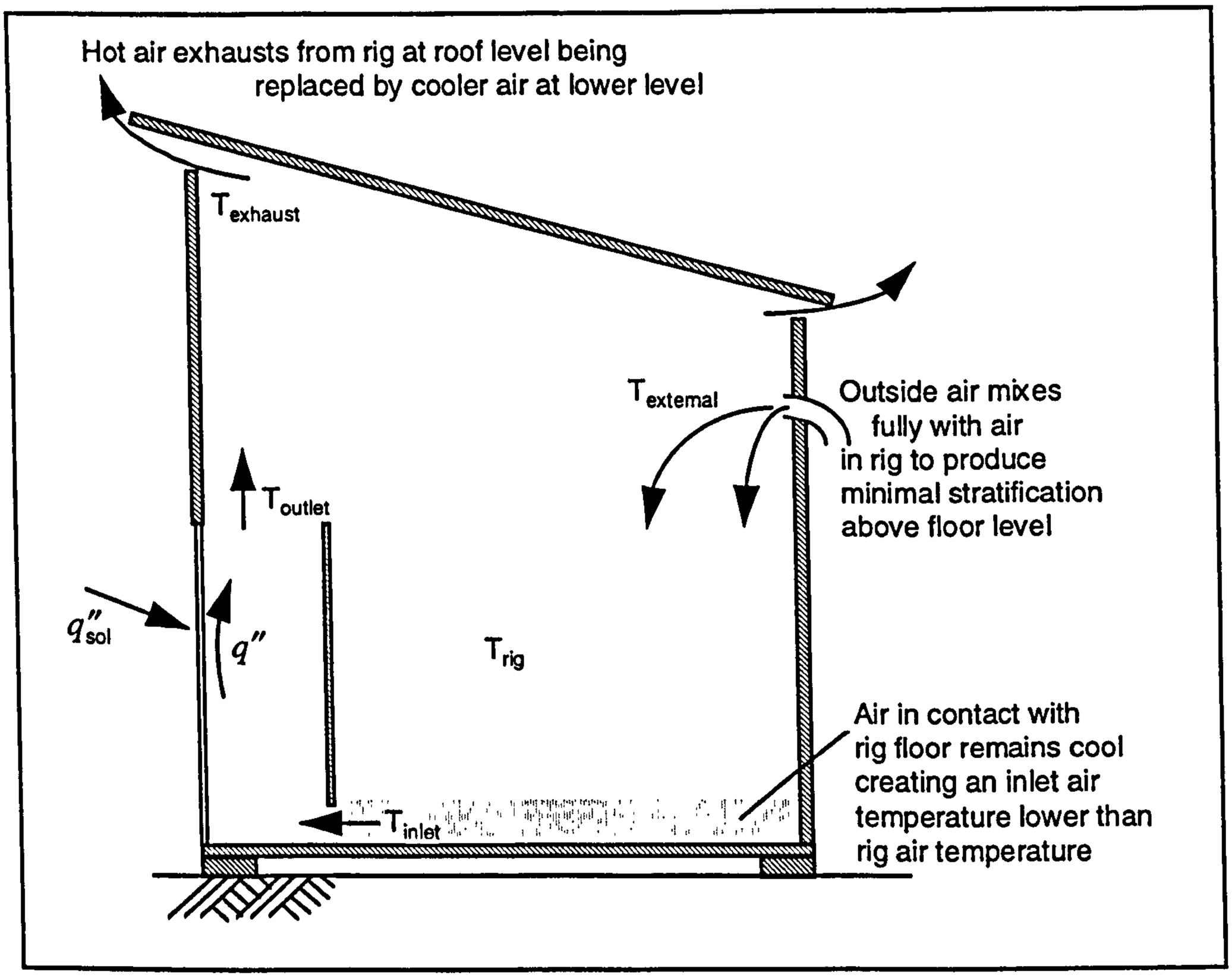

Figure 4.6. Rig stratification creating temperature difference $T_{rig} > T_{inlet}$

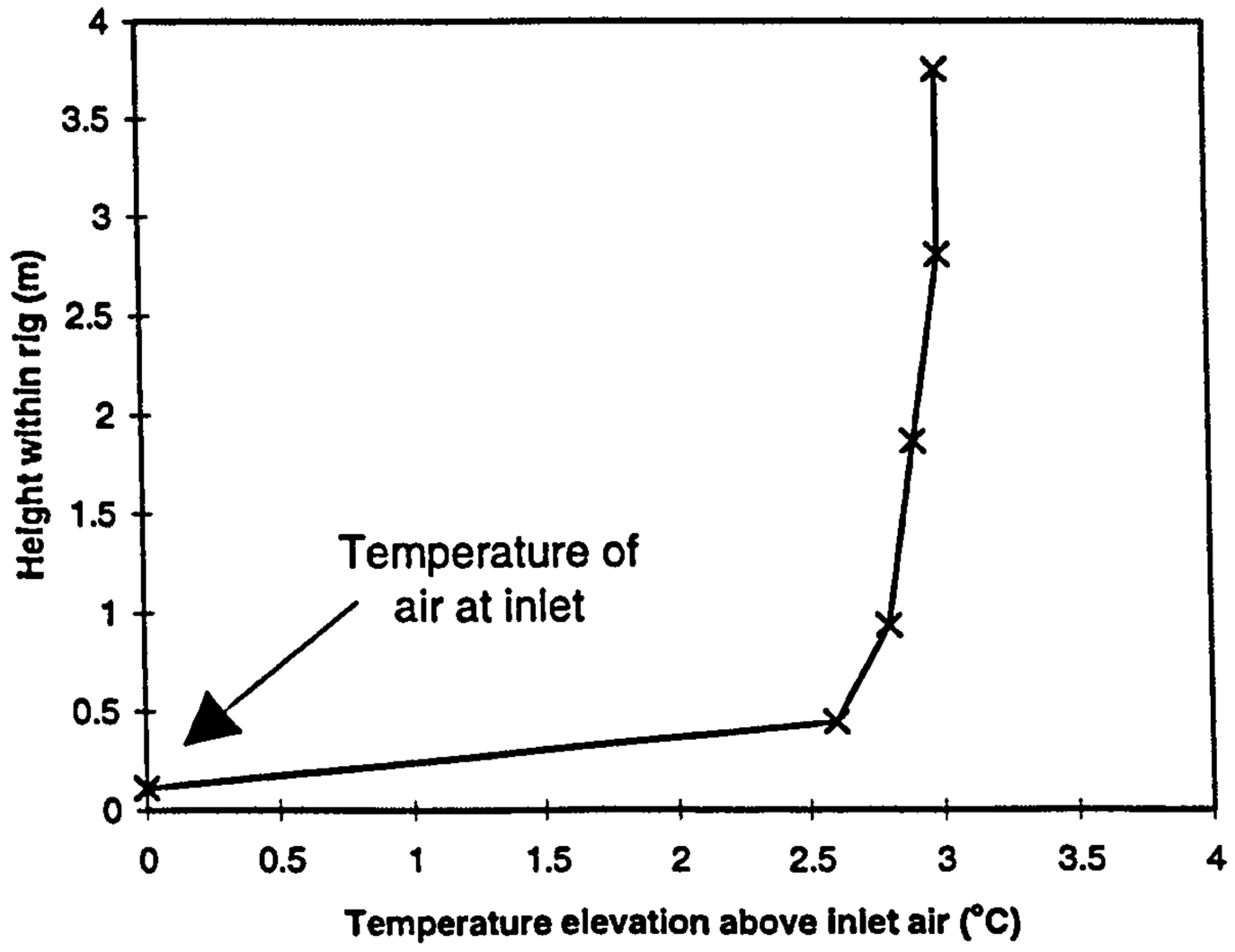

Figure 4.7. Vertical air temperature profile within rig

The mass flow rate through the solar chimney depended upon the stack pressure difference created by the temperature elevation and consequent fall in density of the air within the chimney compared with that within the rig. In situations where the temperature of the air within the rig rose above that of the inlet air, the stack pressure difference was reduced. This resulted in a reduced mass flow rate. Consequently the temperature of the air within the chimney rose to maintain the overall energy balance within the chimney.

To determine if the changes in mass flow rate could be attributed to the stratification within the rig, the effect of different inlet and rig air temperatures was investigated mathematically by solving equations 4.1. to 4.4.

To calculate T_{outlet}

$$q'' = \frac{\dot{m}\ Cp\ \Delta T}{A} \qquad \text{Equation 4.1}$$

Where $\Delta T = T_{outlet} - T_{inlet}$ Equation 4.2

$$\dot{m} = \rho\ Cd\ A \sqrt{\frac{2\ \Delta P_{inlet}}{\rho}} \qquad \text{Equation 4.3}$$

$$\Delta P_{inlet} = P_s = \rho_0\ g\ h\ 273 \left(\frac{1}{T_{rig}} - \frac{1}{T_{outlet}}\right) \qquad \text{Equation 4.4}$$

Equation 4.4. assumes that the air in both the rig and chimney are fully mixed with bulk air temperatures T_{rig} and T_{outlet} respectively. The correctness of this assumption for application to a solar chimney was discussed in Chapter Two. For investigating the effects of the elevation of T_{rig} above T_{inlet} on the mass flow rate, such an assumption provided a simple test case allowing the likely magnitude of the influence to be assessed.

Equations 4.1 to 4.4 were balanced iteratively for values of q'', T_{rig} and T_{in}. Thus the effects of changing T_{rig} while T_{in} remains constant were calculated.

Figure 4.8. shows that as the temperature of the air mass within the rig increased above that of the inlet air the effect on the mass flow rate is

significant, causing a decrease in mass flow rate of in excess of 7.0 kg/s per °C temperature elevation.

q'' = 100 W/m^2	Cd = 0.61
T_{inlet} = 300 K	ρ = 1.2 kg/m^3
h = 3 m	g = 9.81m/s^2
A = 0.1 m^2	Cp = 1007 J/kg K

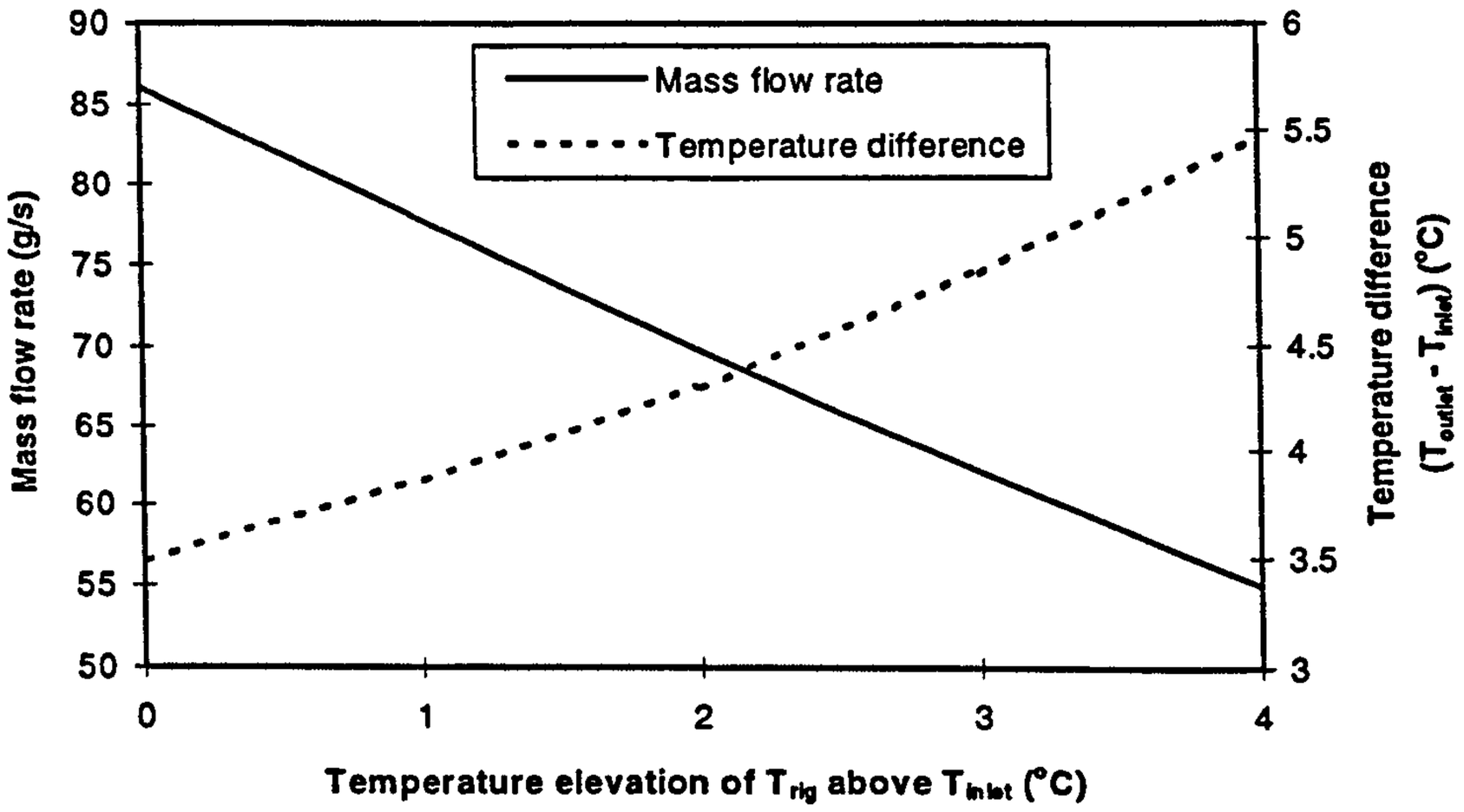

Figure 4.8. Influence of external stack temperature on mass flow rate of a fully mixed space with a heat source.

The results obtained from measurements of the chimney and rig are shown in figure 4.9.

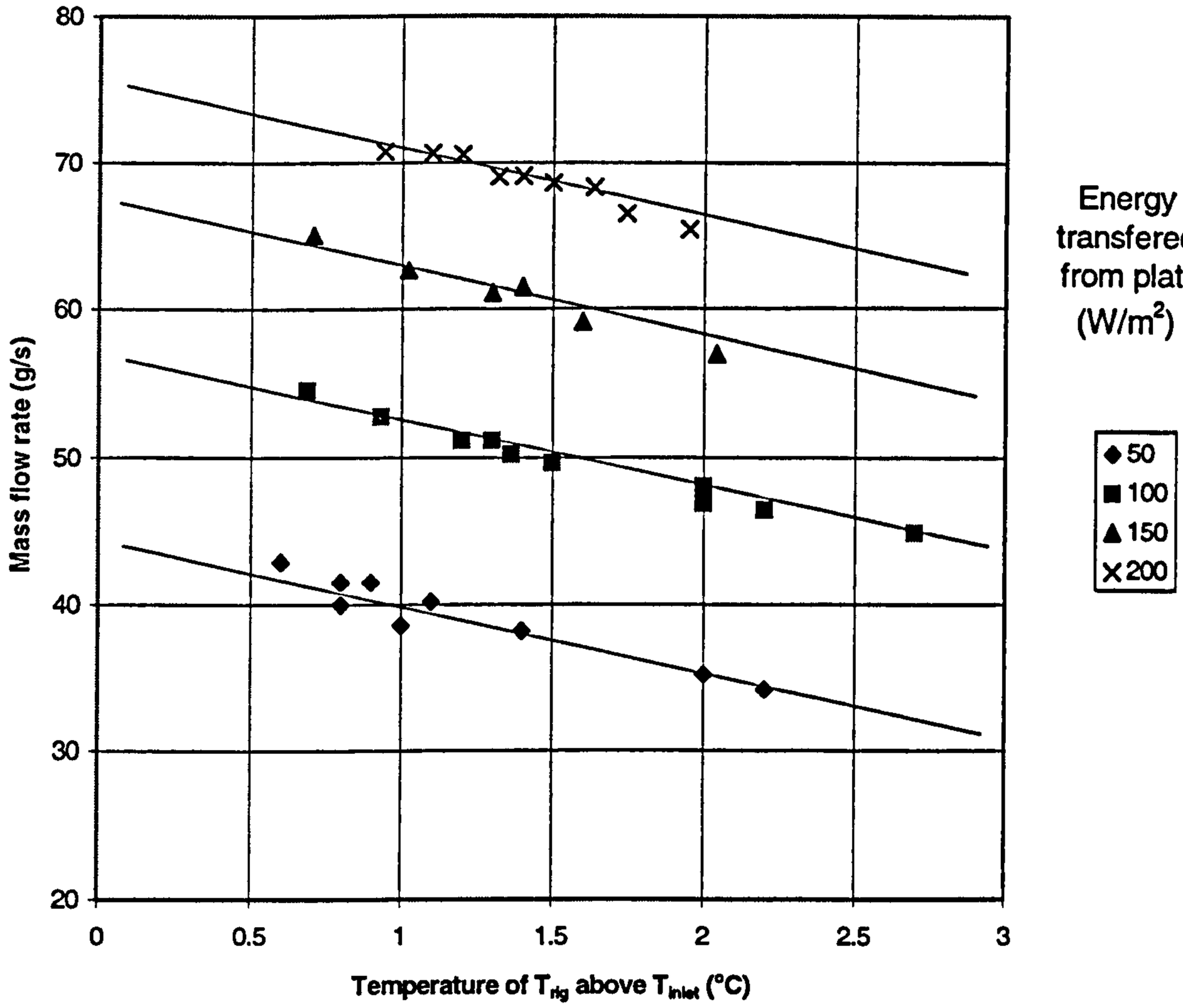

Figure 4.9. Effect on mass flow rate of elevation of rig air temperature above inlet air temperature.

Figure 4.9. shows clearly that as the temperature of the air mass in the rig rose above that of the inlet, the mass flow rate through the chimney fell. Within the accuracy of the measurements taken, the effect was linear and although less than that predicted through the balancing of equations 4.1. to 4.4., the reduction of the flow rate was of a similar order. This therefore, indicated that the differences in mass flow rate at different times of the day for a given value of energy transferred from the plate, could be attributed to different levels of elevation of the rig air temperature above that of the inlet air.

In the experimental investigation undertaken by LaPica[3], he reported up to 0.6°C temperature gradient between the inlet and outlet of his rig. This was not taken into account in the presentation of the results and appears to have been considered as of no consequence to the mass flow rate within the channel. The results presented in figure 4.9. however imply that even such small levels

of elevation of the rig air temperature above that of the inlet air can have significant influences upon the mass flow rate through such a channel.

In light of this, great care was therefore taken to log the temperature distribution of the air within the rig. This allowed the influence of temperature elevation of the rig air mass above that of the inlet air to be fully assessed at all rig configurations and levels of energy transferred from the plate to the air within the chimney. From this data, extrapolation of the mass flow rates at zero temperature elevation was undertaken to allow the results to be compared with the predictions of mathematical models. The CFD model was capable of predicting the effects of the temperature elevation on the mass flow rate given accurate temperature data. The accuracy of this was tested before the model was used to predict the flow rate across the full range of variables investigated experimentally.

4.3 Results of experimental investigation

4.3.1 Experimental results for mass flow rate

To allow the uncertainty in the mass flow rate arising from both the mass flow rate measurements and the calculations of energy transferred from the plate to be estimated, the resulting uncertainties from both sources were added in quadrature using equation 4.5. This approach was suggested as appropriate by Lomas et al[4]. This calculation required that the uncertainty in the mass flow rate due to the uncertainty previously established in the energy transferred form the plate was determined. This was achieved by plotting the mass flow rate across a range of values of energy transferred from the plate and determining the value of change in mass flow rate across the calculated band of uncertainty in the rate of energy transfer.

$$U_{\dot{m}\ \mathrm{Total}} = \sqrt{U_{\dot{m}}^2 + U_{\dot{m}\,(q'')}^2} \qquad \text{Equation 4.5.}$$

Where $U_{\dot{m}\,(q'')}$ is the uncertainty in the mass flow rate resulting from the uncertainty in the calculated rate of energy transferred from the plate.

Figure 4.10. shows the maximum mass flow rate recorded for each chimney height verses the energy transferred from the plate. It is clearly evident that as

both the height of the plate and the level of energy transferred from the plate increased, the mass flow rate increased. It is also evident that increasing of the height of the inlet from 0.075m to 0.15m for the plate heights of 3.0 and 3.75m had a very marked effect upon the flow rate.

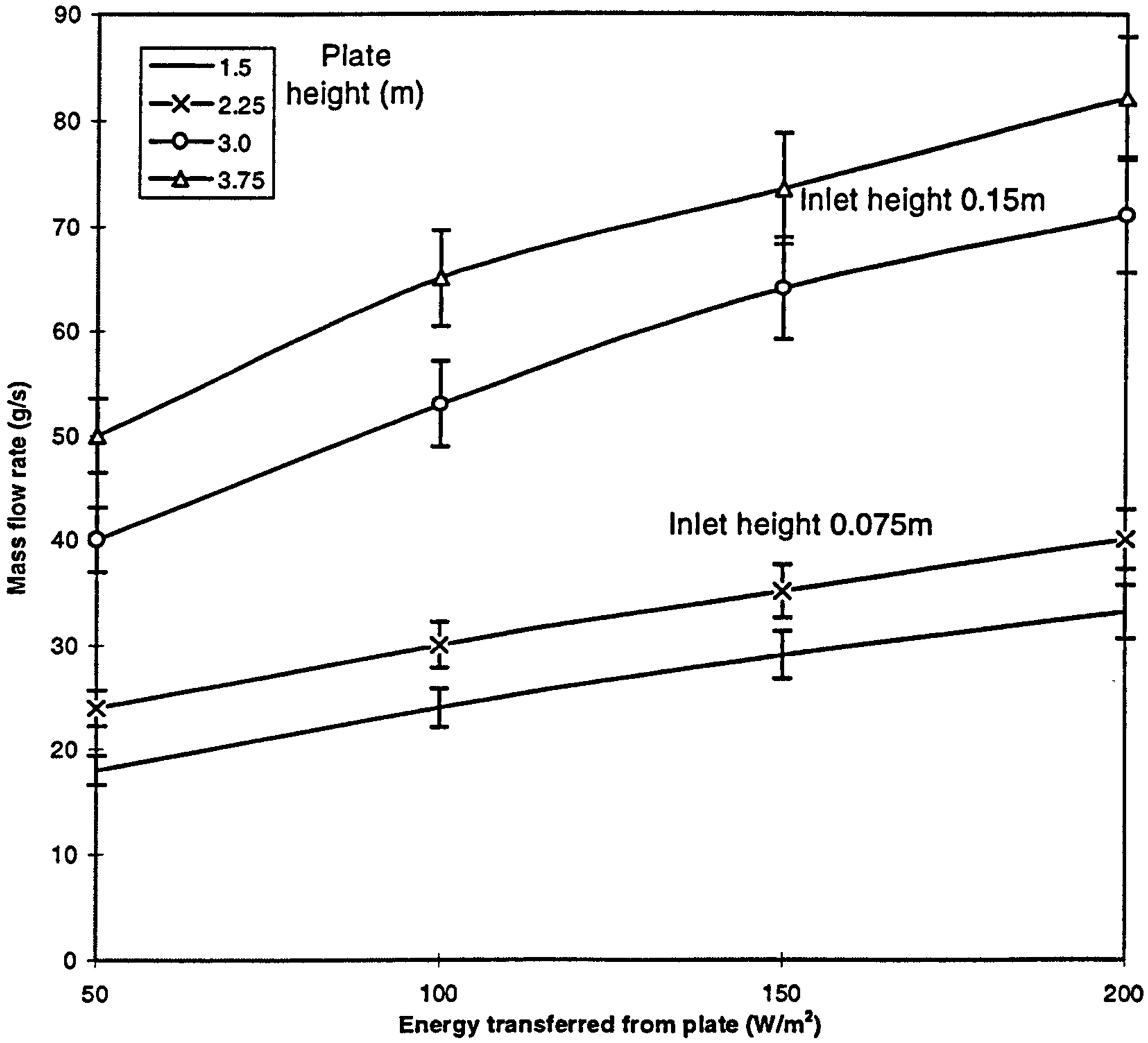

Figure 4.10. Influence of plate height and inlet height on mass flow rate

Figures 4.11. to 4.14. show the influence of the channel depth on the mass flow rate across the range of energy transferred from the plate from 50 to 200 W/m^2.

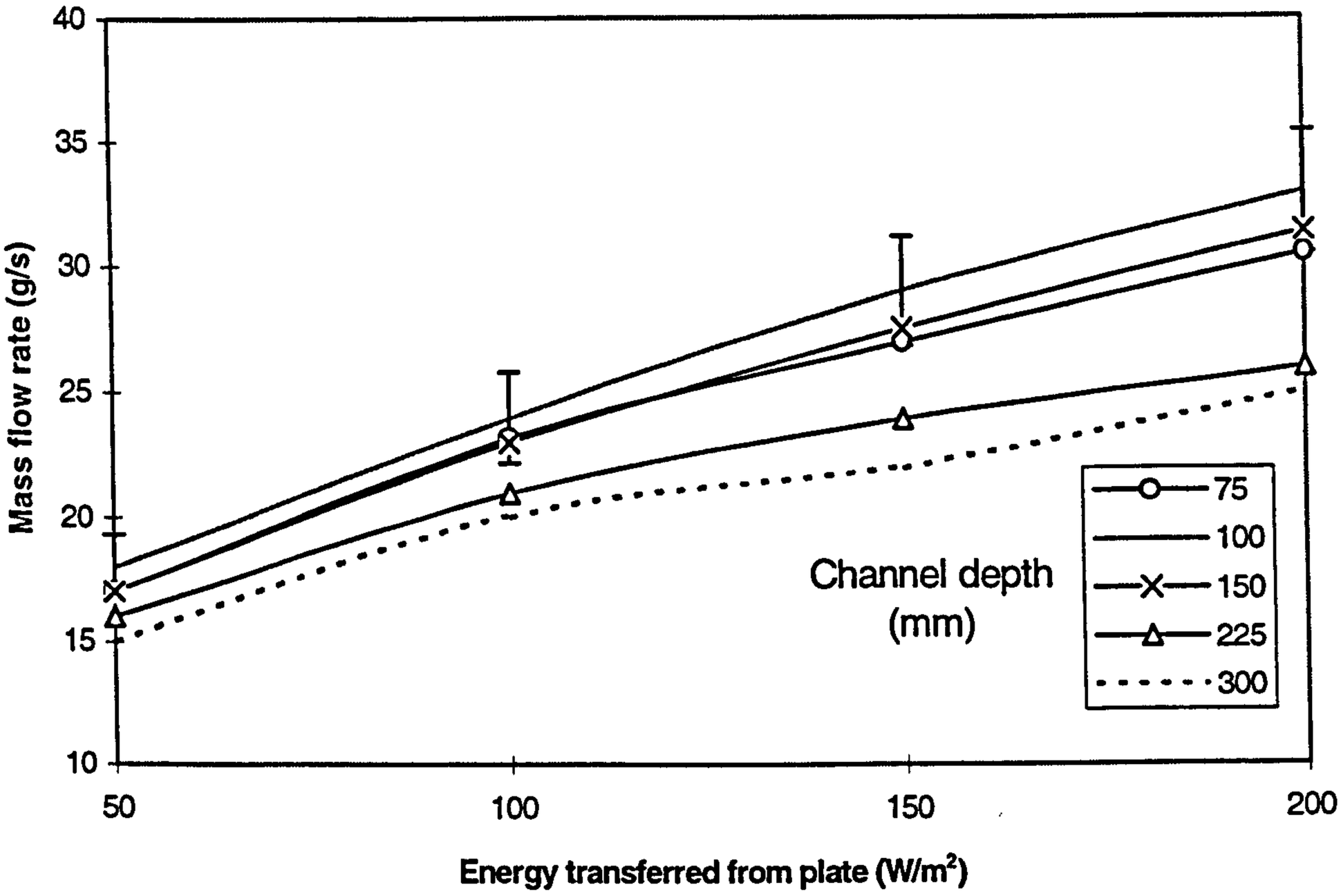

Figure 4.11. Mass flow rate for different aspect ratios with a plate height of 1.5m

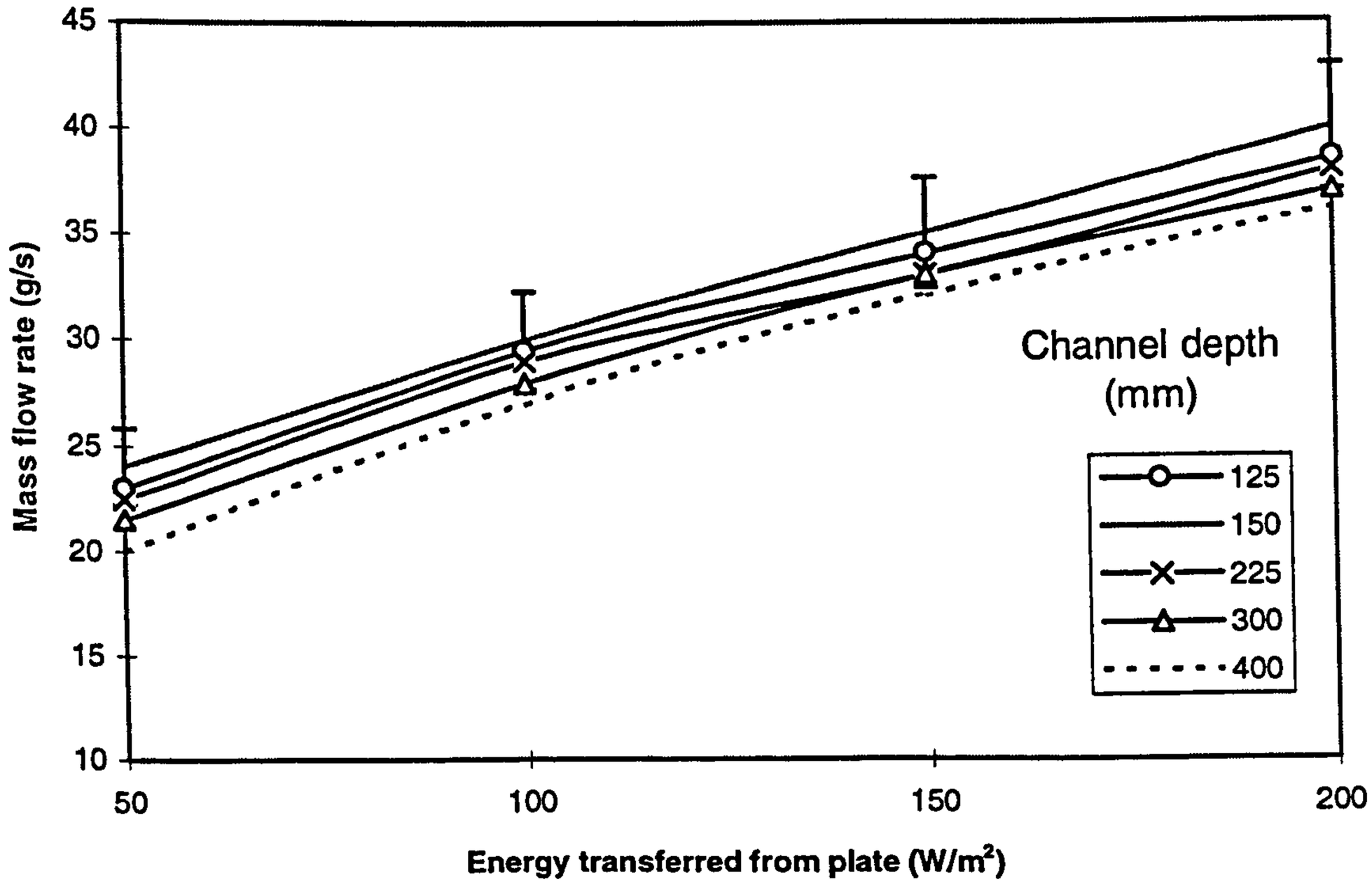

Figure 4.12. Mass flow rate for different aspect ratios with a plate height of 2.25m

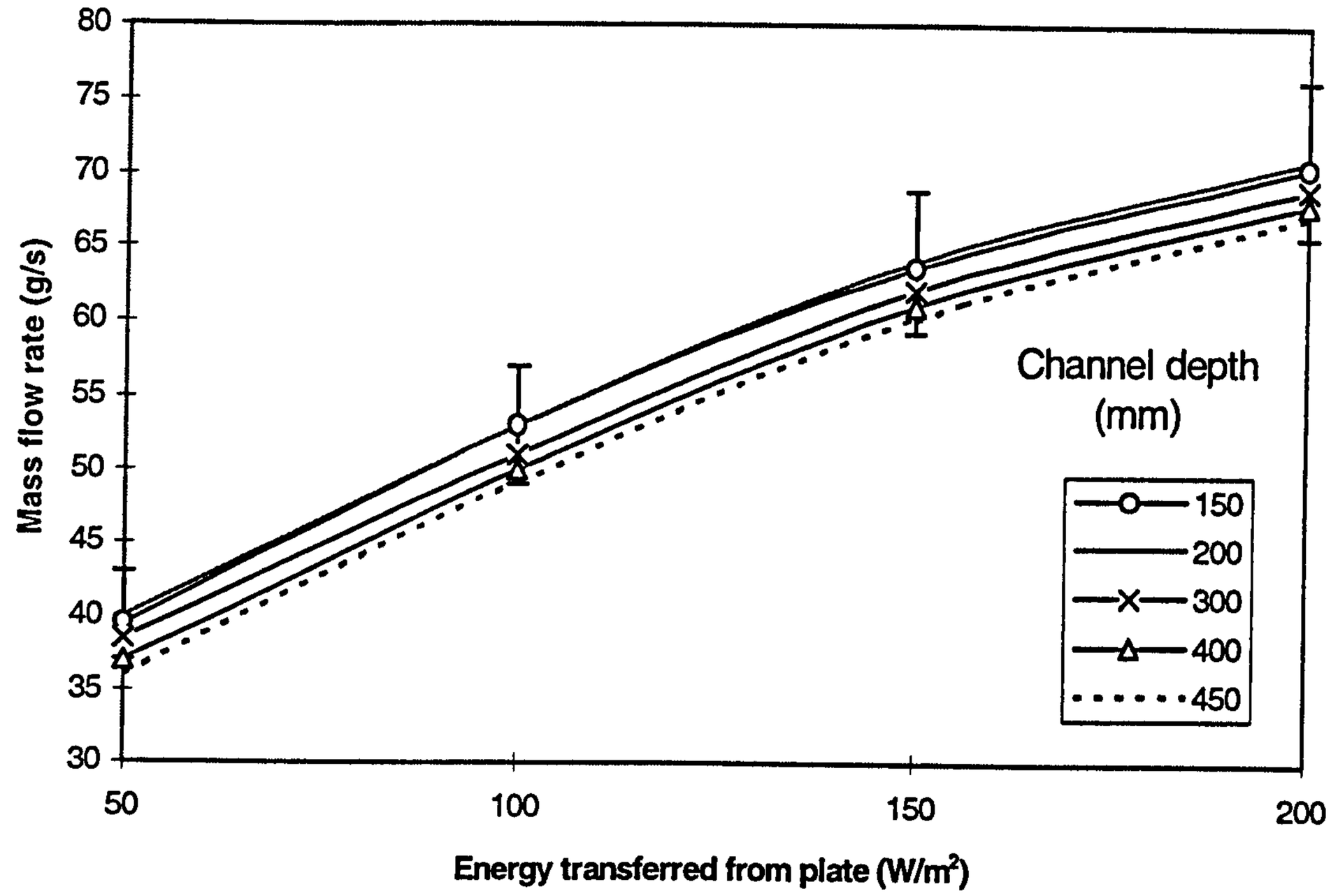

Figure 4.13. Mass flow rate for different aspect ratios with a plate height of 3.0m

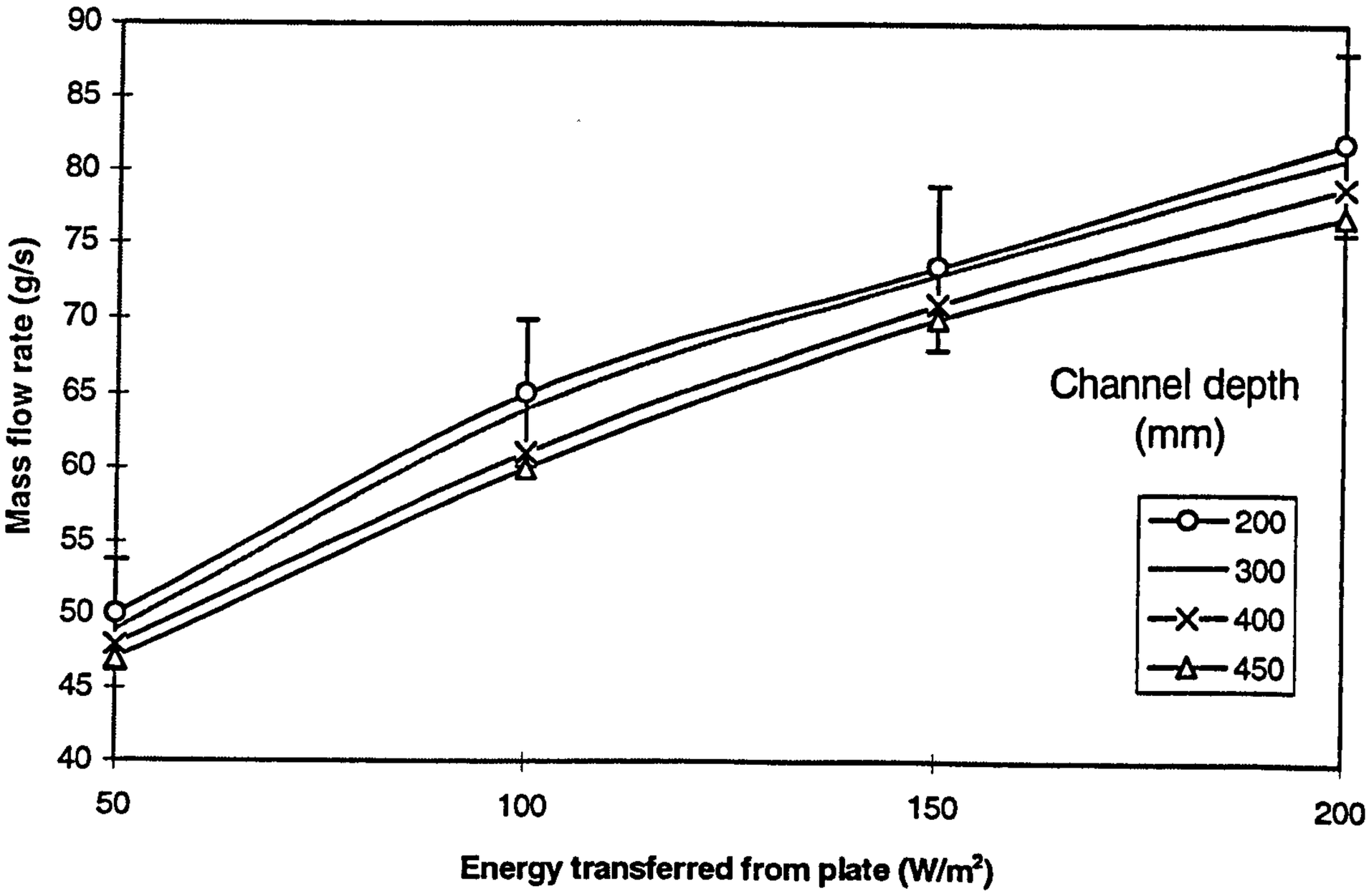

Figure 4.14. Mass flow rate for different aspect ratios with a plate height of 3.75m

Figures 4.11. to 4.14. show that as the aspect ratio of the chimney was changed, the mass flow rate through the inlet of the chimney was influenced. This occurred at all chimney heights. The level of uncertainty indicated in figures 4.11. to 4.15. is that calculated using equation 4.5. To assess if the measured variations were significant, the repeatability of the mass flow measurements was considered. As detailed in Appendix D, a high level of repeatability in the velocity measurements had been ensured through the use of close tolerance components throughout the instruments developed. The major source of uncertainty in the overall uncertainty calculated using equation 4.5. was that associated with the mass flow measurements. Thus as the repeatability of the measurements was considered to be high, significantly better than the +/-6% identified for measurements, the differences in mass flow rate at the different channel depths investigated experimentally were considered to be both significant and relevant. The influence of the channel depth on the mass flow rate was therefore investigated further.

Figure 4.15. clearly shows that at a level of energy transferred from the plate of 100 W/m^2 there is a marked trend shifting the aspect ratio at which the maximum flow rate occurred from approximately 15:1 for a plate height of 1.5m to above 19:1 for a height of 3.75m.

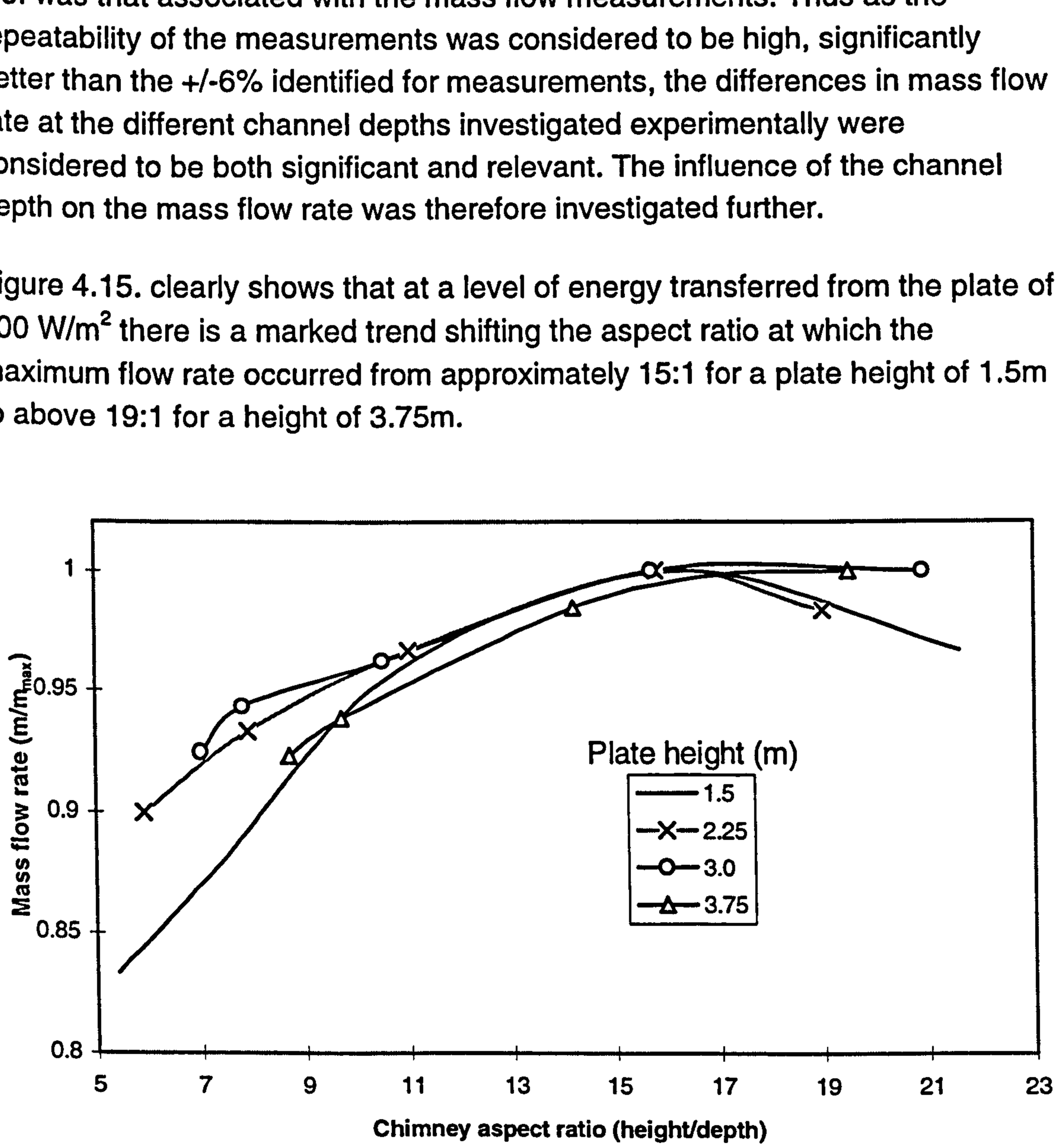

Figure 4.15. Variations in mass flow rate from maximum for all rig heights at an energy transfer rate of 100 W/m^2.

Bouchair[5] stated that the maximum flow rate would occur from a flat plate when the boundary layer just spanned the channel depth of an asymmetrically heated channel. The boundary layer depths were therefore calculated using equation 2.15. to assess whether they corresponded to the channel depths at which maximum mass flow rate occurred.

The boundary layer depths calculated for the experimental rig heights were compared with the channel depths of the maximum flow rates established from figure 4.15. The result of this comparison is shown in figure 4.16.

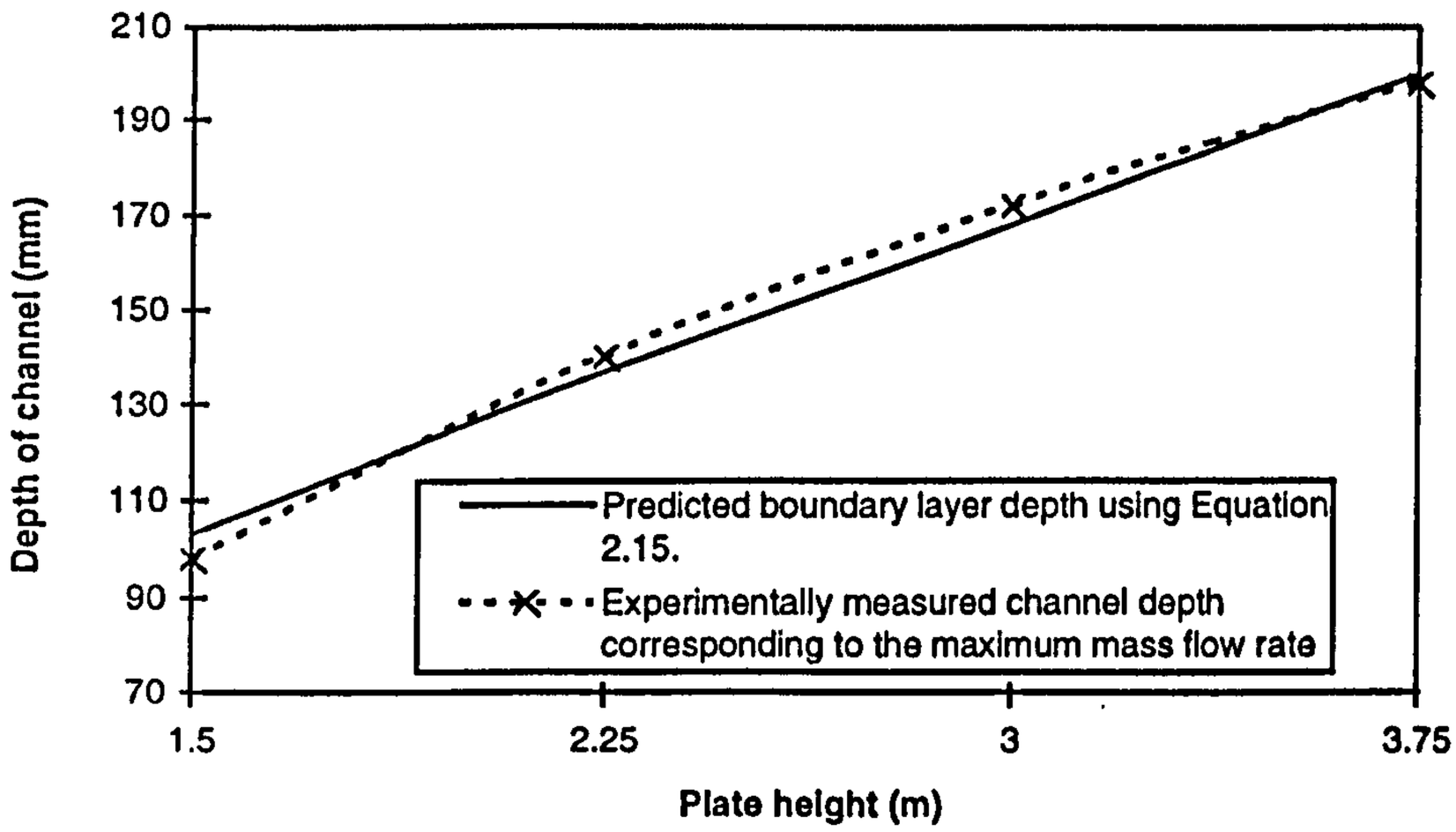

Figure 4.16. Channel depth corresponding to the maximum mass flow rate compared to the depth of a turbulent natural convective boundary layer, calculated using equation 2.15.

Figures 4.15. and 4.16. clearly show that as the height of the plate was increased from 1.5 to 3.75m, the depth of channel at which the maximum flow rate occurred was not set by the physical ratio; chimney height : channel depth, but moved from 15:1 towards 20:1. Comparison with the predictions of the boundary layer depths for a turbulent natural convective flow, calculated using equation 2.15., indicated that the maximum mass flow rate occurred when the channel depth was approximately equal to that of the boundary layer. This confirms the findings of Bouchair who found this to be true for a chimney height of approximately 2.0m.

To assess the relative magnitude of the changes in mass flow rate caused by the changes in aspect ratio, the mass flow rate was plotted against the ratio;

channel depth to depth of channel corresponding to maximum flow rate. The result of this is shown in figure 4.17.

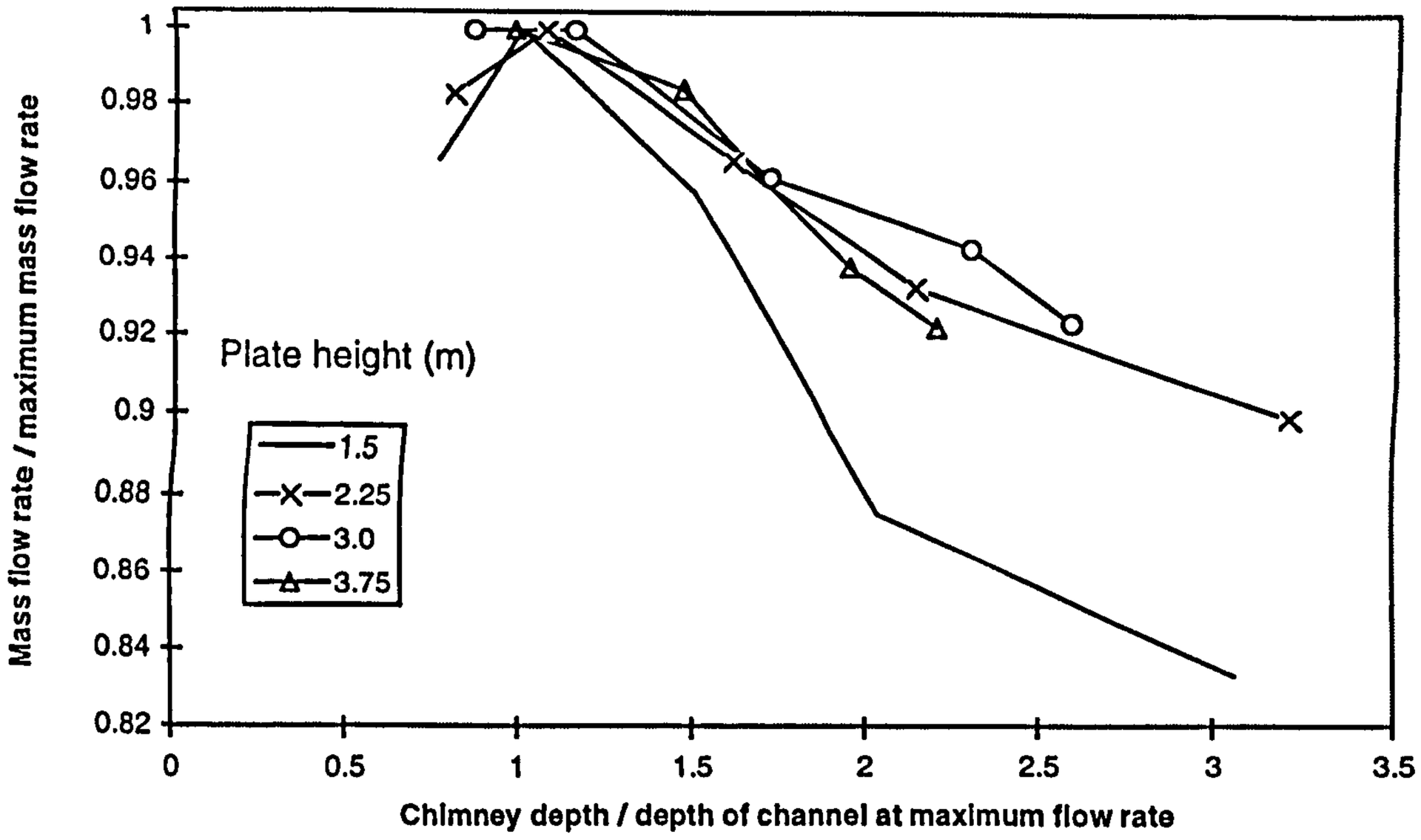

Figure 4.17. Effect of channel depth in relation to depth corresponding to maximum flow rate on mass flow rate for all rig heights at 100 W/m^2.

Figure 4.17. clearly shows that the effect of increasing the channel depth in relation to that corresponding to the maximum flow rate was very similar for all rig heights above 2.25m. It is of interest to note however that when the channel depth was increased to twice that corresponding to the maximum flow rate, the reduction in flow was only of the order of 6%. Thus indicating that the influence of the aspect ratio on the mass flow rate above that corresponding to a maximum flow rate was relatively weak.

At the lowest rig height, of 1.5m, the effect of channel depth upon the mass flow rate was significantly greater than at other heights. Investigation into the results showed no apparent reason for this difference of behavior. It is suggested by the author, that at such relatively low rig heights recirculation penetrated the whole depth of the channel and thus had a much more significant effect on the induced flow rate compared to that at greater rig heights. For channel heights above 1.5m the recirculation was predominantly limited to the upper section of the channel. This however was not investigated

fully and would require detailed experimental measurements to obtain a full explanation.

The trend in mass flow rate with respect to the aspect ratio was largely unaffected by the level of energy transferred from the plate. This indicated that within the level of uncertainty associated with the results obtained, the boundary layer depth at each rig height had remained largely constant.

4.3.2 Plate temperature and convective heat transfer coefficient results

Calculation of a convective heat transfer coefficient required that the plate temperature was established enabling equation 4.6. to be solved.

$$h_c = \frac{q''}{(T_{plate} - T_{reference})} \qquad \text{Equation 4.6.}$$

Where $T_{reference}$ is a conveniently measured air temperature against which to present the heat transfer coefficient.

The temperature of the plate was a dependent variable and thus to eliminate the effect of energy transferred from the plate from the denominator of equation 4.6., an independent input variable was sought as the reference temperature.

The inlet air temperature, which was measured accurately in the experimental investigation, was used as the reference temperature. Use of this variable allowed the heat transfer coefficient to be expressed in terms of two temperature variables that were simple to measure both within the experimental rig and also at actual installed building components. Thus offering the opportunity to compare actual performance of building components with those of this experimental investigation.

The use of the inlet air temperature as $T_{reference}$, however resulted in the local value of the convective heat transfer coefficient varying with distance up the plate as the plate temperature increased with height. Thus direct comparisons of local heat transfer coefficients between chimneys of different heights were possible but average values were not directly comparable.

The overall uncertainty in the plate temperatures at a given value of energy transferred from the plate was calculated by adding in quadrature the uncertainty in the measured temperatures and that caused by the uncertainty in the level of the energy transferred from the plate. This resulted in a level of plate temperature uncertainty of +/- 1.3^{0}C at 100W/m^2.

The effect of chimney height on the temperature elevation of the plate above that of the inlet air i.e. T_{plate} - T_{inlet}, is shown in figure 4.18.

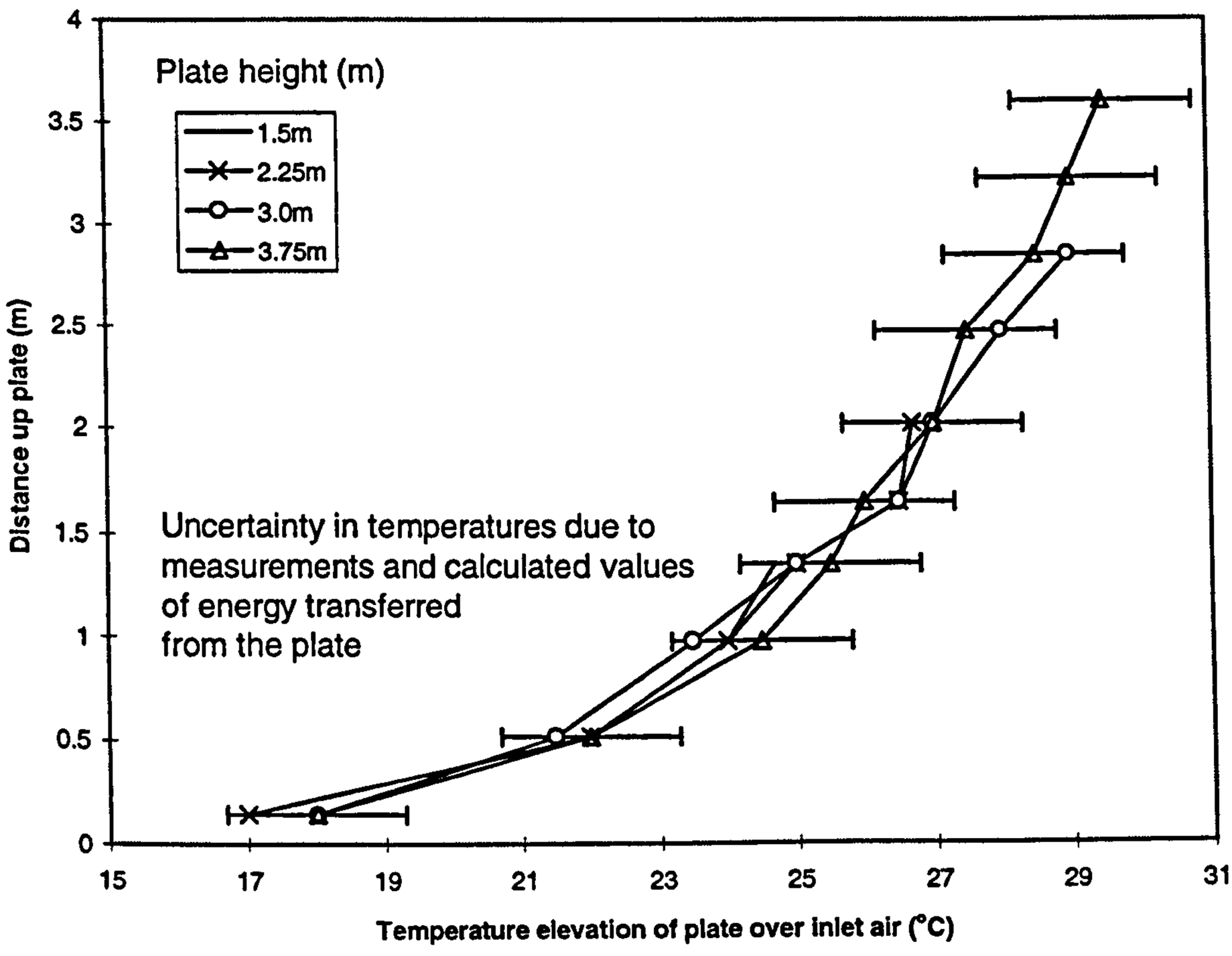

Figure 4.18. Temperature elevation of the plate above inlet air temperature at an energy transfer rate of 100 W/m^2 for each of the experimental plate heights.

Figure 4.18. indicates clearly that within the level of uncertainty identified in the temperature measurements, the temperature elevation of the plate above the inlet air for any given plate height was constant, regardless of the overall chimney height.

Within the uncertainty of the temperature measurements and calculations of energy transferred from the plate, no significant difference in the plate

temperature elevation above the inlet air was found as the depth of the channel was altered.

The uncertainty in the convective heat transfer coefficient, calculated using equation 4.6. was calculated as follows:

$$U_{h_c} = \sqrt{10.9\%^2 + \left(\frac{\sqrt{1.3^2 + 0.2^2}}{T_{mean}}\right)\%^2} = +/- 11.7\%$$

The uncertainty in the temperatures were the combined uncertainties due to measurements and the calculated levels of energy transferred from the plate.

The heat transfer coefficients derived for the plate height of 3.75m are shown in figure 4.19. From this figure it is evident that the error bars calculated for this dependent variable produce a very wide band of uncertainty.

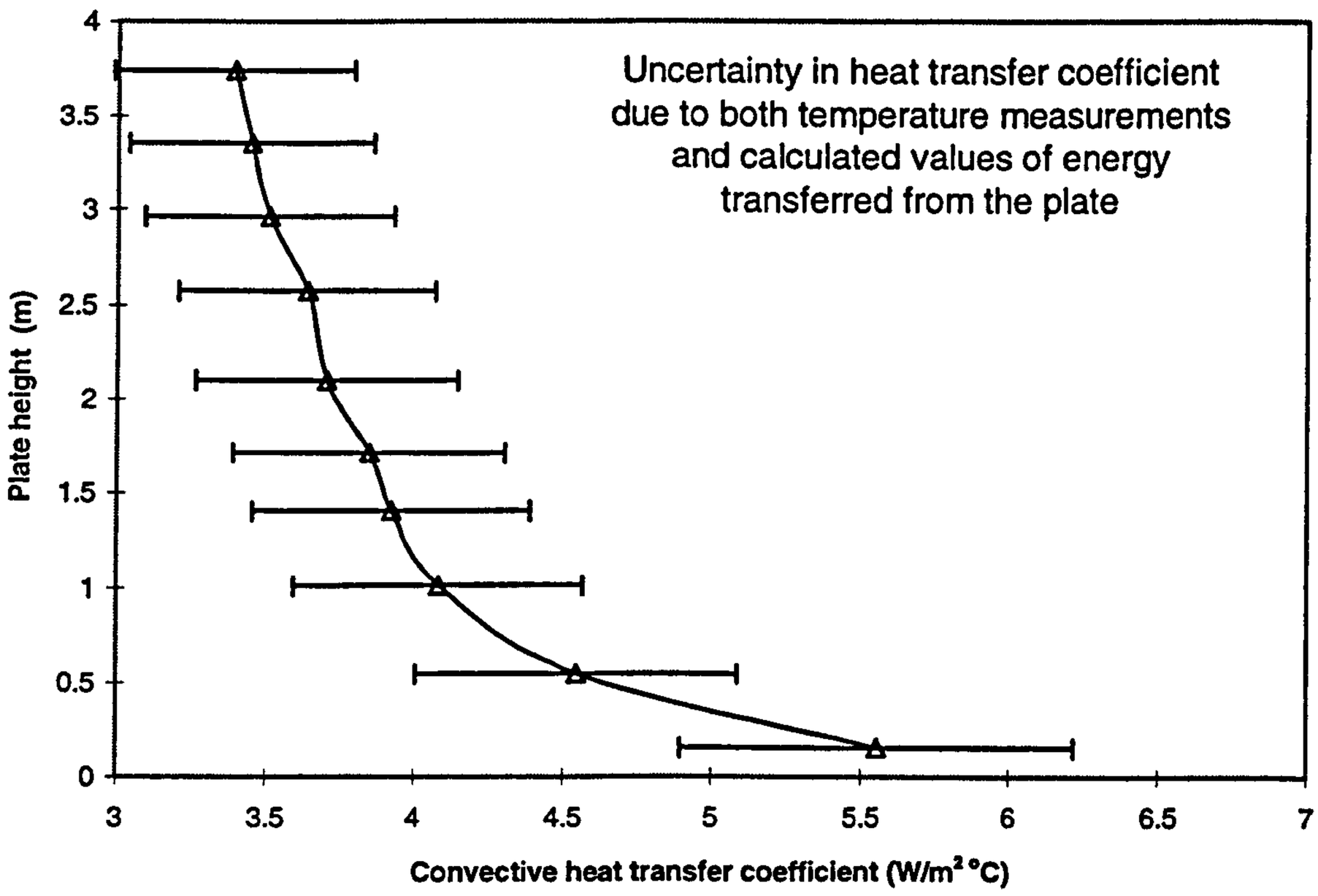

Figure 4.19. Local convective heat transfer coefficient for each of the plate heights at an energy transfer rate of 100 W/m^2.

The mean convective heat transfer coefficient was calculated to occur at approximately 0.45h. This allowed the effects of variations in energy transferred from the plate on the mean convective heat transfer coefficient to

be assessed. This is shown in figure 4.20. The error bars shown were calculated in the same way as those for figure 4.19. across the range of values of energy transferred from the plate and applied to the data for the plate height of 3.75m only.

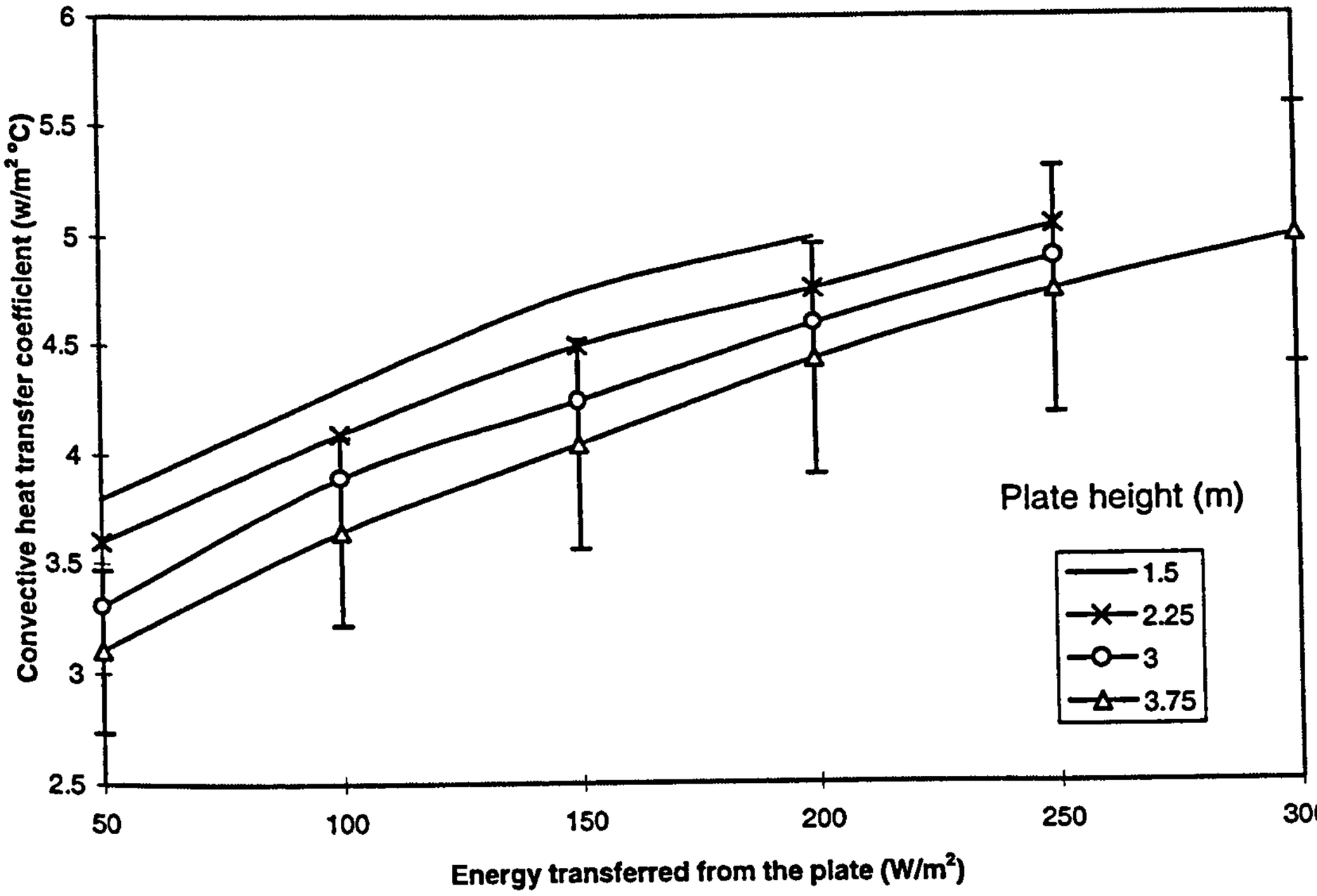

Figure 4.20. Convective heat transfer coefficients for different plate heights across a range of rates of energy transferred from the plate to the air

From figures 4.19. and 4.20. it can be seen that the when the mean convective heat transfer coefficient was calculated, the level of uncertainty, due mainly to that in the calculated value of the energy transferred from the plate to the air, was significant. This therefore reduced the potential of using these experimentally derived values of convective heat transfer coefficient for verification of CFD predictions.

4.4 CONCLUSIONS DRAWN FROM THE EXPERIMENTAL RESULTS

Calculation of the mass flow rate and energy gained by the air at the chimney outlet provided a valuable checking mechanism for the calculation of the key dependent variables to ensure significant random errors were not included in the results.

The variable temperature elevation of the bulk of the rig air above that of the inlet to the chimney resulted in variations of the mass flow rate for a given value of energy transferred from the plate. Investigation showed that over the limited range of temperature elevations of T_{rig} above T_{inlet}, the relationship between temperature elevation and mass flow rate through the experimental rig was linear. This relationship allowed the extrapolation of the mass flow rates at zero temperature elevation for direct comparison with the mathematical model predictions.

The measured mass flow rates showed variations caused by overall rig height, aspect ratio of the chimney, size of the inlet and the level of energy transferred from the plate. Thus the results provided measured data on the influence of all of these key physical variables against which the ability of mathematical and CFD model predictions could be checked.

The level of uncertainty in the results had been established with a high level of confidence ensuring that comparisons with mathematical and CFD models could be undertaken and realistic conclusions drawn.

Evaluation of the aspect ratio corresponding to the maximum mass flow rate for each plate height showed that this maximum occurred when the channel depth was very close to the depth of a turbulent natural convection boundary layer, calculated using equation 2.15. This confirmed the findings of Bouchair[5] that the maximum mass flow rate occurred when the boundary layer just spanned the channel depth. Comparison of the effect of aspect ratios showed that for chimney heights of 2.25m and above, an increase in the ratio of channel depth to boundary layer depth, had a corresponding effect on mass flow rate. The results showed that for a channel depth twice that corresponding to the maximum flow rate, the reduction in flow rate was only around 6%. Thus the sensitivity of the flow rate to changes in channel depth above that corresponding to the maximum flow rate was low.

The plate temperature elevation above the inlet air for any given height and level of heat transferred from the plate remained constant regardless of the overall height or aspect ratio of the chimney. The local convective heat transfer coefficient, based on plate temperature to inlet air difference, also therefore remained constant. The level of uncertainty in the calculated convective heat

transfer coefficient for the chimney was significant and raised doubts as to its usefulness for comparison with CFD predictions of this variable.

4.5 Comparison of experimental results with mathematical model predictions

As highlighted in Chapter Two, the zonal model approach to modeling air flows, universally used in mathematical models, assumes a horizontally fully mixed air mass. Only the complex numerical approach of CFD programmes attempt to describe the flow characteristics and true temperature distribution of air within a space. It is however important that if building designers are to use models to aid in component design then, regardless of their complexity, they must be capable of accurately predicting the mass flow rates and the influence of changes to key physical variables.

The mathematical models described in Chapter Two were therefore tested against the experimental results detailed in this chapter, to assess their suitability for application to a solar chimney.

4.5.1 The zonal model approach

The basic zonal model approach assumes the air within a space is fully mixed. Such a model was used to evaluate the effect of the temperature elevation of the rig air above that of the inlet air using equations 4.1. to 4.4. This model was therefore used as a starting point to assess if a zonal model could predict the mass flow rate through the experimental rig. The physical input variables for the model were as follows:

Plate height (m)	Stack height (m)	Inlet area (m^2)	Plate area (m^2)
1.5	1.6225	0.0675	1.5
2.25	2.3725	0.0675	2.25
3.0	3.135	0.135	3.0
3.75	3.895	0.135	3.75

Table 4.1. Input variables used for zonal model predictions

The inlet was considered to be a sharp edged orifice and thus the value of the discharge coefficient, Cd, used in equation 4.3. was 0.61.

As the mass flow rates recorded within the experimental rig varied with the channel depth, the mathematical models were compared with the maximum flow rates recorded for each of the configurations at a value of energy transferred from the plate of 100 W/m^2. The uncertainty applied to the experimental results was that calculated using equation 4.5.

Figure 4.21. shows clearly that the assumption of a fully mixed air mass significantly over predicted the mass flow rate in all configurations investigated experimentally.

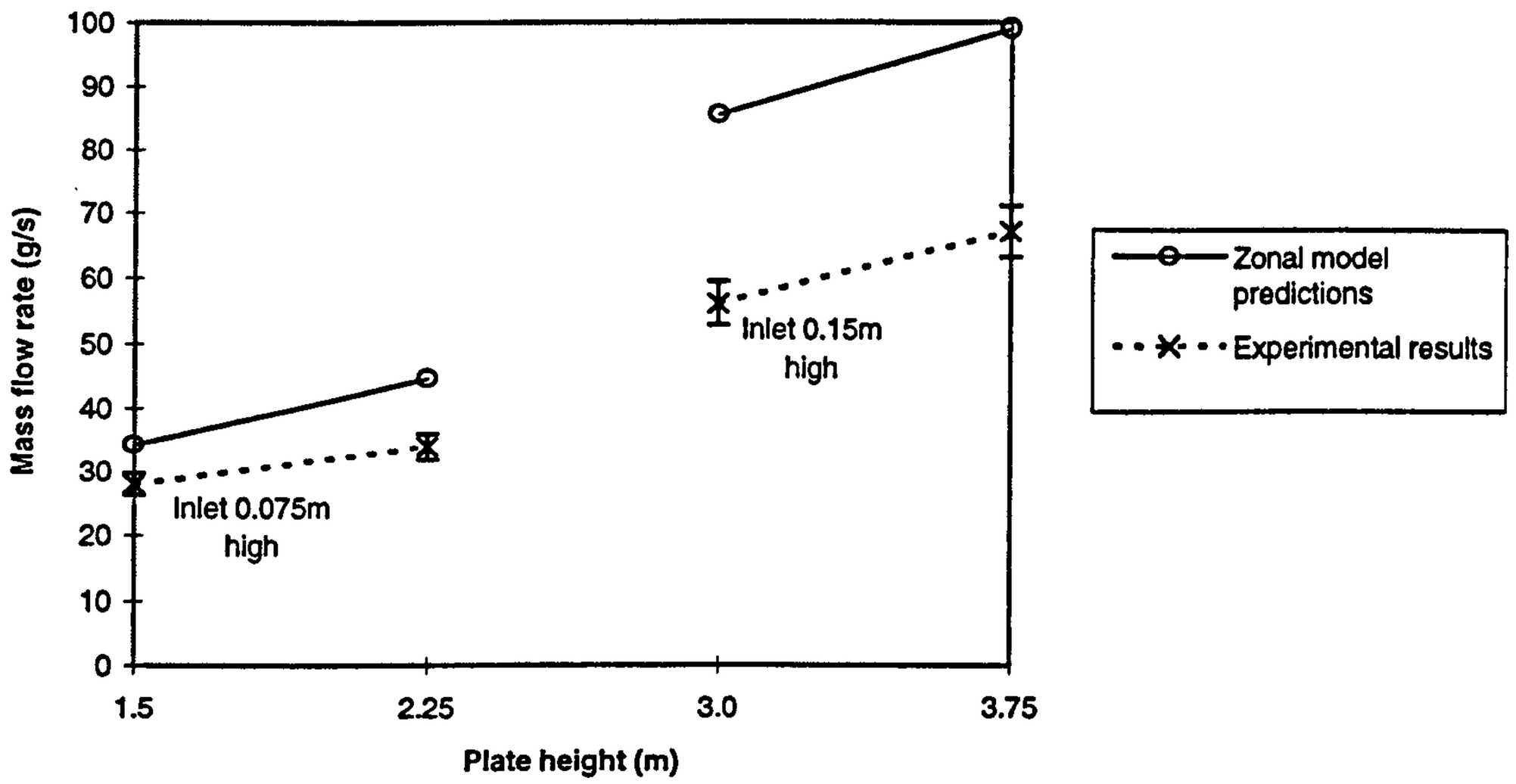

Figure 4.21. Mass flow rate predictions using equations 4.1. to 4.4.

An alternative to the above method suggested by Zikerm et al[6] assumed the temperature rise was linear and that the stack pressure created was due to the difference between the mean air temperature in the chimney and that within the rig. In this case equation 4.4. is modified as follows:

$$P_s = \rho_0 \; g \, h \; 273 \left(\frac{1}{T_{rig}} - \frac{1}{T_{mean}} \right) \qquad \text{Equation 4.7.}$$

$$\text{Where } T_{mean} = \frac{T_{rig} + T_{outlet}}{2} \qquad \text{Equation 4.8.}$$

The mass flow rates predicted by this modification to the basic zonal model are shown in figure 4.22.

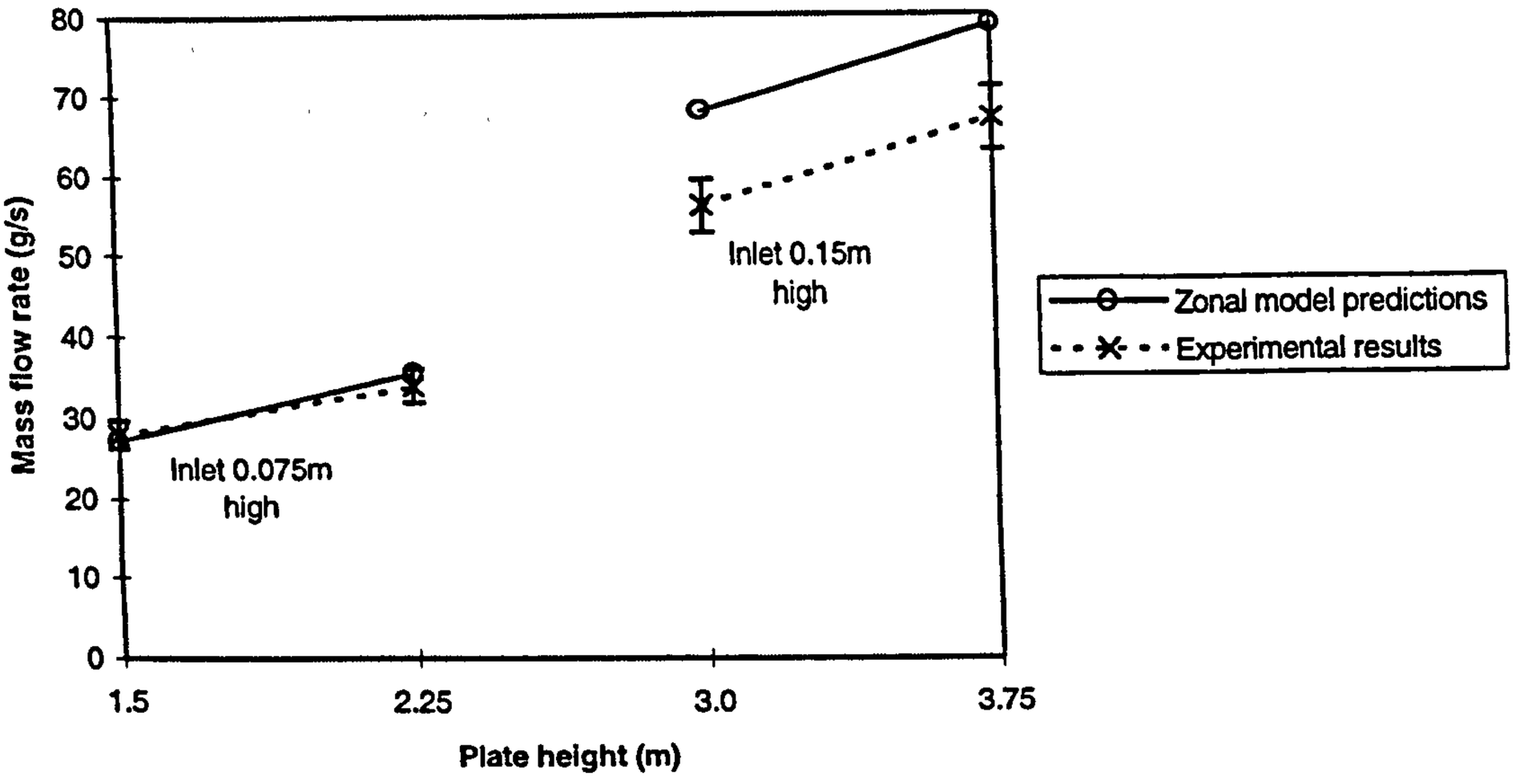

Figure 4.22. Predicted mass flow rates using equations 4.7. to replace equation 4.4.

This model predicted mass flow rates much closer to those measured experimentally than the previous model. However there was still up to a 20% error within the four configurations compared. The model appears to predict the effects of changes in height well but the trend due to changes of size of the inlet was not predicted accurately.

Thus although adjustments to the temperature gradient within the chimney appear to improve the accuracy of the predictions, it is apparent that the influence of the inlet on the flow has a significant effect and this trend was not well predicted by these zonal models.

5.5.2 The model proposed by Borgers et al[7]

The model proposed by Borgers et at[7] and discussed in Chapter Two, accounted for the channel depth, the plate temperature and the temperature of the unheated wall. To allow the model to be tested against the experimental results the variable θ_g, defined by equation 2.25. as the ratio of temperature differences between the unheated wall and the inlet air and the heated wall and the inlet air, was set at 0.1. This implied that the heating of the air by the

second wall of the channel was minimal, i.e. the channel was broadly asymmetrically heated.

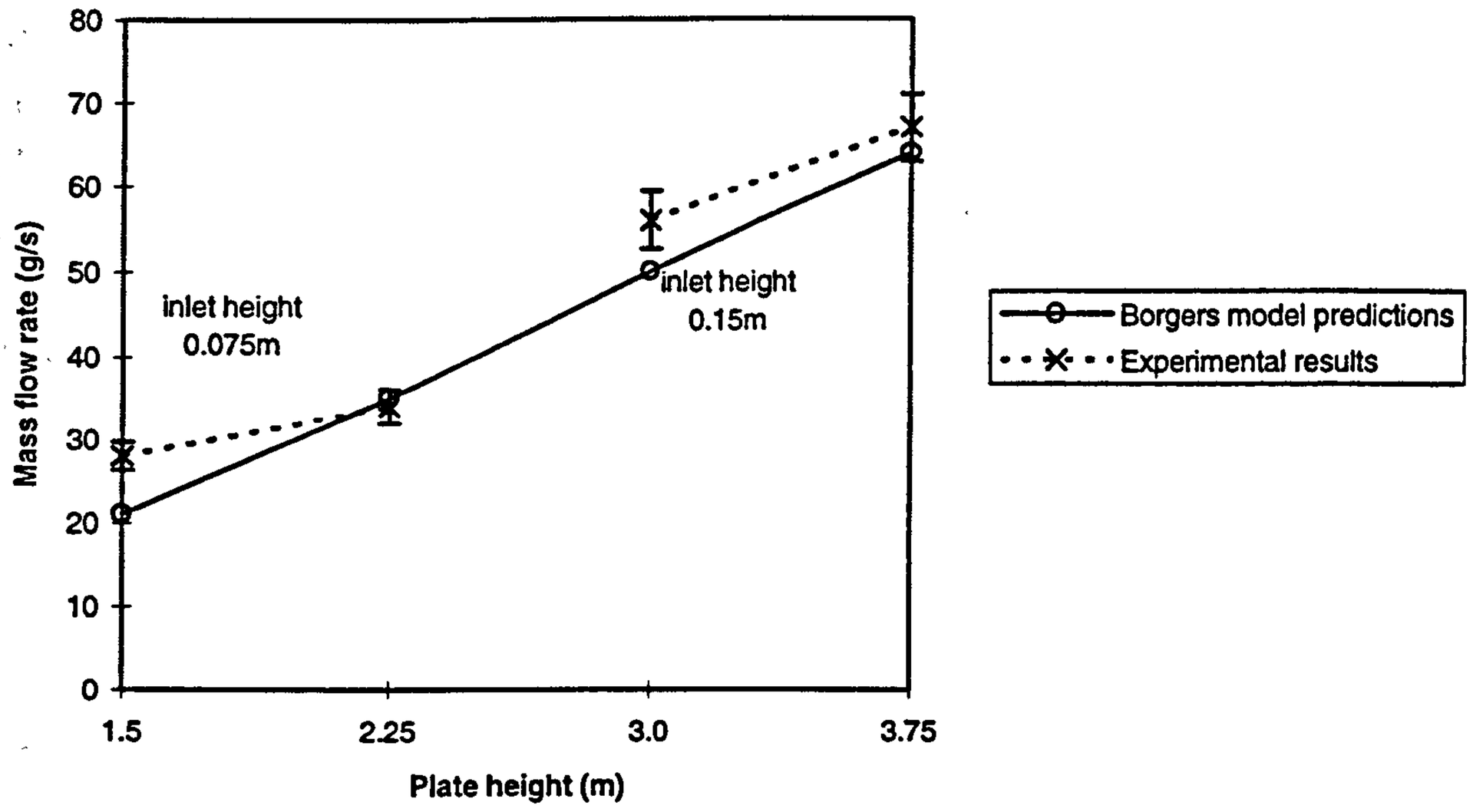

Figure 4.23. Mass flow rates predicted by the model proposed by Borgers et al[7] compared to experimental results.

The model proposed by Borgers et al[7] predicted the mass flow rates induced experimentally relatively well, however the influence of the inlet on the flow was totally omitted. In addition to this the sensitivity of the flow rate to the variable θ_g was high, with the flow rate reducing to zero if the channel was treated as fully asymmetrically heated, i.e. $\theta_g = 0$. This model was therefore not appropriate for the investigation of such building components.

4.5.3 The model proposed by Bouchair[5]

As detailed in Chapter Two, this model was based on balancing the stack pressure with the pressure losses throughout the whole component. In the model presented however the value of the pressure loss coefficient for the inlet was obtained from the experimental results. The applicability of this model to different configurations was therefore questioned. This was tested by comparing model predictions with the experimental results obtained in this investigation.

Bouchair calculated values of the pressure loss coefficient, K, for inlets height of 0.1 and 0.4m. The heights of the inlet to the experimental chimney were

0.075 and 0.15m in this investigation. Therefore for the purpose of comparison, the values of K presented for the inlet of height 0.1 were used in the pressure loss equation, equation 2.29.

Bouchair's model assumes a constant temperature plate and so the mean temperature elevations presented in figure 4.18. for an energy transfer rate of 100 W/m^2 were used as the plate temperatures for the different rig heights.

Values of friction factor, f, based on the Reynolds number calculated using the mean air velocity within the channel were obtained from the Moody chart. Corrections were applied to the hydraulic diameter to allow the chart to be used for flows between parallel smooth plates as suggested by White[8].

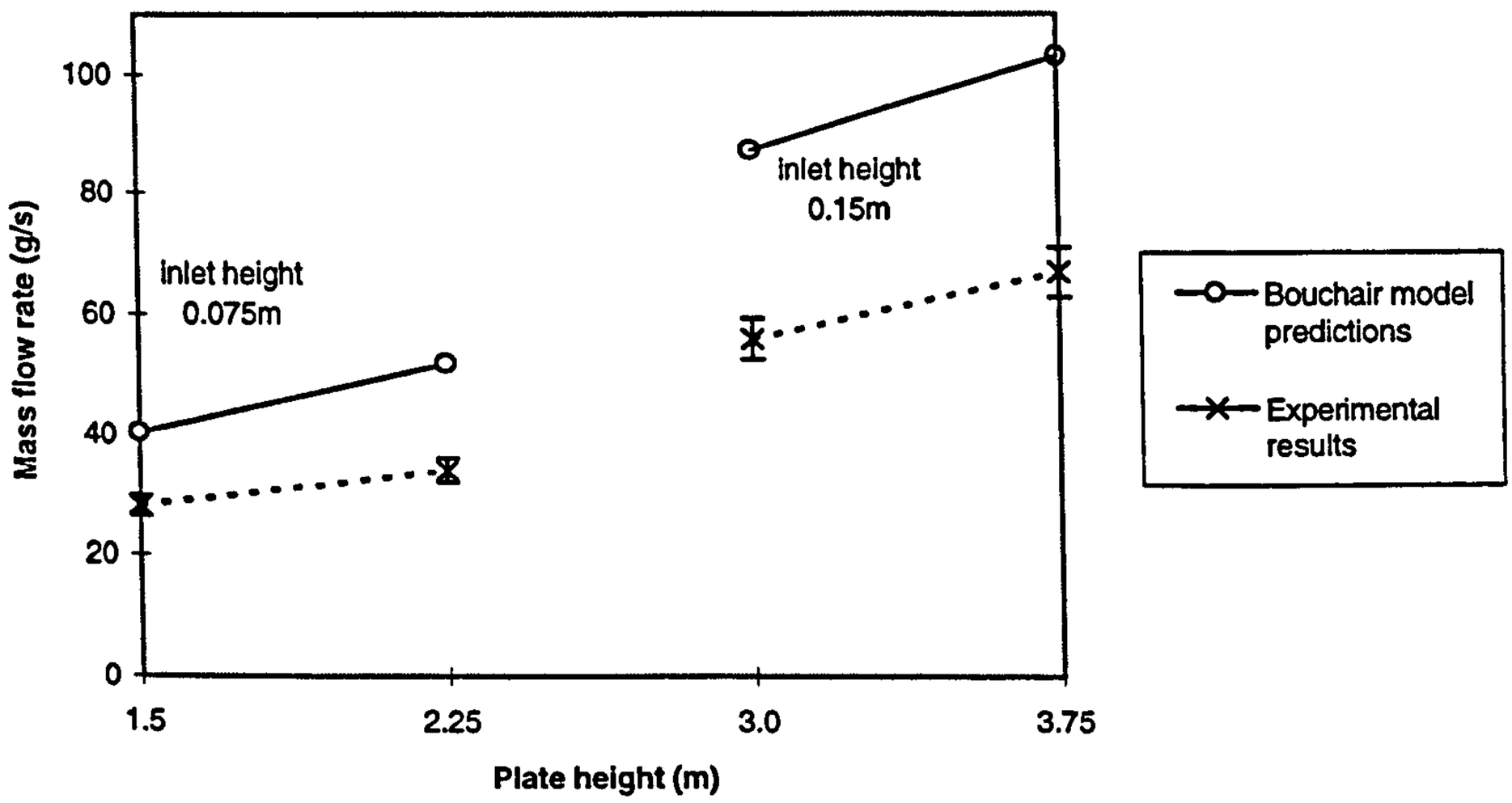

Figure 4.24. Predicted mass flow rates of the model proposed by Bouchair[5] compared to the experimental results.

From figure 4.24. it is evident that the predicted mass flow rates were significantly greater than those measured in the experimental rig. As with the zonal model predictions, the trend in mass flow rate with increase in plate height for the two inlets was well matched. Again however, the effect of changes to the inlet on the flow were less well predicted. As with the simple zonal model, the error in the predicted mass flow rate was markedly greater for the larger inlet. It was concluded therefore that if this model was to accurately predict the effect of different inlet sizes on the mass flow rate through a solar chimney configuration, inlet specific pressure loss data would be required.

Such data would however be configuration specific, and thus significantly limit the generality of the model.

As this model was also able to predict the effect of changes of channel depth, this was also tested. The results of this for a plate height of 3.0m are shown in figure 4.25.

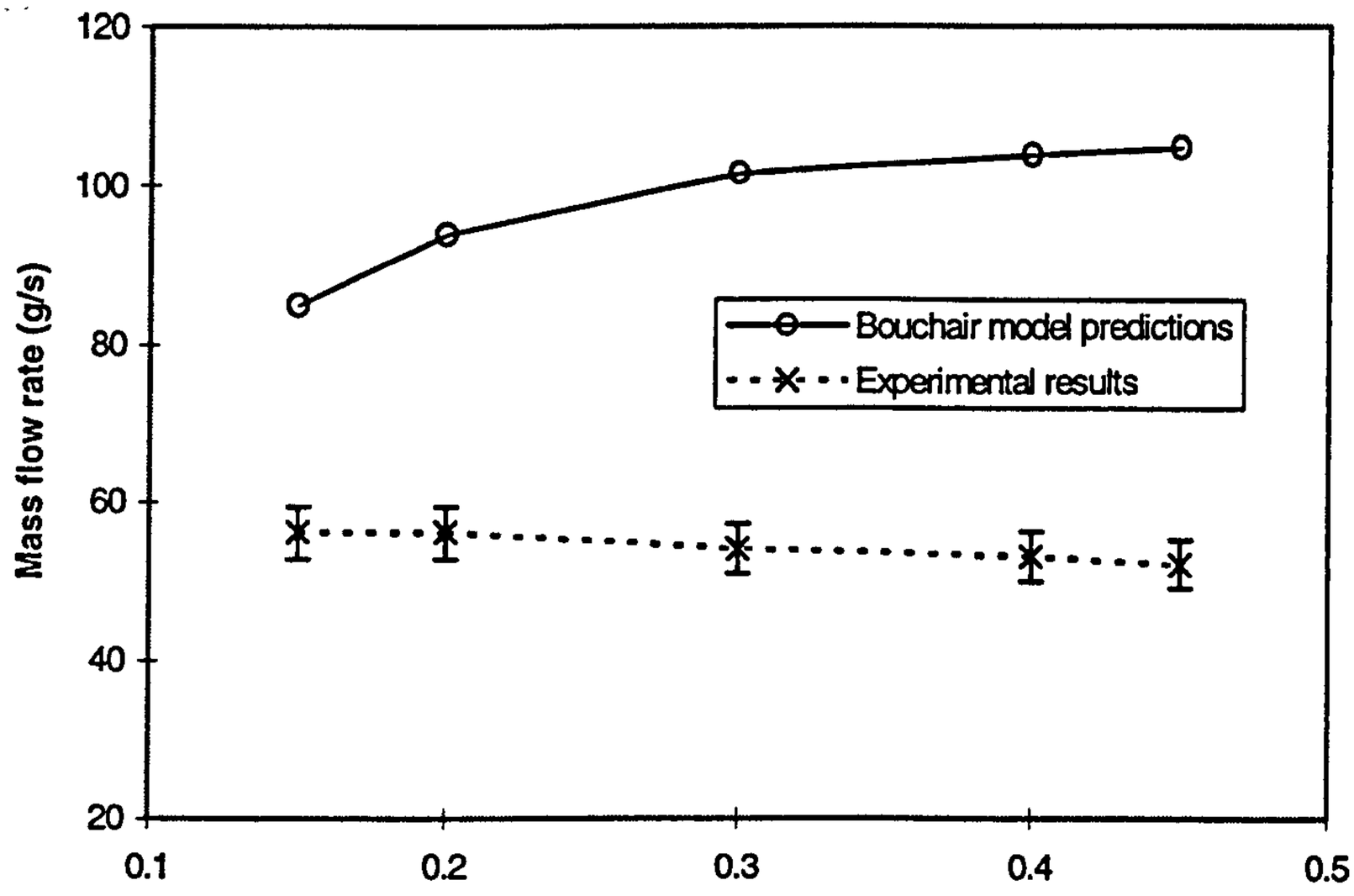

Figure 4.25. Predictions of the mass flow rate using the model proposed by Bouchair[5] compared to the experimental results for a range of channel depths

As described in Chapter Two, the fundamental difference between the zonal model assumption of mass flow rate and that of a boundary layer is that the latter has a finite maximum rate which, once achieved, will not be exceeded by further increases in inlet area or channel depth. The model proposed by Bouchair, based on frictional losses within the channel, predicted that the mass flow rate continued to rise as the channel depth was increased. However this was not the case in either the experiments he undertook or those undertaken in this investigation in which the mass flow rate reached a maximum and then as the channel depth was increased further reduced slightly. The model proposed by Bouchair[5] was therefore neither appropriate for investigating the effects of variations in the channel depth or inlet size.

4.5.4 The model proposed by Awbi[9]

This model is very similar to that proposed by Bouchair[5], with the stack pressure created by the temperature rise in the air being balanced by the pressure losses in the separate components that made up the solar chimney.

Awbi[9] however suggested the use of the common orifice equation, equation 2.3., to describe the induced flow through the inlet. For the purpose of comparing the model with the experimental results, this allowed the sharp edged orifice value of 0.61 to be used for the discharge coefficient, Cd, describing the actual rig inlet with some confidence. The values of friction factor, *f*, used for the purpose of comparison were the same as those used in the evaluation of the model proposed by Bouchair.

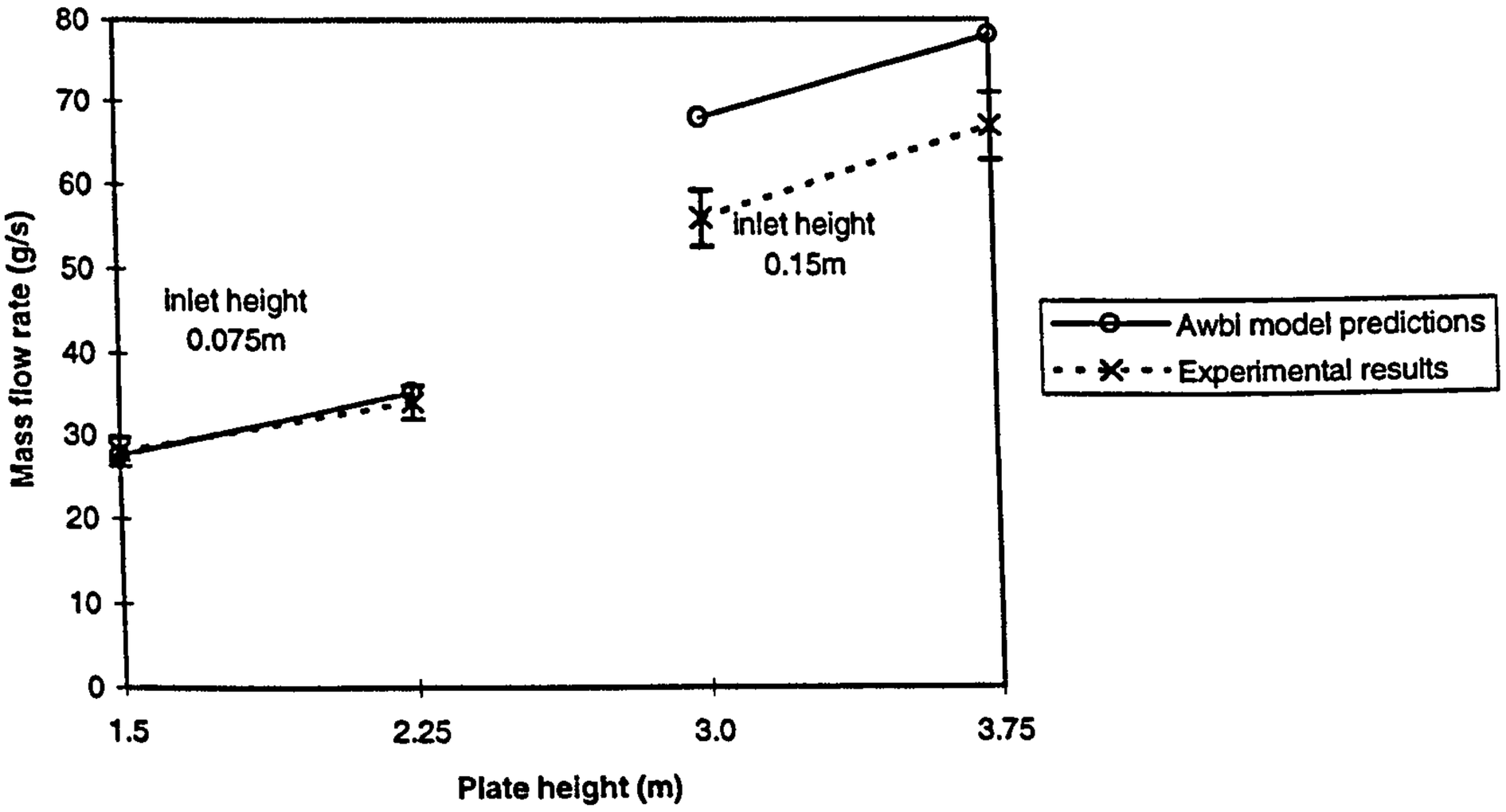

Figure 4.26. Mass flow rate predictions of the model proposed by Awbi[9] compared to the experimental results

Figure 4.26. shows clearly that the model proposed by Awbi[9] predicts the influence of both stack height and inlet area on the mass flow rate similarly to that of the simple zonal models and the model proposed by Bouchair[5]. The ability of the model to predict the influence of channel depth on the mass flow rate was also the same as Bouchair's model, being similarly based on frictional losses within the channel. Thus for general application the model is of limited use.

Conclusion of the comparisons of model predictions with the experimental results

From this comparison of the existing model predictions and the mass flow rates measured in the experimental rig it was apparent that although some of the models were able to predict flow rates close to those measured in some configurations, the influence of variations to physical input parameters overall was not well described.

None of the models were able to accurately predict the influence of the variation of the inlet size on the mass flow rate, with all models overpredicting the increase in mass flow rate when the inlet size was increased. The models incorporating the influence of channel friction offered the opportunity to describe the influence of channel depth on the flow rate. The ability to define a physical maximum flow rate was not included in any of these models resulting in increased predicted flow rates for any increase in channel depth or inlet area. The overall suitability of these models for application to a solar chimney type flow configuration must therefore be questioned.

4.6 Overall conclusion drawn from the experimental investigation and mathematical model predictions

The initial testing of the rig allowed the alternative methods of calculation of the mass flow rate and energy transferred from the plate to be tested. The result of this was that the degree of confidence developed from the uncertainty analysis, undertaken in Chapter Three, was extended to include the ability to detect significant random errors in the resultant data. The testing also highlighted the very high degree of sensitivity of the mass flow rate to variations in the temperature of the air within the rig. An investigation into the effects of this ensured that the results obtained were presented in an appropriate form for comparison with mathematical and CFD model predictions. If such an investigation had not been undertaken the potential usefulness of the results would have been significantly reduced as the influence of the stratification was several times larger than that of the uncertainty identified in Chapter Three.

The measured mass flow rate showed significant variations due to changes in all the key input variables; height, inlet area, energy transferred from the plate and channel depth. Thus the data set provided a full range of influences

against which the mathematical and CFD model predictions could be compared.

The variations in the mass flow rate with channel depth proved to be closely linked to the boundary layer depth, calculated using equation 2.15. proposed by Eckert et al[2]. This finding confirmed that of Bouchair[5] that the maximum mass flow rate occurred when the boundary layer just spanned the channel.

The plate temperature elevations above the inlet air for a given level of energy transferred from the plate were largely constant at any given plate height, within the level of uncertainty identified. Thus the local convective heat transfer coefficient was also constant regardless of overall plate height. For comparison with CFD model predictions however, the level of uncertainty in the convective heat transfer coefficient was significant, with the overall band being in excess of 20%. Thus for comparative purposes this data was of limited practical use.

The comparison of the mathematical model predictions with the experimental results largely proved that none of the models presently available were suitable to evaluate the full effects of variations in the key physical parameters. The models specifically designed to predict the mass flow rate occurring in a solar chimney took account of the channel depth, but the use of channel friction as the only influencing parameter resulted in the true trends in mass flow rate being incorrectly predicted.

Overall therefore the results of this comparison proved that such models were not appropriate for designers who wish to evaluate the effects of the key physical parameters of a solar chimney on the resulting mass flow rate.

4.7 References Chapter Four

1. Taylor, J., An Introduction to Error Analysis, Oxford University Press, USA, 1982.

2. Eckert, E. and Jackson, T., Analysis of turbulent free-convection boundary layer, NACA Technical Note No. 2207, 1950.

3. La Pica, A., Rodono, G. and Volpes, R., An experimental investigation on natural convection of air in a vertical channel, Int. J. Heat Mass Transfer, Vol. 36, No. 3, 611 - 616, 1993.

4. Lomas, K. and Bowman, N., Developing and testing tools for empirical validation, Final Report; An Investigation into Analytical and Empirical Validation Techniques for Dynamic Thermal Models of Buildings, BRE/SERC, Watford, 1988.

5. Bouchair, A. Solar induced ventilation in the Algerian and similar climates, Ph.D. Thesis, University of Leeds, UK, 1989.

6. Zrikem, Z. and Bilgen, E., Theoretical study of a composite Trombe - Mitchel wall solar collector system, Solar Energy, Vol. 39, 409 - 419, 1987.

7. Borges, T. and Akbari, H., Free convective turbulent flow within the Trombe wall channel, Solar Energy, Vol. 33, No. 3/4, 253 - 264, 1984.

8. White, F., Fluid Mechanics, McGraw-Hill Co., 2nd. Ed., New York, 1986.

9. Awbi, H., Design considerations for naturally ventilated buildings, Renewable Energy, Vol. 5, Part 2, 1081 - 1090, 1994.

CHAPTER FIVE

INVESTIGATION OF THE POTENTIAL USE OF COMPUTATIONAL FLUID DYNAMICS FOR THE PREDICTION OF THE PERFORMANCE OF A SOLAR CHIMNEY

5.1 Introduction

As stated in Chapter Two the most appropriate use of a CFD programme once its validity to predict the flow within a given flow regime has been thoroughly tested against experimental results, is the parametric testing of a flow configuration. In this way the amount of experimental investigation can be limited to a range of representative tests to explore the limits of behaviour, reducing both the time and expense incurred. Due to the complex nature of the mathematical processes undertaken to achieve a CFD solution, the level of sensitivity of the output to variations of input parameters must be evaluated if confidence in its ability to predict flows outside the range of the experimental results is to be gained. This chapter examines the sensitivity of the predictions of a CFD programme to user inputs. Taking account of the identified sensitivity, a set of models were run to assess the validity of the CFD programme to predict the flow induced in a solar chimney. The results of this testing allowed the suitability of the CFD programme for further parametric testing to be evaluated.

5.2 Issues that must be addressed before undertaking a CFD analysis

Jones et al[1] reviewed the application of CFD to air flows within buildings and identified some of the aspects that must be considered when it is used in such situations. These were:

- Dependency of the predicted result on the physical configuration of the computational grid used within the flow domain
- Influence of the turbulence model used
- Numerical and computational methods used to solve the equations
- Input data requirements and output data interpretation
- Boundary conditions

These points are now considered in detail and their effects on the CFD output analysed with respect to the investigation of the induced air flow in a solar chimney.

5.2.1 Grid dependency

As detailed in Chapter Two the flow domain is divided into a set of cells to allow the solution of the flow equations to be undertaken at discrete points. In this way the description of a continuous flow can be reduced to a discrete number of equations.

If very few cells are defined i.e. the grid is coarse, then the number of points of solution of the flow equations is small, which results in the definition of the flow being coarse. Jones[1] noted that in such cases the accuracy of the solution may well be dependant upon the grid resolution. Finer grids allow smaller details within the flow to be defined and thus the accuracy of the overall flow predicted will be increased. Li[2] noted that as the grids within a computational domain became finer, the predictions of a CFD programme became closer to those of the experimental results.

Borth[3] however commented that despite computer power increasing markedly over the past few years it was still not possible to define a grid fine enough to get full grid independence in a three dimensional flow within a room. The results of all of his CFD investigations depended to some level upon the degree of grid refinement undertaken. Qualitatively correct results could be obtained from a relatively coarse grid. Quantitatively correct results however required a much finer grid and in areas of flow where recirculation was evident, the predictions remained up to 20% different to those measured, even with the finest grid tested.

The regions of greatest grid dependence are those where steep gradients in the flow variables occur. In these regions significant errors can be produced due to the interpolation procedures used to estimate the values of variables between adjacent grid lines. To reduce these effects, grid spacing in these areas must be reduced such that the value of the flow variables do not change significantly from one cell to the next.

In addition to this the interpolation of the flow variables across cell faces to the cell centres assumes one dimensionality. Thus if the real flow is not in line with

the grid then this assumption of one dimensionality is incorrect. The significance of this error can be reduced by increasing the number of cells in the flow domain where the flow does not align with the grid[4]. This reduces the distances over which interpolation occurs and thus the error incurred.

The computational effort required to achieve a solution however increases disproportionally to the increase in cell numbers. A compromise between accuracy improved by reducing grid size and computational time reduced by increasing grid size must therefore be achieved. This is undertaken by comparing the predictions of a CFD model for increasing grid size refinement. When subsequent reductions in grid spacing make no further difference to the flow predictions, the results are considered to be 'grid independent' and the grid size is appropriate for the investigations of fluid flow within that flow domain.

To enable fine grids to be developed, without the need for the whole flow domain to be defined similarly, local grid refinement has been developed. This allows the regions where the greatest rates of flow variable change occur to be locally treated with a finer grid than the main body of the flow domain. Gunton[5] noted that the changes in cell size should be kept to within a factor of 1.2 for adjacent cells. Thus the use of very fine grids in some areas of a flow domain will have implications over a larger area. The aspect ratio of the cells also should not be allowed to become too large; a value of 5:1 is recommended by Fluent[6] and 10:1 by Gunton[5] again placing restrictions on the level of local grid refinement.

In addition to the requirements for the grid within the flow domain, the positioning of the near wall nodes can have an influence upon the accuracy of the calculation of shear stresses and heat transfer coefficients[6]. (The effect of near wall node spacing in turbulent flows is considered in the next section.) For laminar flows the following relationship has been proposed[6];

$$y\sqrt{\frac{u_\infty}{\nu\, h}} \leq 1 \qquad \text{Equation 5.1}$$

Where y is the distance from the wall to the near wall node
u_∞ is the free stream velocity

Thus for example if the free stream velocity is 0.6 m/s and the point of interest is 0.5 m from the leading edge of a flat plate (the kinematic viscosity (ν) for air at 300K is $16*10^{-6}$), the required distance of the near wall node from the wall, y, is less than 4 mm. By implication, if a large space were being considered, even with an expansion ratio of 1.2, a very large number of cells would be required to fully define the flow domain.

Within a solar chimney the flow will be buoyancy driven and the height of the chimney will generally be a minimum of one storey i.e. 3m. Therefore the likelihood of significant laminar flow existing, up a flat plate subject to a constant heat flux, before the onset of the turbulent transition region was investigated:

A buoyancy driven flow from an isolated isoflux flat plate in stationary fluid will remain laminar if the Grashof number (Gr_h^*) is below $1.6*10^{10}$ [7].

Thus if $Gr_h^* = \frac{g \beta \ q'' \ h^4}{k \ \nu^2}$ Equation 5.2

and $q'' = 100 W/m^2$

Therefore with the properties of air at 300K

$h \approx 0.42m$

In addition to this, the inlet to the solar chimney will not admit air with a uniform velocity profile as used for the development of the above relationship. Etheridge et al[7] noted that with a sharp edged orifice the velocity profile on the outlet side is such that any disturbances are strongly amplified and turbulent flow develops rapidly at values of Reynolds number (Re) greater than about 60. (For details of the layout and dimensions of the rig inlet see figure 3.8)

Therefore if $Re_{d_h} = \frac{u_{mean} \ d_h}{\nu}$ Equation 5.3

For air at 300 K, the values of Re_{d_h} are :

u_{mean} (m/s)	Re_{d_h}
0.05	433
0.5	4327

Thus from the above it can be seen that throughout the range of velocities logged at the inlet of the experimental rig, the value of Re_{d_h} was well above that stated as introducing a high level of turbulence. Therefore the potential of a fully laminar flow existing for any great proportion of the chimney height was minimal. Thus the assumption of turbulence for the whole flow domain was considered valid.

5.2.2. Turbulence models

Schetz[8] noted as recently as 1996 that the modelling of turbulence is an area where the present state of knowledge of the structure of turbulent flows is poor; adding that, in his opinion, there do not appear to be any major advances on the horizon.

The region of the fluid / solid boundary where turbulence is generated in bounded flows is still the subject of considerable research. This near wall region of a fluid flow experiences significant variations in the fluid variables and can be separated into three regions:

- The viscous sub layer. In this region the motion of the fluid is dominated by the viscous shear and turbulent eddying motion is not present. This layer is very thin.

- The log law region. This is where both viscous and turbulent effects are important to the motion of the fluid. In this region a logarithmic relationship between the non dimensional velocities and distance from the wall exists. Investigations have shown that this region extends for values of $0.02 < y/b < 0.2$ [9][4] where b is the depth of the boundary layer.

- The outer layer is where the inertia effects dominate the flow behaviour of the fluid.

To capture the large fluctuations in fluid variables within these layers close to the wall which exist because of turbulent behaviour would require a very large number of nodes. To overcome this Launder and Spalding[10] produced a mathematical model, known as the standard $k\varepsilon$ model, that allowed calculation of the effects of the near wall region through the use of wall functions. The wall functions were developed from experimental data of fully turbulent, high Reynolds number flows, describing the variation of the fluid variables within the near wall region. This allowed the near wall node to be positioned remotely from the near wall region where the rate of change of variables was reduced.

For the model to be used correctly however it is important that the node nearest to the wall is placed correctly. Launder and Spalding[10] state that it must be placed at a position where the viscous effects are overwhelmed by the turbulent ones i.e. within the log law region such that:

$$\left(\frac{k^{1/2}\, y}{\nu}\right) >> 1 \qquad \text{Equation 5.4}$$

Where k represents the turbulent kinetic energy defined as;

$$k = \frac{1}{2}\,\overline{u'^2}\;\overline{v'^2}\;\overline{w'^2} \qquad \text{Equation 5.5}$$

and $\overline{u'}$, $\overline{v'}$ and $\overline{w'}$ are the mean fluctuating Cartesian velocity components of the fluid motion.

Although the standard $k\varepsilon$ model is the most widely used and validated model currently available, Jones et al[1] noted that it still does have general deficiencies, while Holmes[11] pointed out that as the model is semi empirically based, its generality can not be assured in all cases.

The applicability of the standard $k\varepsilon$ model to non high Reynolds number fluid flows was questioned by Li et al[2], with Haghighat et al[12] and Chen et al[13] both noting that a low Reynolds number alternative model would be more appropriate for buoyancy induced flows. Low Reynolds number models do not use wall functions and therefore must resolve the grid to the wall to allow the effects of the near wall region to be fully defined. One of the main reasons for

the preference for a low Reynolds number model was highlighted by Li et al[2] who illustrated the high level of sensitivity of the fluid velocity and heat transfer coefficients calculated by a standard $k\varepsilon$ model to placement of the near wall node. Chen[14] noted that the placement of the near wall node to obtain a correct heat transfer coefficient was arbitrary and that it lacked theoretical support. Both Li et al[2] and Chen[14] concluded that the standard $k\varepsilon$ model was inappropriate for use in building situations, where the heat transfer coefficient was one of the dependant variables of greatest interest. To counter this however Chen et al[13] and Vogl et al[15] both noted that the low Reynolds number models had not been developed or well validated at high Grashof number flows, of the order of 10^{10} and greater. Jones et al[1] commented that Grashof numbers as high as 10^{13} are quite feasible within buildings due to the physical dimensions common in such situations.

Both Vogl et al[15] and Chen et al[13] did find that the low Reynolds number models were able to better predict buoyancy driven flows and heat transfer coefficients in the cases they tested without special considerations of the near wall grid position. This was however later contradicted by Chen[14] who demonstrated that the low Reynolds number models he tested were only good at predicting flows in very specific situations. Their level of generality of application was low.

Chen[14] also noted that pressure gradient flows were not predicted accurately by using turbulence models such as the standard $k\varepsilon$ model. This was due to the assumption of isotropic turbulence throughout the flow domain which for natural convection and recirculation flows was untrue.

Thus although the standard $k\varepsilon$ model has found wide spread use in the engineering world where high Reynolds number fully turbulent flows are common, such as in the aerospace industry, its application to building air flows is less well validated. Low Reynolds number models have been shown to be suitable for use in specific natural convection flows but lack the generality of the standard $k\varepsilon$ model. The detailed experimental results obtained from the solar chimney in this project allowed the validity of a CFD programme to be established. Therefore for the purpose of this investigation the standard $k\varepsilon$ model, available in the CFD programme at Cranfield University was used to describe the turbulence within the flow domain.

The application of CFD predictions to building air flows is receiving increasing coverage, for example Winwood et al[16] Cohen et al[17]. However, despite using the standard $k\varepsilon$ model, few reports discuss the effects of the near wall node positioning or assess the sensitivity of the results obtained.

To test the sensitivity of the standard $k\varepsilon$ model to near wall node position, a CFD model of a flat plate was developed using the CFD programme CFD 2000[18] , as detailed below:

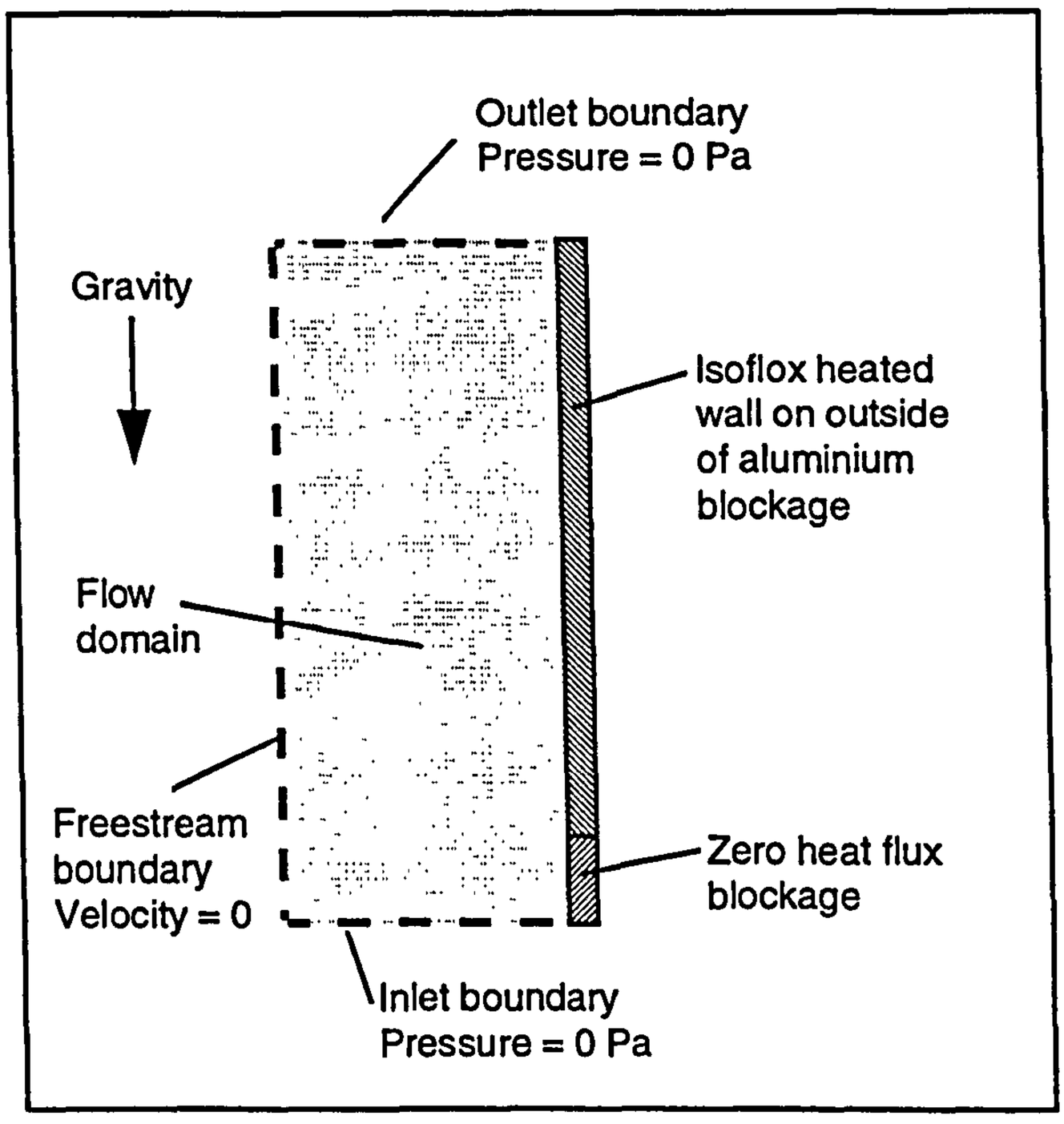

Figure 5.1. Flat plate model used for the testing of the sensitivity of the standard $k\varepsilon$ turbulence model to positioning of the near wall node.

The position of the near wall node is defined by the nondimensional number y^+, where:

$$y^+ = \frac{\rho \, y \, k^{\frac{1}{2}} \, C_\mu^{\frac{1}{4}}}{\mu} \qquad \text{Equation 5.6}$$

Where C_μ is constant at 0.09

This equation is considered valid for values of y^+ greater than 15 which is outside the viscous sub layer[6] .

The turbulent kinetic energy (k) is however directly related to the turbulent shear stress of the fluid which requires the flow equations to be solved before equation 5.6 can be used to calculate y^+. There was therefore a need to be able to calculate y^+ before running the model and thus reduce the need to undertake iterative predictions to set the position of the near wall node correctly. Added to this Chen[13][14] noted that the standard $k\varepsilon$ model predicted values of k that were significantly lower than those measured experimentally in the near wall region. Therefore to check the positioning of the grid before the model was run, and as a manual check on the predicted values of k, the following method of calculating the value of y^+ was adopted.

Incropera[19] proposed the following relationship:

$$\frac{C_f}{2} = \frac{\tau_w}{\rho u_\infty^2} \qquad \text{Equation 5.7.}$$

Where the skin friction coefficient, C_f, was defined by Schetz[8] for a turbulent flow over a smooth flat plate as:

$$\frac{C_f}{2} = \frac{0.185}{(Log_{10} Re_h)^{2.584}} \qquad \text{Equation 5.8.}$$

$$\text{Where } Re_h = \frac{u_\infty h}{\nu} \qquad \text{Equation 5.9.}$$

Burmeister[20] suggested that for a natural convective flow, the velocity u_∞ required for the calculation of Re_h can be interpreted as the maximum velocity in the boundary layer. Thus the value of C_f was calculated based on maximum boundary layer velocity.

Bejan[21]and Versteeg et al[4] proposed that :

$$y^+ = \frac{y}{\nu}\sqrt{\frac{\tau_w}{\rho}} \qquad \text{Equation 5.10.}$$

Therefore substituting equation 5.7 into equation 5.10 the following relationship was obtained, allowing calculation of y^+ for the near wall cell.

$$y^+ = \frac{y}{\nu} u_\infty \sqrt{\frac{C_f}{2}} \qquad \text{Equation 5.11.}$$

Based on the plate configuration in figure 5.1., equation 5.1. for the laminar region and equations 5.7. to 5.11. for the transition and turbulent regions, the relationship between h, y and y^+ is shown in figure 5.2.

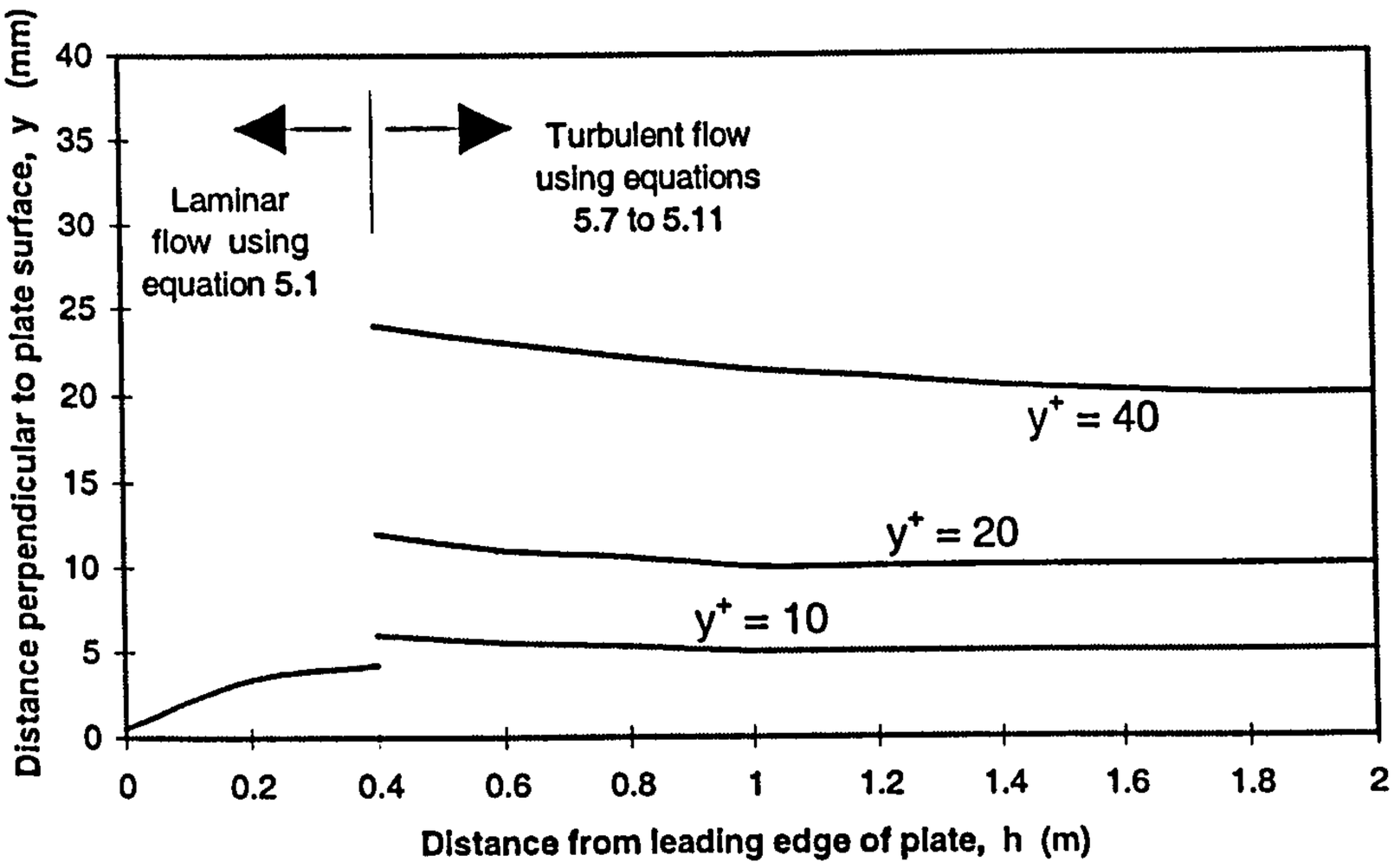

Figure 5.2. Distance of near wall node from a flat plate for a range of values of y^+ for the turbulent region and the maximum distance of the near wall node for the laminar region subject to a constant heat flux of 100 W/m^2.

From figure 5.2. it is evident that the distance of the near wall node from the plate is very dependant upon y^+ . Therefore, if it is required to position the near wall node at a given value of y^+, this will have implications for the grid throughout the remaining area of the flow domain. A very small near wall cell requirement would result in a very fine grid throughout the domain to ensure that the aspect ratio and spacing requirements were met. For the investigation of large spaces, such as building interiors, this implies that very extensive grids must be used, resulting in considerable computer and time resources being required to achieve fully converged solutions.

Effect of grid spacing on velocity profile of a natural convection boundary layer.

For the plate detailed in figure 5.1. velocity profiles were obtained for equal grid spacings equating to a range of values of y^+ from 3 to 96. This corresponds to the near wall node distances given in Table 5.1.

Near wall node distance from wall y (mm)	Value of y^+ of near wall node
2.5	3
5	6
10	18
15	30
20	44
30	73
40	96

Table 5.1. Comparison of near wall node distance and value of y^+ used for velocity profile investigation.

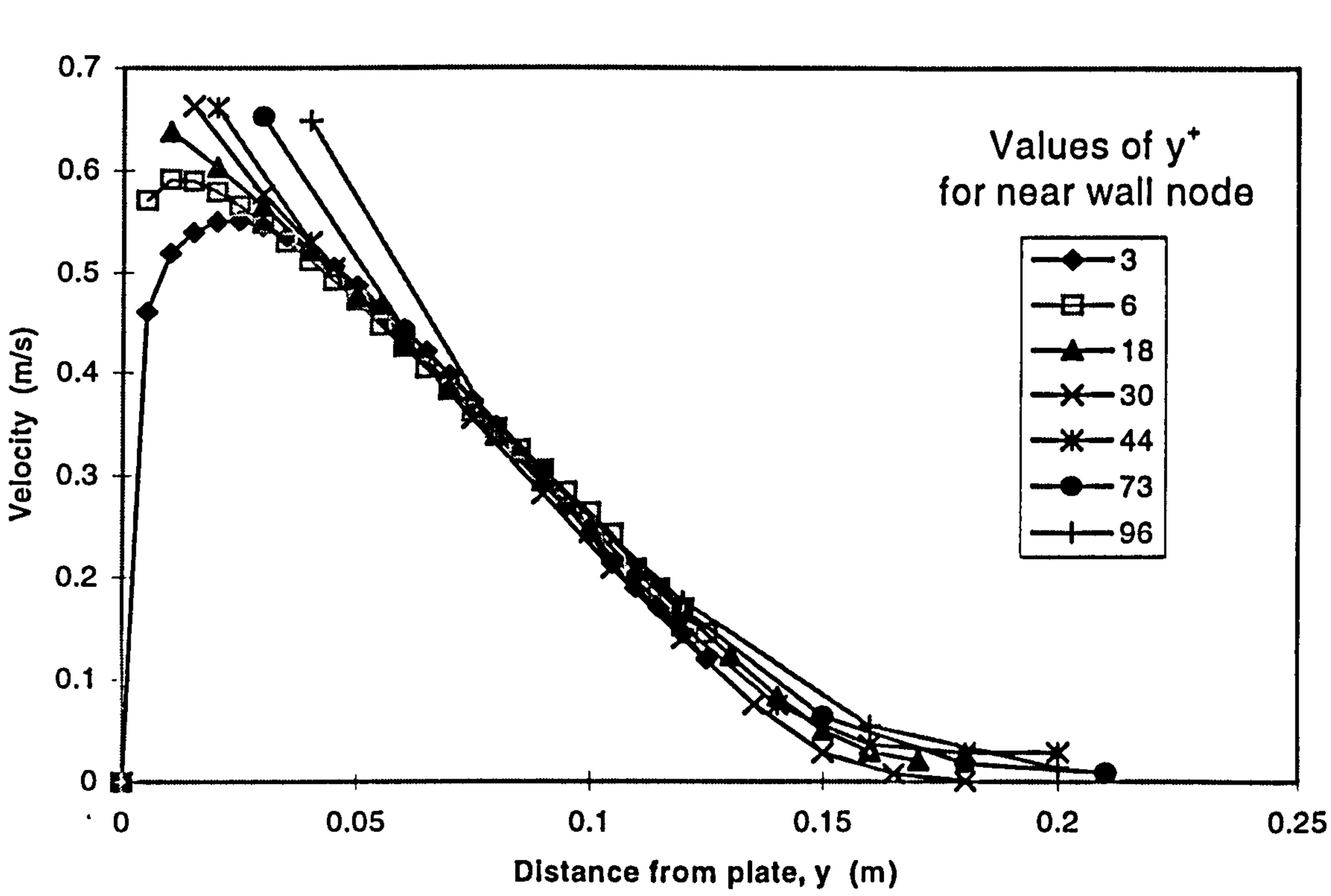

Figure 5.3. Velocity profiles through the boundary layer with a range of equal grid spacing corresponding to values of y^+ for the near wall node ranging from 3 - 96.

As can clearly be seen from figure 5.3., the overall velocity profile was little affected qualitatively by the size of the grid. This agreed with the findings of Borth[3], who found that even a coarse grid gave qualitatively correct results. Quantitatively however the value of the maximum velocity was dependant upon the grid size, only being relatively constant at values of $y^+ \approx 18$ and above. The position where the maximum flow velocity occurred was however affected by all grid refinements.

The conclusion drawn from this was that both the position and value of the maximum velocity of a naturally convection flow along a vertical flat plate are sensitive to the near wall node position. The effect of this on the prediction of the mass flow rate within the boundary layer was however negligible for near wall node values of y^+ greater than 18. Therefore for the purpose of predicting the mass flow rate though a solar chimney, the process of grid refinement was used to ensure that predictions of this dependant variable were independent of the near wall node position.

Effect of grid spacing on convective heat transfer coefficient of a natural convection boundary layer.

The only method of checking the accuracy of CFD model predictions of heat transfer coefficients is to check the values predicted for a simple flow configuration with those of published experimental investigations of the same configuration. For natural convection that is usually a flat plate configuration.

This approach was undertaken by Li et al[2] for an enclosed naturally driven flow with one wall heated to a uniform temperature of 80°C and the other maintained at 34.2°C. Li et al used equally spaced grids ranged from 20 * 20 to 111 * 111 cells within the flow domain.

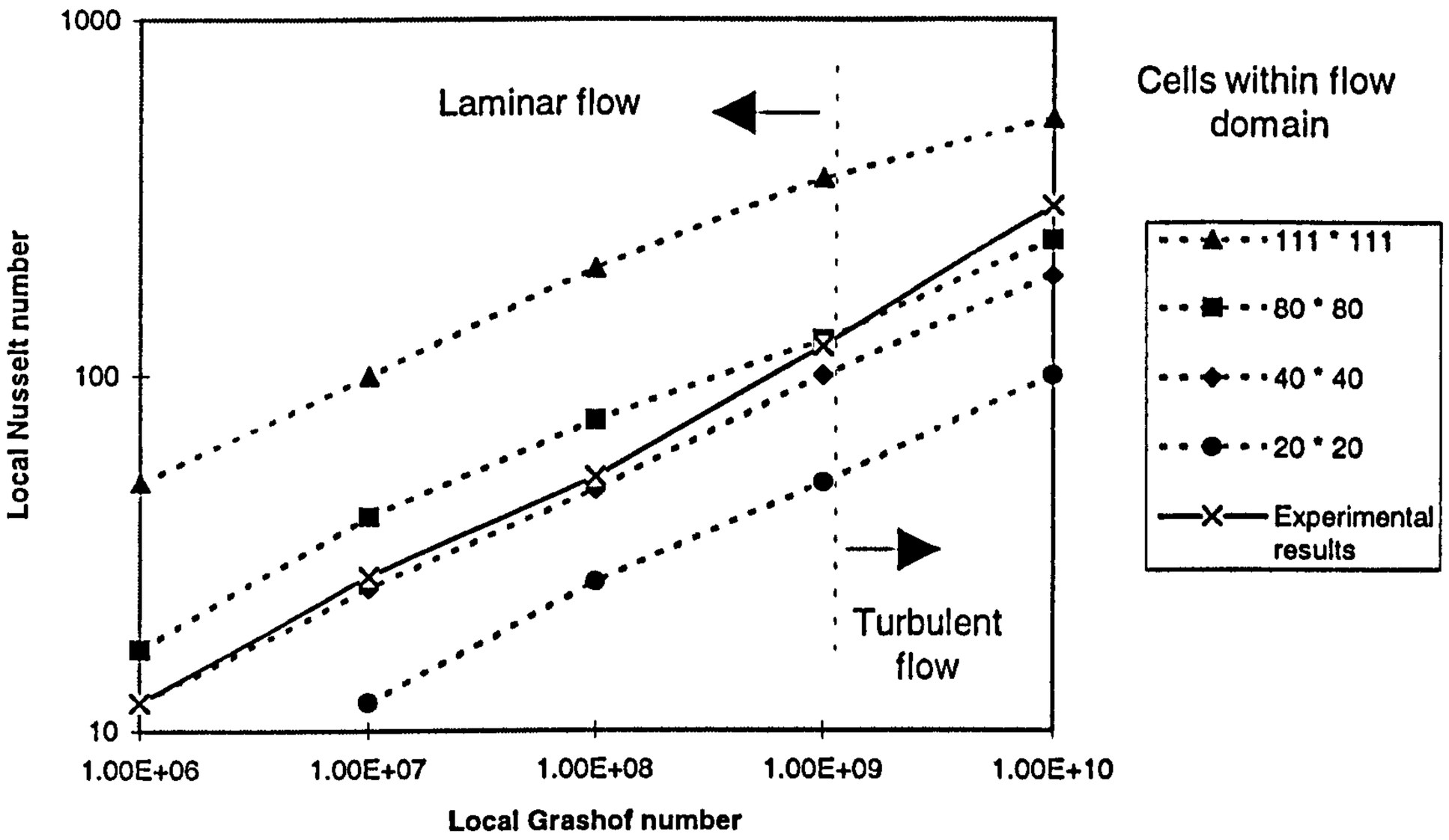

Figure 5.4. Results found by Li et al[2] comparing predicted and experimental local Grashof and Nusselt numbers for an enclosed natural convective flow

Figure 5.4. shows that as the distance of the near wall nodes from the wall was reduced, at a constant value of Grashof number, the value of the predicted Nusselt number increased. This indicated that the position of the near wall node had a direct influence on the predicted convective heat transfer coefficient. Chen[14] undertook a similar validation of CFD predictions and concluded that the positioning of the near wall cell was arbitrary and had to be adjusted, recommended as y^+ =10, before correct convective heat transfer coefficient results could be obtained.

In order that the sensitivity of the proposed modelling configuration could be assessed, a series of tests were run and the results checked against correlations produced from published experimental investigations.

The result of most published investigations into convective heat transfer from a flat plate present their results in the form; local Nusselt number verses local Grashof number. The Grashof number however can be expressed in terms of temperature difference between the wall and the free stream fluid or in terms of the heat flux,:

For isothermal plates

$$Gr_h = \frac{g \beta \Delta T h^3}{\nu^2} \qquad \text{Equation 5.12}$$

Where $\Delta T = (T_{Plate} - T_{fluid})$ and T_{Plate} is constant

For isoflux plates

$$Gr_h^* = \frac{g \beta q'' h^4}{\nu^2 k} \qquad \text{Equation 5.13}$$

Where q'' is the rate of constant heat flux transferred from the plate

$$Nu_h = \frac{h_c h}{k} \qquad \text{Equation 5.14}$$

$$\text{Where } h_c = \frac{q''}{\Delta T} \qquad \text{Equation 5.15}$$

There are two reasons why the use of equation 5.13. was more appropriate for the proposed investigation, rather than the more commonly used equation 5.12.

1. The solar chimney was subject to a constant solar heat flux and as demonstrated in figure 4.18. from the experimental results, the temperature of the plate varied with height. Thus an assumption of an isothermal plate was incorrect.

2. Plotting Nu_h against Gr_h required that the temperature difference was used in both axes. As plate temperature was a dependant variable that changed with positioning of the near wall node, a comparison of such results would tend to mask other relationships due to the changes of plate temperature. Plotting Nu_h against Gr_h^* however allowed the dependant variable of plate temperature to be plotted against the independent variable of heat flux. Thus ensuring that for a given heat flux, changes in plate temperature were identified as being caused by changes to the near wall node positioning.

Bejan[21] reported the following relationship for a vertical isoflux heated plate:

$$Nu_h = 0.55 \left(Gr_h^* Pr\right)^{\frac{1}{5}} \quad \text{for laminar flow} \qquad \text{Equation 5.16}$$

$$Nu_h = 0.17 \left(Gr_h^* Pr\right)^{\frac{1}{4}} \quad \text{for turbulent flow} \qquad \text{Equation 5.17}$$

As the assumption of turbulence was made for the whole flow domain the results of the CFD predictions were compared with those of equation 5.17.

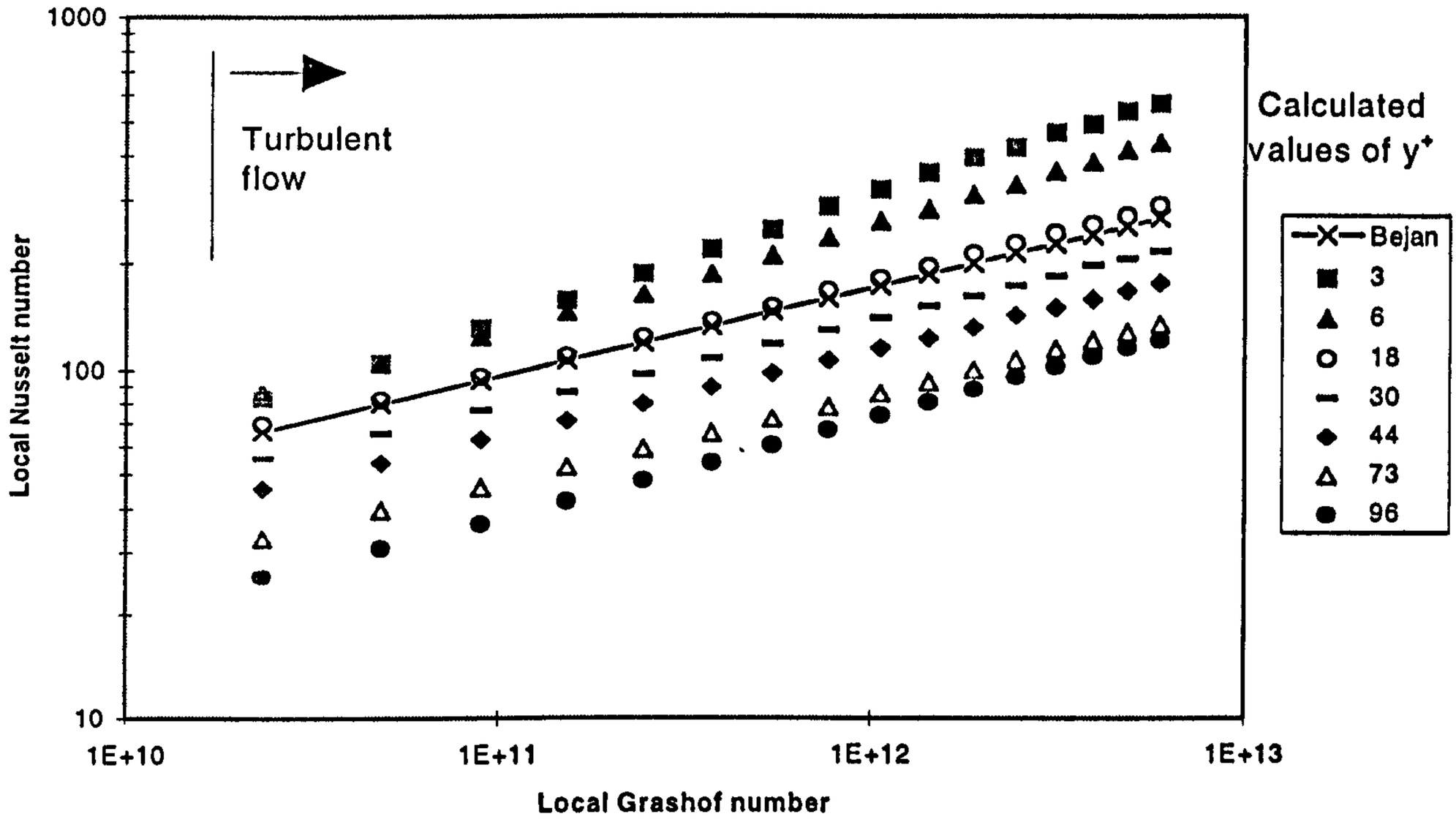

Figure 5.5. Comparison of CFD predicted results for local Nusselt number with those reported by Bejan[21]

As can be seen from figure 5.5. the sensitivity of the heat transfer coefficient, Nu_h, was very similar to that found by Li et al[2] presented in figure 5.4. The value of Nu_h was highly dependant upon the position of the near wall node. For this configuration the calculated value of $y^+ \approx 18$ produced the most consistent values of heat transfer coefficient compared to correlation equation 5.17 reported by Bejan[21]. Thus as Chen[14] noted the value of y^+ required to obtain a correct value of Nu_h appeared to be significantly below the minimum of 25 / 30 recommended[4][6] for high Reynolds number flows.

The reason for this may be explained by the findings of Tsuji et al[22] who investigated the boundary layer of a natural convection flow, concluding that the viscous sub layer was significantly smaller in such a flow than that of a forced convection flow. Tsuji et al[22] stated that the sub layer was only evident up to $y^+ = 1$. If this was the case then the requirement to position the near wall node in the region where viscous effects are overwhelmed by turbulent effects implies that the positioning of the near wall node may be much closer to the plate than $y^+ = 25 / 30$. Thus the values of $y^+ = 10$ recommended by Chen[14] and that found by the author $y^+ \approx 18$ may be appropriate, but as Chen noted the positioning appears to be arbitrary and lacks any theoretical support. This

therefore does not raise confidence in the ability of the CFD programme to predict the heat transfer coefficient for a flow that can not be directly compared with experimental results.

The conclusion drawn from this investigation into the sensitivity of the heat transfer coefficient to the positioning of the near wall node highlighted the high degree of sensitivity of this dependant variable. The implication of this for the prediction of convective heat transfer coefficients was that the CFD predictions were only suitable for comparison with detailed experimental results. The use of CFD for prediction of convective heat transfer coefficients for configurations not investigated experimentally was therefore not undertaken as the high level of sensitivity of this dependant variable meant that unvalidated predictions were unreliable.

5.2.3 Numerical methods

Significant levels of research is being undertaken into the accuracy and efficiency of the numerical methods used in CFD programme[8]. However a discussion of the merits of different methods is outside the scope of this investigation and the default methods of the commercial programme, CFD 2000[18] used at Cranfield University, were adopted.

5.2.4 Input and output parameters

A. Physical parameters

Wall smoothness
The value of this may be varied within the CFD programme. However, as all the internal surfaces of the chimney were aluminium lined, the default assumption within the CFD programme of smooth walls was unchanged.

Conjugate solid
To model the metal plate within the solar chimney to allow the surface temperature to be established, a highly conductive solid layer was created and the heat transfer solved for solid conduction. Aluminium with a conductivity of 237W/m °C was used for the solid. The ratio of conductivities of air to aluminium is 0.026 : 237 i.e. approximately 1 : 9000, the effects of small errors in the assumption of the conductivity of the plate were therefore minimal. As the CFD predictions were of a steady state condition, all the other physical parameters of aluminium were not of importance.

Fluid - Air

To increase the speed of convergence the Boussinesq approximation was used. This approximation allowed the assumption that the density of the fluid remains constant at a value prescribed by the user for all solved equations, except the buoyancy term in the momentum equation, where it is calculated as follows:

$$(\rho - \rho_o)\, g = -\rho_o\, \beta\, g\, (T - T_o) \qquad \text{Equation 5.18.}$$

Equation 5.18. therefore allows the effects of density changes to be calculated without need to calculate density at each node. The validity of the Boussinesq assumption was investigated by Gray et al[23] and shown to be valid for both turbulent and laminar flows where $\Delta T / T_{mean} < 0.1$, ΔT is defined as the change of temperature of the fluid within the flow regime and T_{mean} is the mean temperature within the flow regime. From the experimental results the maximum value of ΔT was 24K when T_{mean} was 293K. Therefore the approximation was valid for the flow investigated.

B. Data interpretation

The output of data from the CFD prediction was evaluated through a post processing visualisation programme. This however integrated the data across the whole flow domain, therefore to obtain data at specified nodes, such as the near wall nodes, the results files of the CFD programme itself were interrogated.

5.2.5 Boundary conditions

The defining of the boundary conditions, in particular that of the inlet, was highlighted by Skovgaard et al[24] as an area of great potential influence on the outcome of a CFD simulation. The reason for this was that the parameters such as turbulence and velocity profile of the fluid at an inlet were dependant upon many factors, in particular the flow upstream of the inlet. Therefore general cases could not be specified. Skovgaard et al[24] noted that inlet specific data must be available if room flows were to be accurately modelled.

The driving force of the solar chimney was the stack pressure created by the changes in temperature, and thus density, of the air within the vertical channel. For this reason the description of the inlet or outlets with predescribed velocities and profiles would be to place an incorrect assumption on the

prediction process. It would also require that the mass flow rate be calculated before the model was run which would require that assumptions about the nature of the flow within the channel had to be made. This would result in the very assumptions used in zonal models being used to predict the flow within a CFD model. To ensure that the CFD programme calculated the flow rate, both the inlet and outlet boundaries were described as pressure boundaries with pressure equal to atmospheric at their respective heights. This allowed the CFD programme to balance the pressure losses due to the fluid flow with the stack pressure created.

A. Inlet profile of air

To test how a sharp edged orifice, such as that use in the experimental rig, figure 3.9, was best modelled, two configurations of the orifice were described, one with the orifice as the inlet boundary and the second using an inlet plenum representing the air outside the orifice, as shown in figure 5.6. These were both tested to evaluate their ability to predict the actual inlet flow profile. The results are shown in figure 5.7.

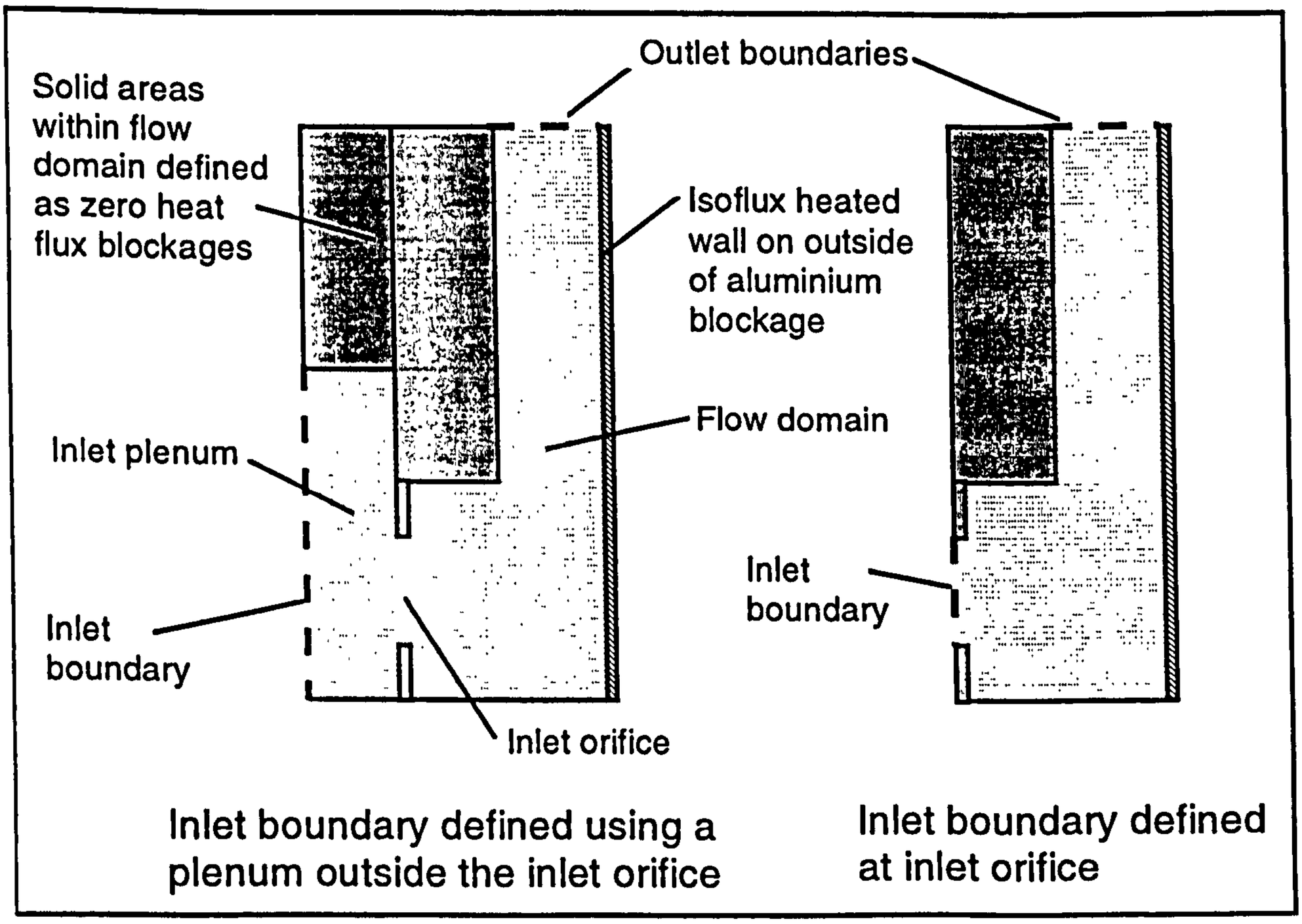

Figure 5.6. Configurations of inlet boundary investigated

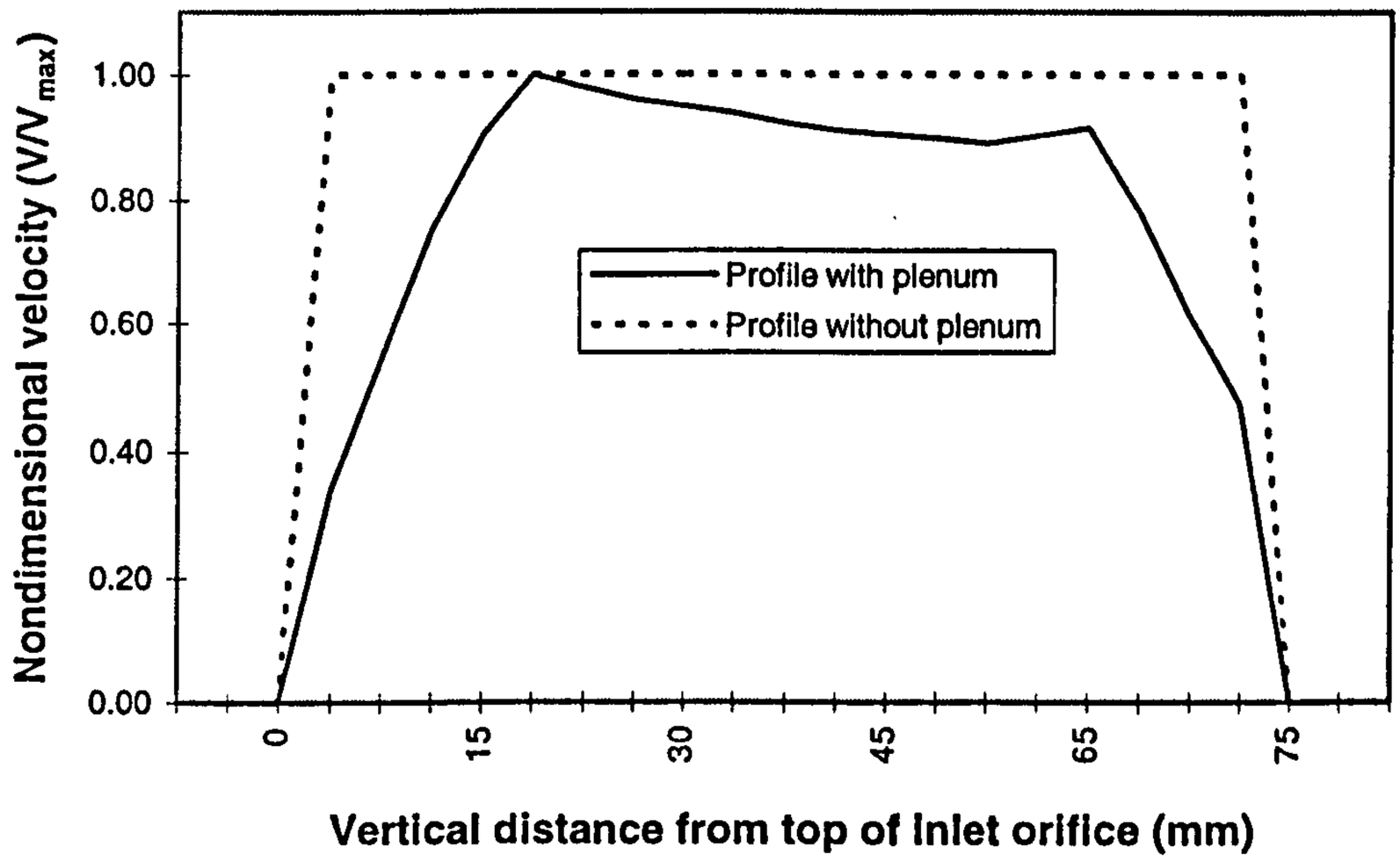

Figure 5.7. Inlet velocity profiles at the sharp edged orifice for the inlet configurations shown in figure 5.6.

From figure 5.7. it was apparent that to obtain a realistic profile, a plenum was required outside the inlet. Cohen et al[17] modelled a room ventilated by an open window and found that inclusion of a plenum outside made only a 6% difference in the bulk flow rate, concluding that such a configuration should only be considered if very accurate modelling was being undertaken. However as can be seen from figure 5.7., regardless of the flow rate, the flow profile was significantly affected by the inclusion of a plenum, which may greatly influence the flow within a space. The effects of the depth of the plenum were therefore checked for the rig configuration. The results of this on the predicted inlet profile are shown in figure 5.8.

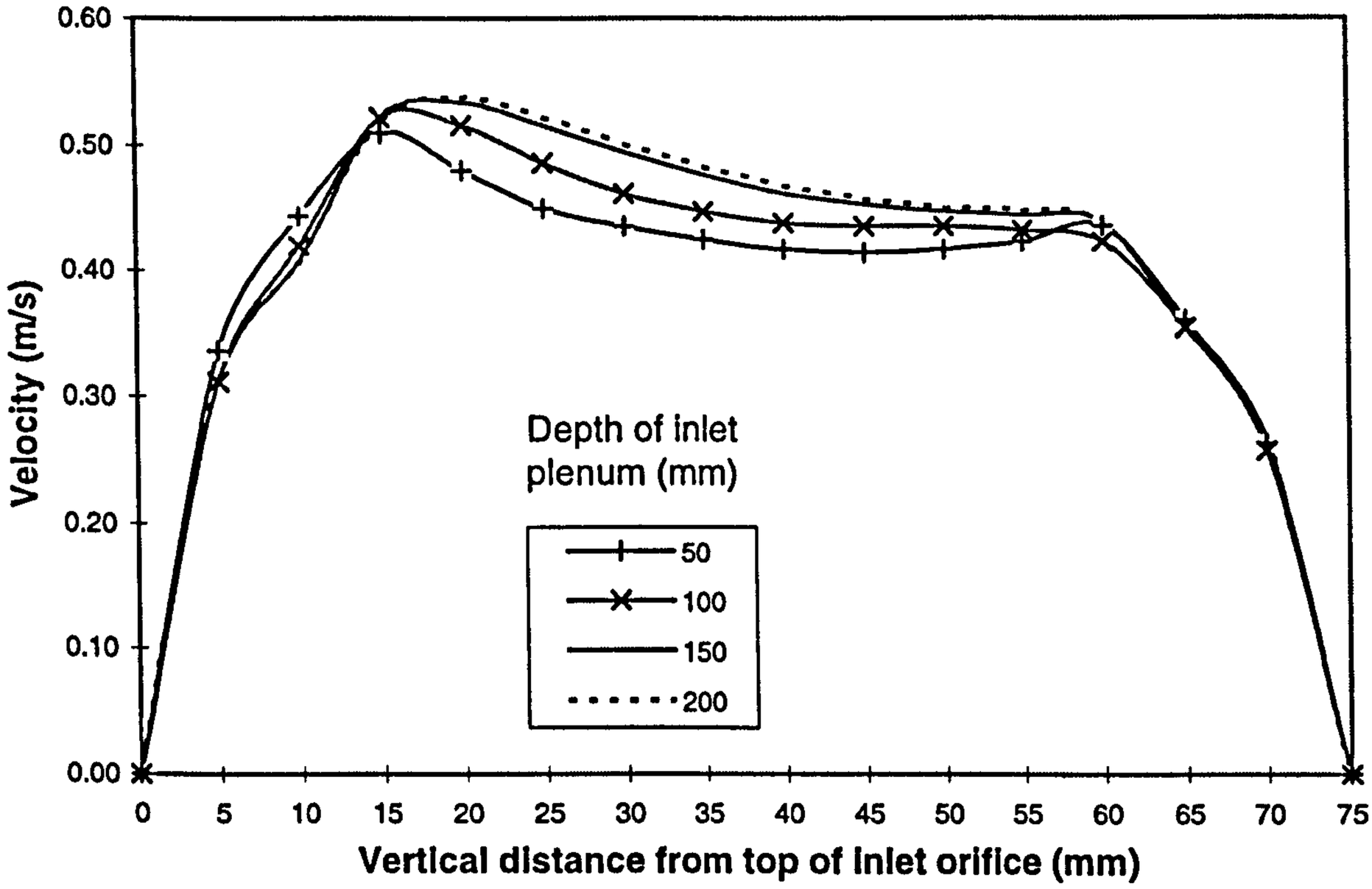

Figure 5.8. Effect of inlet plenum on air inlet profiles

Figure 5.8. clearly shows that an inlet plenum of 150mm and above provides a stable inlet profile. These profiles were then tested against the measured profile obtained from the rig inlet when the positioning of the velocity probes was being investigated.

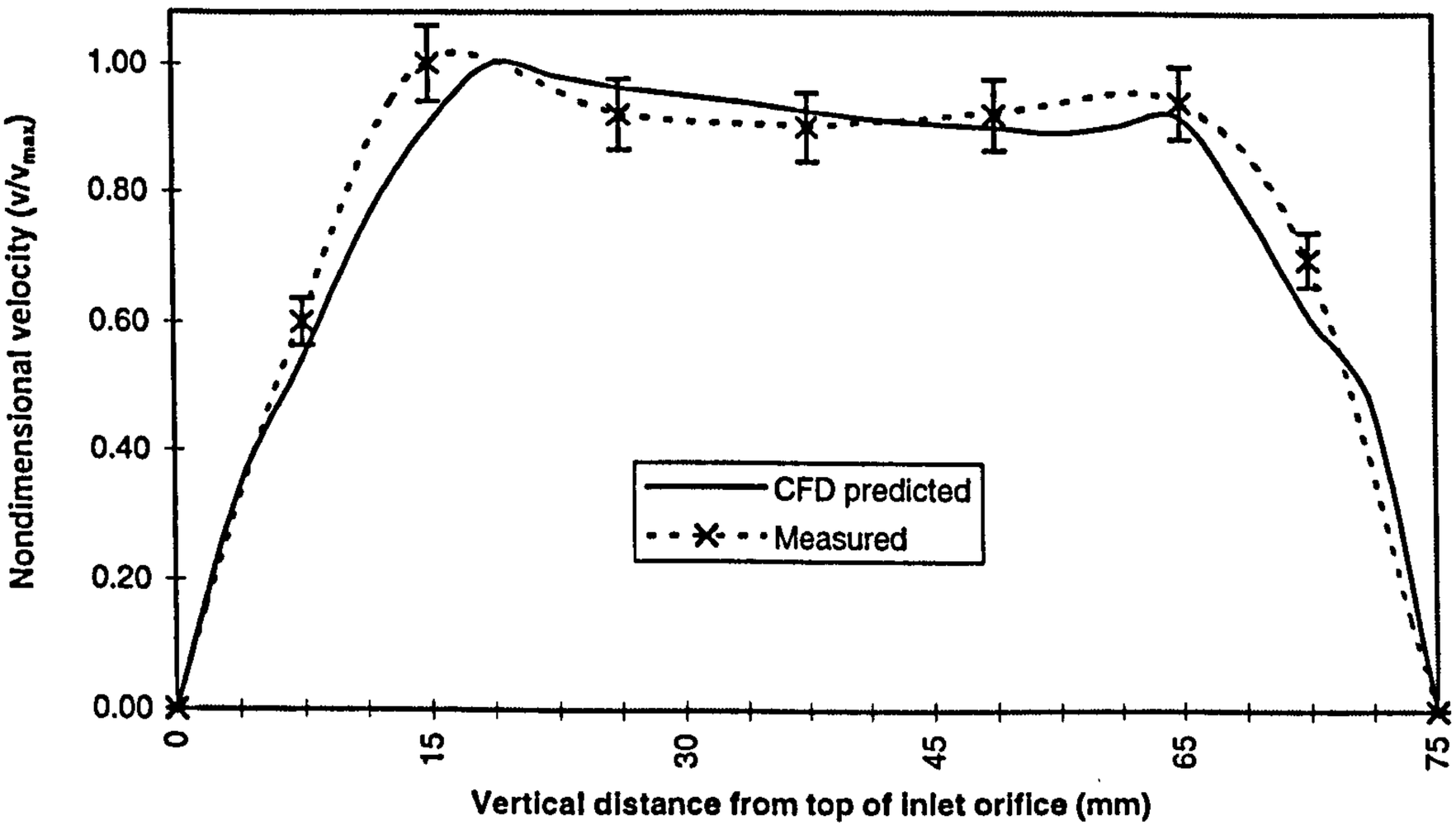

Figure 5.9. Comparison of CFD predicted and measured non dimensional velocity profiles

From figure 5.9. it was evident that the predicted flow profile was very close to that measured and thus the ability of the CFD programme to predict the flow in this region of the rig was qualitatively validated.

B. Mass flow rate through inlet orifice

The mass flow created by the stack pressure difference occurs when the driving pressure and the resistances to flow within the chimney are balanced. For the solar chimney tested experimentally the main pressure loss occurred at the inlet orifice. Therefore having established that the inlet profile of the air was correct, the predicted mass flow rate for a sharp edged orifice was tested to ensure it agreed with the theoretical flow given by equation 5.19.

$$Q = Cd\,A\sqrt{\left(\frac{2\,\Delta P_{inlet}}{\rho}\right)} \qquad \text{Equation 5.19.}$$

The theoretical and experimental value of Cd for a sharp edged orifice was stated by Etheridge et al[7] as 0.61. The model shown in figures 5.10. was developed to test the ability of the CFD programme to predict this flow. The imposed pressure differences between the inlet and outlet were 0.2 - 1.0 Pa. For the modelling of the experimental rig it was also important to establish the required level of grid resolution in the region of the orifice, as the small dimensions of the plate potentially influenced the grid spacing throughout the whole flow domain. The grid was therefore refined to achieve grid independence and then different configurations investigated to assess the sensitivity of the predicted flow rate to different grids.

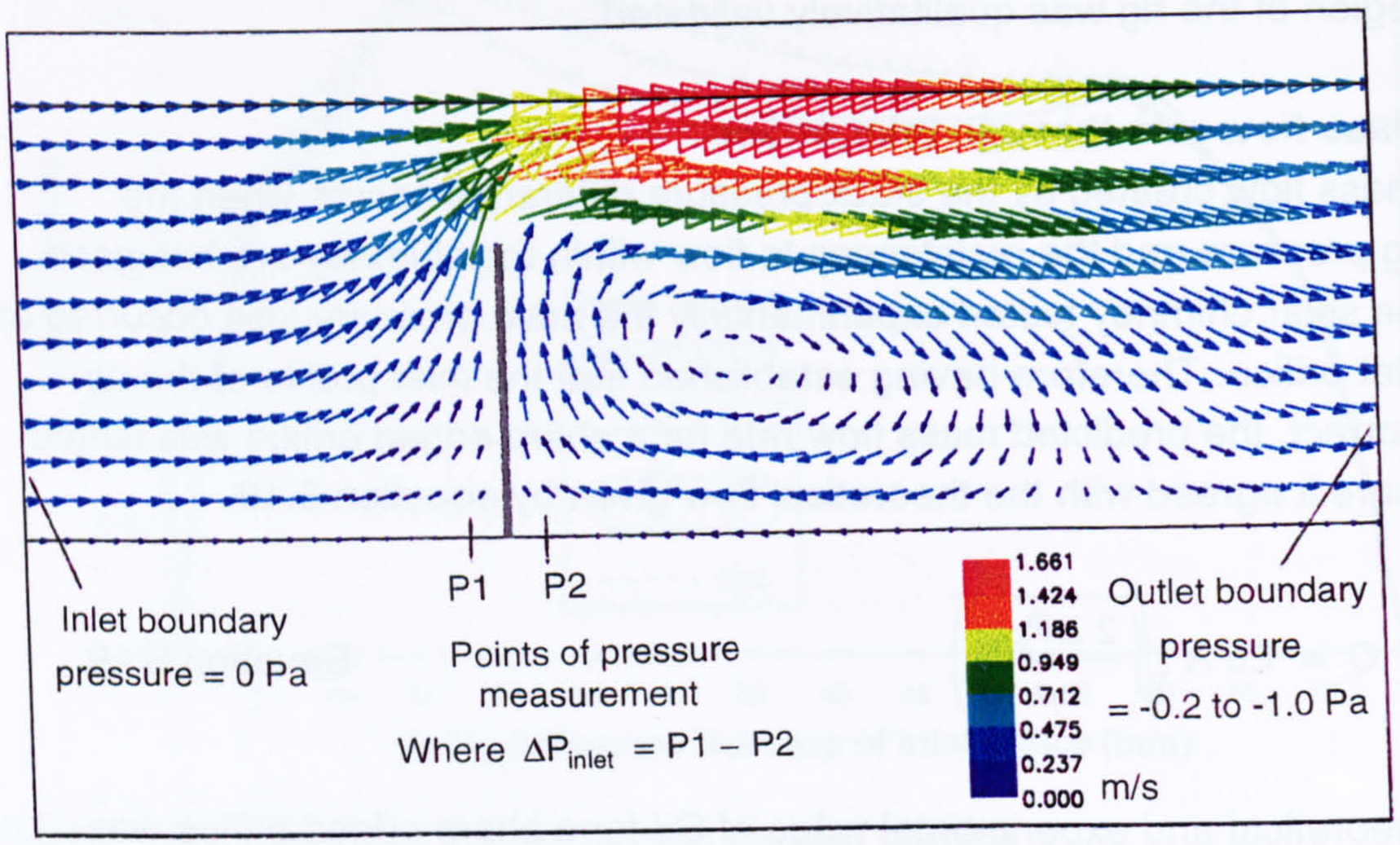

Figure 5.10. Flow through a sharp edged orifice in a pipe. Velocity magnitude vectors for a sample of nodes

Using equation 5.19., the value of Cd was calculated from the pressure differences predicted at the points indicated in figure 5.10. The CFD predictions were found to lie between 0.605 and 0.62, which is within 2% of the recognised value of 0.61. Thus quantitatively validating the CFD predictions of the flow rate for this configuration. The sensitivity of the predicted flow rates was very low to different grid configurations, as defining the orifice plate with a depth of 2mm placed a considerable restriction on the grid used throughout the remaining area of the flow domain.

The conclusion drawn from the investigation into the modelling of the rig inlet was that the CFD programme was able to accurately predict the flow rate through a sharp edged orifice and gave a correct velocity profile, provided an adequate inlet plenum was used upstream of the orifice.

C. Turbulence quantities of air at inlet boundary

As has been described, the flow throughout the flow domain was defined as turbulent. This required that the turbulence quantities of the inlet air were defined. As the air outside the inlet of the experimental rig was largely at rest, the sensitivity of the flow within the chimney to differences in the inlet turbulence parameters was assessed. It was found that with the plenum inlet boundary at a distance 150mm from the orifice the effects of changing the turbulence parameters at the inlet boundary made no noticeable effect to the flow and thus the default value of 2% turbulence intensity was used for all predictions.

D. Heat flux at heated plate

As described above the flux used to simulate the solar heating of the plate was applied to a wall boundary layer on the outside of a thin conjugate aluminium blockage. The values used allowed direct comparison of the CFD predictions with experimentally obtained results.

5.2.6 Other points requiring testing

Although not noted by Jones[1] as an area that must be considered, Cohen et al[17] noted that the method of modelling a real flow domain can have a significant influence on the accuracy of the predictions. One of the frequent assumptions when modelling is that the flow domain is considered as two dimensional and, or symmetrical.

Cohen et al[17] showed that for a room ventilated by a single window that did not run the whole length of the wall, the assumption of two dimensional flow was only correct if the predicted flow was multiplied by the ratio of the openable area to room volume. If this was not undertaken errors up to 50% were found. In addition to the possible errors in flow rates, the distribution of the flow within the space differed significantly between the two and three dimensional models.

The modelling of the inlet orifice of a solar chimney differs from that undertaken by Cohen et al[17] in that the flow is at greater velocities, thus the effect of a three dimensional flow was potentially more marked. In order to check this all possible methods of modelling the flow were investigated to quantify the error arising from modelling simplifications compared to a true three dimensional model of the inlet area. Grid independence was achieved for all models before they were finally run.

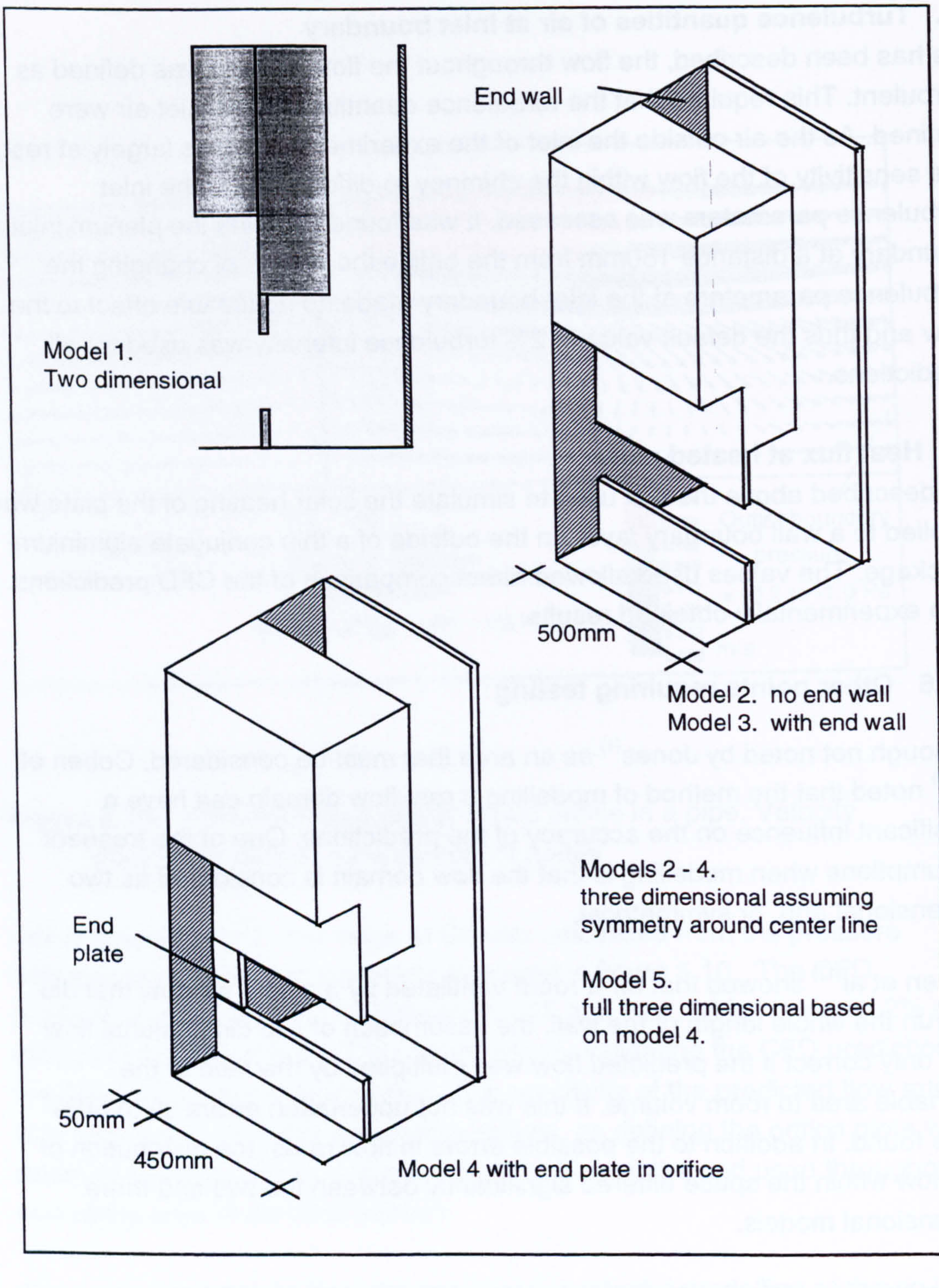

Figure 5.11. Different CFD models used to investigate the effects of model configuration on the predicted mass flow rate

The results of this investigation are shown in the table below:

Model No.	Model configuration	Difference in mass flow rate from base case predictions (%)
1	Two dimensional (all aspect ratios)	+13 ~ 15
2	Three dimensional - no end wall	+ 13 ~ 14
3	Three dimensional - with end wall	+ 11 ~ 12
4	Three dimensional - with end wall and true inlet configuration (all aspect ratios)	+ 1
5	Full three dimensional (all aspect ratios)	Base case

Table 5.2. Results of investigation into the effects of model simplification on the predicted mass flow rates.

As can be seen from Table 5.2. the effect of modelling the inlet configuration correctly had a significant effect on the predicted flow rate. Upon inspection of the flow down stream of the inlet orifice, three dimensional flow was very evident from the CFD predictions of model configurations 4 and 5. This can clearly be seen from the stream lines of the flow shown in figure 5.12.

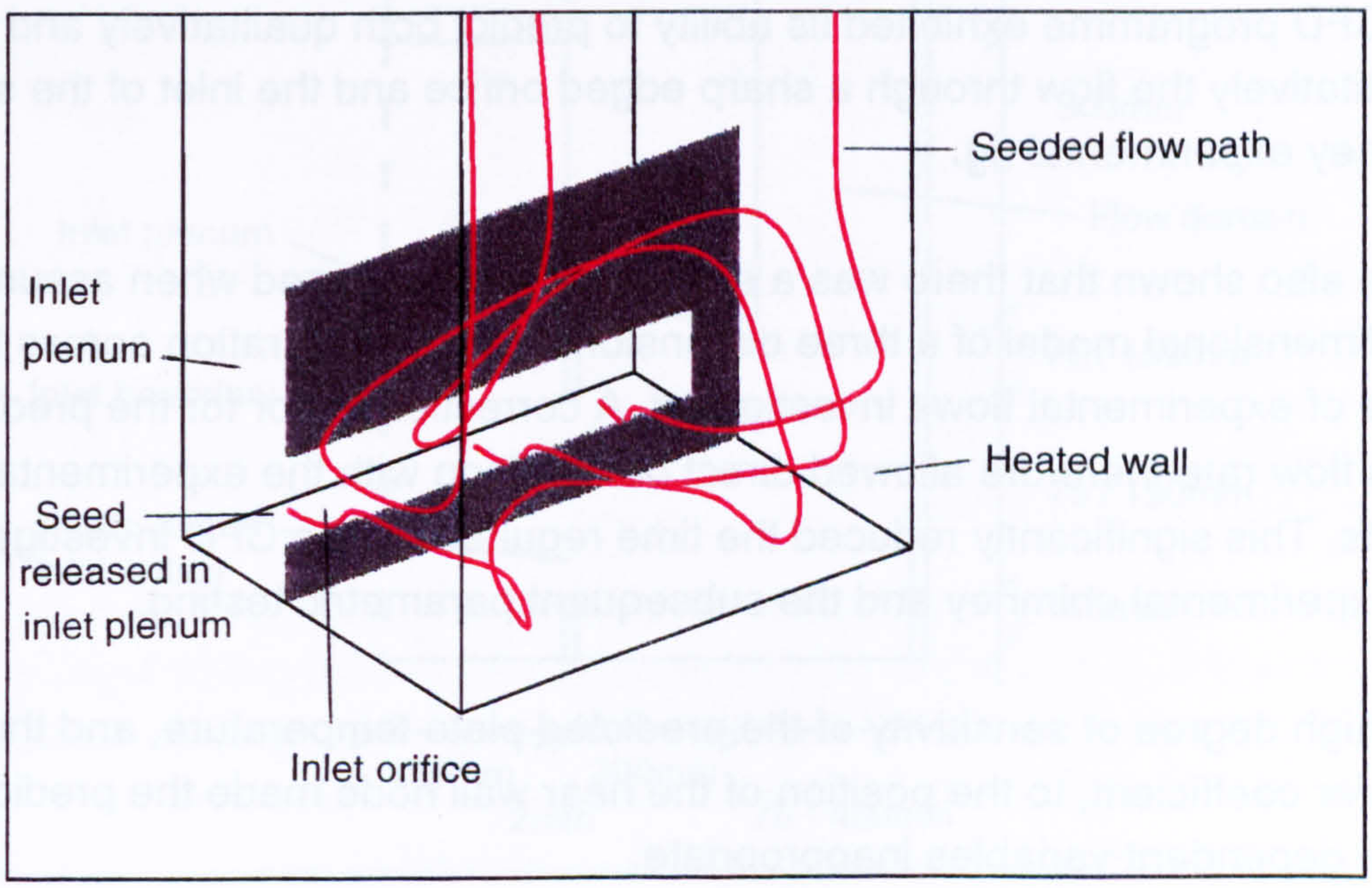

Figure 5.12. Stream lines of flow within the inlet of the three dimensional CFD model number 4.

The results presented in Table 5.2. for model configurations 1, 4 and 5 were undertaken across the full range of aspect ratios investigated experimentally. The difference between the predicted mass flow rates remained largely stable, indicating that the effect on the predicted mass flow rate of assuming a two dimensional model was relatively constant. This offered the opportunity of using a two dimensional model for the investigation and applying a constant correction factor to the results for comparison with the experimental data. Simulations of the two dimensional models required up to 8 hours to reach a converged solution. The three dimensional models required up to 6 times longer to converge. Therefore the time saving of adopting such a modelling regime was significant. In light of this, the two dimensional models were used throughout the investigation of the experimental solar chimney.

5.3 Conclusion drawn from the assessment of the CFD programme to predict natural convection flows and scope of its use in this investigation

This investigation into the potential of CFD to predict the flow within a solar chimney configuration has highlighted the very high level of sensitivity of this modelling technique to user inputs.

The CFD programme exhibited its ability to predict both qualitatively and quantitatively the flow through a sharp edged orifice and the inlet of the solar chimney experimental rig.

It was also shown that there was a systematic error incurred when assuming a two dimensional model of a three dimensional flow configuration across the range of experimental flows investigated. A correction factor for the predicted mass flow rate therefore allowed direct comparison with the experimental results. This significantly reduced the time required for the CFD investigation of the experimental chimney and the subsequent parametric testing.

The high degree of sensitivity of the predicted plate temperature, and thus heat transfer coefficient, to the position of the near wall node made the prediction of these dependant variables inappropriate.

The sensitivity of the predicted velocities and thus mass flow rate, for all but the finest grid sizes, was low and raised confidence that once grid

independence had been achieved, predicted mass flow rates could be directly compared to those measured in the experimental chimney.

5.4 MODEL OF EXPERIMENTAL RIG

The two dimensional CFD model developed of the experimental chimney to test predictions against the experimental results is shown in Figure 5.13.

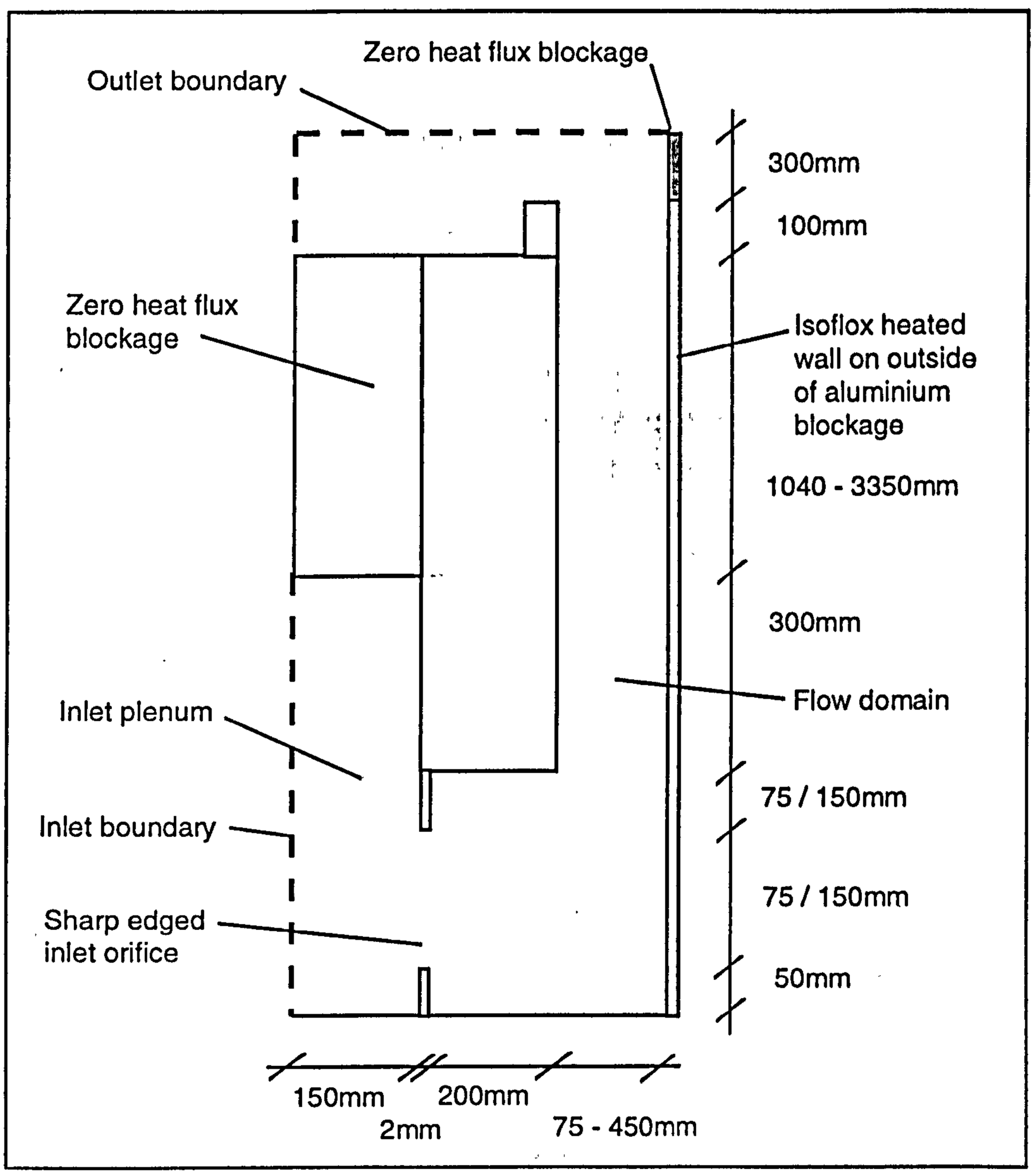

Figure 5.13. Layout of the CFD model developed for predictions of mass flow rate.

The matrix of model testing was the same as that presented in Table 3.8. for the experimental investigation. All models were run with a thermal flux of 100W/m^2 applied to the isoflux wall. A selection of runs with fluxes from 50 to 200W/m^2 were undertaken to assess the effects of the rate of energy transferred from the plate.

For each model it was found that in complying with the requirements to restrict the grid expansion ratio to a maximum of 1.2 and prevent the aspect ratio of any of the cells within the flow domain exceeding 10:1, grid independence had already been achieved. This was proven by increasing the number of cells in both directions by 50% with no noticeable effect on the predicted values of the dependant variables occurring.

The models were deemed to have converged when the whole field residual error was reduced to 1% for mass flow and temperature. CFD2000[18] allowed local monitoring points to be defined where all the variables could be monitored. This allowed areas that were slow to converge, such as areas of flow recirculation, to be monitored specifically. It was found that in such areas the flow did not become stable for a significant period of time after the overall residual error had become stable. Thus simulations were only stopped after both the whole field residual error had reduced to 1% or less and the variables at the local monitored points stabilised.

5.5 Comparison of CFD predicted and experimentally measured mass flow rates

5.5.1 Rig air stratification

A key feature of the experimental results was the elevation of the rig air temperature above that of the inlet air. Investigation of the experimental results, presented in Chapter Four, showed that rig air temperature elevations of between 0 and 3°C above the inlet air temperature had a significant, negative and largely linear effect on the mass flow rate. The first aspect of the results to be modelled was therefore to assess the ability of the CFD model to accurately predict this change in mass flow rate caused by differences in temperature between the rig and inlet air temperatures.

In order to simulate the effect of the temperature of the rig air above that of the inlet air, the pressure of a stack equivalent to a fully mixed mass of air with a height equal to the distance between the top of the inlet and the outlet was calculated using equation 5.20.

$$P_{s\ rig} = \rho_o\ g\ h\ 273 \left(\frac{1}{T_{inlet}} - \frac{1}{T_{rig}} \right) \qquad \text{Equation 5.20.}$$

Where h is the vertical distance from the top of the inlet to the outlet

The use of equation 5.20. assumes that the mass of air was fully mixed at temperature T_{rig}. Justification for this is shown in Figure 4.7. where it can be seen that the air temperature within the rig was constant above that of the inlet throughout the height of the chimney.

The pressure, $P_{s\ rig}$, was applied as a boundary condition to the outlet of the chimney model, acting in opposition to the stack pressure created by the heating of the air by the plate. The effect of applying a range of such pressures to the outlet boundary equivalent to temperature elevations of T_{rig} above T_{inlet} of 0 - 3°C is shown in Table 5.3. below.

Temperature elevation of shed (°C)	Experimental results		CFD predictions	
	Mass flow rate (g/s)	Change in mass flow rate (g/s)	Mass flow rate (g/s)	Change in mass flow rate (g/s)
0	58.0		59.3	
1	53.5	4.5	54.1	5.2
2	49.0	4.5	49.3	4.8
3	44.5	4.5	45.0	4.3

Table 5.3. Comparison of experimental and predicted effects of differences in rig air temperature elevation above that of the inlet air of the solar chimney for a stack height of 3.135m.

The CFD predictions confirm the predictions of the basic model shown in figure 4.8., that the fall in mass flow rate was not linear with changes in shed air temperature above inlet air. However across the range of temperatures experienced during the experimental investigation, the predicted and

measured changes were sufficiently similar to give confidence in the capabilities of the CFD model to predict flows under such situations.

5.5.2 Comparison of predicted and measured mass flow rates subject to changes in key physical variables

Figure 5.14. shows the predicted and measured mass flow rates for all chimney heights and aspect ratios for a value of energy transferred from the plate of 100W/m^2. From figure 5.14. it can clearly be seen that within the level of uncertainty associated with the experimental results, calculated using equation 4.5., there was no significant difference between the CFD predicted and measured mass flow rates across the range of experiments undertaken.

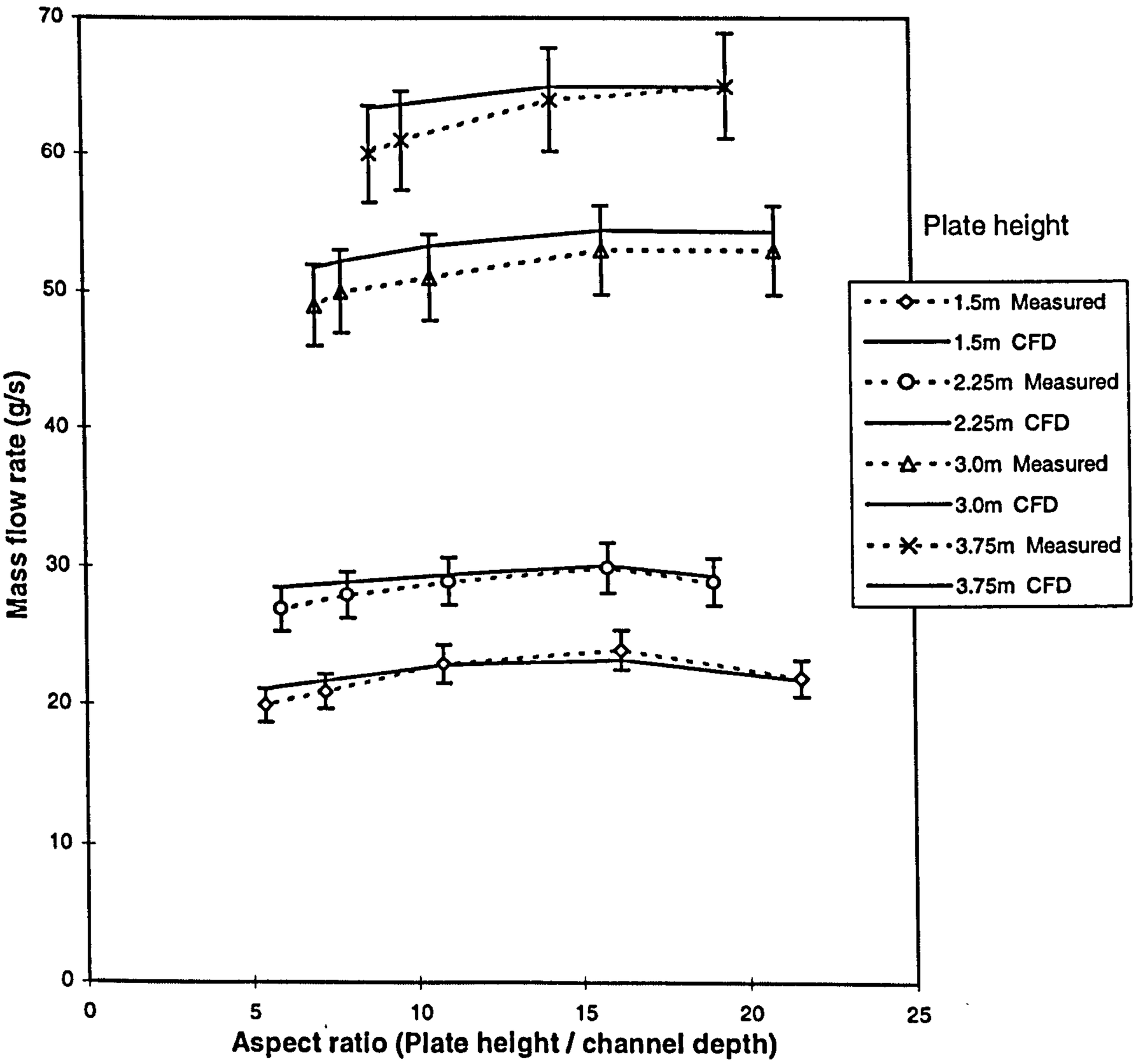

Figure 5.14. Comparison of experimental results and CFD predictions of the mass flow rate at a range of plate heights and aspect ratios for a rate of energy transferred from the plate of 100W/m^2.

From the similarity of the results presented in figure 5.14. it was concluded that the CFD quantitatively predicted the mass flow rate through the chimney and the effects of both height and inlet orifice area variations.

The significance of the variations in mass flow rate to variations in the aspect ratio of the channel within the experimental chimney were discussed in Chapter Four. It was concluded that the variations evident were both significant and relevant. Close inspection of the CFD predictions of mass flow rate across the full range of aspect ratios however showed less variation than that of the experimental results. The result of this was that the aspect ratio corresponding to the maximum flow was less discernible and appears to remain largely constant at around 15:1. The most noticeable difference between the predicted and the measured results was the lower predicted reduction of flow rate as the aspect ratio of the channel decreased. Investigations of the CFD results showed that recirculation, particularly at the lower chimney heights, was evident, but the effect of this on the mass flow rate predicted through the inlet of the chimney was only marginal.

5.5.3 The influence of energy transferred from the plate

Figure 5.15. shows that the measured trend in mass flow rate for variations in the level of energy transferred from the plate was well predicted by the CFD programme.

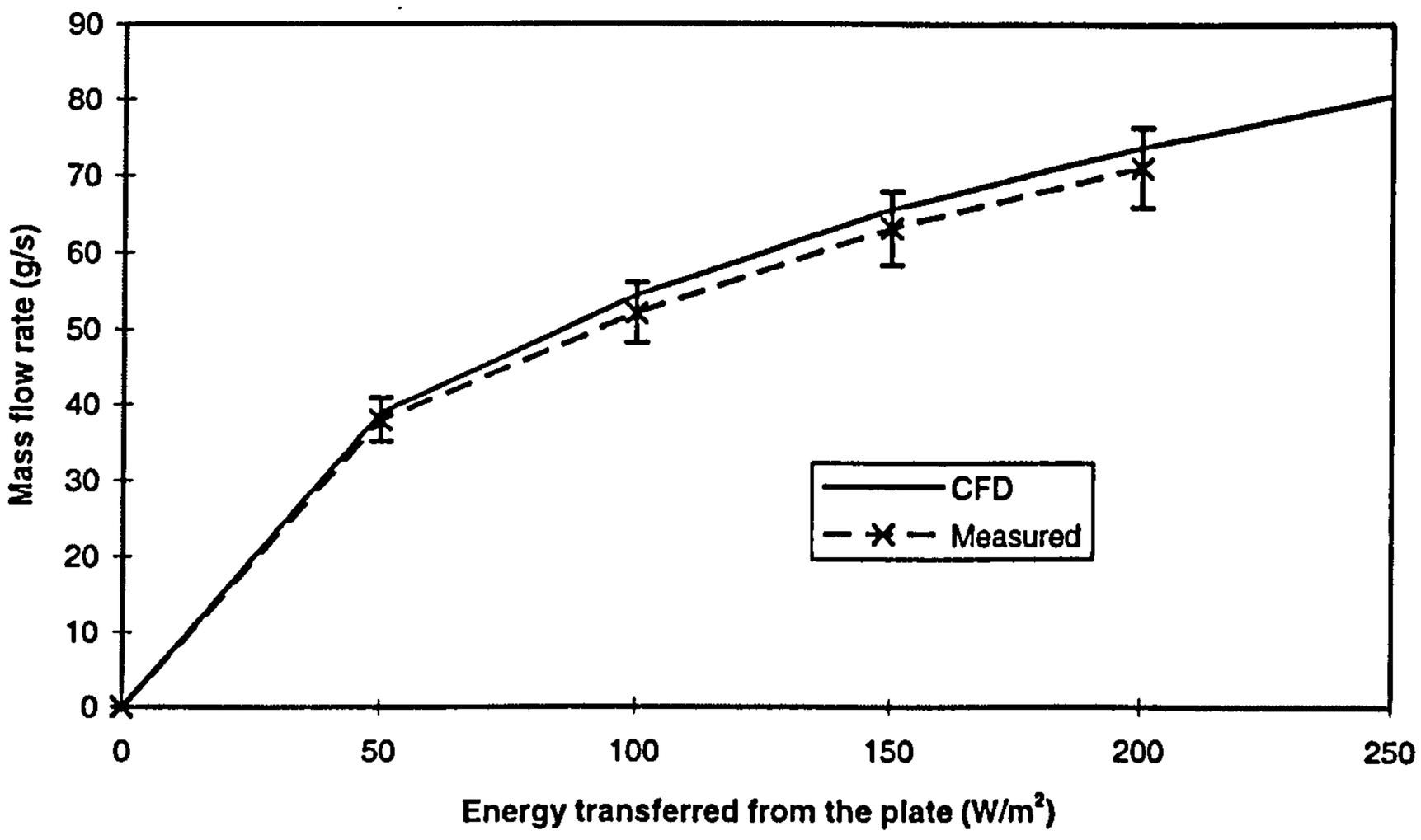

Figure 5.15. Effect of energy transfer rate from the plate on mass flow rate for a stack height of 3.135m.

This level of agreement of variations in mass flow rates was evident at all chimney heights across the range of levels of energy transferred from the plate measured experimentally.

5.5.4 Conclusion drawn from the investigation into the ability of a CFD programme to predict trends in mass flow rate through a solar chimney subject to variations in physical variables

Overall it was concluded that the CFD model was capable of predicting the mass flow rates for the chimney configuration within the accuracy of the experimental results. Bussoletti[25] however noted that the greatest potential use of CFD programmes was the parametric testing of flow configurations once the ability to predict dependant variable trends had been validated. In this respect the CFD model developed of a solar chimney accurately predicted the trends in mass flow rate due to changes in chimney height, inlet area and energy transferred from the plate. The use of the CFD programme for the parametric testing of these variables was therefore considered as appropriate.

The noticeable difference between the measured and predicted trends in mass flow rate due to variations in the channel depth however raised questions as to the ability of the CFD programme to predict the influence of this variable. At channel depths greater than those where the boundary layer spans the channel depth, recirculation was observed in the experimental chimney. This increased as the channel depth increased. The CFD programme predicted recirculation but underestimated the effects on the mass flow rate through the chimney inlet. Chen[14] noted that the assumption of isotropic turbulence in the standard $k\varepsilon$ turbulence model was inappropriate for natural convection flows and areas of flow recirculation. The use of the CFD programme for prediction of flow situations where recirculation was evident was therefore not considered reliable outside the range of experimental results. In light of this, parametric testing was limited to channel depths up to that corresponding to the maximum mass flow rate measured experimentally. In this way the requirement for the CFD programme to predict the occurrence of recirculation flows at the channel outlet was reduced.

5.6 Comparison of CFD predictions of other variables

Although the main aim of using the CFD model was to obtain predictions of the mass flow rate through the solar chimney, the level of information obtained from the experimental investigation also allowed its capability to predict other dependant variables to be evaluated.

5.6.1 Velocity profiles at the chimney outlet

The calculation of the energy gained by the air during experiments required that profiles of both velocity and temperature were measured at the outlet to the chimney. This allowed comparison of these variables with the predictions provided by the CFD model.

The measurement of the direction of the air flow at the chimney outlet could not be undertaken with the instruments developed for measurement of velocity and temperature. Thus for low aspect ratios the occurrence of recirculation, as described in Chapter Four, was established through flow visualisation. However for comparison of actual velocity profiles this method of determining air flow direction was crude and thus limited the usefulness of comparisons at low aspect ratio channel predictions. In addition to this, the velocity measuring instruments were only designed to measure vertical velocity at the chimney outlet and thus air movement across the mouth of the outlet could not be determined.

Predicted velocity profiles for high and low aspect ratio chimney configurations are shown in figures 5.16. and 5.17. respectively.

The error bars presented in figures 5.16. and 5.17. result from the quadratic addition of the velocity measurement uncertainties and that due to the calculation of the energy transferred from the plate using equation 4.5.

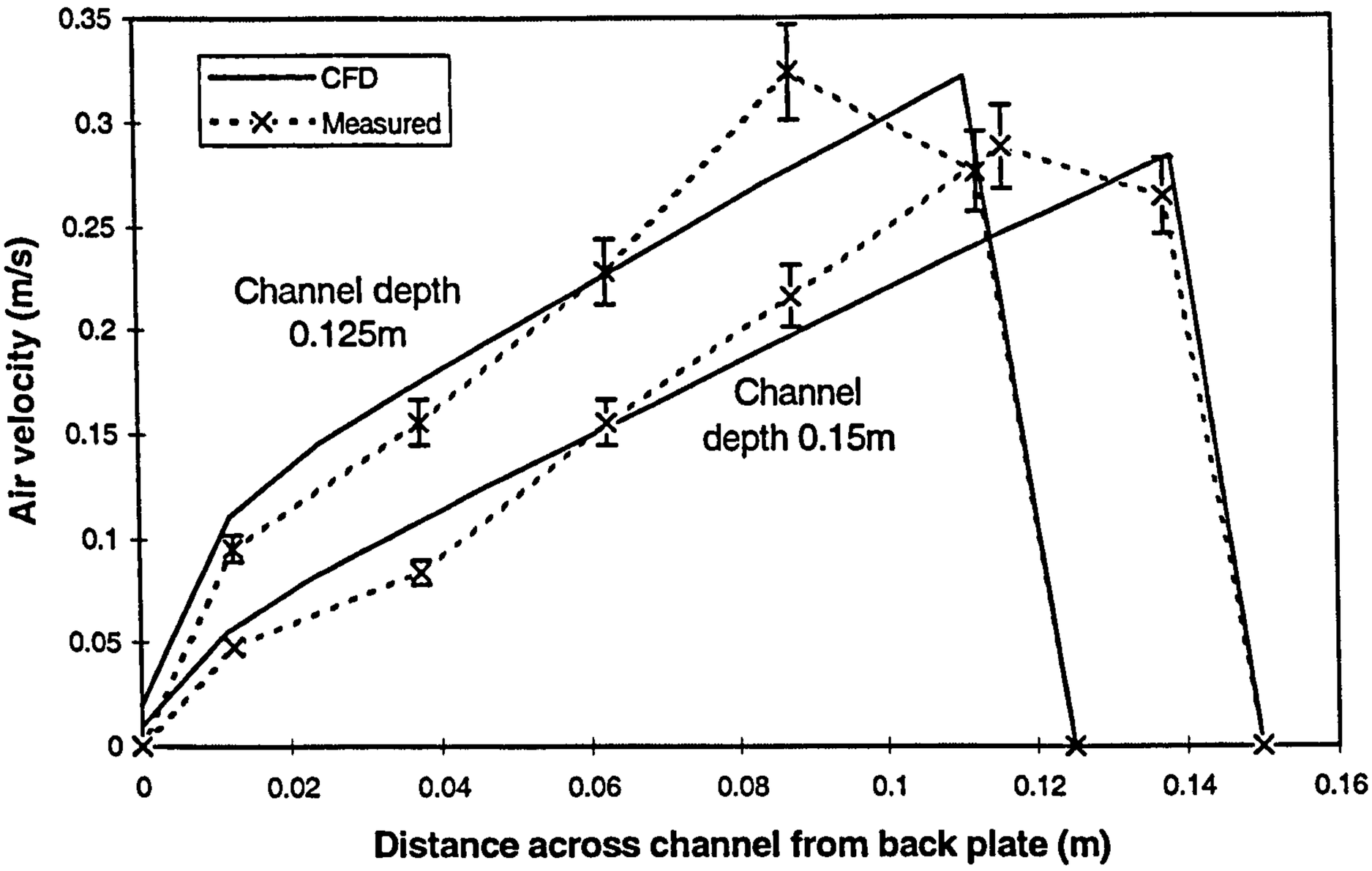

Figure 5.16. Comparison of CFD predicted and experimentally measured air velocity for high aspect ratio chimneys.

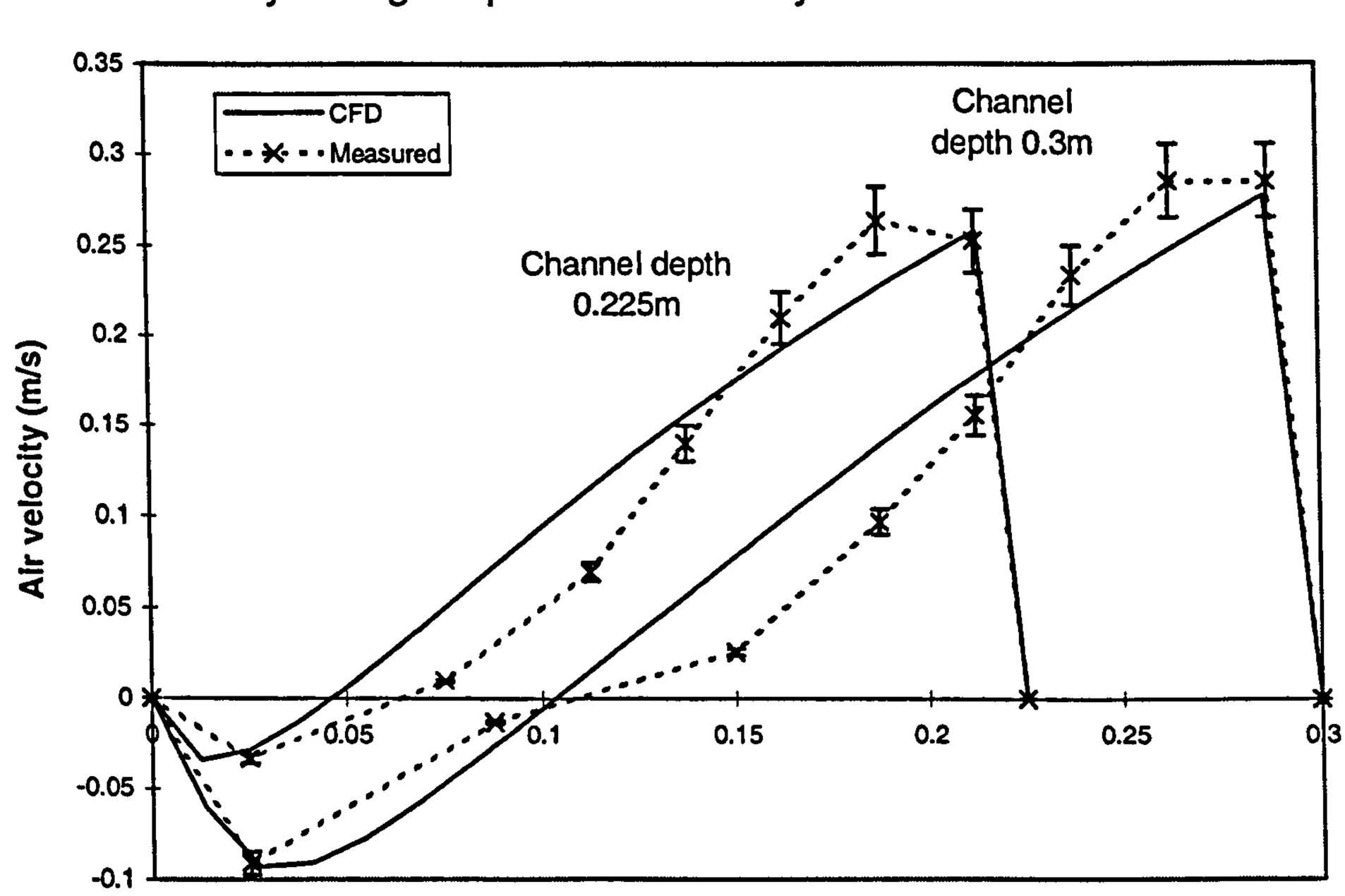

Figure 5.17. Comparison of CFD predicted and experimentally measured air velocity for low aspect ratio chimneys.

At high aspect ratios the measured and predicted velocity profiles were in good agreement. At lower aspect ratios the overall mass flow rate predicted by the CFD model was similar to that measured experimentally, as shown in figure 5.14., however the profiles of the air velocities at the outlet were noticeably different. The CFD predicted a linear decrease in velocity across the channel depth, whereas the measured data indicated a more defined boundary layer with an area of relatively stagnant air in the central region of the outlet. As stated previously however, the velocity measuring instruments were not designed to record air movement across the chimney outlet, therefore the effect of flows non-aligned with the instruments could not be estimated. CFD predictions showed that such flows were evident within this region as shown in figure 5.18. Thus within the limits of the instruments used in the experimental investigation, the predicted flow profiles were broadly similar to those measured. The differences in the central region being attributed to the directional nature of the velocity measuring instruments probes used.

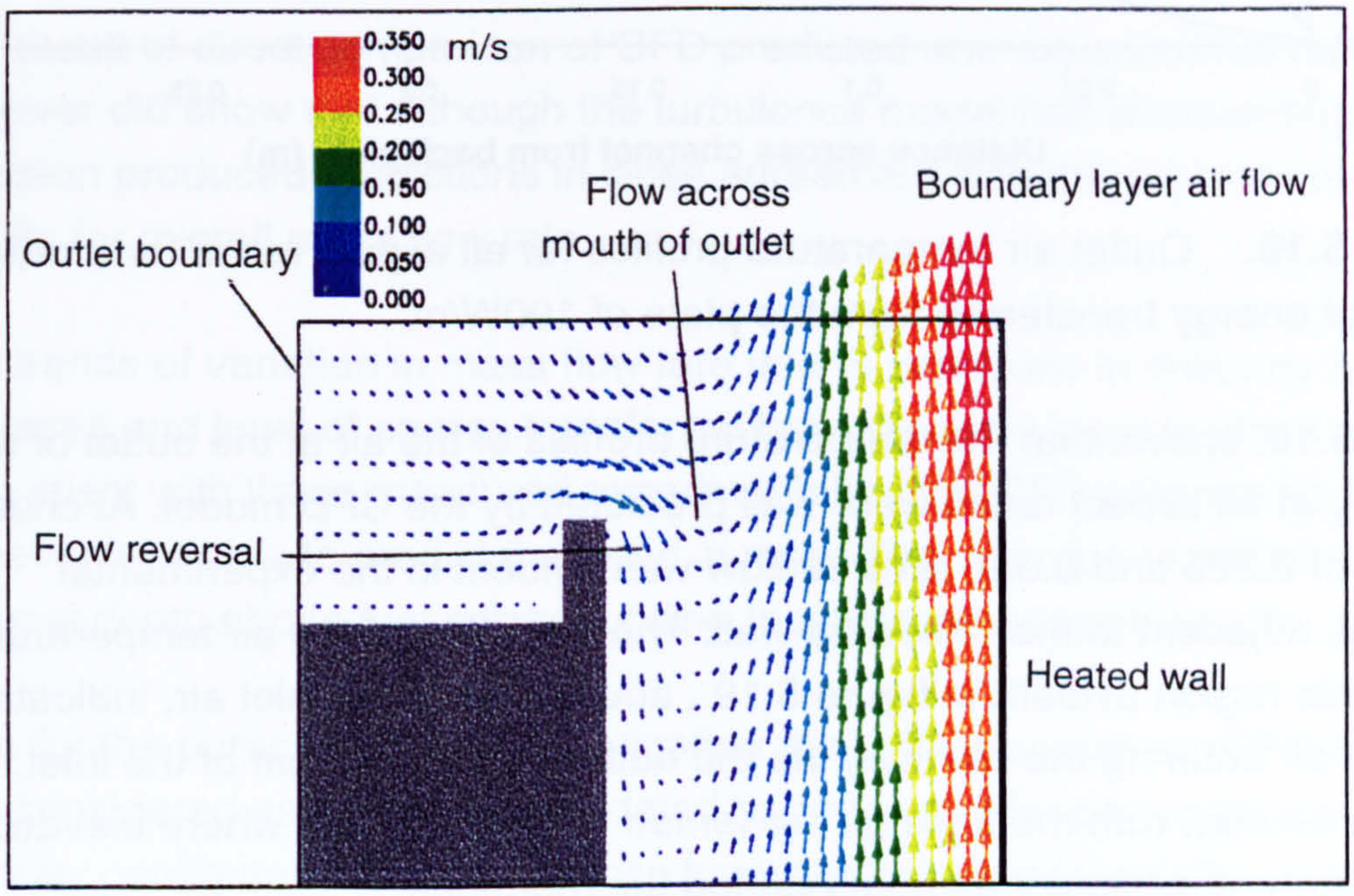

Figure 5.18. CFD predictions of flow at the outlet of the chimney for a low aspect ratio configuration showing the occurrence of reversed flow and the cross flow at the channel outlet.

5.6.2 Temperature profiles at the chimney outlet

Temperature profiles for the channel depths presented in figures 5.16. and 5.17. are shown in figure 5.19.

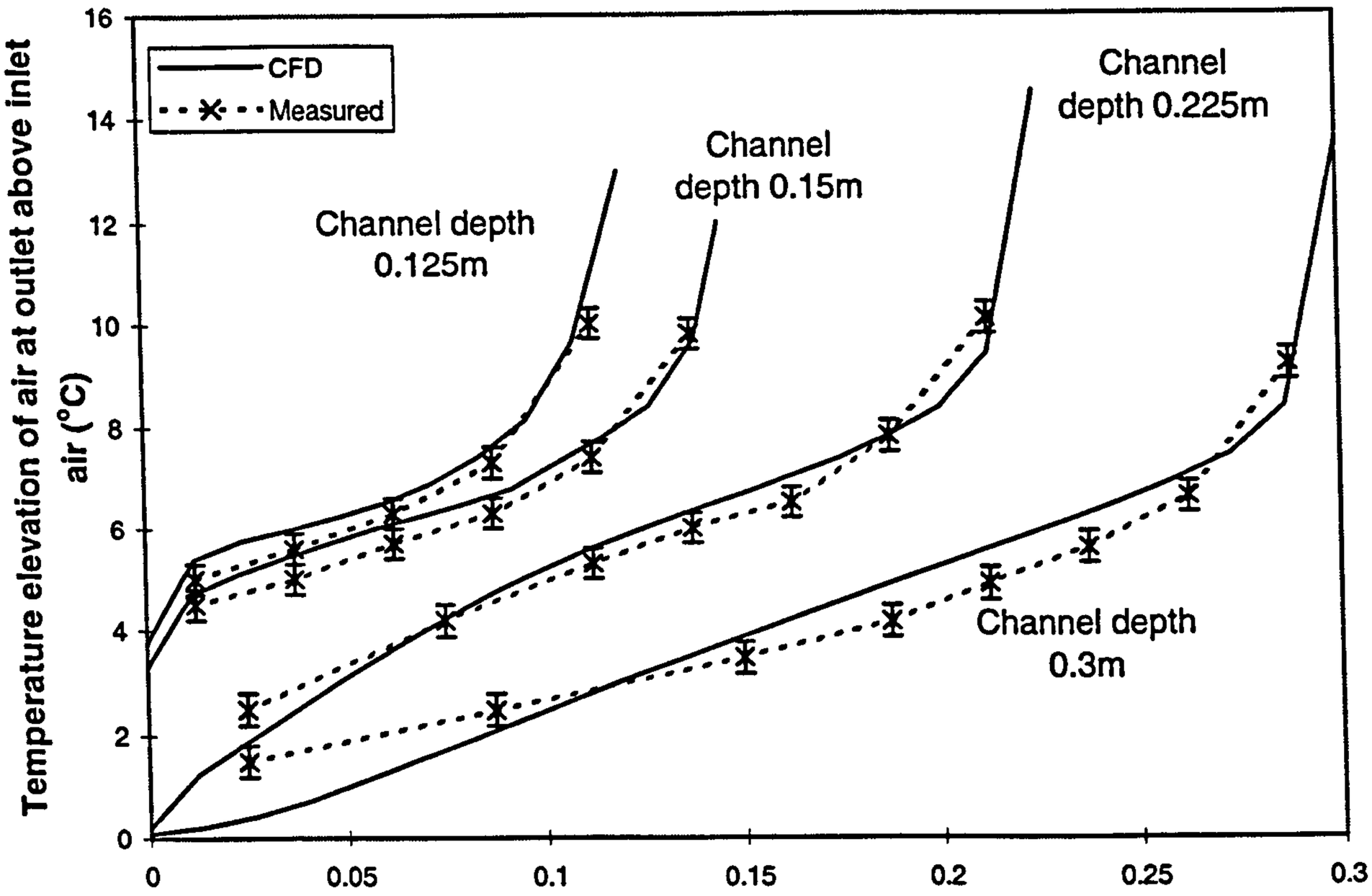

Figure 5.19. Outlet air temperature profiles for all aspect ratios for a rate of energy transferred from the plate of 100W/m^2.

Figure 5.19. shows that the temperature profiles of the air at the outlet of the chimney at all aspect ratios were well predicted by the CFD model. At channel depths of 0.225 and 0.3m, reverse flow was evident in the experimental channel, adjacent to the unheated wall. The elevation of the air temperature within this region evident in figure 5.19., above that of the inlet air, indicated that the air entering the chimney via the outlet was above that of the inlet. This is in agreement with the findings presented in Chapter Four where elevation of the rig air temperature was noted during the mornings.

5.7. Conclusion of the investigation into the use of a CFD programme for predictions of a solar chimney

In this chapter the potential of CFD programmes to accurately model a natural convection flow within a solar chimney configuration has been investigated. The complexity of CFD programmes is such that they can never be checked by manual calculations, and thus the greatest of care must be exercised when they are used and an understanding of both their limits and weaknesses must be obtained.

The major weakness highlighted by this study was that of the turbulence models used in CFD programmes. The most validated model, the standard $k\varepsilon$ model, used frequently for building air flow simulations has a significant influence upon the ability of the CFD programme to predict convective heat transfer coefficients, with this variable being directly influenced by near wall node spacing. This has led practitioners such as Chen[14] to claim that it should not be used if wall temperatures and convective heat transfer coefficients are the dependant variables of interest.

The result of direct comparison of CFD predicted and experimental results however did show that although the turbulence model had shortcomings, its inclusion produced predictions in close agreement with the experimental results for overall mass flow rate.

The trends of variation in mass flow rate due to variations in chimney height, inlet area and level of energy transferred from the plate were in close agreement with those measured experimentally. The CFD programme was however less able to predict the trend in mass flow rate due to variations in the channel depth above that corresponding to maximum mass flow rate.

Thus for the purposes of this investigation the CFD programme; CFD 2000[18], was considered as sufficiently validated to be utilised for parametric testing of chimney configurations outside those investigated experimentally, up to channel depths corresponding to the maximum mass flow rate.

5.8 References Chapter Five

1. Jones, P. and Whittle, G., Computational fluid dynamics for building air flow prediction - current status and capabilities, Building and Environment, Vol. 27, No. 3, 321 - 338, 1992.

2. Li, Y. and Fuchs, L., An evaluation of a computer code for predicting indoor airflow and heat transfer, Proceedings 12th. AIVC Conference, Ottawa, Canada, 1991.

3. Borth, J. and Suter, P., Influence of mesh refinement on the numerical prediction of turbulent air flow in rooms, Proceedings Roomvent 94, Krakow, Poland, June, 1994.

4. Versteeg, H. and Malalasekera, W., An Introduction to Computational Fluid Dynamics, Longman Scientific & Technical, Harlow, UK, 1995.

5. Gunton, M., Private communications about setting up of CFD2000, 1996.

6. Fluent, FLUENT User's Guide, Version 4.3, Fluent Inc., January, 1995.

7. Etheridge, D. and Sandberg, M., Building Ventilation. Theory and Measurement, J. Wiley & Sons., UK, 1996.

8. Shetz, J. and Fuhs, A., Handbook of Fluid Dynamics and Fluid Machinery, Volume 1, J.Wiley & Sons Ltd, USA, 1996.

9. Cebeci, T. and Smith, A., Analysis of Turbulent Boundary Layers. Academic Press Ltd, London, 1974.

10. Launder, B. and Spalding, D., The numerical computation of turbulent flows, Computer Methods in Applied Mechanics and Engineering, Vol. 3, 269 - 289, 1974.

11. Holmes, M. and Whittle, G., How accurate are the predictions of complex air movement models, Building Serv. Eng. Res. Technol., Vol. 8, 29 - 31, 1987.

12. Haghighat, F., Jiang, Z., Wang, J. and Allard, F., Air movement in buildings using computational fluid dynamics, Journal of Solar Energy Engineering, Vol. 114, 84 - 92, 1992.

13. Chen, Q., Moser, A. and Suter, P., A database for assessing indoor airflow, air quality, and draught risk, IEA Annex 20, Subtask 1, Research Item 1.23, 1992.

14. Chen, Q., Comparison of different $k\varepsilon$ models for indoor air flow computations, Numerical Heat Transfer, Part B, Vol. 28, 353 - 369, 1995.

15. Vogl, N. and Renz, U., Comparison of numerically predicted air flow pattern using low-Reynolds turbulence models with laser-doppler-velocimeter measurements in a room with heated walls, Proceedings Roomvent 94, Krakow, Poland, June, 1994.

16. Winwood, R., Benstead, R. and Edwards, R., Advanced fabric energy storage II: Computational fluid dynamics modelling, Building Serv. Eng. Res. Technol., Vol. 18, 7 - 16, 1997.

17. Cohen, R., Davies, R., Seymour, M. and Leppard, J., Application of CFD to naturally ventilated buildings: A guide for practitioners. Proceedings CIBSE / ASHRAE Joint National Conference, Harrogate, UK, 1996.

18. Adaptive Research, CFD 2000, User's Manual, Version 2.2, Adaptive Research Inc., USA.

19. Incropera, F. and DeWitt, D., Fundamentals of Heat and Mass Transfer, 3rd. Ed., J. Wiley & Sons, New York, 1990.

20. Burmeister, L., Convective Heat Transfer, J. Wiley & Sons Inc, 2nd. Edition, 1993.

21. Bejan, A., Heat Transfer, J Wiley & Sons. Inc, USA, 1993.

22. Tsuji, T. and Nagano, Y., Characteristics of a turbulent natural convective boundary layer along a vertical flat plate, Int. J. Heat Mass Transfer, Vol. 8, 1723 - 1734, 1988.

23. Gray, D. and Giorgini, A., The validity of the Boussinesq approximation for liquids and gases, Int. J. Heat Mass Transfer, Vol. 19, 545 - 551, 1976.

24. Skovgaard, M. and Nielsen, P., Modelling complex inlet geometries in CFD - Applied to air flow in ventilated rooms, Proceedings 12 th. AIVC Conference, Ottawa, Canada, 1991.

25. Bussoletti, J., CFD calibration and validation. The challenges of correlating computational model results with test data, Proceedings 18th. AIAA Aerospace Ground Testing Conference, Colorado Springs, USA, June, 1984.

CHAPTER SIX

PARAMETRIC TESTING OF A SOLAR CHIMNEY USING A VALIDATED CFD MODEL

6.1 Introduction

The CFD programme, CFD 2000[1], was shown in Chapter Five to be capable of predicting the mass flow rate through a solar chimney in close agreement with measured results obtained from a full sized experimental rig. Additionally the CFD programme predicted accurately the trends in the mass flow rate due to variations in the rate of energy transferred from the plate to the air and changes to the dimensions of the chimney inlet and overall chimney height. The CFD programme however predicted less accurately the reduction of mass flow rate evident in the experimental investigation as the channel depth increased beyond that corresponding to the maximum flow rate. For the purposes of undertaking parametric testing therefore the channel depth was limited to that at which the maximum mass flow rate was predicted.

Having established the validity of the CFD programme to predict the trends in mass flow rate through a solar chimney identified above, parametric testing was undertaken to establish the effects of these variables outside the range investigated experimentally.

The practical application of the results of this investigation by building designers to the design of solar chimneys, required the results to be presented in an easy to use format. An appropriate format is presented. The proliferation of computers in business meant that a format appropriate for use by such a medium was also important.

Zonal based models were found to be largely inappropriate for the prediction of the variation of mass flow rate found in the experimental investigation. The range of the variables investigated parametrically was, however, outside that undertaken experimentally. Therefore the appropriateness of a zonal based model for the prediction of mass flow rates was evaluated across the range of variables investigated parametrically and the results discussed.

6.2 CFD model developed for parametric testing.

Having validated the CFD programme, CFD 2000[1], for the purpose of investigating the solar chimney configuration, the aim was to develop data in a format practical for use by building designers. The generality of the model used for the parametric testing was therefore of importance if the resulting data was to be applicable to the widest possible range of flow configurations.

The basic model features developed in Chapter Five for the validation testing were maintained, as shown in figure 6.1.

The model developed for the parametric testing was of a 1m wide heated plate and channel, with the inlet being the same width as the channel. The significant number of model variations required to obtain a sufficiently full data set to confidently comment on the influence of all of the physical variables on mass flow rate, meant that the time required for each model to achieve a converged solution was important. An investigation undertaken in Chapter Five highlighted that a three dimensional model required up to six times longer to converge than a two dimensional model based on the same flow configuration. It was also shown that for models where the inlet was of the same width as the channel, only a small systematic error was incurred when using a two dimensional model of a three dimensional flow configuration. This was caused mainly by the inclusion of the end walls of the channel in the model as shown in figure 5.11. and table 5.2.

For practical applications, the use of a solar chimney for the promotion of natural ventilation would be based on modular dimensions used for building cladding systems. A channel width of 1m was therefore considered as a practical minimum for this type of flow configuration. For channel widths greater than 1m where the channel and inlet widths are the same, the effect on the mass flow rate of the end walls of the channel reduces in significance. In view of this, the systematic error reported in table 5.2. of up to 3% over-prediction of the mass flow rate when a two dimensional model, model 1, was used to simulate a three dimensional flow configuration, model 3, was considered as the maximum for channel widths of 1m or greater. Such a small level of uncertainty, at a maximum for channel widths of 1m was considered acceptable for predictions of this nature. Therefore a two dimensional modelling programme was established to investigate the effects of the input variables on the mass flow rate, resulting in a considerable saving of time over

that required to undertake the same investigation using three dimensional models.

For the parametric investigation, the height of the inlet was varied for each stack height. In light of this, the base of the heated plate was set as the mid height of the inlet orifice. In this way the stack height, measured from the mid height of the inlet orifice to the outlet of the channel, was equal to the height of the heated plate. This ensured that the height of the stack remained unaltered as the inlet height was varied across the required range. This is shown in figure 6.1.

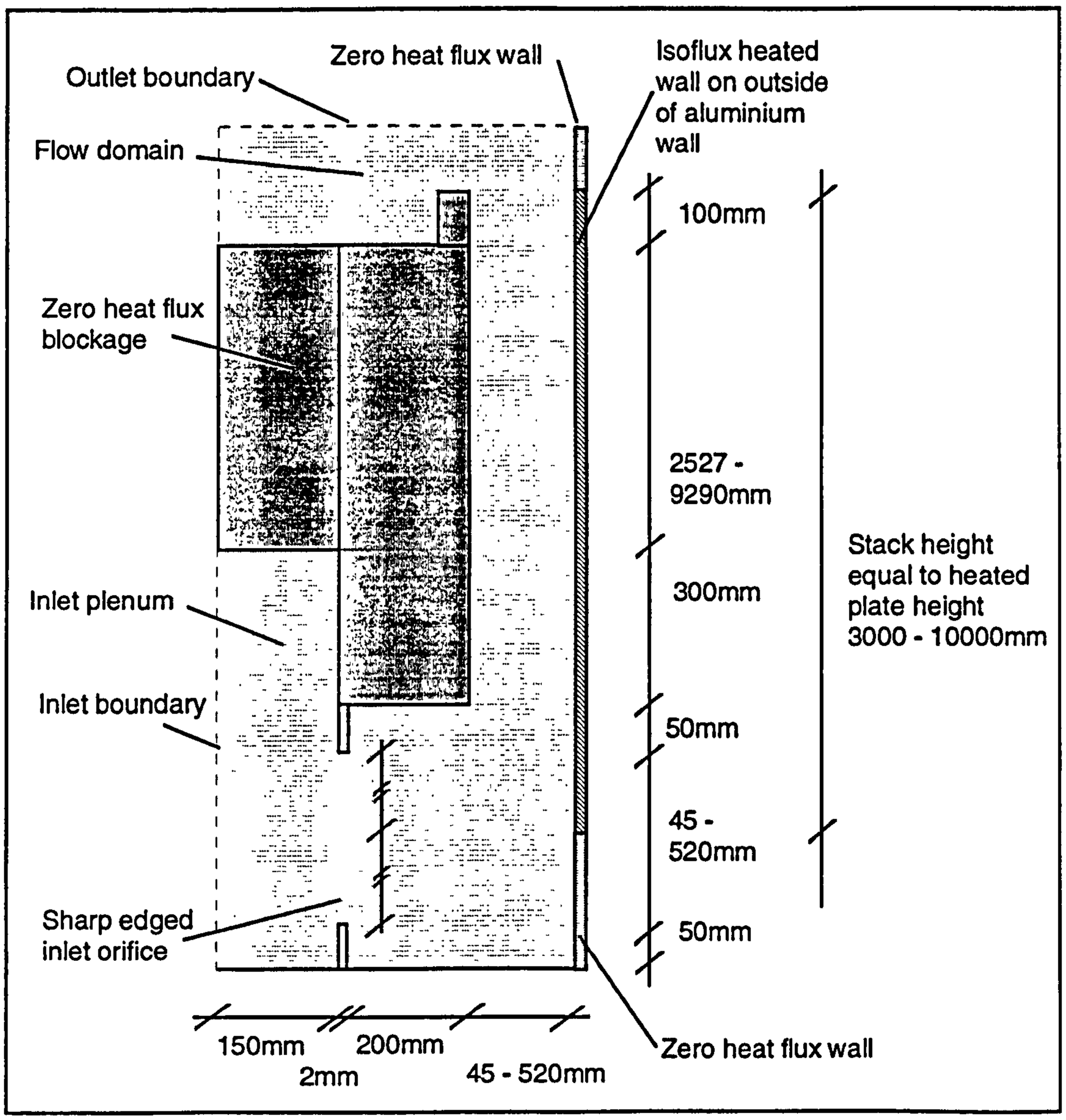

Figure 6.1. Model developed for the parametric testing of the solar chimney flow configuration

The independence of the predicted flow to the computational grid within the flow domain was verified before all models were run.

6.3 Range of parametric tests undertaken

The physical limitations of the experimental rig meant that stack heights greater than 4m could not be investigated. The validity of the CFD programme to predict the trend in mass flow rate due to variations in stack height was however shown to be high. Thus parametric testing was undertaken across a range of stack heights from 3 to 10m. This represented practical chimney heights of between 1 and 3 storeys.

It was shown in Chapter Five that the CFD predictions of the maximum mass flow rate through a chimney were very close to those measured experimentally. The reduction in mass flow rate which occurred in the chimney as the depth of the channel was increased beyond that corresponding to the maximum mass flow rate was, however, less well predicted. Thus the first aspect of parametric testing to be undertaken was to obtain values of the channel depths corresponding to the maximum mass flow rate for stack heights from 3 to 10m.

In practical terms it was decided that the maximum height of the inlet would not exceed the maximum depth of the channel. Thus for the investigation of the channel depth corresponding to the maximum mass flow rate, the channel depth and inlet height were maintained as equal.

Varying the rate of energy transferred from the plate to the air had no noticeable effect on the channel depth at which the maximum mass flow rate occurred.

Figure 6.2. shows the results of the investigation to find the channel depth corresponding to the maximum mass flow rate for channels with stack heights between 3 and 10 m when the inlet height was equal to the channel depth.

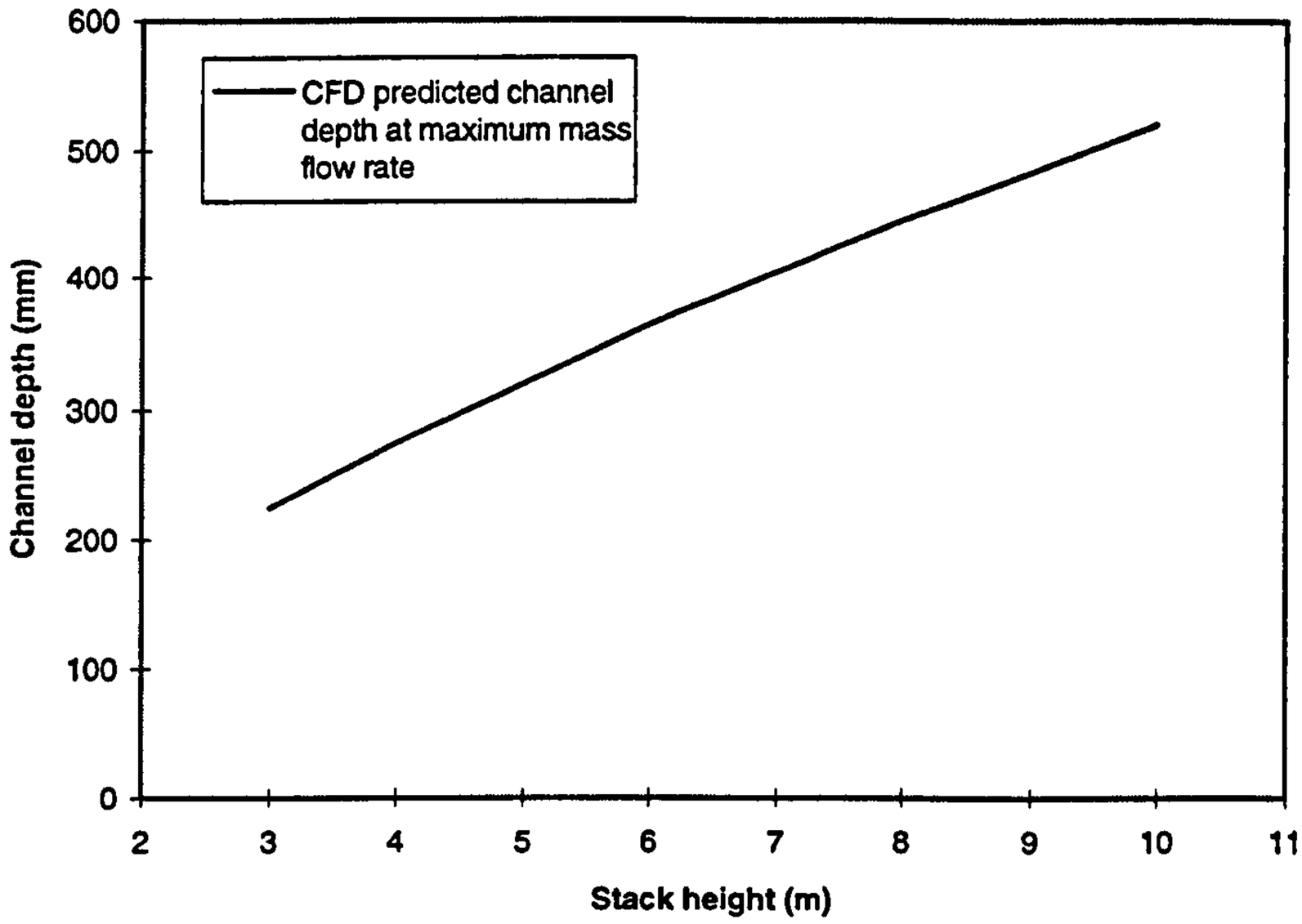

Figure 6.2. Channel depth corresponding to maximum mass flow rate for the parametric investigations at a rate of energy transferred from the plate of 100 W/m^2.

It is apparent from figure 6.2. that the channel depth corresponding to the maximum mass flow rate was an almost linear function of the stack height. The following linear relationship was determined with an r^2 value of 0.998.

$$d_{max} = 105 + 42.05\,h \qquad \text{Equation 6.1.}$$

Where h is the stack height between 3 and 10m.

For the parametric testing, the channel depths and inlet heights at any given stack height were normalised between 0 and 1 in terms of the channel depth corresponding to the maximum mass flow rate, as defined in equation 6.1. i.e.;

$$\text{Normalised channel depth } (D) = \frac{d}{d_{max}} \qquad \text{Equation 6.2.}$$

$$\text{Normalised inlet height } (H) = \frac{h_{inlet}}{d_{max}} \qquad \text{Equation 6.3.}$$

The range of variables to be investigated was therefore defined as follows:

Input variable	Range of values over which input variable investigated					
Stack height (m)	3	4	6	8	10	
Normalised inlet height	0.2	0.4	0.6	0.8	1.0	
Normalised channel depth	0.2	0.4	0.6	0.8	1.0	
Rate of energy transferred from the plate to the air (W/m^2)	50	100	150	200	250	300

Table 6.1. Identified range of input variables for the parametric investigation

With potentially over 700 different model input variable permutations, it was decided that simulations would be undertaken for stack heights 4 and 8m across the full range of input variables identified in table 6.1. Simulations would then be undertaken at other stack heights to ensure that the trends in mass flow rate identified at stack heights 4 and 8m were maintained across the full range of heights, 3 to 10m.

6.4 Results of parametric investigation

The results obtained from the parametric investigation are given in figures 6.3 to 6.8.

Figure 6.3. shows that for any given rate of energy transferred from the plate, the relationship between stack height and maximum mass flow rate was linear.

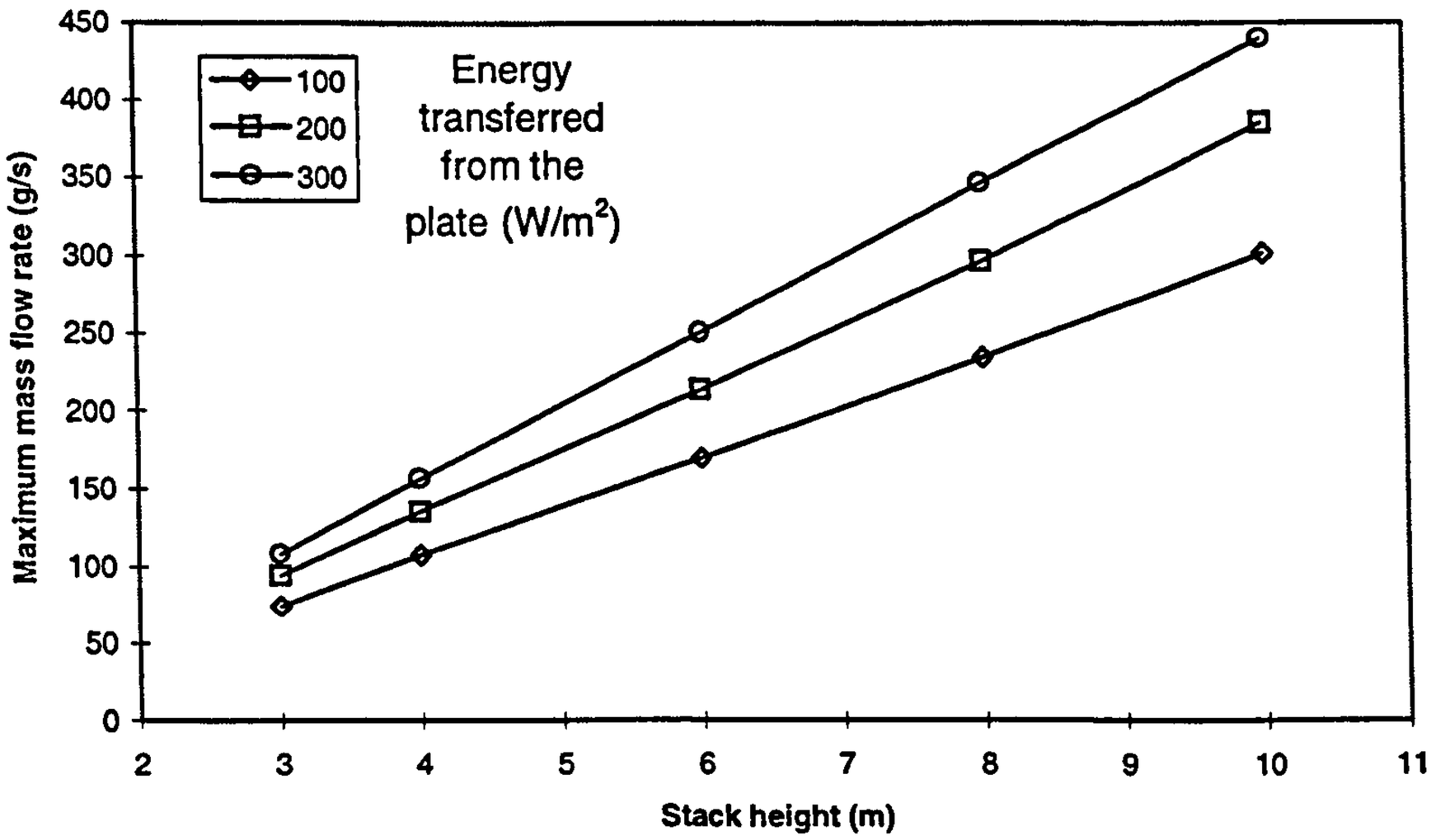

Figure 6.3. The influence of stack height and rate of energy transferred from the plate on the maximum mass flow rate

The effect of increasing the rate of energy transferred from the plate to the air at stack heights 4 and 8m was then assessed. The flow rates were normalised in terms of the flow rate predicted at a rate of energy transferred from the plate of 300W/m^2 for the two respective stack heights, i.e.

$$\text{Normalised maximum mass flow rate for stack heights 4 and 8m} = \frac{\text{Maximum mass flow rate for a given energy input rate}}{\text{Maximum mass flow rate for an energy input rate of 300 W/ m}^2}$$

Equation 6.4.

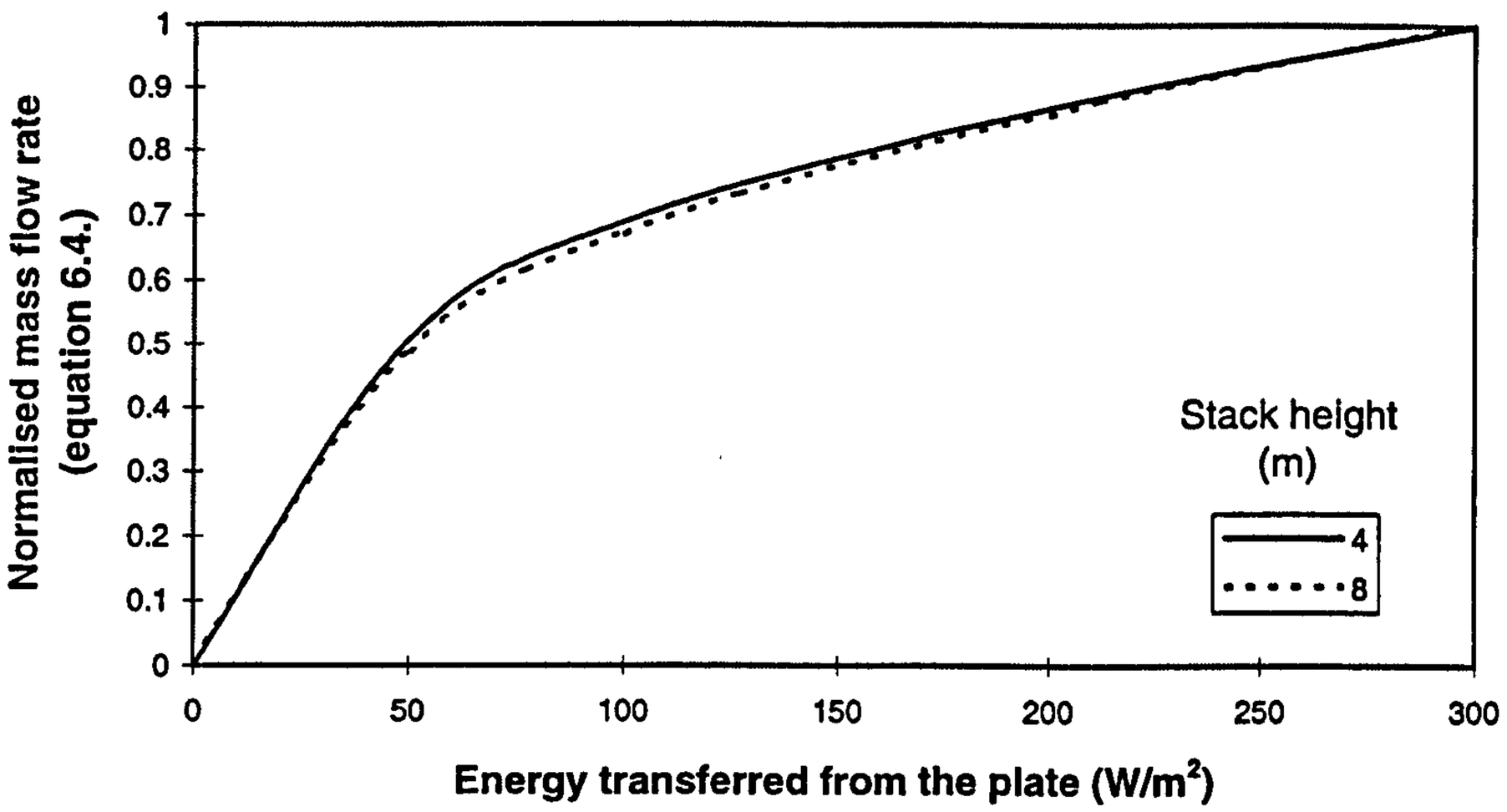

Figure 6.4. Comparison of the effect of the rate of energy transferred from the plate on the normalised maximum mass flow rate for two different stack heights.

Figure 6.4. clearly shows that the influence of the rate of energy transferred from the plate to the air within the channel upon the normalised maximum mass flow rate predicted was practically identical at the two stack heights 4 and 8m.

Having established the relationship between the maximum mass flow rate, the level of energy transferred from the plate and the stack height, the influence of the channel depth and inlet height upon the mass flow rate were then

investigated. Figure 6.5. shows the result of this investigation for a stack height of 4m and a rate of energy transferred from the plate of 100 W/m^2.

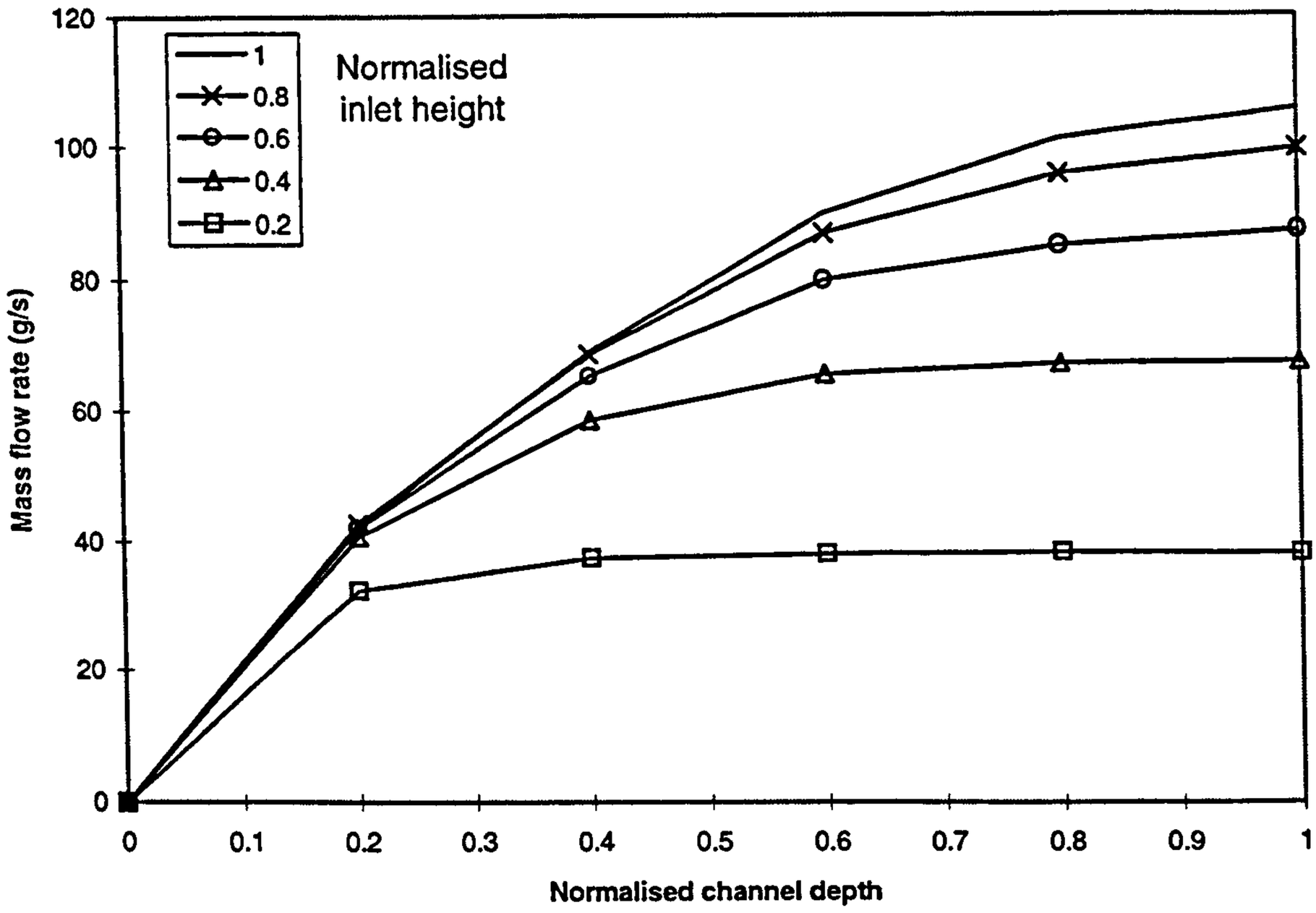

Figure 6.5. Effect of normalised channel depth and inlet height on the mass flow rate for a stack height of 4m and a rate of energy transferred from the plate of 100 W/m^2.

From figure 6.5. it was clear that both the inlet height and channel depth had a marked effect on the mass flow rate predicted through the channel. It was apparent that as either of the normalised variables approached zero, the influence upon the mass flow rate increased markedly. To assess the similarities in the effects of variations of either of the normalised variables on mass flow rate, figure 6.5. was replotted as a surface plot shown in figure 6.6.

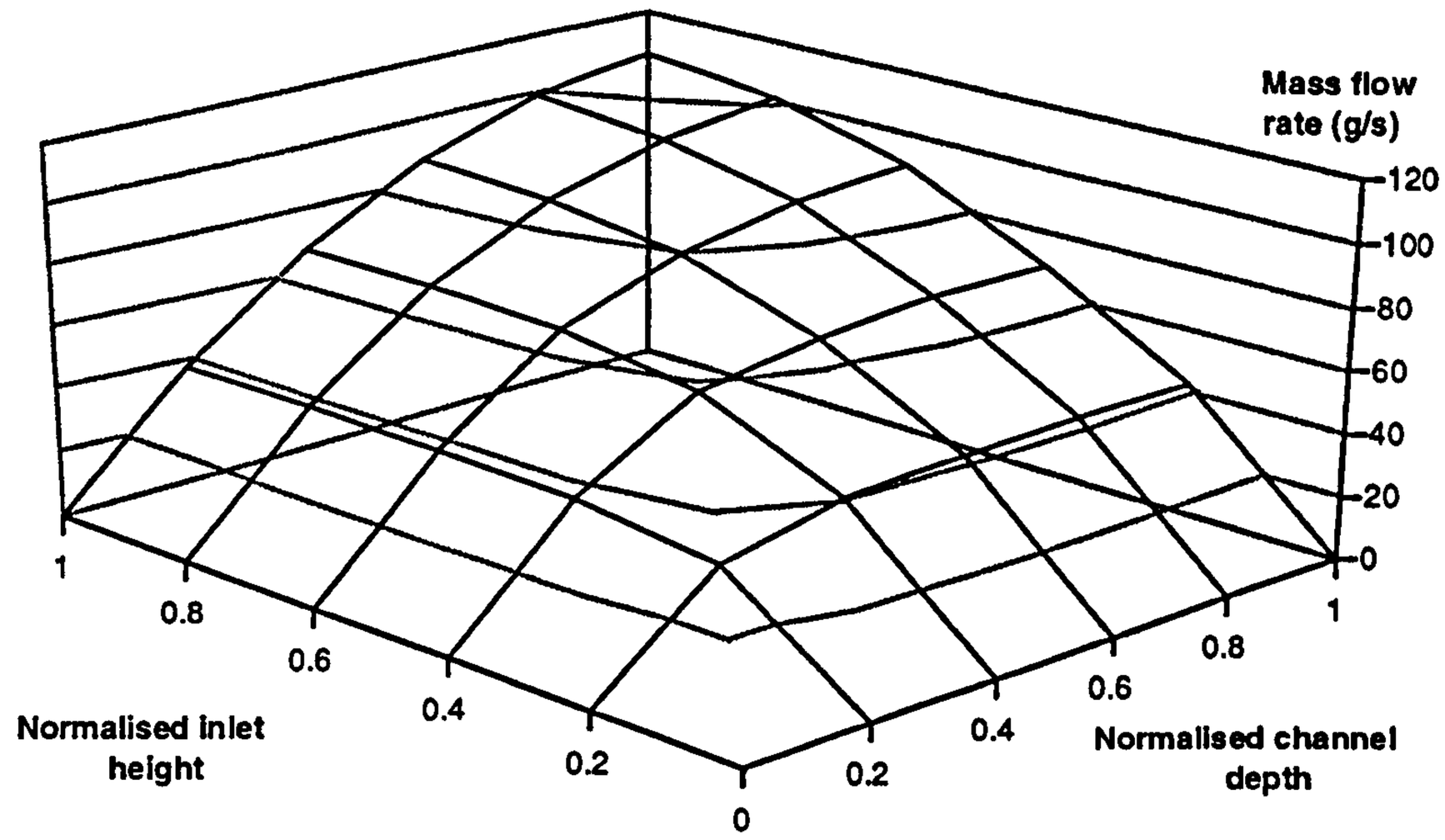

Figure 6.6. Effect of normalised channel depth and inlet height on the mass flow rate for a stack height of 4m and a rate of energy transferred from the plate of 100 W/m^2.

From figure 6.6. it was evident that variations in the predicted mass flow rate were similar in magnitude for variations in either the channel depth or the inlet height.

Having established the influence of the normalised inlet height (H) and channel depth (D) for one value of stack height and rate of energy transferred from the plate, it was important to assess if these trends remained constant at different values of these variables.

To assess the effects of both H and D at different stack heights, the mass flow rates at stack heights 4 and 8m were normalised in terms of the maximum occurring at a rate of energy transferred from the plate of 100 W/m^2.

$$\text{Normalised mass flow rate for stack heights 4 and 8m at 100 W/m}^2 = \frac{\text{Mass flow rate for an energy input rate of 100 W/ m}^2}{\text{Maximum mass flow rate for an energy input rate of 100 W/ m}^2}$$

Equation 6.5.

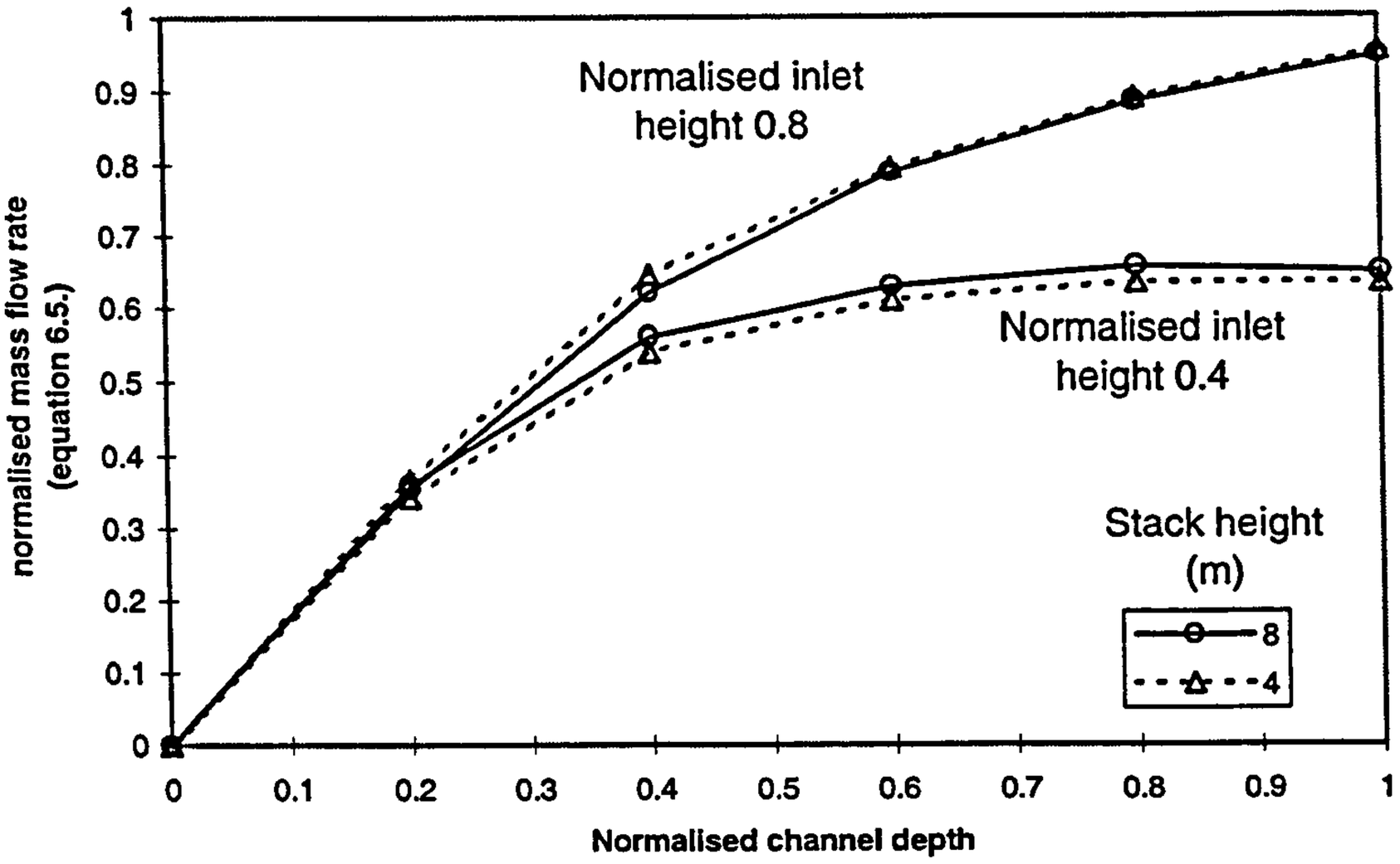

Figure 6.7. The effect of different stack heights on the normalised mass flow rate when the inlet height and channel depth were altered at a constant rate of energy transferred from the plate of 100 W/m^2.

To assess the effects of both H and D at different rates of energy transferred from the plate to the air, the mass flow rate at rates of energy transferred from the plate of 100 and 300 W/m^2 were normalised in terms of the maximum occurring at a stack height of 4m.

$$\text{Normalised mass flow rate for rates of energy transferred from the plate of 100 and 300 W/m}^2\text{ at a stack height of 4m} = \frac{\text{Mass flow rate at a stack height of 4 m}}{\text{Maximum mass flow rate at a stack height of 4 m}}$$

Equation 6.6.

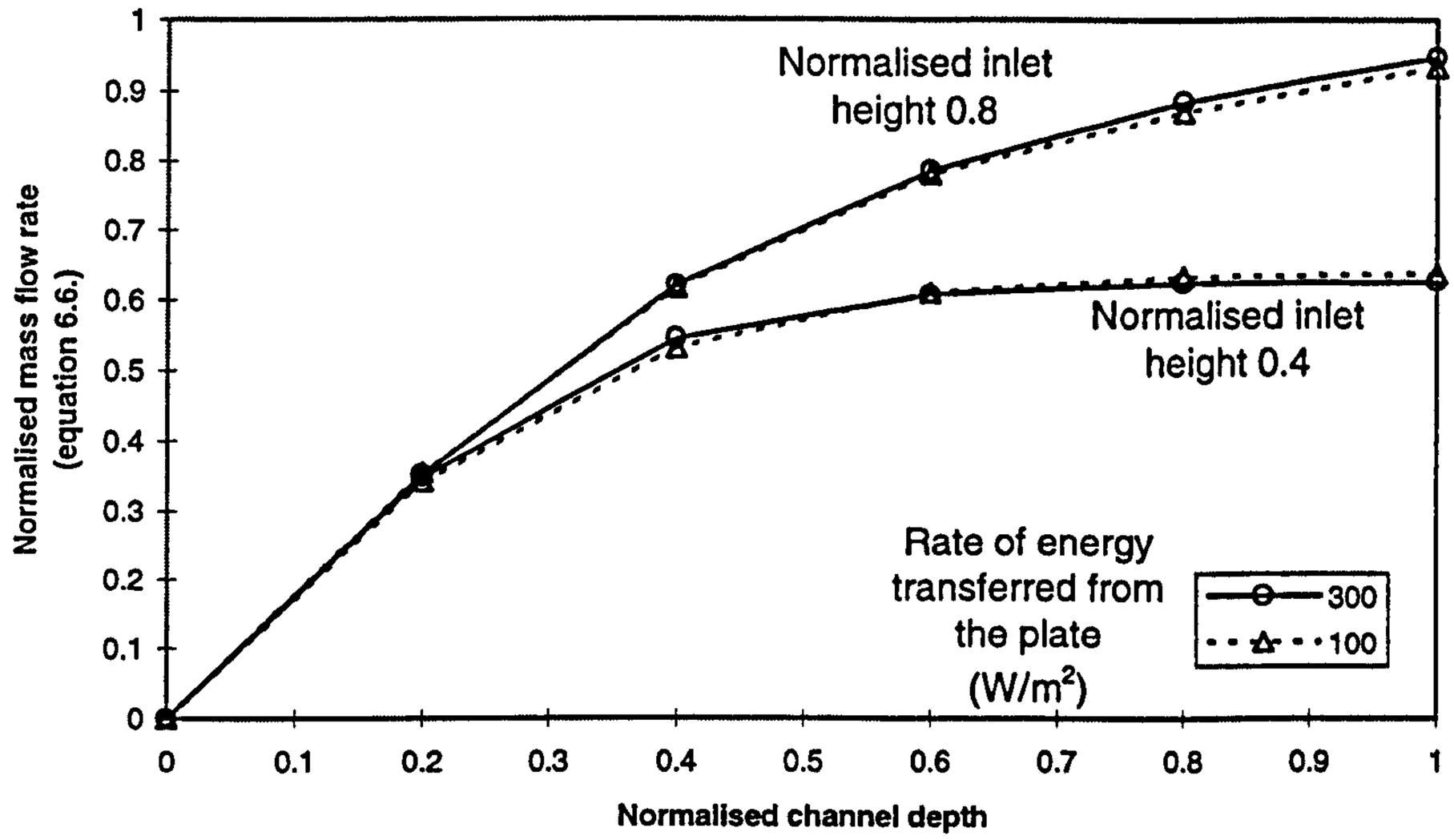

Figure 6.8. The effect of different rates of energy transferred from the plate on the normalised mass flow rate when the inlet height and channel depth were altered at a constant stack height of 4m

From figures 6.7. and 6.8. it was apparent that by normalising the inlet height and channel depth in terms of the channel depth corresponding to the maximum mass flow rate, the effect of variations of these normalised variables on the mass flow rate was the same across the full range of stack heights and rates of energy transferred from the plate investigated. Therefore the relative variations in mass flow rate presented in figures 6.5. and 6.6. for a stack height of 4m and rate of energy transferred from the plate of 100 W/m^2 could be applied across the full range of stack heights from 3 to 10m and rates of energy transferred from the plate from 50 to 300 W/m^2 for the flow configuration modelled.

Conclusions from the parametric investigation

In Chapter Five the predictions of the CFD programme, CFD 2000[(1)], were compared with the results of the experimental investigation. The ability of the CFD programme to predict the trends in mass flow rate due to variations in the physical parameters, except the channel depth beyond that corresponding the maximum mass flow rate, was shown to be good. Therefore it was proposed that the programme could be used in this parametric study, with a high level of confidence in the predictions made.

The parametric investigation undertaken highlighted several relationships between the predicted mass flow rate and the physical variables of such a building component. Over the range of variables investigated these were:

- Variations in the stack height for any given combination of the other variables investigated had a largely linear relationship with the mass flow rate. This is shown in figure 6.3.

- Variations in the rate of energy transferred from the plate to the air had similar effects on the predicted mass flow rate for any given combination of values of normalised inlet height and channel depth across the full range of stack heights investigated. This is shown in figure 6.4.

- By normalising the inlet height and the channel depth in terms of the channel depth corresponding to the maximum mass flow rate, the influence of variations of these variables was shown to be the same for all stack heights and rates of energy transferred from the plate to the air investigated. This relationship is shown in figures 6.5. and 6.6. for a stack height of 4m and rate of energy transferred from the plate of 100 W/m^2.

The model developed for the parametric investigation was similar to that used for the validation investigation detailed in Chapter Five. It required modifications only to ensure that the stack height remained constant when the inlet height was varied. The applicability of the results presented in this chapter to the experimental solar chimney was therefore high due to the similarity of flow configurations. The generality of the results for application to solar chimneys with different component and flow configurations is now considered.

The inlet modelled in this investigation was a sharp edge orifice. The use of grills or dampers at an inlet however may significantly alter the relationship between flow rate and pressure difference across the component. The model also assumed that the channel terminated with no flow resistance. In reality a termination device of some form would be fitted which may offer a considerable flow resistance. The influence of different types of inlet and possible outlet configurations is outside the scope of this investigation. If such studies were undertaken they would allow the generality of the predicted mass flow rates in this investigation to be assessed. The application of these results quantitatively to chimney configurations other than that modelled in this

investigation must therefore be undertaken with great caution. Qualitatively the trends in flow rate due to variations in the physical variables are considered as more general and applicable to a wide range of similar flows configurations.

6.5 Presentation of parametric investigation results in a format appropriate for use by designers

6.5.1 Graphical presentation of results

From the results presented for the parametric investigation it was shown that the effect of variations in both channel depth and inlet height could be presented in a normalised format across the full range of stack heights and rates of energy transferred from the plate investigated. Thus because this relationship held true for all stack heights and rates of energy transferred from the plate, a graphical presentation of these results was possible. This offered an easy to use method of evaluating the effects of variations in any of the input variables studied in this investigation. The presentation of the results in this format is shown in figures 6.9. through to 6.12.

Figure 6.9. allows the determination of the normalised values of the inlet height and channel depth for any stack height from 3 to 10m.

Having obtained the normalised values of these two variables, figure 6.10. allows the effects of variations in the values of either of these variables to be assessed in terms of a normalised mass flow rate, M_A.

$$M_A = \frac{\text{Mass flow rate}}{\text{Maximum mass flow rate for a given stack height and energy input rate}} \qquad \text{Equation 6.7.}$$

Figures 6.9. and 6.10. allow the relative effects on the mass flow rate due to variations in either inlet height or channel depth to be evaluated. For example if a normalised inlet height of 0.2 is proposed for a flow configuration, it is evident from figure 6.10. that variations in the channel depth between the normalised values of 0.6 and 1.0 make no noticeable effect on the mass flow rate through a chimney. This is true for any stack height and rate of energy transferred from the plate.

Figure 6.11. allows the evaluation of the effects of the rate of energy transferred from the plate on the mass flow rate. Using the normalised mass flow rate M_A and the rate of energy transferred from the plate, a second normalised mass flow rate M_B is obtained.

$$M_B = \frac{\text{Mass flow rate for a given energy input rate}}{\text{Maximum mass flow rate for an energy input rate of 300 W/m}^2} \qquad \text{Equation 6.8.}$$

Finally figure 6.12. allows the actual mass flow rate to be determined from the stack height and the normalised mass flow rate M_B.

To demonstrate the use of the figures 6.9. to 6.12., the mass flow rate resulting from the following combination of input variables has been presented.

Input variable	Value of input variable
Stack height (m)	7
Channel depth (mm)	300
Inlet height (mm)	200
Rate of energy transferred from the plate to the air (W/m^2)	150

Table 6.2. Values of input variables used in the example calculation of mass flow rate presented in figures 6.9. to 6.12.

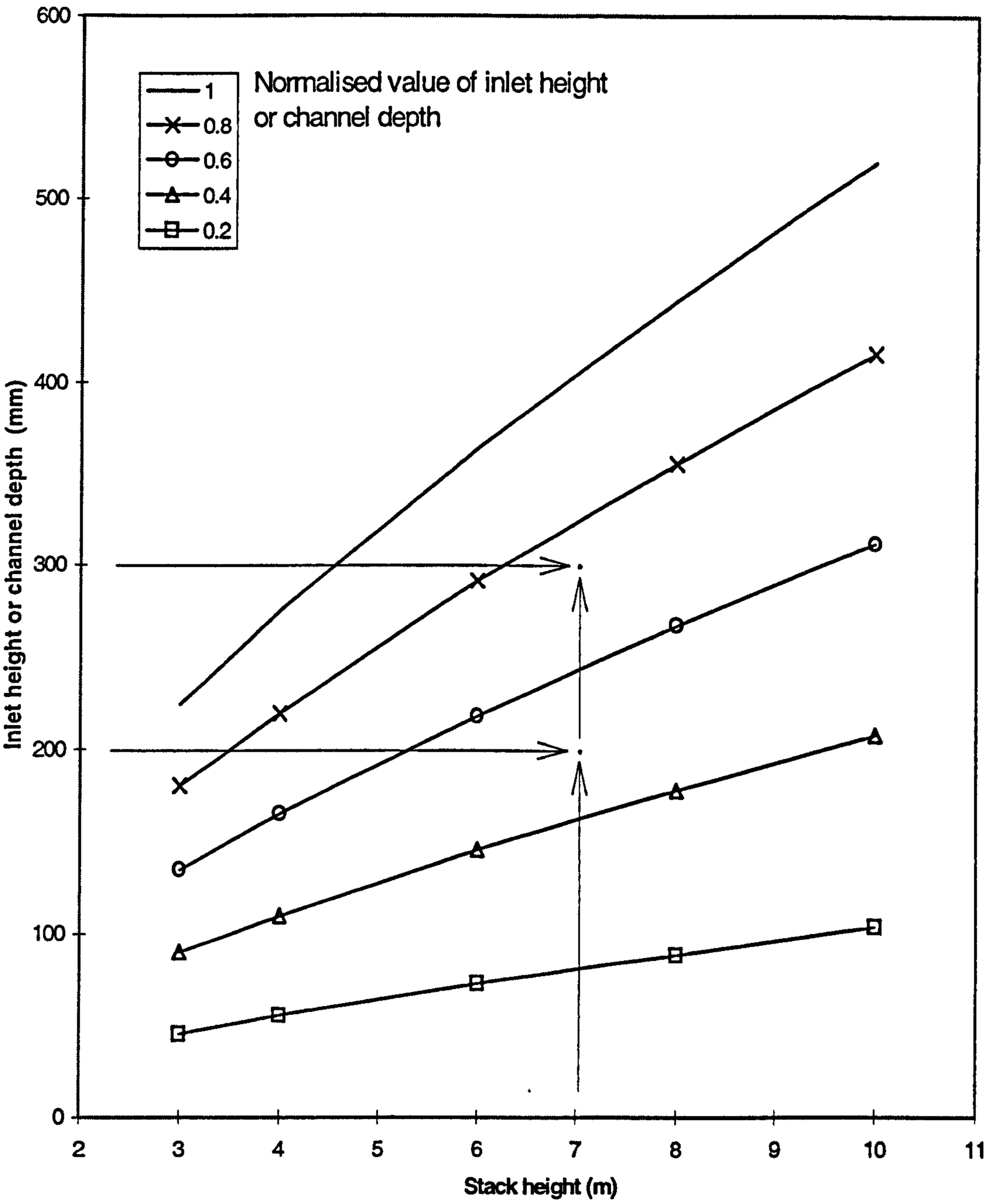

Figure 6.9. Determination of the value of the normalised inlet height and channel depth from the actual dimensions (mm)

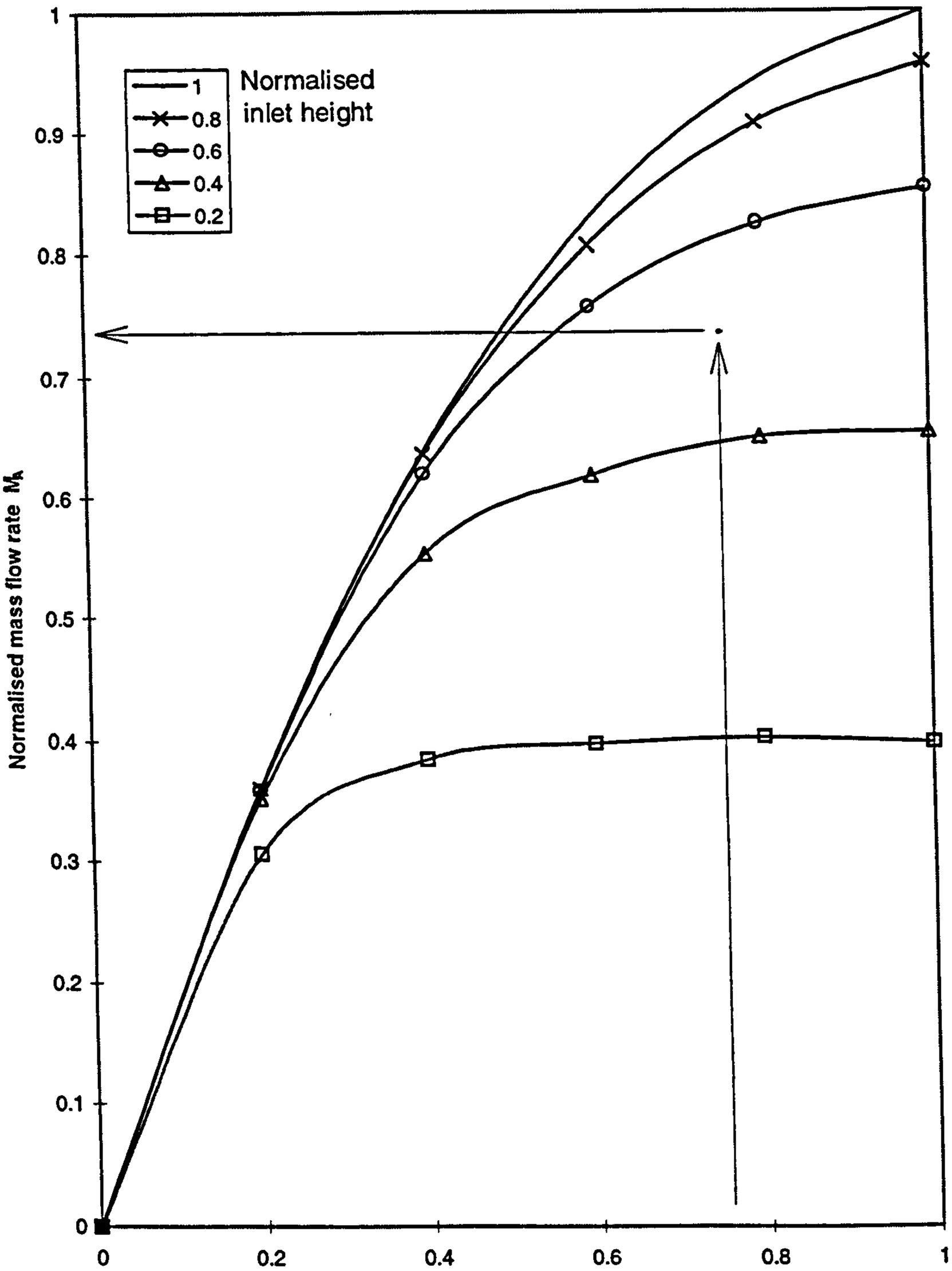

Figure 6.10. Determination of the normalised mass flow rate M_A from normalised values of the inlet height and channel depth

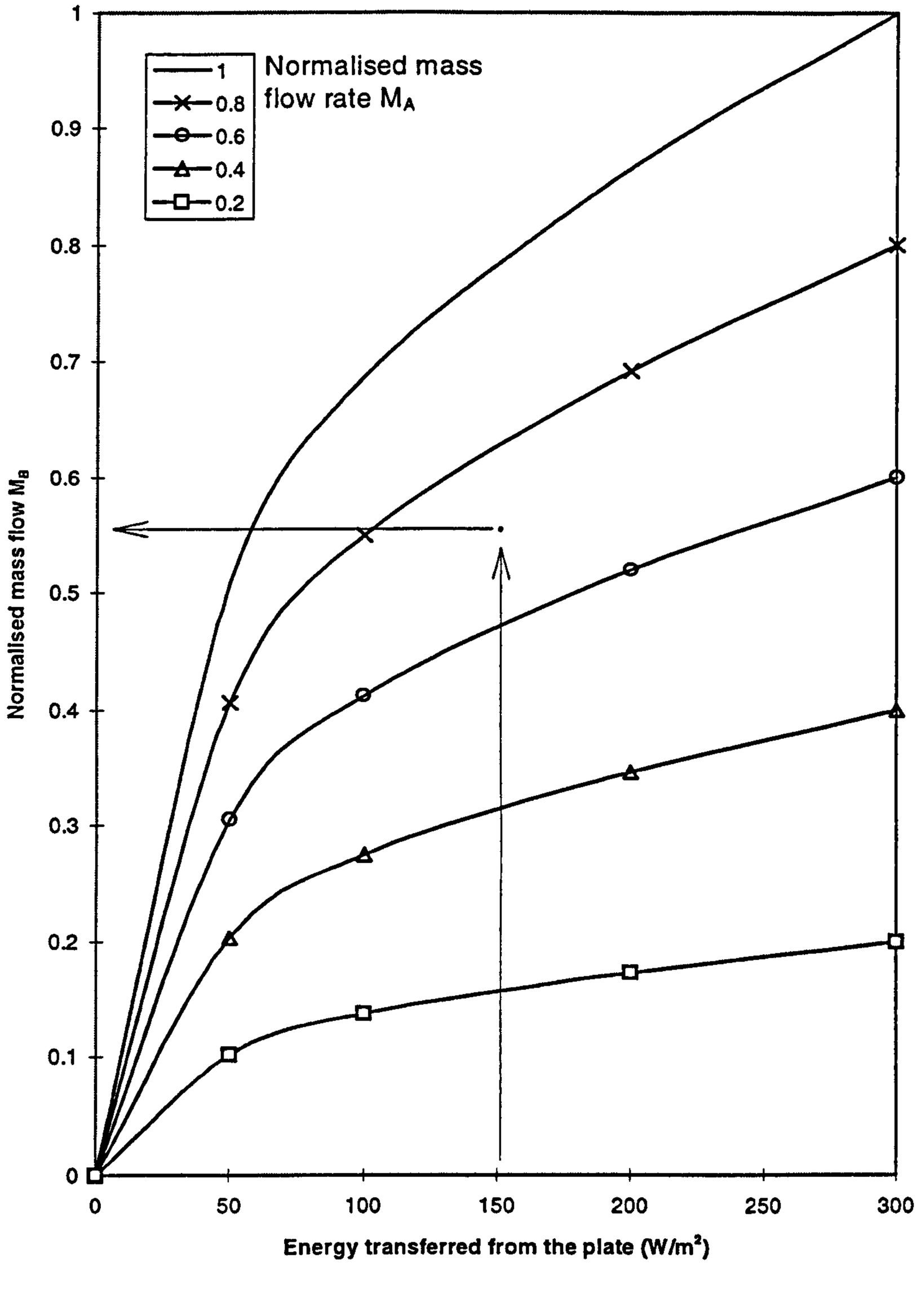

Figure 6.11. Determination of the normalised mass flow M_B from the normalised mass flow rate M_A and the rate of energy transferred from the plate (W/m^2)

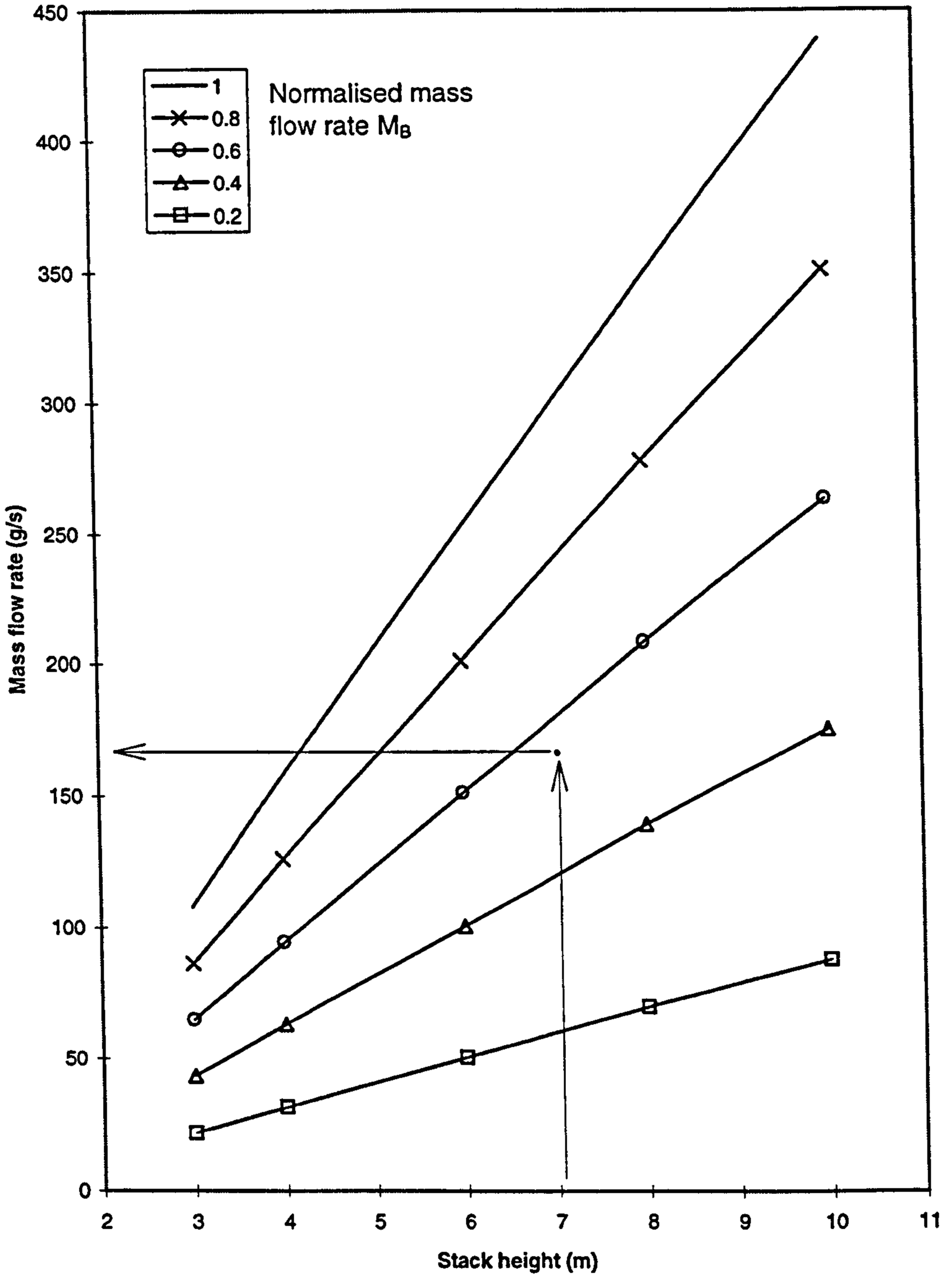

Figure 6.12. Determination of the mass flow rate (g/s) from the normalised mass flow rate M_B and stack height (m)

The mass flow rate resulting from the combination of input variables presented in table 6.2. is 170 g/s.

As noted previously, the quantitative value of the results obtained from this investigation are limited to flow configurations close to that modelled. Qualitative indications of the influence of variations in the key physical parameters will however offer considerable scope to evaluate the effects of such variations at an early stage in the design process. Thus allowing designers to make an early decision as to the appropriateness and influence on mass flow rate of a given set of physical parameters of a solar chimney.

6.5.2 Presentation of results in a format appropriate to spread sheet application

Development of a single relationship between the mass flow rate and all of the input variables was not considered appropriate, as manual calculation from a single complex equation would be cumbersome. Therefore a spread sheet application of figures 6.9. to 6.12. was developed and is described below by equations 6.9. to 6.13.

1. Calculation of the normalised inlet height (H) and channel depth (D) from the stack height and proposed inlet height and channel depth.

$$H = \frac{h_{inlet}}{105 + 42.05\ h} \qquad \text{Equation 6.9.}$$

$$D = \frac{d}{105 + 42.05\ h} \qquad \text{Equation 6.10.}$$

2. Calculation of the normalised mass flow rate M_A. The family of curves presented in figure 6.10 could be defined as individual polynomial curves. This would however require interpolation between the curves to obtain the full relationship between D, H and M_A. An alternative method of defining the output, M_A, in terms of the two continuous inputs, H and D, was therefore sought.

Neural networks allow an output variable to be expressed as a function of a set of input variables. This is achieved by allowing a neural network to learn the functional relationship between the inputs and outputs from a set of data containing all the variables of interest. The result of such an operation is a set of weights that can be applied, through a set relationship, to the input data to determine the corresponding value of the output. A more detailed description of the process is given in Appendix E.

The result of allowing the neural network to learn the relationship between the output M_A and the normalised inputs of D and H obtained from the parametric investigation is presented below:

It was found that the relationship between the inputs and outputs was defined to within +/- 2% for normalised input values of greater than 0.1 using 9 neurons in one hidden layer.

The following relationship allows determination of the output for any combination of normalised inputs between 0.1 and 1.0. The inputs and weights are expressed as matrices.

$$M_A = W_{output}^T \cdot \left[\text{Tanh}\left(W_{input} \cdot \text{Input}\right)\right] + \text{Offset} \qquad \text{Equation 6.11.}$$

Where W_{output}^T is the transpose of vector W_{output}.

The input vector is defined as; $\text{Input} = \begin{bmatrix} D \\ H \\ 1 \end{bmatrix}$

Neuron input weights $W_{input} = \begin{bmatrix} -6.309211 & 3.947574 & 1.15121 \\ 0.87819 & 9.620393 & -0.469006 \\ 0.488163 & -2.631925 & -0.260346 \\ 0.179838 & 0.991806 & -0.613458 \\ -3.552815 & 3.225209 & -0.248714 \\ 1.392716 & 0.751457 & 1.273349 \\ 1.171577 & 0.527113 & 1.682916 \\ 2.923094 & -0.996726 & 0.657121 \\ -5.72084 & -7.035315 & 0.0043646 \end{bmatrix}$

Offset = -0.169044

Neuron output weights $W_{output} =$

$$\begin{bmatrix} 0.0860467 \\ 0.0838518 \\ -0.441308 \\ 0.571685 \\ -0.211255 \\ -0.0229080 \\ -0.371362 \\ 0.585819 \\ 0.188713 \end{bmatrix}$$

3. Calculation of the normalised mass flow rate M_B . A fourth order polynomial curve was fitted to the curve $M_A = 1$ in figure 6.11. to allow definition of M_B in terms of the rate of energy transferred from the plate to the air with an r^2 value of 0.998.

$$M_B = M_A \left(-1.096*10^{-10}\, q''^4 + 1.108*10^{-7}\, q''^3 - 4.122*10^{-5}\, q''^2 + 8.03*10^{-3}\, q'' + 0.196\right)$$

Equation 6.12.

4. Calculation of the mass flow rate. The linear function of mass flow rate with variations in stack height was established for the normalised mass flow rate M_B with an r^2 value of 1.0.

$$\dot{m} = M_B\,(47.29\,h - 32.40)$$

Equation 6.13.

The routine identified through equations 6.9. to 6.13. allows the calculation of the mass flow rate per meter channel width through a solar chimney to within +/-4% of that predicted in the parametric investigation for the range of input variables detailed in table 6.3.

Input variable	Range
q''	50 - 300 W/m^2
h	3 - 10 m
d	0.1 - 1 normalised to the channel depth corresponding to the maximum flow rate
h_{inlet}	0.1 - 1 normalised to the channel depth corresponding to the maximum flow rate

Table 6.3. Range of input variables appropriate for use in equations 6.9. to 6.13.

6.5.3 Evaluation of a zonal model to predict the variations in mass flow rate found in the parametric investigation

An evaluation of the application of zonal models to predict flow rates at and above the channel depth corresponding to the maximum mass flow rate was presented in Chapter Four. The zonal model approach was largely unable to accurately predict the trends in mass flow rate due to variations in inlet height or channel depth for such configurations. To assess whether the zonal modal approach was more appropriate to flows occurring when the channel depth was less than that corresponding to the maximum, the CFD predicted mass flow rates from the parametric investigation were compared with such a model.

The mathematical model proposed by Bouchair[2] required the use of pressure loss coefficients at both the inlet and the outlet which, as noted in Chapter Four, are specific to the flow configuration and velocity profile of the air passing through these flow components. The modification of this model, by Awbi[3], allowed the use of the common orifice equation for the inlet orifice with a value of discharge coefficient, Cd, of 0.61. The flow configuration modelled by CFD in this investigation was a sharp edged orifice and thus the use of the common orifice equation to describe the flow through the inlet orifice was appropriate. The mathematical model proposed by Awbi[3] was therefore used as the basis for this investigation. Pressure losses at the channel outlet were not included in the model developed as the pressure loss coefficient, K, was dependent upon the velocity profile of the air at the exit[4]. This varied with channel depth and thus could not be accurately defined.

To allow direct comparison with the CFD predictions, the model was based on the level of energy transferred from the plate to the air, rather than plate temperatures as Awbi[3] had used. The proposed model is given by equations 6.14. to 6.20.

$$\dot{m} = \frac{q'' \, A_{plate}}{Cp \, \Delta T} \qquad \text{Equation 6.14.}$$

$$\Delta T = T_{outlet} - T_{inlet} \qquad \text{Equation 6.15.}$$

$$P_s = \rho_0 g h 273 \left(\frac{1}{T_{inlet}} - \frac{1}{T_{inlet} + \frac{\Delta T}{2}} \right)$$ Equation 6.16.

$$\dot{m} = Cd \rho A_{inlet} \sqrt{\frac{2 \Delta P_{inlet}}{\rho}}$$ Equation 6.17.

$$\Delta P_{inlet} = P_s - 4 f \frac{h}{d_h} \frac{\rho u^2_{mean}}{2}$$ Equation 6.18.

$$d_h = \frac{4 d w}{2 (d + w)}$$ Equation 6.19.

$$u_{mean} = \frac{\dot{m}}{\rho d w}$$ Equation 6.20.

Where f is the friction factor for a duct.

Bouchair[2] suggested that the friction factor should have a value of 0.011, which he determined from the Moody diagram[5] based on the channel roughness and the mean channel velocity Reynolds number. To compare the model with the CFD predictions, corrections were applied to the Reynolds number to allow the Moody diagram to be used for flows between smooth parallel plates, as suggested by White[6].

Equations 6.14. to 6.20. were solved for an inlet air temperature of 300K, a rate of energy transferred from the plate of 100 W/m^2 and normalised inlet heights and channel depths ranging from 0.2 to 1.0. The predictions of mass flow rate were compared with those obtained from the CFD model with the percentage differences presented in figure 6.13.

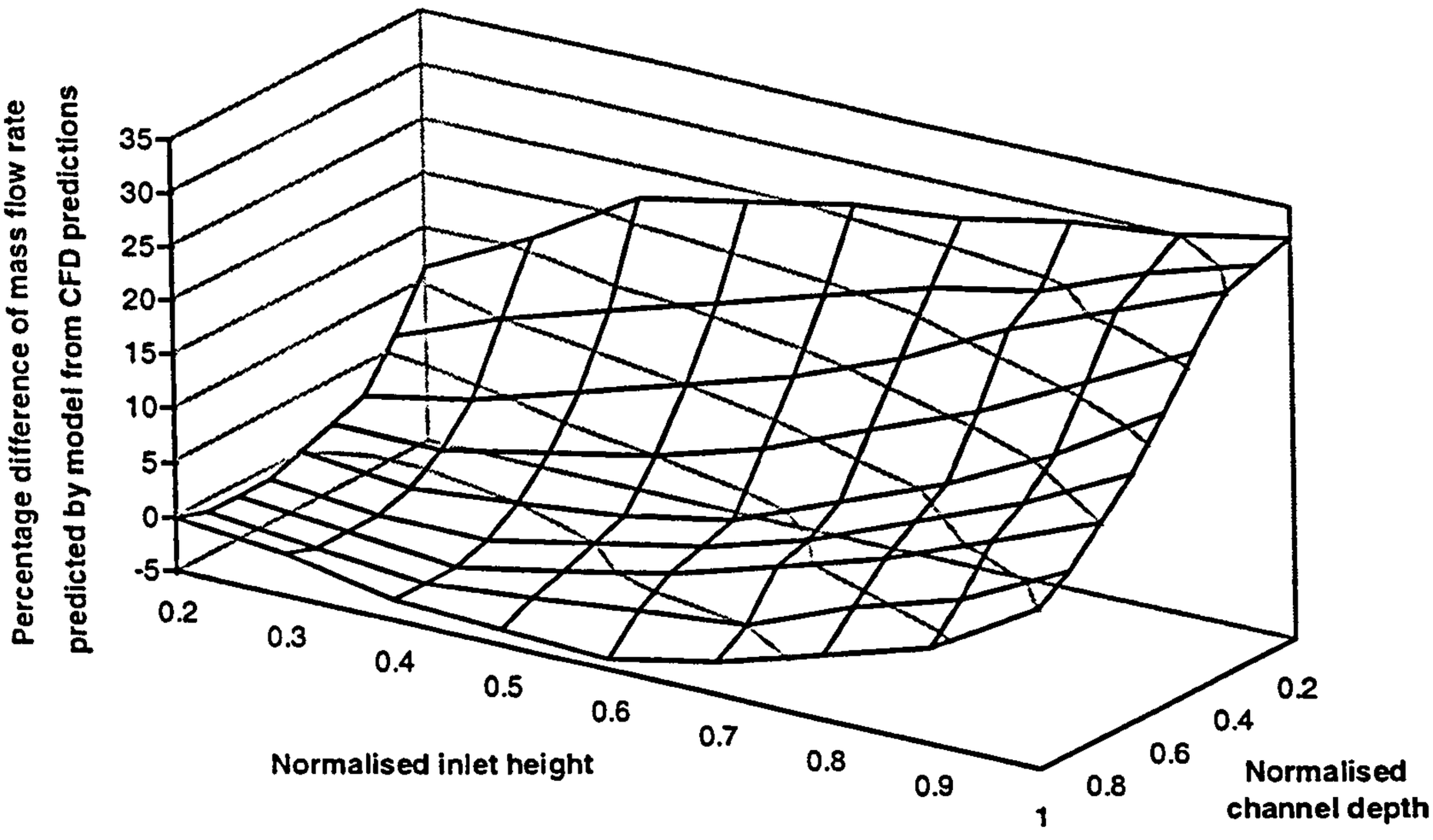

Figure 6.13. Percentage difference between predicted mass flow rate of model using equations 6.14. to 6.20. from that predicted by the CFD model

From figure 6.13. it is apparent that the model proposed in equations 6.14. to 6.20. does not predict accurately the variations in mass flow rate due to variations in inlet height or channel depth when compared to predictions from a validated CFD model.

For normalised channel depths above the minimum of 0.2, increases in the inlet height generally caused the mass flow rate to increase above that predicted by the CFD model. This confirmed the findings presented in Chapter Four, that the zonal model approach always returned an increased mass flow rate when the resistance to flow was reduced through an increase of the inlet height. For a naturally convective boundary layer this was not the case, as for a given rate of energy transferred from the plate to the air a definite maximum mass flow rate exists which once achieved was not exceeded by subsequent increases in either the inlet height or channel depth.

As the channel depth was reduced below that corresponding to the maximum mass flow rate, the difference between the predicted mass flow rates increased. This indicated that the reduction of flow rate presented in figure 6.5. due to variations in channel depth, were not well described by the channel frictional losses as defined in equation 6.18.

It is of interest to note that the area of greatest agreement between the two model predictions, was that where the inlet height was small and the channel depth large. In channel configurations such as this, the overwhelming majority of the pressure losses occur across the inlet orifice. The relatively close agreement of the models in this area showed that when such pressure losses predominate, then the orifice equation, equation 6.17., linked to a zonal model gave relatively accurate mass flow predictions. As the inlet height increased and the pressure losses in other areas of the flow path became important, the accuracy of the model reduced significantly.

Overall therefore the zonal model appeared to offer only limited application in the format presented for the prediction of the influence of physical variables on the mass flow rate of a solar chimney.

6.6 Discussion of the results of the parametric investigation and presentation of the results in a format appropriate for design use

The aim of this project has been to evaluate existing methods of investigating the potential of a solar chimney, however it is of interest to place the results of the parametric investigation into context with respect to the potential to drive natural ventilation.

As noted in Chapters One and Two, a solar chimney uses a plate heated by solar energy to heat air within the chimney. To allow evaluation of the potential of different tools to predict the mass flow rate through a solar chimney this project has concentrated upon the critical period for natural ventilation; that of little wind and the external air temperature rising to equal those experienced internally. In such situations the natural stack effect between the internal and external air masses will reduce towards zero.

The use of a solar chimney in such situations would however allow the exhaust air from the building to be heated above the external air temperature. It is this potential to provide ventilation when the stack effect due to differences in internal and external air temperatures is minimal, that makes the solar chimney a valuable addition to a natural ventilation strategy for a building.
To assess the effectiveness of a solar chimney, it is appropriate to calculate the temperature elevation of the internal air mass that would be required to

achieve the same mass flow rate had the solar aspect of the chimney not been included in the chimney design.

If it is assumed that the chimney configuration is the same as that of the solar chimney, i.e. the pressure losses are concentrated at the inlet orifice then the required temperature rise of the internal air mass can be calculated as follows:

If the example set out in table 6.2. is considered where a mass flow rate of 170 g/s was predicted.

$$\Delta P_{inlet} = \left(\frac{\dot{m}}{\rho \ Cd \ A} \right)^2 \frac{\rho}{2} \qquad \text{Equation 6.21.}$$

Where for a sharp edged orifice the value of the discharge coefficient Cd is 0.61.

$$\Delta P_{inlet} = 0.809 \quad Pa$$

If the pressure difference across the inlet (ΔP_{inlet}) is equal to the stack pressure (P_s) and the air within the unheated chimney is considered to be fully mixed then;

$$P_s = \rho_o \ g \ h \ 273 \left(\frac{1}{T_{external}} - \frac{1}{T_{internal}} \right) \qquad \text{Equation 6.22.}$$

If the external air mass is assumed to be at 300K then;

$$T_{internal} = 303.1K$$

From this simple calculation it can be seen that the temperature rise required to obtain the same mass flow rate, through the same chimney configuration, would be over 3°C. Although this is not large, its significance with an internal air temperature around 27°C could be the difference between tolerable internal conditions on a hot summers day and unacceptably high internal air temperatures. Thus in such situations, the addition of a solar chimney to a building allows the ventilation rate to be significantly enhanced.

Through the use of a validated CFD model, the variations of the mass flow rate through a solar chimney have been shown to be a function of the following four variables;

- level of energy transferred from the plate to the air within the channel,
- stack height,
- channel depth,
- inlet orifice area.

The relationship between the mass flow rate, the normalised inlet height when the inlet width was equal to that of the channel, and the normalised channel depth has been shown to be constant across the range of stack heights and rate of energy transferred from the plate investigated parametrically.

The result of this finding allowed the development of a simple graphical method to evaluate the influence of either of the normalised variables on the mass flow rate for a given stack height and rate of energy transferred from the plate. This was included in a series of figures that allowed the determination of the mass flow rate resulting from any given combination of input variables.

This relationship was also presented in a format appropriate for inclusion on a spread sheet based computer programme.

For early design stage evaluation of the potential of a solar chimney such methods are appropriate, however their use to investigate a whole building ventilation strategy would not be appropriate. For this, zonal models linked to dynamic thermal models are most often used. The inputs required for a zonal model of this type are either the temperature of the air mass within the space or a pressure difference across a defined opening, usually within the building envelope. The use of a modified zonal model to predict the mass flow rate through natural ventilation chimneys was therefore evaluated, as one of the independent variables of such a model is the pressure difference across the inlet opening. If the output of such a model gave accurate predictions it could be used to supply pressure data for a whole building zonal model, allowing the inclusion of such a component in the investigation of the buildings overall ventilation strategy.

Modification of an existing zonal model proposed by Bouchair[2] and modified by Awbi[3] for application to a solar chimney building component was however shown to be largely unable to predict the trends in mass flow rate identified in

this parametric investigation. The basic zonal model assumption of a fully mixed air mass within a solar chimney resulted in an overprediction of mass flow rate as the inlet orifice area was increased. This was due to the fact that the temperature distribution within a solar chimney is governed by the boundary layer adjacent to the heated wall. This results in a maximum mass flow rate existing, that once achieved is independent of further increases in the inlet orifice area.

The attempt to define variations in mass flow rate due to changes in channel depth by considering the frictional losses in a duct also proved to be largely inaccurate. The frictional losses were defined using the Moody diagram based on the mean velocity Reynolds number of the air flow within the channel.

Consideration of the flow configurations appropriate for the application of the Moody diagram highlights the significant difference between such flows and those existing in a solar chimney. The Moody diagram was developed for fully developed flows in a circular duct[7]. Correction factors can be applied to obtain data for a flow between parallel plates[6]. However, again the flow regime was fully developed. If the velocity profiles from the parametric investigation are investigated, figure 6.14., it can be seen that the flow profiles at the mid height of the channel, were significantly different from those of fully developed turbulent flows with the same mass flow rate.

From figure 6.14. it can be seen that the velocity profile of the air adjacent to the heated wall was the same in both channel configurations. It can therefore be concluded that the influence of the unheated wall upon the profile of the flow near the heated wall was very small. This will remain true until the flow within the channel approaches a fully developed state, then subsequent changes to the channel depth will cause equal variations in the profile of the flow adjacent to both walls. Variations in the depth of the channel for the flow configurations presented in figure 6.14. therefore mainly effected the flow of air adjacent to the unheated wall. As the distance from the heated plate increased the velocity of the flow within the channel reduced. The use of a mean channel velocity to define the flow adjacent to the unheated wall therefore significantly overestimated the true velocity of the air in this region. In addition to this, for a given stack height, as the channel depth was reduced, the mean channel velocity based Reynolds number fell towards the critical value of 2300. This implies that the flow regime was moving from a turbulent to a laminar flow. In Chapter Five however it was shown that the flow within the

channel would be turbulent in nature due to the heating of the air by the wall and by the effects of the inlet orifice both generating turbulence. The use of the friction factor based on the mean channel velocity Reynolds number as proposed by Bouchair[2] and Awbi[3] for a non forced flow within a channel must therefore be questioned.

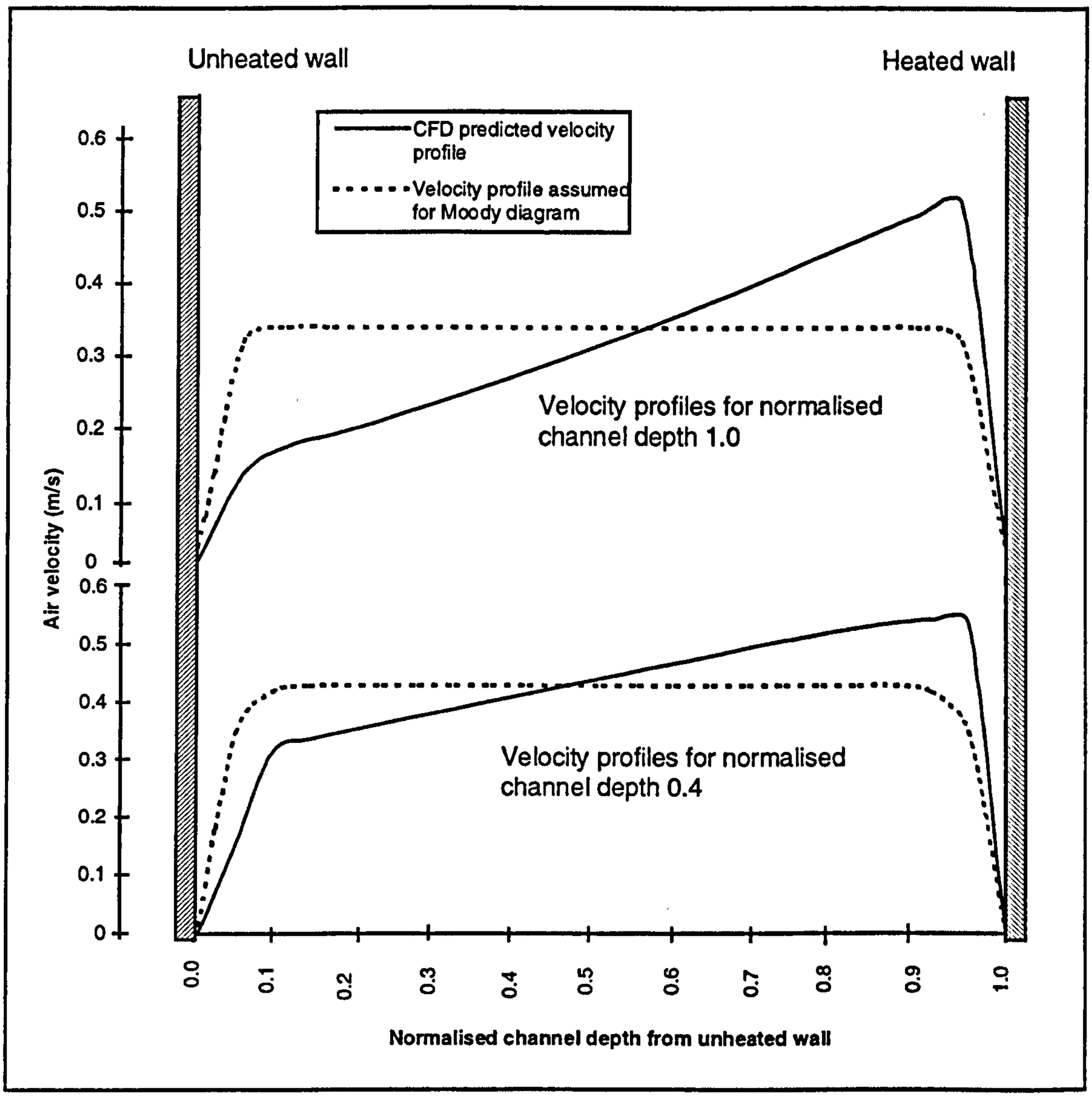

Figure 6.14. Comparison of the actual velocity profile within a solar chimney as predicted in the parametric investigation with that of a turbulent fully developed flow of the same mass flow rate

The justification for using any velocity other than the channel mean for the determination of the friction factor from the Moody diagram, or an alternative method of evaluating the channel friction, would however require a significant

level of further investigation if it is to be based on sound physics and offer a general, rather than a case specific solution.

Overall therefore, quantitative values of mass flow rate obtained from this investigation are only appropriate to flow configurations similar to those modelled in this investigation. Qualitatively however, the results may be used to obtain an understanding of the effects of variations in the physical variables on the mass flow rate through similar building components. The use of the friction factor determined from the Moody diagram within zonal models is not considered appropriate for application to asymmetrically heated natural convective channel flows such as that within a solar chimney.

6.7 References Chapter Six

1. Adaptive Research, CFD 2000, User's Manual, Version 2.2, Adaptive Research Inc., USA.

2. Bouchair, A. Solar induced ventilation in the Algerian and similar climates, Ph.D. Thesis, University of Leeds, UK, 1989.

3. Awbi, H., Design considerations for naturally ventilated buildings, Renewable Energy, Vol. 5, Part 2, 1081 - 1090, 1994.

4. Fried, E. and Idelchik, I., Flow Resistance, A Design Guide For Engineers, Hemisphere Publishing Corp., New York, 1989.

5. CIBSE, Flow of Fluids in pipes and Ducts, CIBSE Guide C4, 1988.

6. White, F., Fluid Mechanics, McGraw-Hill Co., 2nd. Ed., New York, 1986.

7. Sabersky, R., Acosta, A. and Hauptmann, E., Fluid Flow, A First Course in Fluid Mechanics, Macmillan Publishing Co., 3rd. Ed., London, 1989.

CHAPTER SEVEN

CONCLUSIONS AND RECOMMENDATIONS FOR FURTHER WORK

7.1 Introduction

The adoption of natural ventilation strategies for buildings requires that designers are able to fully evaluate the potential of such strategies to meet the ventilation requirements of a buildings occupants throughout the year. To achieve this, accurate design tools capable of predicting the operation of building components, such as solar chimneys, must be available. If this is not the case then inappropriate designs may be adopted that subsequently are unable to meet the ventilation needs of the building occupants.

The aim of this project was to investigate if the potential of a solar chimney to drive natural ventilation could be accurately evaluated with the design tools that are currently available. If such tools were not appropriate, then a tool was to be developed.

The potential of design tools currently available was evaluated for application to a solar chimney along with work in all areas of similar flow configurations. It was evident from this investigation that very little work had been undertaken in quantifying the flow rates through such building components and the applicability of the general models available was questionable.

In light of this an experimental rig was constructed to allow mass flow rate data to be obtained for a solar chimney across a limited range of physical variables. The resulting data set allowed the ability of zonal models to predict the performance of a solar chimney to be determined.

To obtain sufficient experimental data to develop a reliable design tool capable of predicting the effect of a full range of physical variables would have required a very extensive investigation. The potential of CFD programmes to predict the performance of a solar chimney was therefore investigated. Within specific variable limits a validated CFD model was developed that allowed a parametric investigation of the effect of physical variables to be undertaken. This allowed the range of the physical variables investigated to be increased significantly above that practical with an experimental rig.

The resulting data from the parametric investigation allowed two design tools to be developed. The generality of the tools developed was however limited quantitatively to flow configurations close to that investigated parametrically.

This project, therefore, highlights the significant limitations of the design tools that are currently available to building designers when applied to a solar chimney. It also provides the first step to the development of a comprehensive tool describing the operation of a solar chimney, that will allow its potential to be evaluated throughout the design process.

7.2 Conclusions

1. There are two design tools that are currently available to designers for the investigation of air movement within buildings; zonal models and CFD programmes. Evaluation of the potential of these tools proved that neither zonal models or CFD programmes are suitable for the prediction of mass flow rates through a solar chimney without modification or extensive validation respectively.

    - Zonal models assume that the air mass within a space is fully mixed. This is not the case in a solar chimney where the flow is largely contained within a natural convective boundary layer. The result of this simplification is that the mass flow rate continues to increase with increases in inlet orifice area when a zonal model is used to make predictions. In a solar chimney a maximum flow rate does exist and once achieved will not be exceeded by increases in the inlet orifice area.

    - Predictions of the effects of varying channel depth on mass flow rate through a solar chimney with modified zonal models, using the Moody diagram based friction factor, proved that such models are inappropriate for such applications. The friction factor obtained from the Moody diagram requires that significant assumptions are made about the flow within a chimney which do not reflect the complex nature of such flows and so are not based on sound physical principles.

- The complexity of CFD programmes is such that the predicted results of a simulation cannot be checked by manual calculation. The programmes are also highly sensitive to both the model configuration and input variables used. Such sensitivity, therefore, makes predictions using unvalidated CFD models highly unreliable. The validation of CFD models requires that accurate data is available for similar flow configurations against which the predictions can be compared. A thorough review of work in this area however proved that little empirical data for realistic and practical flow configurations exists. Consequently future investigations into such flow configurations will be limited by this lack of data for model validation.

2. The experimental investigation of building components, such as solar chimneys, to obtain data to validate mathematical and CFD models requires that great care is taken in the design of the experimental rig to ensure that any uncertainties are both minimised and quantifiable. If this is not undertaken the level of confidence in and usefulness of the data for comparison with model predictions will be very limited.

3. The experimental investigation into the operation of a solar chimney subject to a range of physical input variables demonstrated that:

    - The channel depth corresponding to the maximum mass flow rate for a given chimney height was very close to the depth of a turbulent natural convective boundary layer;

    - The mass flow rate was largely insensitive to variations in the channel depth beyond that corresponding to the maximum mass flow rate;

    - For a given rate of energy transferred from the plate to the air within the channel, the temperature elevation of the plate above that of the inlet air was constant regardless of the overall channel height.

4. Comparison of the predictions of a CFD model using the standard $k\,\varepsilon$ turbulence model and the experimentally measured results proved that the CFD programme was able to predict the effects on mass flow rate of variations in; stack height, inlet orifice area and the rate of energy

transferred from the plate to the air within the channel. The CFD programme was, however, not able to accurately predict the variations in mass flow rate due to channel variations above that corresponding to the maximum mass flow rate. This was due to the inability of the programme, using the standard $k\,\varepsilon$ turbulence model, to accurately predict flow recirculation which occurs at the channel outlet when the channel depth exceeds the depth of the turbulent natural convective boundary layer.

5. The CFD programme predictions of the convective heat transfer coefficient were highly sensitive to the position of the near wall node. The prediction of this variable outside the range of flow configurations investigated experimentally was, therefore, unreliable. This further demonstrated the limitations of using unvalidated CFD models for the prediction of dependant variables in natural convective flow configurations.

6. The use of two dimensional CFD models to make predictions regarding three dimensional flow configurations offers considerable time savings for detailed investigations. The error in using such a modelling technique for a solar chimney was found to be systematic in nature. The magnitude of the error was, however, specific to the flow configuration investigated and must be quantified across the full range of model variations before being used.

7. The parametric investigation of the performance of a solar chimney by a validated CFD programme model demonstrated that:

    - For any given combination of channel depth, inlet orifice area and rate of energy transferred from the plate, the effect of stack height on the mass flow through a solar chimney was largely linear;

    - By normalising the channel depth and inlet height in terms of the channel depth corresponding to the maximum mass flow rate, the effects of variations in either of these variables remained the same across the full range of stack heights and rates of energy transferred from the plate investigated;

    - For any given combination of normalised channel depth and normalised inlet height, the effect of variations in the rate of energy

transferred from the plate was similar for all stack heights within the range investigated.

8. The results of this investigation are only quantitatively applicable to flow configurations very similar to those investigated. Qualitatively, the results from this investigation can be applied to a wide range of similar flow configurations to evaluate the effect of variations of the key physical variables.

7.2 Recommendations for further work

7.2.1 Natural ventilation as a whole year strategy

The adoption of natural ventilation as a ventilation strategy for a building requires a very detailed analysis of the natural driving forces available to drive the ventilation. This project highlights the inadequacy of the design tools currently available for the evaluation of the potential of a solar chimney to drive natural ventilation. In addition to this, the lack of guidance on the use of chimneys and especially solar chimneys, indicates that little work has been undertaken in this area or on the use of such components to meet whole year ventilation requirements. This area needs to be urgently addressed if appropriate schemes are to be adopted that meet the requirements of the building occupants.

In addition to the design of chimneys, the control of ventilation provided by such components requires investigation before their true potential can be evaluated. The use of a full fresh air ventilation system in winter requires that tight control is essential if significant energy losses are not to be incurred. At such times the possibility of exhaust air heat recovery may offer a solution and requires investigation.

7.2.2 Development of tools appropriate for the design of solar chimneys

The use of a validated CFD model for the investigation of a solar chimney has been shown to be appropriate for the evaluation of the effects of variations of a range of input variables. However, the validity of the CFD model was not universal and limits were set on the range of some input variables investigated parametrically. To allow the validity of CFD models to be assessed, there is a

need for an extensive range of data sets of realistic flow configurations. This will allow parametric investigations to be undertaken without the need to obtain data from experiments first, thus ensuring that simplified models are developed based on correct data.

The use of modified zonal models for the prediction of mass flow rates through solar chimneys has been shown to be at best, very specific to the flow configuration on which they were based. The possibility of modifying the zonal model approach does offer significant advantages over that of CFD; simplicity, speed of convergence and the potential to incorporate such models into whole building ventilation models. Any alternative approaches to the Moody diagram based friction factor developed must offer a wide range of generality and, therefore, be based on sound physics.

7.2.3 Extend the scope of the variables investigated

This project has concentrated on the potential of existing tools to predict the operation of a solar chimney subject to variations in a range of physical variables. In reality the range of variables that will influence the performance of the chimney will be significantly greater than those studied here. It is, therefore, necessary that all of these factors are investigated and methods of evaluating their effect on the performance of a chimney produced.

7.2.4 Demonstrate the potential of solar assisted chimneys

The lack of guidance on the design and potential of solar assistance for chimney driven ventilation is one possible reason for such components not being adopted. A working example would overcome this and allow in use problems to be addressed and provide a valuable source of data for the validation of design tools.

APPENDIX A

A REVIEW OF PHYSICAL MODELLING TECHNIQUES TO AID IN THE DESIGN OF NATURAL VENTILATION BUILDING COMPONENTS

Paper presented at CIBSE National Conference, Eastbourne, October, 1995.

A REVIEW OF PHYSICAL MODELLING TECHNIQUES TO AID IN THE DESIGN OF NATURAL VENTILATION BUILDING COMPONENTS

M. J. Swainson, W. J. Batty
Dept of Applied Energy, CRANFIELD UNIVERSITY.

Current trends towards the natural ventilation of buildings have led to the adoption of both atria and chimneys. In order for them to be effective a detailed understanding of the physical processes involved is required. To this end the use of physical models has been employed. However, at present most models assume similarity of the flows through an assumption of high levels of turbulence, thus allowing boundary layer flows to be ignored. When turbulence cannot be globally assumed, then either full scale models or reduced scale models with alternative working fluids must be employed. Previous use of CFC based refrigerant gases in reduced scale models is now unacceptable on environmental grounds and the new HCFC and HFC gases have been investigated as potential replacements. From the data presently available only moderate scale reductions are possible while maintaining both thermal and dynamic similarity.

INTRODUCTION

Recently an interest has developed into the natural ventilation of commercial and educational buildings. The techniques proposed to achieve this rely upon the stack effect, created by temperature differences between the internal and external air masses, and wind induced pressure differences.

However, the performance of wind induced ventilation is very variable and for a passive ventilation strategy the critical situation is one of high external temperatures and calm or very low wind speeds. Thus ventilation will be driven by stack pressure differences alone.

To date the methods utilised for the enhancement of the stack effect in non domestic buildings have led to the adoption of both atria and chimneys.

One of the fundamental problems of atria as a method of enhancing the stack effect is that the effectiveness of a stack is dependant upon the height over which the elevation of temperature occurs. In atria, significant temperature elevation is limited to the area above the occupied space (CIBSE [1]). Consequently, the stack induced pressure differences may be relatively small if external temperatures are high.

One approach taken to provide large stack heights, is the thermally massive chimneys developed at De Montfort University. These are driven by internal heat gains some of which is stored in the massive structure. This stored heat then helps to drive ventilation throughout the night.

However, in lighter weight buildings ventilation is required mainly during the day with particular emphasis on offsetting high solar gains. This function may potentially be achieved by low thermal mass, solar driven thermosyphoning panels or chimneys. In such devices the air is heated after it has left the occupied space enhancing the natural stack effect.

Attempts to predict the effectiveness of simple chimneys, have employed mathematical models assuming fully mixed interzonal air movement (Dorer and Weber [2], Raatschen [3]). However, an investigation into a free standing solar chimney (Swainson [4]) drawing air from and venting to ambient, showed that a simple fully mixed zonal air flow model was inappropriate. This experiment represented a situation where the internal and external air temperatures were identical and the air flow was driven entirely by the thermosyphoning air panel. When the fully mixed zonel model was replaced by one employing a linear temperature gradient throughout the height of the panel, the predictions of mass flow rate were significantly improved. However, the model continued to over predict the flow rate.

Visualisation of the chimney flow patterns across a range of aspect ratios of chimney height to depth, showed that large areas of recirculating and stationary air were present at low aspect ratios with the flow being more uniform as aspect ratio increased.

Consequently there is a need to understand the flow behaviour within a chimney more fully so that correlation equations can be developed that will allow the effects of changing such characteristics to be predicted. The development of such equations requires performance data from an actual chimney or a physical model.

PHYSICAL MODELS

Many studies have been undertaken to physically model ventilation systems, with models constructed at either full or reduced scales (references [5 - 15]).

Full Scale Models.

Full scale models or actual buildings have been used to investigate the performance of single components to complete buildings. The major problems of using full scale models are the expense of construction and the lack of control over natural variables that occurs when models are constructed and investigated outside laboratory conditions. The advantage of such an approach is that the results can be used to predict directly the performance of a similar component or building.

Reduced Scale Models.

When considering the use of reduced scale models it is evident that the results obtained must be able to predict the behaviour of a full scale building component. In order to achieve this it is important that the laws of similitude between the parameters describing the model and the full scale component are fully observed and that the effects of any assumptions made, are minimised. The physical parameters involved in the process of convective heat transfer can be reduced to a number of dimensionless groups through the process of dimensional analysis. Similarity between a model and a building component is then achieved by similarity between sets of dimensionless groups describing the behaviour of both the model and the building component.

For convective heat transfer the important groups are;

- Prandtl number (Pr) the relationship of the temperature distribution with the velocity distribution within a fluid.

$$\text{Where} \quad \Pr = \frac{\mu \ c_p}{k} \qquad (1)$$

- Grashof number (Gr) the relationship of the buoyancy forces to the viscous forces.

$$\text{Where} \quad Gr = \frac{\rho^2 \ g \ \beta \ \Delta T \ L^3}{\mu^2} \qquad (2)$$

- Reynolds number (Re) the relationship of the inertial forces to the viscous forces

$$\text{Where} \quad Re = \frac{u \ L}{\nu} \qquad (3)$$

In the past several approaches have been taken:

Moog [5] suggested that if, when investigating flows within rooms, the temperature distribution of the air mass is not isothermal then all of the dimensionless numbers have the same importance and thus none can be ignored. He concluded that this condition requires scales of 1:1 if results are to be transferable.

However, it has been assumed (Nevrala [6], Nielsen [7]) that, provided the flow is highly turbulent, and consequently well mixed, then velocity profiles within such flows are dimensionally similar regardless of physical scale. This suggests that for forced convection, provided the Re number is maintained above the critical value at which flows become turbulent, velocity similarity will be achieved and similarity will then only be governed by the Archimedes (Ar) number, where,

$$Ar = \frac{Gr}{Re^2} \qquad (4)$$

Scale models to investigate room air movement resulting from inlet jets have used air as the working fluid on this basis [6].

This approach has also been used in an investigation of passive cooling, where the assumptions of turbulence allowed similarity between the Re and Gr numbers to be assumed when developing the scale models (Imbabi [8]). Again, air was used as the working fluid and a scale of 1:10 was adopted.

However, both of the above mentioned modelling methods assume that any wall boundary flow patterns can largely be ignored. If this is not the case then, for buoyancy driven flows, similarity of both the Pr and Gr numbers must be achieved.

The use of the same working fluid allows the prime criterion of similarity of Pr numbers to be achieved. Therefore similarity of the Gr numbers requires that;

$$\left(\frac{\rho^2\, g\, \beta\, \Delta T\, L^3}{\mu^2}\right)_m = \left(\frac{\rho^2\, g\, \beta\, \Delta T\, L^3}{\mu^2}\right)_c \qquad (5)$$

Equation [5] indicates that if when developing a scale model all fluid parameters remain constant, the temperature difference within the model must change to the third power of the scale reduction. Radiative energy interchange is related to the fourth power of the temperature difference, so any significant reduction in scale may not only be impractical due to the elevated temperatures required, but the relative magnitude of the convective and radiative heat transfer mechanisms will be significantly distorted.

To allow temperature similarity to be maintained different working fluids must be used for the reduced scale model.

Gases as working fluids. To maintain the similarity of Pr and Gr numbers while still allowing the physical scale to be altered, high density gases such as the refrigerants R12 and R114 have been used in the past.

Investigations involving the use of refrigerant gases have to date been primarily used to establish convective heat transfer coefficients within passive solar houses. Similarity of the Pr numbers has been used by investigators (Wray et al [9], White et al [10]) to claim that the use of alternative gases will allow results to be directly scaled between the model and a full scale building component for model scales ranging from 1:5 to 1:8. The value of the Pr number for refrigerant gases is however far more temperature dependant than that of air. In response to this a proposal to mix a number of gases offering greater stability has been suggested (Maldonado [11]).

Water as working fluid. Working models of a scale of 1:5 are still large and often expensive to construct. In an attempt therefore to reduce the scale of experiments

further, and also to use fluids that do not require gas-tight chambers, several liquids have been investigated.

Water has been considered. However, the difference between the Pr numbers is significant with air being approximately stable at 0.71 and water varying from 6.8 at 20 °C to 1.8 at 100 °C. To overcome this, models using water at temperatures around 150 °C and consequently at high pressure have been attempted (Barber et al [12]). In this case the Prandtl number is of the order 1.2.

For the investigation of whole-building ventilation strategies, the air flows are assumed to be predominately turbulent in nature i.e. Re and Peclet (Pe) numbers will be large, where Pe = Re * Pr. The use of density differences between water and saline solutions, introduced into the model to represent a heat source has been undertaken with differences in density being such as to guarantee turbulent flow (Lane-Serff [13]). In turn, this allows the assumption of independence of flow, from both of these numbers for water based models, allowing scales from 1:30 to 1:100. Both velocities and temperatures can then be scaled off the model and claimed agreement between calculated and experimental data suggests that the modelling technique is effective (Linden et al [14]).

However, the use of water/brine based models at relatively small scale reductions is not appropriate for detailed studies as fluid flows will not be independent of Re or Pe. At such scales the viscosity and thermal diffusivity of the fluids become significant parameters [13,14].

Conclusion drawn from previous work

It can be seen therefore that if physical modelling is to be undertaken, similarity of both the Gr and Pr numbers requires that it is achieved either through the use of a full scale model or a model of reduced scale with an alternative gas as working fluid.

The development and testing of full scale building components such as a solar chimney up to three stories high, does have practical problems, therefore it was decided to investigate the potential of reduced scale models to provide performance data. Experiments to date at Cranfield University using reduced scale modelling (Wills [15], Guerin [16]) have been primarily interested in obtaining heat transfer data. For the investigation of a solar chimney the prime importance is that dynamic similarity exists, so that fluid flow rates can be scaled from the model to a full scale building component.

Dimensional analysis of all the relevant variables shows that the dimensionless groups that must be maintained in order to achieve dynamic and thermal similarity are the Gr and Pr numbers. With such similarity maintained the dimensionless velocities will also be equal, thus allowing scaling of the model results to a full scale component.

USE OF ALTERNATIVE HCFC AND HFC GASES

Due to the environmental concerns regarding CFC refrigerant gases, the search for alternatives has concentrated on the new HCFC and HFC gases.

Similarity of the Pr numbers requires that;

$$\left(\frac{\mu\ c_p}{k}\right)_m = \left(\frac{\mu\ c_p}{k}\right)_c \qquad (6)$$

One of the major differences between the refrigerant gases and air is the greater rate of change in Pr number with temperature of the refrigerants. Fig. 1 shows the behaviours of the Pr numbers of air and a selection of the gases.

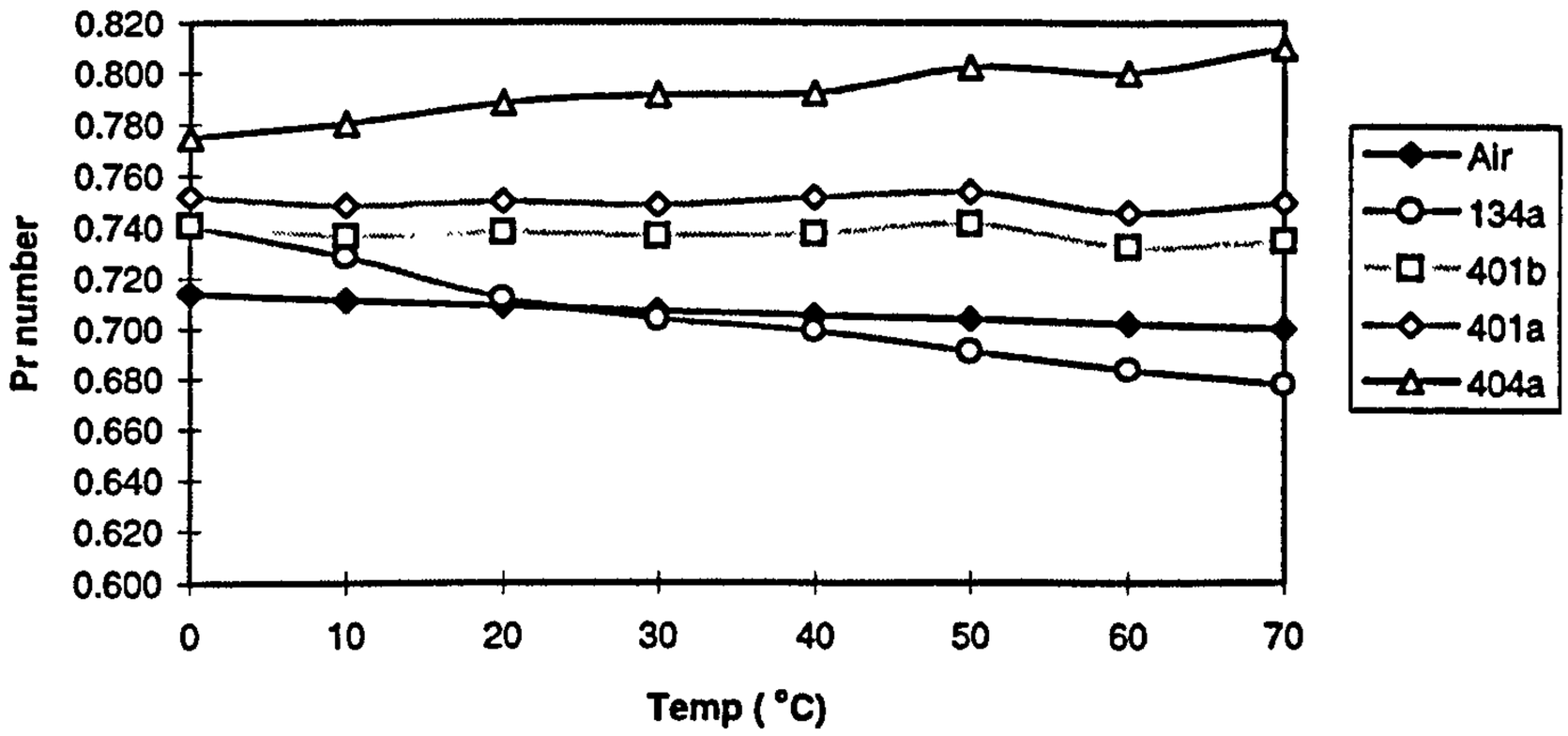

Fig 1. Comparison of the variations of Pr number with temperature (ref. [17]).

With Pr number similarity achieved, similarity of the Gr numbers will dictate the scale of the model.

$$\frac{L_m}{L_c} = \left[\frac{\Delta T_c}{\Delta T_m}\ \frac{\beta_c}{\beta_m}\left(\frac{\nu_m}{\nu_c}\right)^2\right]^{\frac{1}{3}} \qquad (7)$$

If the temperatures are to be maintained equal in both model and building component and both gases considered ideal, this reduces to;

$$\frac{L_m}{L_c} = \left[\left(\frac{\nu_m}{\nu_c} \right)^2 \right]^{\frac{1}{3}} \qquad (8)$$

From the values obtained for the properties of the refrigerant gases in references [17,18,19], the following scale reductions between the model to the building component are possible;

Refrigerant	Scale Factor (model : component)
R 124	1 : 3.9
R 142b	1 : 3.3
R 134a	1 : 3.1
R 401b	1 : 2.9

The figures given above are for 25 °C. For many of the gases little detailed thermophysical data exists at present across a range of temperatures and therefore from the data available, the most suitable working fluid appears to be R134a, offering reasonable similarity of its Pr number with that of air across a suitable range of temperatures.

Example of Scaling

To show how the preceding scaling procedure can be put into practice, the following example shows how the scales for a solar chimney of 6.0m height are calculated.

Similarity of Pr numbers is the first criterion. In previous experiments [4] the elevation of the working fluid at the chimney exit was found to be up to ambient plus 20 °C. Thus close correspondence of Pr numbers in the range of 20 to 40 °C is required. From the data collected refrigerant 134a has the most appropriate characteristics, differing by less than 1% from that of air across this temperature range (see Fig. 1).

Similarity of the Gr numbers is also required. If temperature similarity is maintained then the scale reduction can be calculated with equation [8]. The results of which are shown below;

Fluid temp. (°C)	$\frac{L_c}{L_m}$
20	3.16
30	3.13
40	3.12

Thus a chimney of 6.0m would require a geometrically similar model of 1.92m. In addition to this height the model chamber would require sufficient space for the chimney to vent freely, which would increase the required model height to over 2.0m.

With geometric, dynamic and thermal similarity achieved, the dimensionless velocity, which is a dependant variable in both the model and full scale component, will be equal [9] i.e. $Re_m = Re_c$.

$$\text{Therefore} \qquad \frac{u_c}{u_m} = \frac{\nu_c L_m}{\nu_m L_c} \qquad (9)$$

Thus, if the scale reduction is assumed to be 1 : 3.13, the flow rate through the chimney can be calculated from the following velocity scales:

Fluid temp. (°C)	$\frac{u_c}{u_m}$
20	1.79
30	1.77
40	1.76

With full similarity achieved the dimensionless heat transfer will also be maintained such that $Nu_m = Nu_c$. Thus the convective heat flux ratio can be calculated;

$$\frac{h_c}{h_m} = \frac{L_m k_c}{L_c k_m} \qquad (10)$$

Fluid temp. (°C)	$\frac{h_c}{h_m}$
20	0.57
30	0.56
40	0.54

The ratio of the heat fluxes can then be calculated. The radiative exchange rate is maintained through temperature similarity therefore;

$$\text{Ratio of heat fluxes} = \frac{h_c + k_c}{h_m + k_m} \qquad (11)$$

Fluid temp. (°C)	Component heat flux / Model heat flux
20	1.022
30	0.985
40	0.951

CONCLUSION

The use of scale models is a suitable method of collecting the data required to develop correlation equations for the prediction of the effectiveness of large building components such as solar chimneys. With such components the boundary layer flows cannot be

ignored and assumptions of fully turbulent flows are inappropriate. Thus similarity must be achieved between both the Gr and Pr numbers, which requires the use of air in full scale models, or alternative gases in reduced scale models. A detailed search of the available data supplied for the new refrigerant gases shows that moderate scale reductions of around 1:3 are achievable with such fluids. The preceding example highlighted the still considerable model heights that would be required, which along with the practical considerations of the construction of a gas tight model chamber and the equipment needed to recover the gas after each experiment, would make marginal any cost savings over the use of full scale models. Additionally HCFCs are to be phased out by 2015 and the use of HFC gases is in question as their potential environmental impact as greenhouse gases becomes more apparent.

Consequently, the viability of utilising scale models with refrigerant gases is marginal at best.

SYMBOLS USED

Ar	Archimedes number	
c_p	Specific heat capacity at constant pressure	(J/kg °C)
CFC	Chlorofluorocarbons	
g	Acceleration due to gravity	(m/s^2)
Gr	Grashof number	
h	Convective heat transfer coefficient	(W/m^2 °C)
HCFC	Hydrochlorofluorocarbons	
HFC	Hydrofluorocarbons	
k	Thermal conductivity	(W/m °C)
L	Length	(m)
Nu	Nusselt number	
Pr	Prandtl number	
Re	Reynolds number	
T	Temperature	(°C)
u	Velocity of fluid flow	(m/s)
β	Coefficient of thermal expansion	
μ	Viscosity	(N s/m^2)
ν	Kinematic viscosity	(m^2/s)
ρ	Density	(kg/m^3)

Subscripts

m	Model
c	Full scale building component

REFERENCES

1. CIBSE, 1994, "CIBSE Application Manual. Natural Ventilation in Buildings", Draft version 16/12/94, CIBSE.

2. Dorer, V., and Weber, A., 1994, "Simulation of passive cooling and natural facade driven ventilation", 15th AIVC Conference, Buxton, UK.

3. Raatschen, W., 1994, "Energy and ventilation performance of double facade office building", BEP 94 Conference, York, UK.

4. Swainson, M., 1994, "Investigation into the potential of thermosyphoning air panels to drive natural ventilation in buildings", MSc. Thesis, Cranfield University.

5. Moog, W., 1981, ASHRAE Trans. CH 81-17, N° 4, 1162.

6. Nevrala, D., 1979, "Modelling of air movement in rooms", PhD Thesis, Cranfield University.

7. Nielsen, P., 1994, "Air distribution in rooms. Research and design methods", Roomvent 94 Conference, Poland,

8. Imbabi, M., 1990, "A general procedure for the small scale modelling of buildings" Int. J. of Energy Research, 14, 311 .

9. Wray, W., and Weber, D., 1979 "Hot zone/cold zone: A quantitative study of natural heat distribution mechanisms in passive solar buildings", 4th National Passive Solar Conference. Kansas City, USA.

10. White, M., Winn, C., Jones, G., and Balcomb, J., 1985 "The influence of geometry on natural convection in buildings", 10th National Passive Solar Conference, USA.

11. Maldonado, E., Junkhan, G., and Woods, J., 1982 "Use of a gas mixture for experimental modelling of mixed free and forced convection in enclosures", 7th International Heat Transfer Conference, Munich.

12. Barber, E., Bettge, D., and Powell, F., 1970 "Development of a modelling technique for evaluation of natural convection and ventilation in rooms", ASHRAE Symposium Bulletin SF - 70 - 9.

13. Lane-Serff, G., 1989, "Heat flow and air movement in buildings", PhD Thesis, University of Cambridge.

14. Linden, P., Lane-Serff, G., and Smeed, D., 1990, J. of Fluid Mechanics, 212, 309.

15. Wills, M., 1986, "The determination of convective heat transfer within telephone exchanges using experimental scale models", Cranfield University.

16. Guerin, F., 1987, "Optimisation of the design of a lightweight survival tent", MSc. Thesis, Cranfield University.

17. Du Pont. Transport properties of Suva refrigerants.

18. HRPR. Forane software.

19. Allied Signal Chemicals. ASIDATA refrigeration software.

APPENDIX B

MODEL OF SOLAR TRANSMISSION THROUGH GLAZING OF SOLAR CHIMNEY FOR USE IN SENSITIVITY ANALYSIS.

The following model was set up to read from a file of stored solar data to calculate; the solar energy transmitted through the glazing, the solar energy absorbed by the plate and the solar energy absorbed by the glazing.

Day angle (D);

$$D = \frac{360(\text{Day N}^{\underline{o}} - 1)}{365} \qquad \text{Equation B.1.}$$

Where Day N$^{\underline{o}}$ is the number of the day, January 1st. is 1.

Equation of time (E) in minutes;

$$E = 229.18\left(\begin{array}{r} 0.000075 + 0.001868\,\text{Cos}D - 0.032077\,\text{Sin}D - \\ 0.014615\,\text{Cos}2D - 0.04089\,\text{Sin}2D \end{array}\right) \qquad \text{Equation B.2.}$$

Local apparent time (LAT) i.e. the time based on the position of the true sun in relation to the observers meridian;

$$\text{LAT} = \text{GMT} - \frac{\text{Longitude}}{15} + E \qquad \text{Equation B.3.}$$

Where longitude is measured in degrees west of Greenwich.

Local hour angle (LHA);

$$\text{LHA} = (\text{LAT} - 12) * 15 \qquad \text{Equation B.4.}$$

Declination of sun (Dec);

$$\text{Dec} = 23^\circ\ 27'\ \text{Sin}\left[\left(\frac{284 + \text{Day N}^{\underline{o}}}{365}\right)360\right] \qquad \text{Equation B.5.}$$

Angle of incidence of the direct solar radiation on a vertical surface (θ_{direct})

$$\theta_{direct} = \mathrm{Cos}^{-1}\left(\begin{array}{l} -\mathrm{Sin\,Dec\ Cos\,Latitude\ Cos\,Azinuth} + \\ \quad \mathrm{Cos\,Dec\ Sin\,Latitude\ Cos\,Azimuth\ Cos\,LHA} + \\ \quad \mathrm{Cos\,Dec\ Sin\,Azimuth\ Sin\,LHA} \end{array}\right)$$

Equation B.6.

Where Azimuth is the angle between the normal to the glazing and the meridian passing through the rig, measured east or west from true south. East is negative.

Angle of refraction (θ_{ref})

$$\theta_{ref} = \mathrm{Sin}^{-1}\left(\frac{\mathrm{Sin}\,\theta_{direct}}{n}\right)$$

Equation B.7.

Where n is the refractive index of the glass

Path length of the direct solar radiation through the glass (L)

$$L = \frac{d}{\mathrm{Cos}\theta_{ref}}$$

Equation B.8.

Where d is the thickness of the glass

Fraction of the direct solar radiation transmitted through the glass taking into account the absorption by the glass only $(\tau_{abs\ direct})$

$$\tau_{abs\,direct} = e^{-KL}$$

Equation B.9.

Where K is the absorptivity of the glass per meter

As the solar radiation incident upon the glazing was unpolarised the calculation of the reflected component of the direct radiation considered both parallel and perpendicular polarised components of the incident radiation.

Reflected perpendicular radiation $(r_{\perp})$

$$r_{\perp} = \frac{\mathrm{Sin}^2\left(\theta_{direct} - \theta_{ref}\right)}{\mathrm{Sin}^2\left(\theta_{direct} + \theta_{ref}\right)}$$ Equation B.10.

Reflected parallel radiation $(r_{\shortparallel})$

$$r_{\shortparallel} = \frac{\mathrm{Tan}^2\left(\theta_{direct} - \theta_{ref}\right)}{\mathrm{Tan}^2\left(\theta_{direct} + \theta_{ref}\right)}$$ Equation B.11.

The fraction of direct solar energy transmitted through the glazing taking into account both absorption of the glass and the reflection of the direct solar radiation at the surfaces of the glass (τ_{direct}) was then calculated as follows[1].

$$\tau_{direct} = \frac{1}{2}\left[\left(\frac{\tau_{absdirect}\left(1-r_{\perp}\right)^2}{1-r_{\perp}^2\,\tau_{absdirect}^2}\right) + \left(\frac{\tau_{absdirect}\left(1-r_{\shortparallel}\right)^2}{1-r_{\shortparallel}^2\,\tau_{absdirect}^2}\right)\right]$$ Equation B.12.

Equations B.7. to B.12. were repeated for the diffuse solar radiation incident upon the glass to calculate the component of diffuse radiation transmitted $(\tau_{diffuse})$ and that absorbed by the glass $(\tau_{abs\ diffuse})$. For this an effective angle of incidence of the diffuse radiation upon the glazing was required. Duffie[2] suggested that for isotropic diffuse radiation the effective angle of incidence could be taken as 59.5°. The validity of this was tested as part of the sensitivity analysis reported in Chapter Three.

The solar radiation transmitted through the glass was therefore calculated for the direct and diffuse as follows:

$$q''_{trans\ direct} = \left(\tau_{direct}\ q''_{direct}\right)$$ Equation B.13.

$$q''_{trans\ diffuse} = \left(\tau_{diffuse}\ q''_{diffuse}\right)$$ Equation B.14.

The total solar radiation transmitted $q''_{sol\ trans}$ was thus:

$$q''_{\text{sol trans}} = q''_{\text{trans direct}} + q''_{\text{trans diffuse}}$$ Equation B.15.

This value of total solar radiation was used as the dependant variable for the sensitivity analysis into the input variables of the solar radiation calculations of solar radiation absorbed by the plate of the solar chimney described in Chapter Three.

To calculate the solar radiation absorbed by the plate (q''_{sol}) the following calculation was used to determine the transmittance - absorptance product:

$$q''_{\text{sol}} = \frac{q''_{\text{sol trans}}\ \alpha}{1-(1-\alpha)r_d}$$ Equation B.16.

Where α is the absorptance of the plate to solar radiation and r_d is the reflectance of the glass to diffuse solar radiation reflected from the plate, defined as:

$$r_d = \tau_{\text{abs diffuse}} - \tau_{\text{diffuse}}$$ Equation B.17.

The solar radiation absorbed by the glass $\left(q''_{\text{abs glass}}\right)$ was also required as an input to the dynamic model used in the sensitivity analysis. This was calculated as follows:

$$q''_{\text{abs glass direct}} = \frac{q''_{\text{direct}}}{2}\left[\frac{(1-r_{\perp})(1-\tau_{\text{abs direct}})}{1-r_{\perp}\tau_{\text{abs direct}}} + \frac{(1-r_{\text{II}})(1-\tau_{\text{abs direct}})}{1-r_{\text{II}}\tau_{\text{abs direct}}}\right]$$

Equation B.18.

Equation B.18. was repeated for the diffuse radiation allowing calculation of the total energy absorbed by the glazing:

$$q''_{\text{abs glass}} = q''_{\text{abs glass direct}} + q''_{\text{abs glass diffuse}}$$ Equation B.19.

References Appendix B

1. Allen, J., Solar processes, Final Report; An Investigation into Analytical and Empirical Validation Techniques for Dynamic Thermal Models of Buildings, BRE/SERC, Watford, 1988.

2. Duffie, J. and Beckman, W., Solar Engineering of Thermal Processes, 2nd. Ed., J. Wiley & Sons Inc., USA, 1991.

APPENDIX C

MATHEMATICAL MODEL OF FLAT PLATE TO UNDERTAKE SENSITIVITY ANALYSIS

C.1. Introduction

The solution of transient heat transfer problems in all but the simplest geometries requires the use of finite difference methods. Such methods allow realistic models to be built, describing true physical configurations and allow variation of any of the variables within the model. Thus for the sensitivity analysis undertaken in this investigation, the finite difference method allowed the sensitivity of a defined dependent variable to be evaluated when input variables were varied across their identified range of uncertainty.

C.2. Nodal model of flat plate

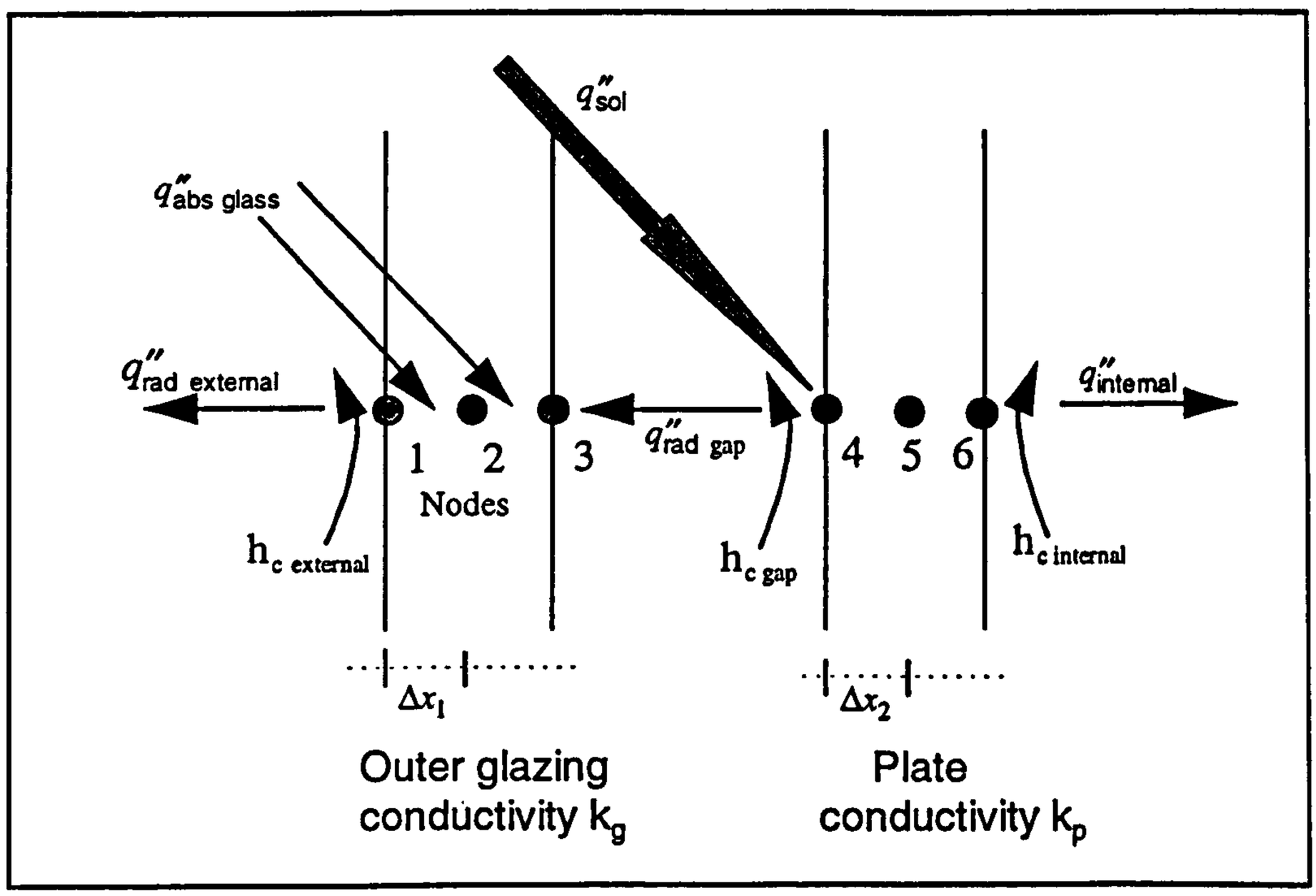

Figure C.1. Nodal model developed of the flat plate arrangement

For the purpose of this investigation the heat transfer through the glazing and plate of the solar chimney was assumed to be one dimensional.

C.3. Choice of method of solution

Two methods of solving the finite difference equations are commonly used. These are the explicit and the implicit methods.

The explicit method is so called because the temperatures at the nodes at the new time step are determined from the temperatures at the nodes at the previous time step. Thus this method of calculation is straightforward. However this method is not unconditionally stable and the time steps must not exceed a critical value as defined in equation C.1. Heat transfer texts[1] provide proofs of this limiting criteria.

$$1 - 2Fo - 2FoBi \geq 0 \qquad \text{Equation C.1.}$$

Where $$Fo = \frac{\Delta t\, \alpha}{\Delta x^2} \qquad \text{Equation C.2.}$$

$$\alpha = \frac{k}{\rho\, Cp} \qquad \text{Equation C.3.}$$

and $$Bi = \frac{h_c\, \Delta x}{k} \qquad \text{Equation C.4.}$$

Thus to calculate the limiting time interval;

$$\Delta t \leq \frac{0.5}{1 + Bi}\left(\frac{\Delta x^2}{\alpha}\right) \qquad \text{Equation C.5.}$$

If node number one is taken as an example from figure C.1. with the following variables;

Variable		Value
ρ	(kg/m^3)	2500
k^g	(W/Km)	1.1
Cp	(J/kg K)	800
Δx	(m)	0.002
h_c	($W/m^2\,^oC$)	16.6

From this the maximum time interval using the limit presented in equation C.5. is 3.5 seconds. Such a short time interval would require considerable computer time to run models for a full day.

An alternative method of solution is the implicit method. This method never becomes unstable, however large the time steps adopted. This offered the scope to match the time interval to the same as that of the data logging.

C.4. Nodal equations for the flat plate model

Development of the nodal equations was undertaken based on the energy balance at each node, i.e. rate of energy into a node is equal to the rate of change of energy within a node. (The subscript numbers refer to the node number and ^{P} is the time step identifier)

For node 1 therefore:

$$q''_{\text{rad external}} + \frac{q''_{\text{abs glass}}}{4} + h_{c\,\text{external}}\left(T^{P+1}_{\text{external}} - T^{P+1}_{1}\right) + \frac{k_g}{\Delta x_1}\left(T^{P+1}_{2} - T^{P+1}_{1}\right) = \left(T^{P+1}_{1} - T^{P}_{1}\right)\frac{\rho_1\, Cp_1\, \Delta x_1}{2\ \Delta t}$$

Equation C.6.

$$\frac{\Delta x_1}{k_g}\, q''_{\text{rad external}} + \frac{\Delta x_1}{4\ k_g}\, q''_{\text{abs glass}} + Bi_1\left(T^{P+1}_{\text{external}} - T^{P+1}_{1}\right) + \left(T^{P+1}_{2} - T^{P+1}_{1}\right) = \frac{1}{2\ Fo_1}\left(T^{P+1}_{1} - T^{P}_{1}\right)$$

Equation C.7.

$$\frac{2\ Fo_1\ \Delta x_1}{k_g}\, q''_{\text{rad external}} + \frac{2\ Fo_1\ \Delta x_1}{4\ k_g}\, q''_{\text{abs glass}} + 2\ Fo_1\, Bi_1\left(T^{P+1}_{\text{external}} - T^{P+1}_{1}\right) + 2\ Fo_1\left(T^{P+1}_{2} - T^{P+1}_{1}\right) = \left(T^{P+1}_{1} - T^{P}_{1}\right)$$

Equation C.8.

Defining T^{P} in terms of T^{P+1}, the equation for node 1 becomes:

$$T^{P}_{1} + \frac{2\ Fo_1\ \Delta x_1}{k_g}\left(q''_{\text{rad external}} + \frac{q''_{\text{abs glass}}}{4}\right) = -2\ Fo_1\, Bi_1\, T^{P+1}_{\text{external}} + T^{P+1}_{1}\left(1 + 2\ Fo_1 + 2\ Fo_1\, Bi_1\right) - 2\ Fo_1\, T^{P+1}_{2}$$

Equation C.9.

Similarly the equations for all remaining nodes become:

Node 2

$$T_2^P + \frac{Fo_1\ \Delta x_1}{k_g}\left(\frac{q''_{abs\ glass}}{2}\right) = -\ Fo_1\ T_1^{P+1} + T_2^{P+1}(1 + 2\ Fo_1) - Fo_1\ T_3^{P+1}$$

Equation C.10.

Node 3

$$T_3^P + \frac{2\ Fo_1\ \Delta x_1}{k_g}\left(q''_{rad\ gap} + \frac{q''_{abs\ glass}}{4}\right) = -2\ Fo_1\ T_2^{P+1} + T_3^{P+1}(1 + 2\ Fo_1 + 2\ Fo_1\ Bi_3) - 2\ Fo_1\ Bi_3\ T_4^{P+1}$$

Equation C.11.

Node 4

$$T_4^P + \frac{2\ Fo_4\ \Delta x_2}{k_p}\left(q''_{rad\ gap} + q''_{sol}\right) = -2\ Fo_4\ Bi_4\ T_3^{P+1} + T_4^{P+1}(1 + 2\ Fo_4 + 2\ Fo_4\ Bi_4) - 2\ Fo_4\ T_5^{P+1}$$

Equation C.12.

Node 5

$$T_5^P = -\ Fo_4\ T_4^{P+1} + T_5^{P+1}(1 + 2\ Fo_4) - Fo_4\ T_6^{P+1}$$

Equation C.13.

Node 6

$$T_6^P + \frac{2\ Fo_4\ \Delta x_2}{k_p}\left(q''_{rad\ internal}\right) = -2\ Fo_4\ T_5^{P+1} + T_6^{P+1}(1 + 2\ Fo_4 + 2\ Fo_4\ Bi_6) - 2\ Fo_4\ Bi_6\ T_{Rig\ wall}^{P+1}$$

Equation C.14.

Where $q''_{rad\ external} = \varepsilon_g \sigma \left(T_1^4 - T_{external}^4\right)$ Equation C.15.

$$q''_{rad\ gap} = \frac{\sigma\left(T_4^4 - T_3^4\right)}{\frac{1}{\varepsilon_g} + \frac{1}{\varepsilon_p} + 1}$$

Equation C.16.

$$q''_{rad\ internal} = \varepsilon_p \sigma \left(T_6^4 - T_{rig\ wall}^4\right)$$

Equation C.17.

To allow the above nodal equations to be solved they were written in matrix format and then solved in the programme Mathcad[2].

$$\left[T^{p}\right] + \left[Q''\right] = [B] \cdot \left[T^{p+1}\right] \qquad \text{Equation C.18.}$$

Therefore

$$\left[T^{p+1}\right] = [B]^{-1} \cdot \left(\left[T^{p}\right] + \left[Q''\right]\right) \qquad \text{Equation C.19.}$$

Where B =

$$\begin{bmatrix}
1 & 0 & 0 & 0 \\
-2Fo_1Bi_1 & 1+2Fo_1+2Fo_1Bi_1 & -2Fo_1 & 0 \\
0 & -Fo_1 & 1+2Fo_1 & -Fo_1 \\
0 & 0 & -2Fo_1 & 1+2Fo_1+2Fo_1Bi_3 \\
0 & 0 & 0 & -2Fo_4Bi_4 \\
0 & 0 & 0 & 0 \\
0 & 0 & 0 & 0 \\
0 & 0 & 0 & 0
\end{bmatrix}$$

$$\begin{bmatrix}
0 & 0 & 0 & 0 \\
0 & 0 & 0 & 0 \\
0 & 0 & 0 & 0 \\
-2Fo_3Bi_3 & 0 & 0 & 0 \\
1+2Fo_4+2Fo_4Bi_4 & -2Fo_4 & 0 & 0 \\
-Fo_4 & 1+2Fo_4 & -Fo_4 & 0 \\
0 & -2Fo_4 & 1+2Fo_4+2Fo_4Bi_6 & -2Fo_4Bi_6 \\
0 & 0 & 0 & 1
\end{bmatrix}$$

$$Q'' = \begin{bmatrix}
0 \\
\frac{2\ Fo_1\ \Delta x_1}{k_g}\left(q''_{\text{rad extemal}} + \frac{q''_{\text{abs glass}}}{4}\right) \\
\frac{Fo_1\ \Delta x_1}{k_g}\left(\frac{q''_{\text{abs glass}}}{2}\right) \\
\frac{2\ Fo_1\ \Delta x_1}{k_g}\left(q''_{\text{rad gap}} + \frac{q''_{\text{abs glass}}}{4}\right) \\
\frac{2\ Fo_2\ \Delta x_2}{k_p}\left(q''_{\text{rad gap}} + q''_{\text{sol}}\right) \\
0 \\
\frac{2\ Fo_2\ \Delta x_2}{k_p}\left(q''_{\text{rad internal}}\right) \\
0
\end{bmatrix}$$

References Appendix C

1. Incropera, F. and DeWitt, D., Fundamentals of Heat and Mass Transfer, 3rd. Ed., J. Wiley & Sons, New York, 1990.

2. Mathsoft, Mathcad Plus 6.0, Mathsoft Inc., USA, 1995.

APPENDIX D

A COMBINED THERMISTOR THERMOMETER AND LOW VELOCITY ANEMOMETER

Notation

A, B & C	Constants equation 1.
D, E & F	Constants equation 2.
C1 & 2	Capacitors 1 & 2 (μF)
H	Power dissipated by thermistors (W)
R1 to 10	Resistors 1 to 10 (Ω)
RT1 & 2	Thermistors (Ω)
T	Temperature of thermistor (°C)
Te	Temperature elevation of thermistor RT2 above thermistor RT1 (°C)
T1 & 2	Temperatures of thermistor RT1 and RT2 respectively (°C)
U	Uncertainty
V	Supply voltage (Volts)
v	Air velocity (ms^{-1})
X & Y	Potential difference indicated by voltmeters X and Y respectively (Volts)

D.1 Introduction

The need to measure both air temperature and velocity at a series of points within a low velocity stream is one of the prime requirements of investigations into both thermal comfort and air quality within buildings and the performance of components designed to assist in the driving of natural ventilation in buildings. However, accurate measurement of low velocity air flows remains problematic.

Generally, several individual sensors are required for velocity measurements of such processes. Thus, there is a need for multiple devices capable of accurately measuring velocities within the range 0 - 1 m/s that are not prohibitively expensive.

D.2 Instruments presently available

Hot wires and hot spheres have been used traditionally[1]. The self heating effects of the former create uncertainties of up to +/-15% for velocities between 0.05 - 0.1 m/s [2] and the slow response of the latter [3] limit their use for some 'in situ ' experiments where transient conditions are experienced. More sophisticated systems, such as Laser Doppler Anemometry, are not suitable for extended monitoring in remote sites and are very expensive.

An alternative, widely used device for air velocity measurement is the thermistor based anemometer. However, the cost of multiple channel instruments presently commercially available limits options significantly. An investigation into the possibilities of constructing a low cost, low power consumption multiple channel instrument with high resolution at low air velocities was therefore undertaken.

D.3 The proposed instrument

McNair [3 & 4] proposed a very simple thermistor based instrument that, it was claimed, offered an ideal combination of high resolution at low air velocities and accuracies better than +/-5% down to values of 0.05m/s over a temperature range of 0 to 60°C. This seemed to offer an ideal solution for the investigation currently being undertaken by the authors into the potential of solar chimneys to drive ventilation within buildings.

D.3.1 The theory

Air velocity measurements made using thermistors rely upon the resistive heating of the thermistor when an electrical current passes through it. The temperature the thermistor attains, for a given electrical current, will depend upon the rate at which heat is removed from its surface. For a particular air temperature this will relate to the speed of the air flow.

McNair's instrument used two precision, negative temperature coefficient thermistors in a bridge circuit arrangement (Figure D.1.) one to measure the air temperature, the other to measure air velocity.

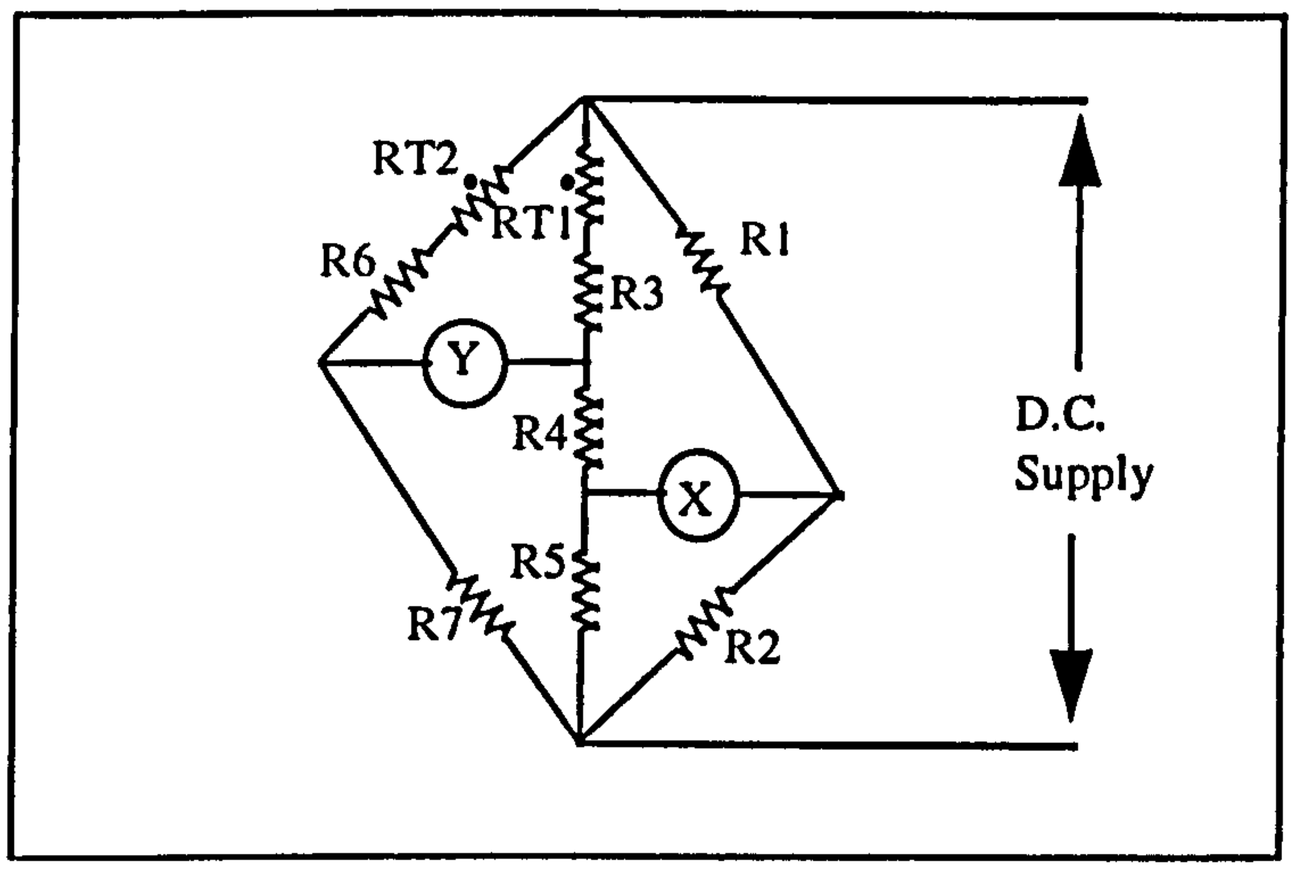

Figure D.1. Basic bridge circuit proposed by McNair

Precision thermistors (+/-0.2%) are widely commercially available and are supplied with tables of resistance for a range of temperatures. From the data tables supplied, equations to describe the variation of resistance with temperature can be established in the form given below, e.g.

$$RT1 = A\, e^{\left(\frac{B}{C+T}\right)} \qquad \text{Equation D.1.}$$

From the thermistor manufacturer's data supplied, the constants for equation D.1. were calculated as follows:

	1MΩ @ 25°C	3KΩ @ 25°C
A	$7.49 * 10^{-4}$	$9.51 * 10^{-4}$
B	8537.03	5106.08
C	381.28	316.20

Table D.1. Values of constants for thermistors in equation 1.

Thermistor RT1 is of high resistance (1MΩ @ 25°C) which only heats marginally above ambient when a small current is passed through it. This ensures that its temperature is not affected by air velocity. The resistance of RT1 and thus temperature can be established by measuring the potential difference at X.

$$\text{Temp}(T1) := \left[\frac{8537.03}{\ln\left[\frac{\frac{V \cdot R5}{X + V \cdot \left(\frac{R2}{R1+R2}\right)} - R3 - R4 - R5}{7.49\,10^{-4}} \right]} \right] - 381.28$$

Equation D.2.

Thermistor RT2 is of low resistance (3KΩ @ 25°C) and thus heats several degrees above ambient when a current is passed through it. The resistance and thus temperature of RT2 can be established by measuring the potential difference at Y.

$$\text{Temp}(T2) := \left[\frac{5106.08}{\ln\left[\frac{\frac{V \cdot R7}{Y + V \cdot \left[\frac{R4+R5}{R3+R4+R5+(RT1)}\right]} - R6 - R7}{9.51 \cdot 10^{-4}} \right]} \right] - 316.20$$

Equation D.3.

The power dissipated from RT2 can then be calculated:

$$H_{RT2} = \frac{V^2 \; RT2}{(R6 + R7 + RT2)^2}$$

Equation D.4.

The temperature elevation of RT2 above ambient (Te) was related to air velocity by McNair using King's law Equation D.5. The values for the constants D, E and F being established by calibration.

$$v = D + E\left(\frac{H_{RT2}}{Te}\right)^F$$

Equation D.5.

D.3.2 The proposed instrument design

McNair's instrument was designed such that power dissipated from thermistor RT2 was at a maximum at the mid value of the temperature range of interest. The investigation undertaken into the solar chimney required air temperatures and velocities to be measured in temperature ranges of 5 - 30°C and 15 - 60°C. The lowest air velocities being measured in the higher of these two ranges.

Thus to ensure that the maximum power dissipated by thermistors RT2 was at the mid point of the air temperature range and that the temperature elevation was sufficient to ensure good resolution at low air velocities, the following values for the other resistances in the circuit were chosen:

	Temperature range (°C)	
	5 - 30	15 - 60
R1	1M Ω	1M Ω
R2	15KΩ	15K Ω
R3	82K Ω	82K Ω
R4	82K Ω	82K Ω
R6	2700 Ω	800 Ω
R7	800 Ω	700 Ω
Supply	12 V	9 V

Table D.2. Values of resistors used to adjust power dissipation from thermistor RT2 to temperature band of interest

This provided the following power dissipation characteristics for thermistors RT2 for the two temperature ranges of interest:

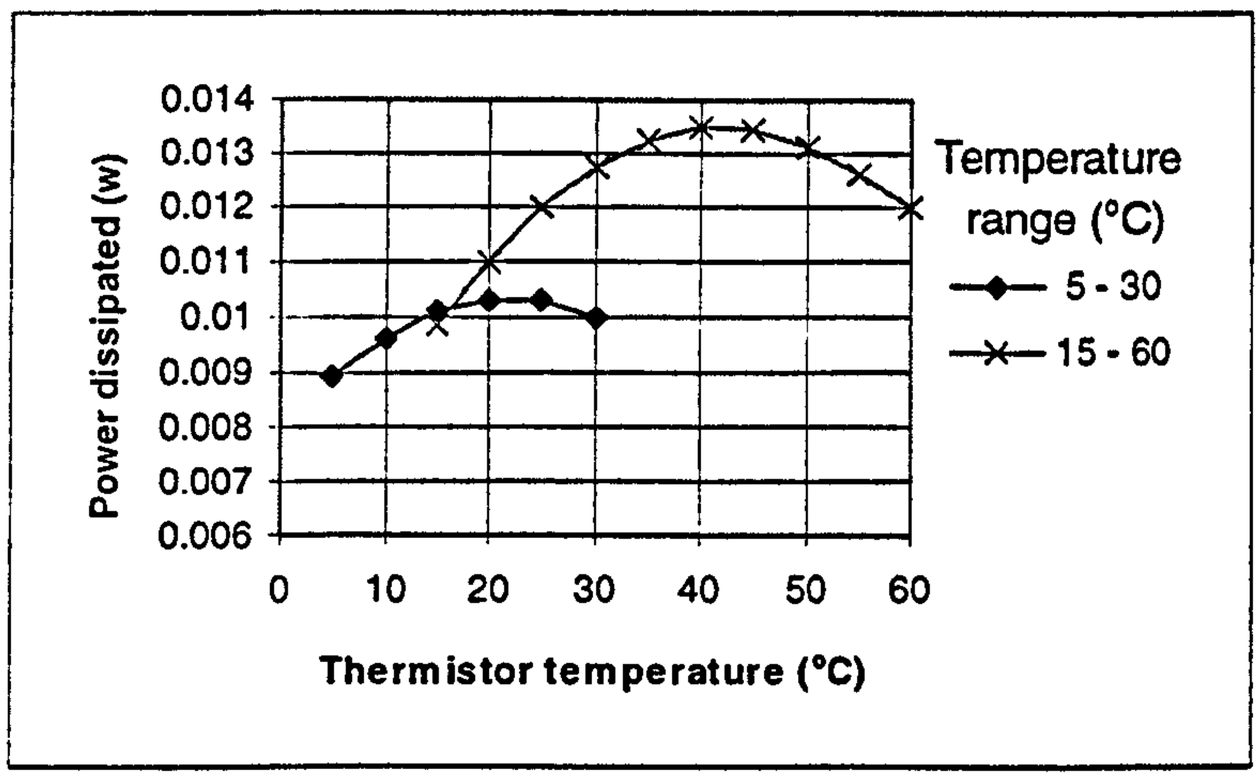

Figure D.2. Power dissipated by thermistors RT2 for different temperature applications

The proposed use of the instruments to measure air flow in positions where radiative heat transfer could be high required that the thermistors were shielded from such sources of heat. This was achieved by shielding the

thermistors as shown in Figure D.3. It was also important to ensure that the self heating of the velocity thermistor RT2 did not influence the temperature readings of thermistor RT1. Thus in both instruments RT1 was placed below RT2.

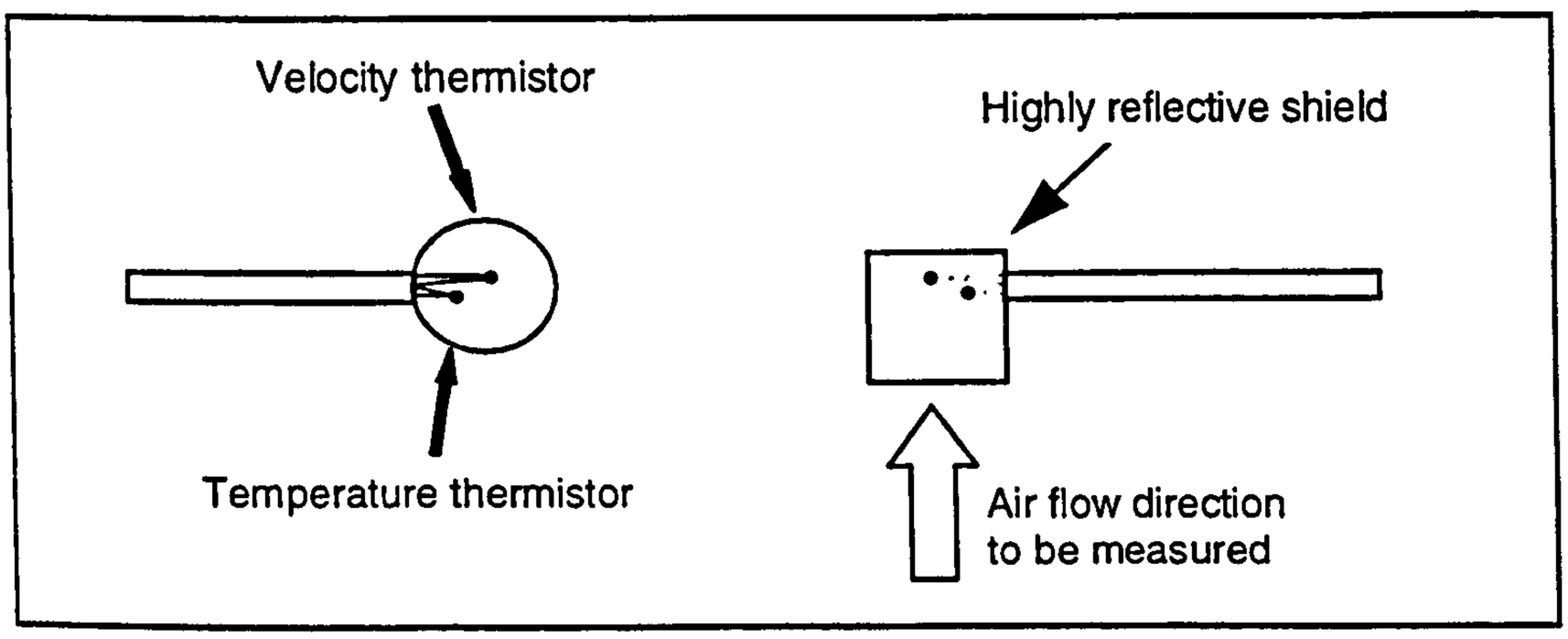

Figure D.3. Sensing heads showing shield and thermistor positioning

To ensure that all other components retained constant values and thus the repeatability of the instruments was maximised, precision resistors (+/- 0.1%) were used throughout.

With cable lengths of up to 3 meters, measures were taken to minimise the potential of picking up electrical interference. Consequently for the final instrument design all leads were shielded and earthed as shown in Figure 4.

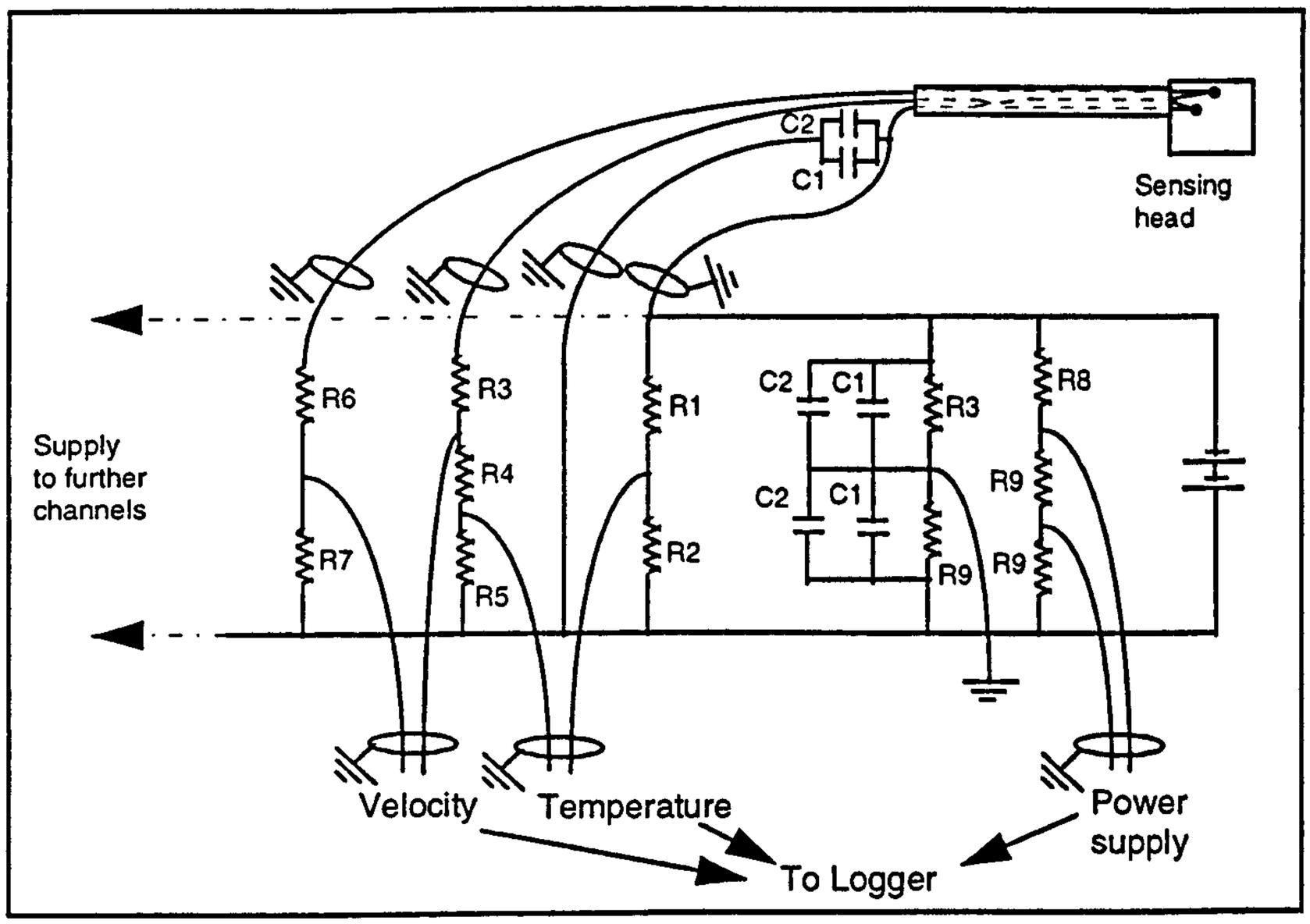

Figure D.4. Circuit layout for power supply and one channel of final instrument

Common components between instruments in the final design

R 8	15 K Ω	C 1	4.7 μF
R 9	1 K Ω	C 2	0.1 μF

D.4 Calibration

With the fitting of shielding it was found that the sensors were marginally sensitive to mounting orientation. Consequently, the sensors were calibrated in the same orientation as their final mounting.

A rotating arm rig was developed that allowed the sensing heads to be moved horizontally at speeds between 0.02 and 1.0 m/s through a stationary air mass. This is shown in figure 5.

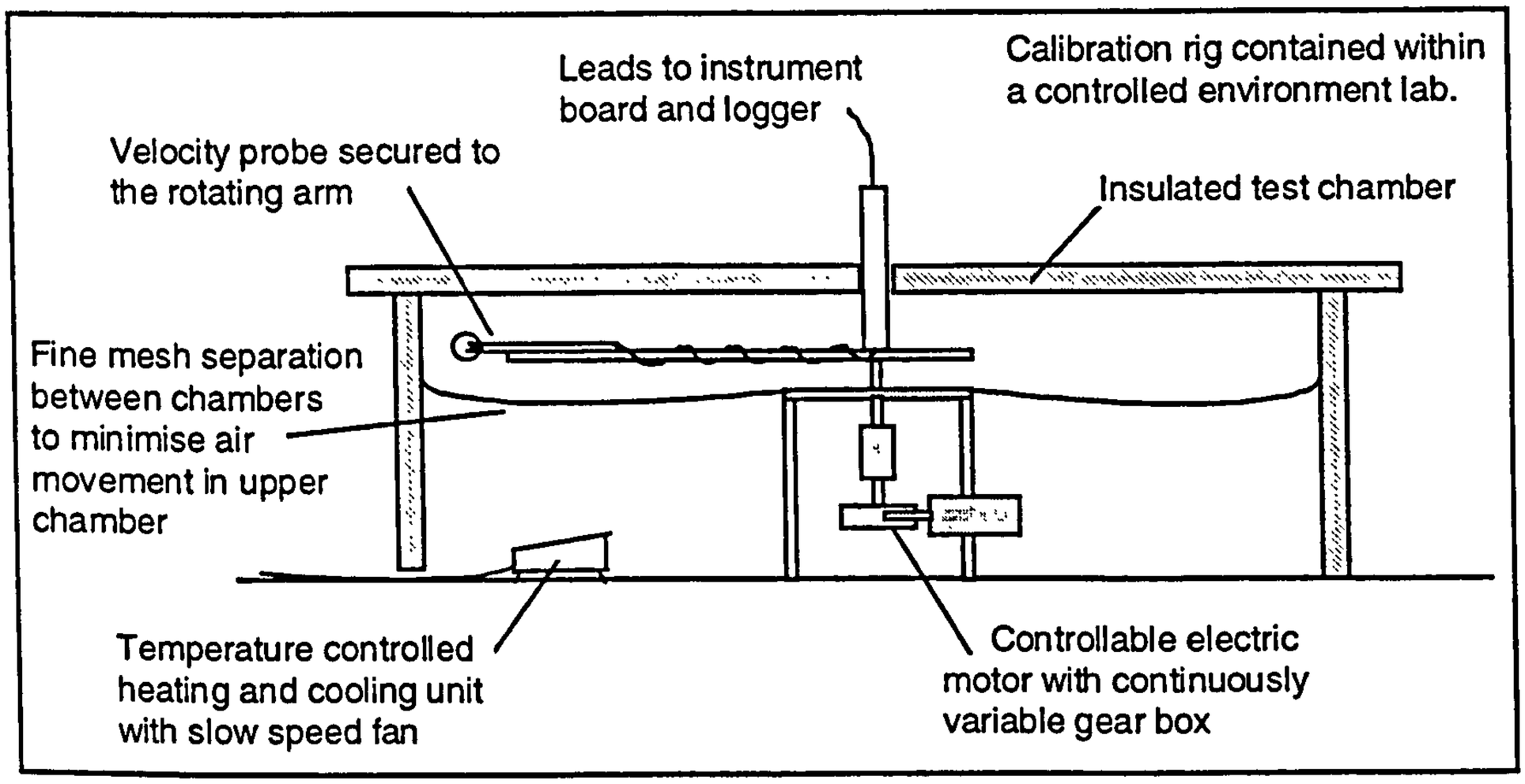

Figure D.5. Rotating arm calibration rig developed for inlet sensor calibration

The rig developed in figure 5. allowed the calibration of the sensors to be used at the inlet of the solar chimney across a temperature range of 5 - 30°C for velocities from 0.05 to 0.8 m/s with an estimated accuracy of +/- 2%.

To calibrate the sensors used at the exit of the solar chimney a simple wind tunnel that produced a flat velocity profile at the test section was designed and constructed. Through the use of a precision orifice plate mounted in the manufacturers recommended test section and a precision micro manometer the sensors were calibrated across a range of velocities of 0.05 to 0.8m/s for temperatures varying from 15 to 60°C.

The rig developed is shown in figure D.6.

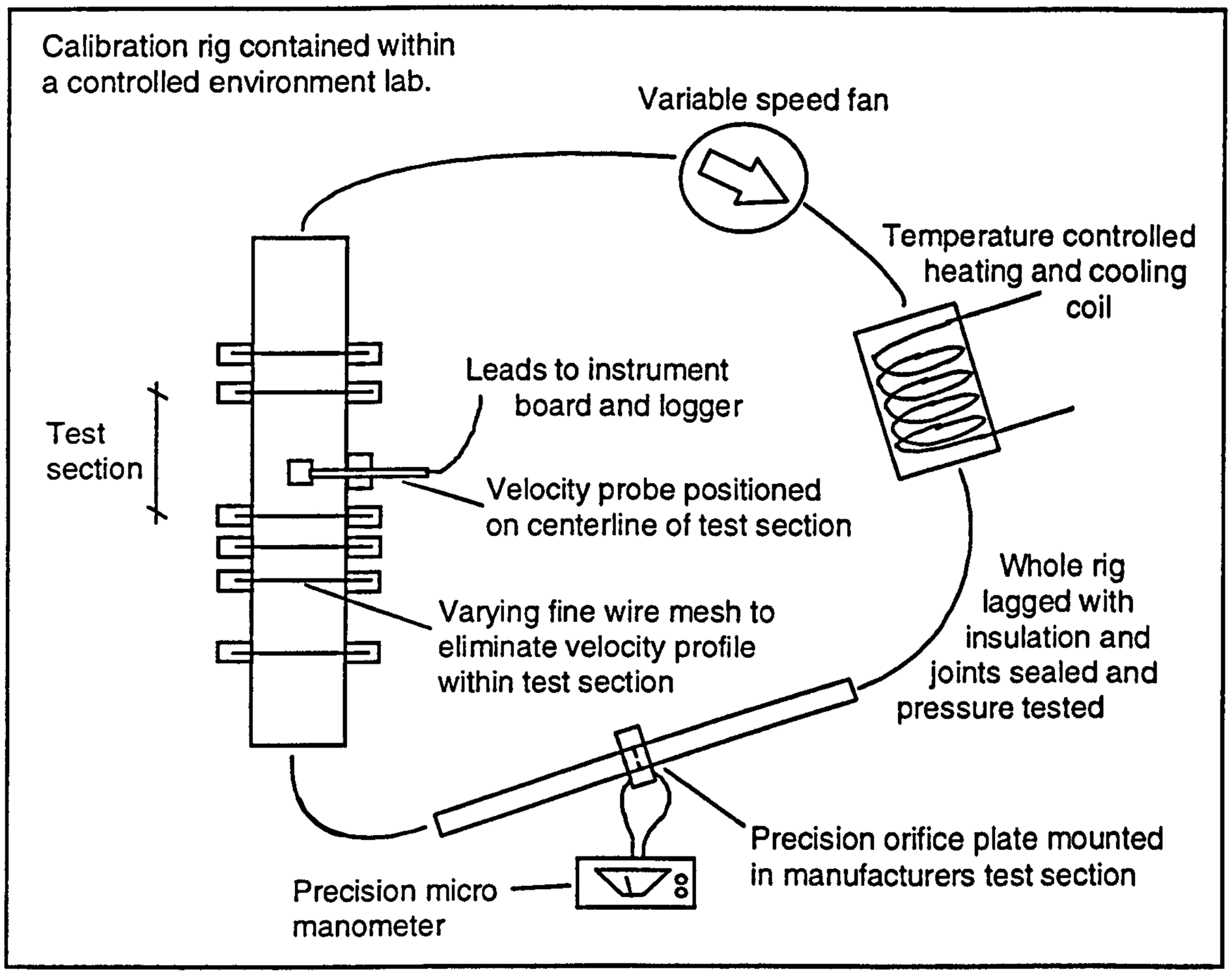

Figure D.6. Wind tunnel designed and constructed for the testing of sensors to be used at the exit to the solar chimney.

The accuracy of the calibrations was estimated to be +/- 3%.

Each sensor was calibrated at a mid range temperature to obtain the constants required for equation D.2. At a single temperature it was possible to fit a curve to all sensing heads to within +/- 2% of the imposed velocities. Two sensing heads of each type were then calibrated across their respective temperature ranges allowing the temperature stability of the instruments to be fully tested. The constants obtained at the mid range temperatures were found to be within +/-5% for both instruments for velocities between 0.05 and 0.8 m/s across the temperature ranges required.

Using the method of quadrature addition proposed by Taylor[5] to calculate the total level of uncertainty in the velocity measurements the following maximum level of uncertainty was:

$$U = \sqrt{5^2 + 3^2}$$ Equation D.6.

Therefore $U \approx \pm 6\ \%$

D.5 Results of use

The instruments described above have been used successfully in a remote location requiring battery operation for a period of eight months. Upon recalibration of the instruments after this period of operation, it was found that there had been no discernible changes to the calibration curves fitted at the outset.

D.6 Conclusion

The instruments described were constructed for the investigation of a building component to promote natural ventilation. This required up to 16 sensors to measure the inlet and outlet flow characteristics of the device. The output of the instrument developed was tailored to the data logging instrument used and was battery operated successfully on a remote site over an eight month period. The use of precision components throughout and the overall simplicity of the instrument ensured that calibration equations remained valid throughout an eight month period of use. Thus the ability to calibrate to a high level of accuracy with good resolution of the output across the range 0.05 - 0.8 m/s resulted in the development of an instrument suitable for remote logging in many applications.

D.7 References Appendix D

1. Nielsen, P., Air distribution in rooms - Research and design methods, Proceedings Roomvent 94, Poland, 1994.

2. Zhang, J., Wu, G., and Christianson, L., Hot wire / film anemometry for room air motion studies, Proceedings 12th. AIVC Conference, Ottawa, Canada, 1991.

3. McNair, H. and Russell ,M., Design of a thermistor thermometer and anemometer for room air measurement, The Gas Council, Report No. R&D/69/127, 1969.

4. McNair, H., A combined thermistor thermometer and anemometer, Fluid Dynamic Measurement in the Industrial and Medical Environments, Leicester University Press, 1974.

5. Taylor, J., An Introduction to Error Analysis, Oxford University Press, USA, 1982.

APPENDIX E

THE USE OF NEURAL NETWORKS FOR THE DETERMINATION OF A FUNCTIONAL RELATIONSHIP BETWEEN INPUT AND OUTPUT DATA SETS

The fitting of meaningful equations to accurately describe the relationship of more than one input to an output can result in unwieldy and complex results. The relationship between the normalised inputs of channel depth and inlet height and the normalised output of mass flow rate M_A, presented in figure 6.10. posed such a problem.

An alternative approach to curve fitting was therefore sought. This raised the question of the potential of a neural network to define the output M_A as a function of the two inputs, normalised inputs of channel depth (D) and inlet height (H). The advantage of a neural network is that it estimates a functional relationship between the inputs and outputs without recourse to a mathematical model of the relationship. Thus a functional relationship can be produced where a mathematical model would be impractical to resolve.

The basic structure of a neural network is shown in diagram E.1.

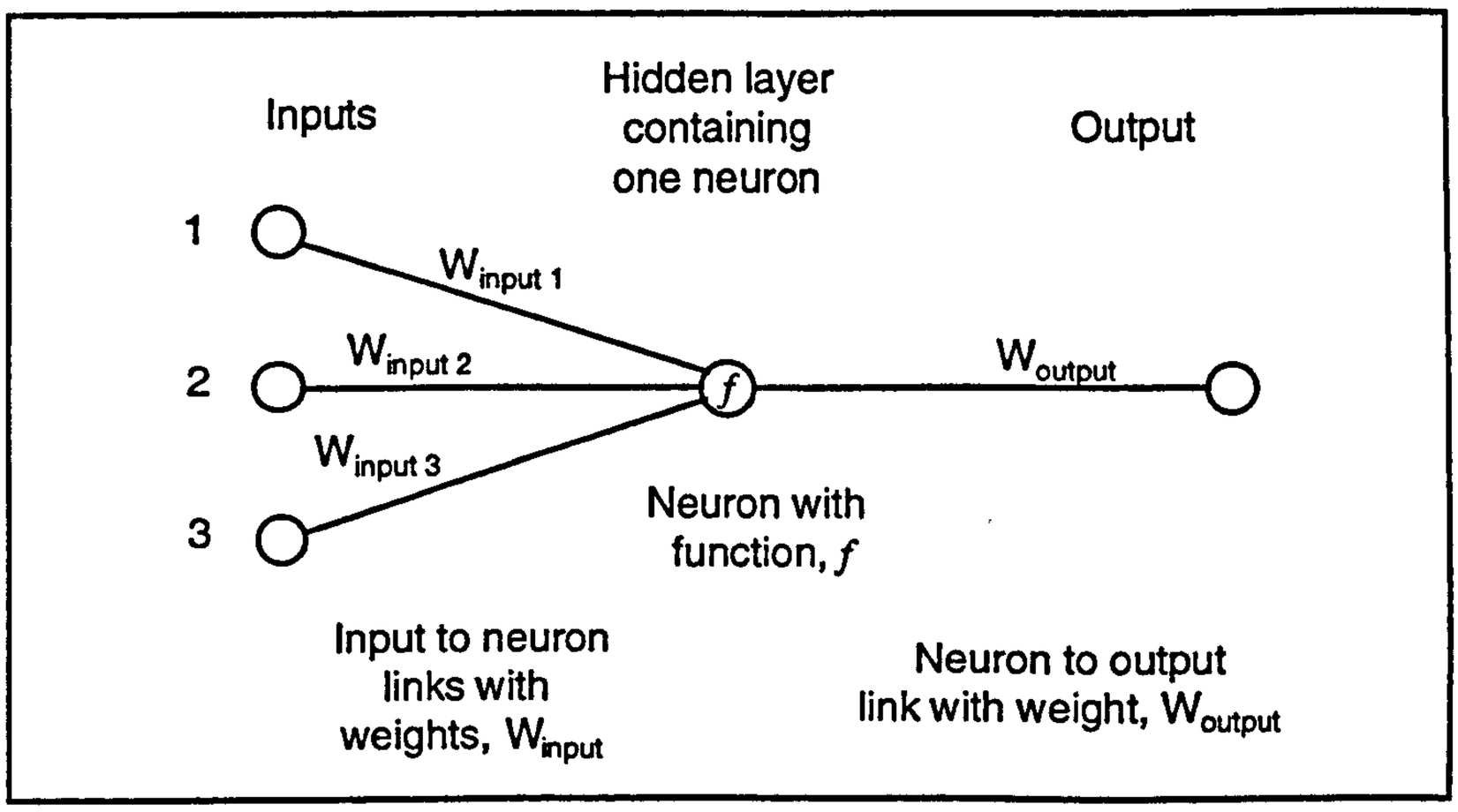

Figure E.1. Structure of a neural network using a hidden layer of one neuron.

In the network presented in figure E.1. the following relationships exist:

$$\text{Neuron output} = f\left(\sum W_{input}\,\text{Input}\right) \qquad \text{Equation E.1.}$$

where f is the neuron function

$$\text{Output} = \text{Neuron output}\ W_{output} \qquad \text{Equation E.2.}$$

The neuron presented in figure E.1. receives three inputs. Each of these are multiplied by weights W and then summed to give a single neuron input. If multiple neurons are used in the hidden layer then this would be undertaken at each neuron. The output of the neuron is then made a function of the input. Kosko[1] notes that there is no limit to the different functions that can be used. Usually a sigmoidal curve is used that approaches limits for very small and large input values. In the network used for this investigation a hyperbolic tangent function was used. Thus the output of each neuron is equal to; $\tanh\left(\sum W_{input}\,\text{Input}\right)$. The output is then calculated by multiplying the neuron output by a second weight. If multiple neurons are used then the output is the sum of the neuron outputs multiplied by their respective weights.

The relationship between the inlet and output is achieved by training the neural network on a data set that contains known values of the output for a range of input combinations. Such a data set was available from the parametric investigation in terms of the normalised channel depth and inlet heights inputs and the output, M_A. The data set was then used as an input for the neural network. The output values of the network were calculated based on the input combinations and an initial guess for all weights. The neural network then uses back propagation to modify the weights to minimise the squared error between the calculated output from the network and the actual output contained in the data set. This back propagation is undertaken until the error is minimised for the data set used.

The network used for the determination of the relationship between the input and output data presented in figure 6.10. contained nine neurons in one hidden layer. In addition to the inputs of H and D, a third input of 1 was used as a bias input. This ensured calculation of outputs when the inputs H and D were both zero.

The input vector for each set of data was defined as:

$$\text{Inlet} = \begin{bmatrix} D \\ H \\ 1 \end{bmatrix}$$

The weights determined by the neural network to be multiplied by the inputs to obtain the neuron inputs, are presented in matrix format below. The three columns correspond to the weights for the three inputs; D, H and 1.

Neuron input weights

$$W_{input} = \begin{bmatrix} -6.309211 & 3.947574 & 1.15121 \\ 0.87819 & 9.620393 & -0.469006 \\ 0.488163 & -2.631925 & -0.260346 \\ 0.179838 & 0.991806 & -0.613458 \\ -3.552815 & 3.225209 & -0.248714 \\ 1.392716 & 0.751457 & 1.273349 \\ 1.171577 & 0.527113 & 1.682916 \\ 2.923094 & -0.996726 & 0.657121 \\ -5.72084 & -7.035315 & 0.0043646 \end{bmatrix}$$

Thus the output of each neuron, expressed in matrix format was:

$$\text{Neuron output} = \tanh(W_{input} \cdot \text{Input}) \qquad \text{Equation E.3.}$$

The weights determined by the neural network to be multiplied by the neuron outputs, presented in matrix format were:

Neuron output weights

$$W_{output} = \begin{bmatrix} 0.0860467 \\ 0.0838518 \\ -0.441308 \\ 0.571685 \\ -0.211255 \\ -0.0229080 \\ -0.371362 \\ 0.585819 \\ 0.188713 \end{bmatrix}$$

The output was then calculated as the sum of the neuron outputs multiplied by the weights *W*. The neural network used for this investigation applied a weight to a tenth neuron that maintained an output value of 1. Thus this effectively acted as an offset to be added to the calculated output. Therefore the output M_A was defined by the functional relationship presented in equation E.4. for any combination of inputs. The relationship was found to predict the values of M_A to within +/- 2% for normalised inputs of between 0.1 and 1.0.

Equation E.4. is presented in matrix format to allow the data to be entered onto a spreadsheet computer programme for the calculation of output M_A.

$$M_A = W^T_{output} \cdot \left[\text{Tanh}\left(W_{input} \cdot \text{Input}\right)\right] + \text{Offset} \qquad \text{Equation E.4.}$$

Where W^T_{output} is the transpose of vector W_{output}.

Reference Appendix E

1. Kosko, B., Neural Networks and Fuzzy Systems, Prentice-Hall Inc., USA, 1992.